CHARACTERISATION OF COLLAGEN TYPE I / TYPE II COMPOSITE SCAFFOLDS FOR OSTEOCHONDRAL TISSUE ENGINEERING



Maryam Tamaddon

Hertford College

Michaelmas Term 2014

A Thesis Submitted for the Degree of Doctor of Philosophy

Department of Materials, University of Oxford

CHARACTERISATION OF COLLAGEN TYPE I / TYPE II COMPOSITE SCAFFOLDS FOR OSTEOCHONDRAL TISSUE ENGINEERING

Maryam Tamaddon, Hertford College

D.Phil. Thesis, Michaelmas Term 2014

ABSTRACT

The field of tissue engineering has potential to provide a superior alternative to current surgical treatments. Biologically inspired scaffolds have recently gained considerable attention in this field. The goal of this thesis was to develop and characterise the layers of an osteochondral scaffold following the composition and structure of cartilage, the cartilage-bone interface and underlying bone to treat osteoarthritis or defects in bone and cartilage. Monomeric collagens were used as the basis of these scaffolds, as they can mitigate the issue of antigenicity and may improve the reliability of the scaffolds due to the lack of native crosslinks.

Monomeric collagen type I alone and mixed with different amounts of hydroxyapatite formed the layers corresponding to calcified cartilage and subchondral bone. Collagen fibrils were made by *in vitro* fibrillogenesis. The preparations were characterised in terms of their molecular interaction; hydroxyapatite was attached electrostatically and covalently to collagen. The addition of hydroxyapatite and the formation of fibrils increased the rigidity of the collagen chains and subsequently increased the viscosity of the preparations. This affected the pore size of the final scaffolds; the pores were more dependent on growth than nucleation of ice crystals and more greatly influenced by suspension viscosity. The increase in rigidity of collagen chains with hydroxyapatite or fibrillogenesis led to an increase in the compressive modulus of the scaffolds up to 10 times. The modulus of the solid material and pore anisotropy were the main factors affecting the compressive modulus. The scaffolds were biocompatible and able to induce bone marrow stem cells to produce matrix-molecule collagen type I without any differentiation or growth factors.

Monomeric collagen type II alone and mixed with equal amounts of chondroitin sulphate formed the layers corresponding to different zones of cartilage. Fibrillogenesis was performed *in vitro*. Chondroitin sulphates attached to collagen mainly by electrostatic forces, which were weakened when the collagen was made fibrillar. This interaction caused the loss of chondroitin sulphate in the cell culture media and thus a negative or no contribution to cell proliferation, but significantly increased chondrogenic differentiation. The addition of chondroitin sulphate and fibrillogenesis increased the rigidity of the collagen chains and the viscosity of suspensions, thereby affecting the pore structure of the final scaffolds. A very important finding was that stem cells produced mostly collagen type II matrix molecules on these scaffolds, which differed from the production of collagen type I on type I scaffolds.

The hypothesis that the chemical differences in composition lead to different microstructure, mechanical properties and cell behaviour is confirmed. The developed scaffolds were greatly promising for osteochondral regeneration. The scaffolds were invaded, resorbed and remodelled by stem cells, and they were able to direct chondrogenesis and osteogenesis by tailoring the scaffold properties. This has great implications for clinical use. The main shortcomings were 1) their low compressive modulus, 2) their extreme contraction in cell culture media and 3) loss of chondroitin sulphate.

This thesis is dedicated to the loving memory of my dad, Kazem Tamaddon.

ACKNOWLEDGEMENTS

I would like to express my heartfelt gratitude to my supervisor Prof. Jan Czernuszka, who has been a tremendous mentor for me. Thank you for giving me freedom to explore; I would not have grown as much if it wasn't for this. Thanks for trusting me and providing me invaluable guidance throughout this time. I could not have hoped for a better supervisor.

I also wish to thank Dr. Eileen Gentleman in the Department of Craniofacial Development & Stem Cell Biology at King's College London. Thank you for my first ever experience with cells! I learnt from you immensely. I cannot express enough thanks for your kindness, calmness and support.

I would also like to thank Professor C.R.M Grovenor, head of Materials department at Oxford University for providing the laboratory facilities. I also wish to thank Dr. David Brand for kindly providing me with the collagen; this work would not have been possible without it! My special thanks to the past and present members of Biomaterials group for helpful discussions.

To my lovely family, my mom and grandparents, who encouraged me and provided me with the means to continue my studies; thank you for your unconditional love, support and unwavering belief in me. Without you, I would not be the person I am today.

This thesis would not have been possible without the support of my partner Dr. Farhad Hassani Mehraban; thank you for the being there and standing by me every step of the way. Your kindness and emotional support got me through the hard times. Thanks for caring for me, feeding me and comforting me when things got busy.

PREFACE

The research described in this thesis was undertaken by the author in the Department of Materials, University of Oxford, between October 2010 and January 2015, under the supervision of Prof. Jan Czernuszka. It is original in its contents except where reference to the work of others is acknowledged in the text. No parts of this thesis have been submitted or accepted for a degree at this university or elsewhere. Various parts of the work in this thesis have been published in peer-reviewed journals as follows:

Peer-reviewed papers:

[1] M. Tamaddon, R. S. Walton, D. D. Brand and J. T. Czernuszka. Characterisation of freeze-dried type II collagen and chondroitin sulfate scaffolds. *J. Mater. Sci. -Mater. Med. 24(5),* pp. 1153-1165. 2013. . DOI: 10.1007/s10856-013-4882-9.

[2] M. Tamaddon and J. T. Czernuszka, "The need for hierarchical scaffolds in bone tissue engineering," *Hard Tissue,* vol. 2, pp. 4-37, 2013.

TABLE OF CONTENTS

ABSTRACT……..i
ACKNOWLEDGMENTS …… iii
PREFACE……..……iv
TABLE OF FIGURES……...ix
LIST OF TABLES……..……..xiv
LIST OF ABBREVIATIONS……xv

Chapter 1. Introduction 1

Chapter 2. Literature Review 6
2.1 Introduction 7
2.2 Biology, anatomy and properties of cartilage 8
2.2.1 Composition 8
2.2.1.1 Cells 9
2.2.1.2 Extracellular matrix (ECM) 10
2.2.2 Structure 15
2.2.3 Mechanical properties 18
2.2.3.1 Compression 19
2.2.3.2 Tensile 21
2.2.4 Healing behaviour 23
2.3 Biology, anatomy and properties of bone 25
2.3.1 Composition 25
2.3.1.1 Cells 26
2.3.1.2 ECM 27
2.3.2 Structure 30
2.3.3 Mechanical properties 32
2.3.4 Bone healing behaviour 35
2.4 Cartilage-bone interface 36
2.5 Bone and cartilage defects 39
2.6 Current treatments 43
2.7 Tissue engineering (TE) 46
2.7.1 Scaffolds 47
2.7.2 Cells 52
2.7.3 Growth factors 53
2.8 Osteochondral tissue engineering 56
2.8.1 Osteochondral scaffold materials 57
2.8.1.1 Collagen 57
2.8.1.2 Chondroitin sulphate (CS) 63
2.8.1.3 Collagen-chondroitin sulphate composites 64
2.8.1.4 Hydroxyapatite (HAp) 66
2.8.1.5 Collagen-hydroxyapatite composites 67
2.9 Scaffold fabrication techniques 70
2.10 Scaffold-cell interaction 72
2.11 Basis and aims of this research 77

Chapter 3. Experimental Procedures: Scaffolds Fabrication 80

3.1 Introduction **81**
3.2 Preparation of collagen-based scaffolds **82**
3.2.1 Materials 82
3.2.2 Collagen solutions 82
3.2.3 Dialysis and Fibrillogenesis 83
3.2.4 Casting and Freeze-drying 85

Chapter 4. Fourier Transform Infrared Spectroscopy **87**
4.1 Introduction **88**
4.2 Experimental Procedures **89**
4.2.1 Statistical Analysis 90
4.3 Results **91**
4.4 Discussion **96**
4.4.1 Changes in molecular structure of Type-I scaffolds 98
4.4.2 Changes in molecular structure of Type-II scaffold 100
4.5 Summary **104**
4.6 Conclusion **104**

Chapter 5. Rheological properties of preparations **106**
5.1 Introduction **107**
5.2 Experimental Procedures **107**
5.3 Results **110**
5.3.1 Linear Viscoelastic Region (LVR) 110
5.3.2 Shear rate dependency 118
5.3.3 Dynamic Frequency Sweep 121
5.4 Discussion **128**
5.4.1 Rheological behaviour during rotational shear measurements 132
5.4.2 Rheological behaviour during oscillatory measurements 134
5.4.2.1 Storage (G') and loss (G'') moduli 137
5.5 Summary **139**
5.6 Conclusion **140**

Chapter 6. Microstructural Evaluations **141**
6.1 Introduction **142**
6.2 Experimental Procedures **142**
6.2.1 Statistical Analysis 143
6.3 Results **144**
6.3.1 Microstructure evaluation 144
6.3.1.1 Type-I composite scaffolds 144
6.3.1.2 Type-II composite scaffolds 148
6.3.2 Pore size analysis 150
6.4 Discussion **159**
6.4.1 Scaffold formation 159
6.4.1.1 Mechanism of formation of collagen suspensions 159
6.4.1.2 Scaffold synthesis from collagen suspensions 160
6.4.2 Microstructure 164
6.4.2.1 Type-I collagen scaffolds 164
6.4.2.2 Type-II collagen scaffolds 167
6.4.3 Pore sizes 168

6.4.4 Pore circularity 171
6.4.5 Measurement method 172
6.5 Summary 175
6.6 Conclusion 176

Chapter 7. Mechanical Properties of Scaffolds 177
7.1 Introduction 178
7.2 Experimental Procedure 178
7.2.1 Statistical Analysis 179
7.3 Results 180
7.4 Discussion 184
7.4.1 Mechanical behaviour of type-I scaffolds 190
7.4.2 Mechanical behaviour of type-II scaffolds 191
7.5 Summary 193
7.6 Conclusion 193

Chapter 8. Biological Properties of composite scaffolds 195
8.1 Introduction 196
8.2 Experimental Procedure 196
8.2.1 Scaffold sterilization 196
8.2.1.1 Sterilisation effectiveness 197
8.2.2 Cells and Media 197
8.2.3 Live/Dead assay (cell viability) 199
8.2.4 Cytoskeletal immunostaining (cell morphology) 200
8.2.5 Cell Proliferation 200
8.2.6 Histological examination 201
8.2.7 Immunohistochemistry 203
8.2.8 Statistical Analysis 204
8.3 Results 206
8.3.1 Scaffold size evaluation and cell mediated contraction 206
8.3.2 Live/Dead assay (cell viability) 209
8.3.3 Cytoskeletal immunostaining (cell morphology) 212
8.3.4 Alamar Blue 215
8.3.5 Histological examination 217
8.3.5.1 H&E 217
8.3.5.2 Trichrome 222
8.3.5.3 Alizarin Red 225
8.3.6 Immunohistochemistry 227
8.4 Discussion 234
8.4.1 Scaffold sterilization 234
8.4.2 Changes in scaffold sizes in culture 234
8.4.2.1 Cell-mediated changes 235
8.4.2.2 Solution-mediated changes 236
8.4.3 Cellular behaviours 237
8.4.3.1 Cell viability and scaffold biocompatibility 238
8.4.3.2 Cell attachment 239
8.4.3.3 Cellular metabolic activity 242
8.4.4 Histological evaluations 243

8.4.5 Matrix molecules production by cells 244
8.5 Summary 248
8.6 Conclusion 249
Chapter 9. Thesis Summary & Conclusions 250
Chapter 10. Future Works 258

LIST OF FIGURES

Figure 2.1 Composition of articular cartilage, redrawn from (Aigner and Stove, 2003) 8
Figure 2.2 Organisation of different collagen types in articular cartilage (Cremer et al., 1998) 10
Figure 2.3 Schematic sketch of a proteoglycan monomer (Newman, 1998) 12
Figure 2.4 Structure of articular cartilage according to the distance of its elements from the joint surface-tidemark denotes a discrete band between mineralized and non-mineralized cartilage (Madry et al., 2010); adapted from (Yang and Temenoff, 2009) 16
Figure 2.5 Structure of articular cartilage according to its distance from the cells, adapted from (Stockwell, 1979) 17
Figure 2.6 Schematic stress-strain curves for samples of human femoral condyle. Vertical arrows (↑) show the stress parallel to surface cleavage and horizontal arrows (→) show the stress perpendicular to surface cleavage. Black lines illustrate the surface of articular cartilage and red lines the deep layer. As seen, surface of articular cartilage has higher tensile strength than deep layer; redrawn from (Kempson et al., 1973) 22
Figure 2.7 Types of repair tissue, from (Aigner and Stove, 2003) 24
Figure 2.8 Bone matrix components by weight % 25
Figure 2.9 Bone hierarchical structure (Suchanek and Yoshimura, 1998) 30
Figure 2.10 Two cartilage layers in contact having a plane of symmetry; (a) the contact problem is equivalent to a rigid plane contacting a bone-cartilage layer or (b) a rigid sphere indenting a flat cartilage-bone layer (Ateshian et al., 1994) 37
Figure 2.11 Contact with force P between a rigid sphere and two layers with (a) sharp interface, which leads to delamination between the layers caused by the tensile and shear stresses at the interface due to abrupt change in modulus E, (b) graded interface with gradual increase in E, which suppress delamination; diagram from (Giannakopoulos, 1998) 38
Figure 2.12 Partial-thickness, full-thickness and osteochondral defects; adapted from (O'Shea and Miao, 2008), picture from (Leng et al., 2013) 40
Figure 2.13 Schematic representation of the main structures of a healthy (left) and degenerated (right) joint; modified from (Aigner and Stove, 2003), picture modified from http://thinkloud65.files.wordpress.com/2012/05/oa2.jpg 41
Figure 2.14 Three key ingredients of TE; adapted from (O'Shea and Miao, 2008) 47
Figure 2.15 Schematic of forces on femur bone; the center represents the cancellous bone and the outer represents the cortical bone. Cancellous bone is subjected predominantly to compression while cortical bone is exposed to both tensile and compressive forces 50
Figure 2.16 Hierarchical structure of collagen, showing the amino acid sequence, alpha-chain, triple helix and molecular structures and assembly into fibrils of quarter staggered pattern (67nm) consisting of gap (40nm) and overlap regions; redrawn from (Tamaddon and Czernuszka, 2013, Lane and Weiss, 1975) .59
Figure 2.17 Typical stress-strain curve for collagen and calcium-phosphate-collagen composites; redrawn from (Lawson and Czernuszka, 1998) 68
Figure 2.18 Freeze-drying principle to produce porous structures; adapted from (Deville, 2008) 71
Figure 2.19 Cell and material interaction; adapted from (Martino et al., 2012, Anselme, 2000) 74
Figure 2.20 Effect of cell spreading/adhesion on subsequent cell behaviour. Blue refers to cell nuclei and black dots represent focal adhesions; redrawn from (Bacakova et al., 2004) 75
Figure 2.21 Proposed scaffold for osteochondral TE 78
Figure 3.1 TEM micrographs of reconstituted fibrillar type-I atelocollagen (left) and of reconstituted fibrillar type-II atelocollagen (right) (Walton, 2010) 84
Figure 3.2 Plastic tubing mould to produce samples for characterisation 85
Figure 3.3 PTFE mould to produce samples for cell study 85
Figure 4.1 FTIR spectra of type-I composite scaffolds (n=3) in 800-3500cm^{-1} range 91
Figure 4.2 FTIR spectra of type-I composite scaffolds (n=3) in 800-3500cm^{-1} range 92
Figure 4.3 Second derivative spectra (900-1700 cm-1) of type-I composite scaffolds 95

Figure 4.4 Second derivative spectra (800-1700 cm-1) of type-II composite scaffolds 95
Figure 4.5 Collagen and HAp interaction and bond formation, redrawn from (Ficai et al., 2009).....100
Figure 4.6 Proposed bonding between a) collagen and b) chondroitin sulphate. Circles indicate the sulphate and hydroxyl/carboxyl groups; drawings from (National Center for Biotechnology Information) 103
Figure 5.1 Storage modulus G' vs. strain of type-I collagen composite preparations in a strain sweep (0.1-100%) mode of an oscillatory shear test (strain=0.1-100%, T=20C) 111
Figure 5.2 Storage modulus G' vs. strain of type-II collagen composite preparations in a strain sweep (0.1-100%) mode of an oscillatory shear test (strain=0.1-100%, T=20ºC).....112
Figure 5.3 The effect of fibrillogenesis on Linear Viscoelastic Region of the preparations: A) 1af, 1rf B)1af-HAp1:1, 1rf-HAp 1:1 C)1af-HAp 1:3, 1rf-HAp 1:3 D)2af, 2rf E) 2af-CS, 2rf-CS. The red line indicaes the flat part of the curve corresponding to the LVR. Strain=0.1-100%, T=20ºC 115
Figure 5.4 The effect of HAp and CS addition on LVR of different preparations: A)1af, 1af-HAp 1:1, 1af-HAp 1:3 B)1rf, 1rf-HAp 1:1, 1rf-HAp 1:3 C)2af, 2af-CS, 2rf, 2rf-CS; shear stress versus strain and storage modulus versus strain shown. Strain=0.1-100%, T=20ºC.....117
Figure 5.5 Flow curves and hysteresis loops of preparations showing the effect of particle addition to type-I preparations; shear rate=0.1-100 1/s. T=20C. Filled symbols (■) and downward arrow show increasing shear rate, while open symbols (□) and upward arrow show decreasing of shear rate.....118
Figure 5.6 Flow curves and hysteresis loops of preparations showing the effect of fibrillogenesis of type-I preparations; shear rate = 0.1 – 100 1/s, T= 20C. Filled symbols (■) and downward arrow show increasing shear rate, while open symbols (□) and upward arrows show decreasing of shear rate 119
Figure 5.7 Flow curves and hysteresis loops of preparations showing the effect of shear rate on viscosity of type-II preparations; shear rate = 0.1 – 100 1/s, T= 20ºC. Filled symbols (■) and downward arrow show increasing shear rate, while open symbols (□) and upward arrows show decreasing of shear rate.119
Figure 5.8 Storage (G') and loss (G'') modulus cross-over of a) 1af, b) 1af-HAp 1:1, c) 1af-HAp 1:3, d)1rf, e)1rf-HAp 1:1, f)1rf-HAp 1:3 in frequency sweep test; angular frequency = 100-0.1 rad/s , strain amplitude γ = 1%, T =20ºC.....121
Figure 5.9 Storage (G') and loss (G'') modulus of a) 2af, b) 2af-CS, c) 2rf and d) 2rf-CS in frequency sweep test; angular frequency = 100-0.1 rad/s , strain amplitude γ = 1%, T =20ºC 122
Figure 5.10 Phase angle between shear stress and strain in oscillatory shear test in frequency sweep (angular frequency = 100-0.1 rad/s , strain amplitude γ = 1%, T =20ºC) 123
Figure 5.11 Complex modulus (G*) and complex viscosity (η*) in oscillatory shear test; frequency sweep (angular frequency = 100-0.1 rad/s , strain amplitude γ = 1%, T =20C). Effect of HAp addition on type-I preparations (A) and (B); effect of fibrillogenesis on type-I preparations (C), (D) and (E); type-II preparations (F).....125
Figure 5.12 Schematic illustration of worm-like polymer chains with continuous flexibility and Kuhn chains with rigid and flexible domains (Larson, 1999).....128
Figure 5.13 Concentration regimes for rodlike rigid molecules, redrawn from (Larson, 1999, Doi and Edwards, 1986) 130
Figure 5.14 Schematic illustration of three zone model in dynamic rheological measurements; G' and G'' vs angular frequency. Adapted from (Ferry, 1980, Larson, 1999).....138
Figure 6.1 SEM images of *1af* at a) low magnification, b) high magnification with the red arrow indicating a secondary pore 144
Figure 6.2 SEM images of *1af-HAp 1:1* at a) low magnification, b) high magnification with red arrow indicating a secondary pore and blue arrow a colony of HAp deposit on collagen sheet.....145
Figure 6.3 SEM images of *1af-HAp 1:3* a) low magnification, b) high magnification with red arrow indicating a secondary pore 145
Figure 6.4 SEM images of *1rf* at a) low magnification, b) high magnification with red arrow indicating a secondary pore 146

Figure 6.5 SEM images of *1rf-HAp 1:1* at a) low magnification, b) higher magnification with the red arrow indicating a secondary pore and green circles fibrous struts and c) high magnification with the blue arrows showing clusters of HAp deposit on collagen sheet.....147
Figure 6.6 SEM images of 1rf-HAp 1:3 at a) low magnification, b) and c) high magnifications with the blue arrows showing clusters of HAp deposit on collagen sheet.....148
Figure 6.7 SEM images of *2af* at a) low magnification, b) high magnification with red arrow indicating a secondary pore 149
Figure 6.8 SEM images of *2af –CS* at a) low magnification, b) high magnification with red arrow indicating a secondary pore 149
Figure 6.9 SEM images of *2rf* at a) low magnification, b) high magnification with red arrow indicating a secondary pore 149
Figure 6.10 SEM images of *2rf –CS* at a) low magnification, b) high magnification the red arrow indicating a secondary pore and c) high magnification with green circles showing fibrous struts.....150
Figure 6.11 Frequency plots of circularised pore diameters Type I collagen composite scaffolds (number of measured pores, n = 100).....151
Figure 6.12 Frequency plots of circularised pore diameters for Type II collagen composite scaffolds (number of measured pores, n = 100) 152
Figure 6.13 Frequency plots of cross-sectional elliptical pore areas for afibrillar Type I collagen. Ellipses represent proportioned, averaged pores, with mean major and minor axis dimensions, (A = mean cross-sectional area of pores, Q = mean isoperimetric quotient of circularity), (n = 100) 155
Figure 6.14 Frequency plots of cross-sectional elliptical pore areas for reconstituted fibrillar Type I collagen. Ellipses represent proportioned, averaged pores, with mean major and minor axis dimensions, (A = mean cross-sectional area of pores, Q = mean isoperimetric quotient of circularity), (n = 100) 156
Figure 6.15 Frequency plots of cross-sectional elliptical pore areas for Type II collagen. Ellipses represent proportioned, averaged pores, with mean major and minor axis dimensions, (A = mean cross-sectional area of pores, Q = mean isoperimetric quotient of circularity), (n = 100) 158
Figure 6.16 Temperature dependency of nucleation and growth rates; it can be seen that at -20C growth rate is dominant in determining the microstructure. Adapted from (Xie et al., 2013).....170
Figure 6.17 Thermal gradient across the scaffold leads to pore anisotropy in the direction of the heat transfer; red arrows show high thermal gradient while orange arrows show lower gradient due to the thickness of the mould wall 171
Figure 7.1 Stress-strain curves of type-I collagen composite scaffold under compression (n=5). The inset shows the linear portion of the curve, through which a line was fitted (ending points for *1rf-HAp 1:1* and *1:3* were 20%, for the rest 10% strain); the slope of this line was considered as the compressive modulus 180
Figure 7.2 Compressive modulus (E*) of type-I composite scaffolds (n=3); * indicates a significant difference at p=0.05 181
Figure 7.3 Stress-strain curves of type-II collagen composite scaffold under compression (n=5). The inset shows the linear portion of the curve, through which a line was fitted (ending points 10% strain); the slope of this line was considered as the compressive modulus.....182
Figure 7.4 Compressive modulus (E) of type-II composite scaffolds (n=5); * indicates a significant difference at p=0.05 182
Figure 7.5 Schematic stress-strain curve of a low density foam under compression; σ*is collapse stress and ε_d is densification strain. Adapted from (Ashby, 2006, Gibson and Ashby, 1997).....185
Figure 7.6 Buckling dominated behaviour of a pore (Ashby, 2006) 186
Figure 7.7 Fracture-dominated behaviour of a pore (Ashby, 2006) 187
Figure 7.8 Schematic diagram of stress-strain curve of a hypothetical scaffold with regions marked for typical loads generated by thumb, firm thumb and strong thumb pressures. Adapted from (Harley et al., 2010b) 192
Figure 8.1 Cell culture and characterisation assays 199

Figure 8.2 Percentage of change in scaffold diameter before cell seeding and after 1 and 28 days of culture. Symbols show significant difference at $p<0.05$: # significantly different from *1af*; * significantly different from *1af-HAp*; Δ significantly different from *1rf-HAp*; + significantly different from *2af*. No significant difference between groups at day 1 ($p<0.05$) 206
Figure 8.3 Scaffold sizes after 1 day (black column) and 28 days (blue column) of cell seeding in culture media. The dashed columns represent scaffold diameter after 1 day (gray) and 28 days (light blue) in media only (no cells). The diameter of scaffolds before cell seeding is denoted by dashed line. The "*" of different colours demonstrates significant difference between groups at day 28. There was no significant difference at day 1 ($p<0.05$) (n=3) 207
Figure 8.4 Live/Dead cytotoxicity assay showing cell viability of type-I scaffolds at day 1 and 14 (D, x5). Green color indicates live cells and red color dead cells 210
Figure 8.5 Live/Dead cytotoxicity assay showing cell viability of type-I scaffolds at day 1 and 14 (D, x5 and x10). Green color indicates live cells and red color dead cells 211
Figure 8.6 Cytoskeletal and DAPI images of type-I scaffolds; red indicates the cytoskeletal of cells; blue indicates the cell nuclei. Green circles indicate a cell and its cytoskeleton. Magnification 40x 213
Figure 8.7 Cytoskeletal and DAPI images of type-II scaffolds; red indicates the cytoskeletal of cells; blue indicates the cell nuclei. Green circles indicate a cell and its cytoskeleton. Magnification 40x 214
Figure 8.8 AlamarBlue activity of cells on different scaffolds on 1, 7 and 28 days. Symbols show the significant difference at level 0.05 in the same day: # significantly different from *1af*, Δ significantly different from *1rf-HAp* and + significant difference from *2af*. At day 7, *1af-HAp* and *2rf-CS* showed significantly lower activity compared to other scaffolds. Significant decrease in 1af-HAp at day 28 compared to day 7 215
Figure 8.9 Alamar Blue activity change from day 1 in different groups 216
Figure 8.10 H&E staining of *1af* sections, at A) week 1 and B) week 4; black arrows show the cell nuclei 219
Figure 8.11 H&E staining of *1af-HAp* sections at week 4, cell nuclei stained dark brown 219
Figure 8.12 H&E staining of *1rf-HAp* sections at week 4; black arrow shows the cell nuclei 220
Figure 8.13 H&E staining of *2af* sections at week 4; black arrow shows the cell nuclei 220
Figure 8.14 H&E staining of *2af-CS* sections at week 4; black arrow shows the cell nuclei 220
Figure 8.15 H&E staining of *2rf-CS* sections at week 4. Cell nuclei stained dark brown 221
Figure 8.16 Trichrome staining of sample *1af* at A) week 1 and B) week 4 at different magnifications. Scale bar shown in image. Black arrows show the cell nuclei, orange arrows correspond to collagen and blue arrow shows GAGs 222
Figure 8.17 Trichrome staining of sample *1af-HAp* at A) week 1 and B) week 4 at different magnifications. Scale bar shown in image. Black arrows show the cell nuclei, orange arrows correspond to collagen and blue arrow shows GAGs 223
Figure 8.18 Trichrome staining of sample *1rf-HAp* at week 4 at different magnifications. Scale bar shown in image. Black arrows show the cell nuclei and orange arrows correspond to collagen 223
Figure 8.19 Trichrome staining of sample 2af at week 4 at different magnifications. Scale bar shown in image. Black arrows show the cell nuclei and orange arrows correspond to collagen 224
Figure 8.20 Trichrome staining of sample *2af-CS* at week 4 at different magnifications. Scale bar shown in image. Black arrows show the cell nuclei and orange arrows correspond to collagen 224
Figure 8.21 Trichrome staining of sample 2rf-CSat week 4 at different magnifications. Scale bar shown in image. Black arrows show the cell nuclei, orange arrows correspond to collagen and blue arrow shows GAGs 225
Figure 8.22 Alizarin Red staining of sample 1af at week 4; black arrow indicates an example of the regions stained positive for calcium. 225
Figure 8.23 Alizarin Red staining of sample 1af-HAp at week 4; black arrow indicates an example of the regions stained positive for calcium 226
Figure 8.24 Alizarin Red staining of sample 1rf-HAp at week 4; black arrow indicates an example of the regions stained positive for calcium 227

Figure 8.25 Alizarin Red staining of sample 2af at week 4; black arrow indicates an example of the regions stained positive for calcium.....227
Figure 8.26 Col II and DAPI staining of 1af scaffolds at week 4 at different magnifications. Red arrows indicate examples of col II expressed by the BMMSCs 228
Figure 8.27 Col II and DAPI staining of 1af-HAp scaffolds at week 4. Red arrow indicates examples of col II expressed by the BMMSCs 229
Figure 8.28 Col II and DAPI staining of 1rf-HAp scaffolds at week 4 at different magnifications. Red arrows indicate examples of col II expressed by the BMMSCs 230
Figure 8.29 Col I and II and DAPI staining of 2af scaffolds at week 4 at different magnifications. Red arrows indicate examples of col I and II expressed by the BMMSCs 231
Figure 8.30 Col II and DAPI staining of 2af-CS scaffolds at week 4 at different magnifications. Red arrows indicate examples of col II expressed by the BMMSCs 232
Figure 8.31 Col II and DAPI staining of 2rf-CS scaffolds at week 4 at different magnifications. Red arrows indicate examples of col II expressed by the BMMSCs 233
Figure 8.32 Effect of matrix elasticity on mesenchymal stem cell fate, adapted from (Engler et al., 2006); MSCs are initially small and round but develop increasingly branched, spindle, or polygonal shapes when grown on matrices respectively in the range typical of E brain (0.1–1 kPa), E muscle (~10 kPa), or E collagenous bone (~100kPa).....247

LIST OF TABLES

Table 2.1 Structure of articular cartilage according to distance from joint surface 15
Table 2.2 Structure of cartilage according to distance from chondrocytes 17
Table 2.3 Mechanical properties under compression using different methods in different species 20
Table 2.4 Tensile properties of articular cartilage (Roth and Mow, 1980, Akizuki et al., 1986, Kempson et al., 1973); S=Surface, D=Deep 23
Table 2.5 Mechanical properties of cortical and cancellous bone 34
Table 2.6 Bone graft methods comparison (Porter et al., 2009, Wahl and Czernuszka, 2006, Puppi et al., 2010, Tenhuisen et al., 1995). 44
Table 2.7 Scaffold matrix properties, modified after (Sharma and Elisseeff, 2004) 51
Table 2.8 Commercial scaffolds currently available (Place et al., 2009). 55
Table 2.9 Collagen molecules families. 60
Table 2.10 Currently investigated collagen-CS scaffolds; DHT=dehydrothermal crosslinking, EDC=1-ethyl-3-(3-dimethylaminopropyl) carbodiimide, GTA=Glutaraldehyde crosslinking; FD= freeze-drying 65
Table 2.11 Currently researched collagen-HAp scaffolds. GTA =glutaraldehyde , DDPA=glutaraldehyde. Diphenylphosphorylazide, EDC/NHS =carbodiimide/N-hydroxy succinimide. 69
Table 3.1 Collagen solution types and acronyms used throughout the text. 84
Table 4.1 FTIR second derivative band assignment in type-I composite scaffolds; # denotes a shoulder rather than peak. 92
Table 4.2 FTIR second derivative band assignment in type-II composite scaffolds; the unit is cm^{-1} and refers to the wavenumber 93
Table 5.1 Phase angle of different preparations. 124
Table 6.1 Mean pore areas, distribution of pore area sizes (% of pores between x and y mm^2), and isoperimetric quotient of circularity Q. Symbol * denotes significant difference from 1af, • denotes significant difference from 1rf, + denotes significant difference from 1rf-HAp 1:1, ■ denotes significant difference from 2af and # from 2rf; symbol ♦ indicates significant difference with all other scaffolds in type-II. Significant level is at 0.05 using Mann-Witney test. 153
Table 6.2 filtering of pore sizes for type-I scaffolds, % pores with both axes between 50-600um and with the circularised pore diameter between 50-600um. 174
Table 6.3 filtering of pore sizes for type-II scaffolds; % pores with both axes between 30-500um. 175
Table 7.1 Compression modulus of type-I and II composite scaffolds (n=5), SD= standard deviation. 183
Table 7.2 relative density of type-I scaffolds; no significant difference at level of 0.05 between afibrillar scaffolds; significant difference between 1rf and afibrillar scaffolds, and between 1rf and 1rf-HAp 1:1, and between 1rf-HAp 1:3 and all other scaffolds. 187
Table 7.3 Relative density of type-II scaffolds; no significant difference at level of 0.05 was observed. 188
Table 7.4 Anisotropy ratio, R, of different scaffolds. 189
Table 8.1 The overall, cell-mediated and solution-mediated changes in scaffold diameter at day 1. The overall reduction was calculated as (original diameter-diameter at day1)/original diameter; SD= standard deviation (n=3). 208
Table 8.2 cell-mediated and overall reduction in scaffold diameter at day 28; SD= standard deviation (n=3). 209
Table 8.3 The % of change in Alamar Blue activity in different scaffolds after 7 and 28 days; SD denotes standard deviation (n=3). 217
Table 8.4 Storage modulus, compressive modulus and pore sizes of scaffolds vs overal changes (OC) and cell-mediated changes (CMC) in size after 1 and 28 days. 237
Table 8.5 Scaffolds properties (surface area, compressive modulus and pore sizes) and Alamar Blue activity at day 1 (divided by 10000). 241

LIST OF ABBREVIATIONS

AB …….……..…….. Alamar Blue
ACI ……...Autologous Chondrocyte Implantation
ALP ……..…..……Alkaline Phosphatase
ANOVA……..……Analysis of variance
BCP……...…....Biphasic Calcium Phosphate
BMPs ……..Bone Morphogenetic Proteins
BSA …….……... Bovine Serum Albumin
CMC …….. Cell-mediated changes in size
COL1A1…… Collagen type I alpha chain 1
CS …….…….…….…… Chondroitin Sulfate
DAPI……..... 4',6-diamidino-2-phenylindole dihydrochloride
DDPA…….……....Glutaraldehyd Diphenylphosphorylazide
DHT……..... Dehydrothermal crosslinking
DNA……..…….Deoxyribonucleic Acid
DPX …… ….…….Distrene-80 Plasticizer Xylene
ECM…….……..……Extracellular Matrix
EDC…….……...……1-Ethyl-3-(3-Dimethylaminopropyl) Carbodiimide
ES……Embryonic Stem Cells
FBS…….…….. Fetal Bovine Serum
FD…….……...…….……Freeze Drying
FDA……Food and Drug Administration
FEG……..…….....Field Emission Gun
FGF…….. ……..……Fibroblastic Growth Factors
FTIR…….…..... Fourier Transform Infrared Spectroscopy
GAGs……... Glycosaminoglycans
GFs……...……...Growth Factors
GTA……...Glutaraldehyde Crosslinking
H&E……. Hematoxylin and Eosin
HAp……...…… Hydroxyapatite
hBMMSCs …… ……..Human Bone Marrow Mesenchymal Stem Cells
HCL…….……. Hydrochloric Acid
IGF…….…..…Insulin-like Growth Factors
IHC……....…Immunohistochemistry
IMS ……..…Industrial Methylated Spirit
IR …….....Infrared
LVR……...…Linear Viscoelastic Region
M-CSF…….Macrophage Colony-Stimulating Factor
MSCs…….…..…… Mesenchymal Stem Cells
NCPs……Non-Ccollagenous Proteins
NHS……..…… N-hydroxy Succinimide
OA…….……..……...Osteoarthritis
OC…….…Overall changes in size

OSX……...…… Osterix
PBS……...……...Phosphate Buffered Saline
PDGF……...….Platelet-derived Growth Factor
PF.....Paraformaldehyde
PG .....…….….Proteoglycan
PTFE ……..……..…… Polytetrafluoroethylene
RANK Ligand……...……...Receptor Activator of Nuclear Factor κ B
RGD ..…….……..…….Arg-Gly-Asp
RUNX2…….…... Runt-related Transcription Factor 2
SBF……...….Simulated Body Fluids
SD……...…….Standard Deviation
SEM……..…...….Scanning Electron Microscopy
TBS…….…...……... Tris Buffered Saline
TCP……...……...Tricalcium Phosphate
TE…….……...…...….Tissue Engineering
TEM……...……..... Transmission Electron Microscopy
TGF…….……....…....Transforming Growth Factors
TKA ……...……Total Knee Arthroplasty
VEGF……Vascular Endothelial Growth Factor
α-MEM ...……...……..….Minimum Essential Medium Eagle Alpha Modification

Chapter 1.

Introduction

The failure of organs and the damage to tissues are recurrent problems facing healthcare systems. Orthopaedic reconstruction of defects originating from trauma, tumour, degeneration and an aging population form a large part of this challenge (Wu et al., 2014).

Human tissues generally consist of two parts: cells and an *extracellular matrix*. Cells are responsible for the maintenance and synthesis of the extracellular matrix (Buckwalter and Mankin, 1997a), and the matrix provides a supportive microenvironment for the cells. However, when this matrix is destroyed beyond a critical extent (critical size defect), the cells are unable to fully repair the matrix, at which point other treatment routes (e.g. surgical) must be employed. In the case of bone and cartilage, marrow stimulation techniques, arthroscopic repair and tissue grafts can postpone the need for total joint replacement; however, these treatments usually lead to formation of an inferior tissue, donor site morbidity, pain, hematoma and inflammation (Porter et al., 2009, Lynn et al., 2004a). As a potential solution, tissue engineering (TE) has been developed, wherein scaffolds are designed and fabricated to interact with cells and prompt tissue regeneration. Although the realisation of this solution has been limited, the development of novel scaffold materials, designs and fabrication methods have made TE more realistic (Bajaj et al., 2014).

Recently, biomimetic scaffolds have attracted attention among researchers as an approach to improve the biological response and mechanical fixation of scaffolds when implanted in a defect. Here, the extracellular matrix of the target tissue serves as the scaffold because it provides the physical, chemical and biological cues that influence cell function. Therefore, biomimetic scaffolds imitate important features of the extracellular matrix chemistry and architecture, even at the nanoscale (Kim et al., 2012).

A common obstacle to successful cartilage regeneration by TE is a lack of scaffold and newly formed tissue integration with the surrounding and underlying tissue. At the same time, scaffolds aiming to regenerate only bone neglect the need for formation of healthy hyaline cartilage. Therefore, the concept of the regeneration of articular cartilage and underlying bone (osteochondral defect), and the development of a well-defined tissue-to-tissue interface (Schaefer et al., 2000) have drawn considerable attention, especially as techniques for promoting superior cartilage integration and a treatment for osteochondral defects (O'Shea and Miao, 2008).

Therefore, utilising the concept of biomimetic scaffolds to regenerate an osteochondral defect was the aim of this research. A composite of collagen types I and II, which are respectively the major constituents of bone and articular cartilage, was used as the basis of the scaffolds. It was hypothesised that *the chemical gradient in scaffolds leads to microstructural and mechanical differences, which affects the behaviour of cells differently*. These layers were produced to mimic the zonal structure and interface of cartilage and bone.

It was postulated that the interactions between different constituents of the scaffolds would affect the viscosity of preparations, which in turn would influence the microstructure of the scaffolds. This assumption was based on the process of scaffold fabricating. A common method for the fabrication of three-dimensional porous scaffolds is freeze-drying aqueous or camphene-containing suspensions. The way the water or camphene freezes depends on the viscosity of the suspension, and affects the microstructure because the pores are negative replicas of the formed ice crystals. It was further assumed that these chemical interactions and pore structure elements would affect the mechanical properties of the scaffolds. Cell behaviour,

including attachment, proliferation and differentiation was thought to be moderated by these chemical, microstructural and mechanical factors.

This thesis examines the preparation of composite types I and II collagens for osteochondral TE scaffolds. It further investigates whether the hypothesis developed earlier in this chapter holds true. Since a biomimetic approach to TE is taken, a comprehensive review of the bone and cartilage biology, structure, properties and defects, as well as relevant literature in the area of TE is presented in Chapter 2. The main experimental objectives and hypotheses of this research were:

Chapter 3

Objectives: To synthesise composite preparations from monomeric collagen extractions (type I and II) incorporating hydroxyapatite or chondroitin sulphate to fabricate porous three-dimensional scaffolds.

Chapter 4

Objectives: To characterise the fabricated scaffolds using *Fourier Transform Infrared Spectroscopy* to develop an understanding of their properties and behaviours at the molecular level.

Hypothesis: It is hypothesized that the synthesis of composite scaffolds in Chapter 3 has led to interactions between chondroitin sulfate/hydroxyapatite and different types of collagen (I and II) at molecular levels.

Chapter 5

Objectives: To study the rheological properties of preparations using a *rheometer*, and to understand the behaviour of suspensions at the molecular level before freeze-drying (Chapter 5).

Hypothesis: It is hypothesized that the molecular interactions between different constituents of scaffolds examined in Chapter 4, leads to differences in viscosity of suspensions and their rheological properties, which can in turn affect their microstructure (Chapter 6).

Chapter 6

Objectives: To evaluate the microstructure, including pore structures, pore sizes and shapes of different scaffold types using *Scanning Electron Microscopy* (Chapter 6).

Hypothesis: It is hypothesized that the differences in viscosity of preparations shown in Chapter 5 affects scaffolds microstructures.

Chapter 7

Objectives: To use *Compression Testing* and assess the mechanical properties of fabricated scaffolds to examine their suitability for implantation (Chapter 7).

Hypothesis: It is hypothesized that differences in molecular (Chapter 4 and 5) and microstructures (Chapter 6) of composite scaffolds affect their compressive modulus.

Chapter 8

Objectives: To determine the biological response to scaffolds, and test whether the scaffolds alone would provide cues for *Mesenchymal Stem Cells* to guide them towards a specific lineage (Chapter 8).

Hypothesis: It is hypothesized that the chemical/molecular composition (Chapter 4 and 5), scaffold microstructures (Chapter 6) and mechanical properties (Chapter 7) affect cellular response, in terms of proliferation and differentiation.

An overall summary and key conclusions of the work in this thesis are presented in Chapter 9 and suggestions for further work are given in Chapter 10.

Chapter 2.

Literature Review

2.1 Introduction

Tissue engineering is concerned with regenerating damaged tissues using appropriate combinations of scaffolds, cells and growth factors. This thesis endeavours to develop and characterise collagen composite scaffolds for bone and cartilage repair (osteochondral). As explained in Chapter 1 to design the ideal biomimetic scaffold, a full understanding of the compositions, structures, biomechanical and biochemical properties of the natural tissue is required. Thus, this chapter presents the literature background for the study. The first two sections describe the structure, composition and biomechanical properties of cartilage and bone, followed by a description of the interface between these two tissues and an outline of their possible defects and the current surgical treatments. The principles of TE, especially osteochondral TE, are then examined with a focus on scaffold materials and a brief description of fabrication techniques. The final section explains the cell–scaffold interaction, and the chapter concludes with a description of the aims of the thesis.

2.2 Biology, anatomy and properties of cartilage

Controlled motion between bones is made possible by the functional connections of synovial joints. The articulating bone ends are covered with cartilage 0.1–5 mm thick, depending on species, age and the location of the joint (Athanasiou et al., 1991). Cartilage is an avascular connective tissue with high compressive, tensile and shear strengths.

2.2.1 Composition

Cartilage consists of chondrocytes, which are cartilage-specific cells, embedded in an extracellular matrix (ECM). This matrix mainly comprises collagen, proteoglycans and non-collagenous proteins. The composition of articular cartilage is shown in Figure 2.1.

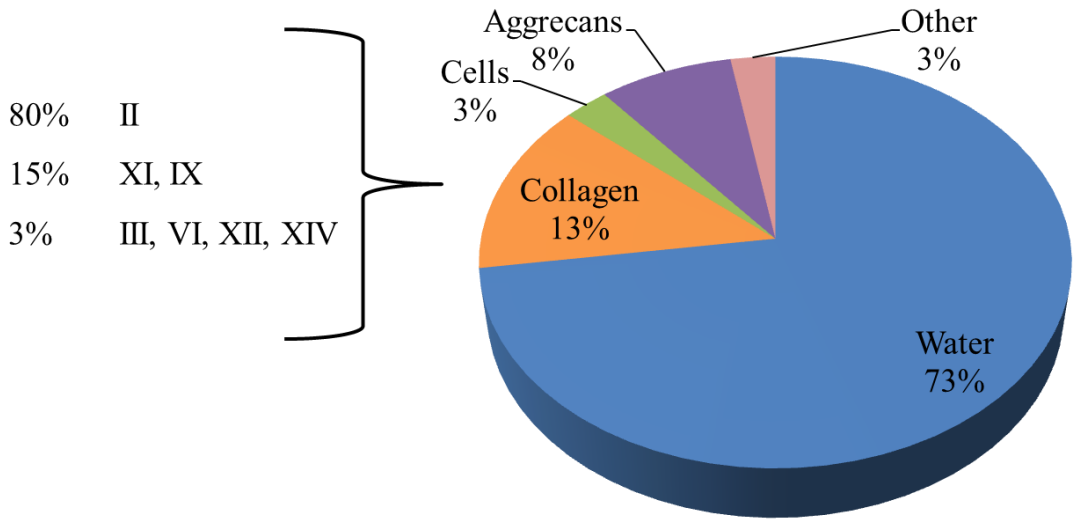


Figure 2.1 Composition of articular cartilage, redrawn from (Aigner and Stove, 2003)

Articular cartilage functions via its ECM, and not cells, to provide mechanical stability. Therefore, while in parenchymal organs (e.g. liver), more than 95% of the tissue volume consists of the cells, in connective tissues, more than 95% of the volume consists of the functional

element, ECM. The cells are responsible for the maintenance of the ECM by an appropriate anabolic activity, which leads to a balanced matrix turnover needed for the integrity of the ECM (Aigner and Stove, 2003).

2.2.1.1 Cells

Chondrocytes originate from mesenchymal stem cells (MSCs). During embryogenesis, the MSCs differentiate to chondrocytes and produce a cartilaginous matrix (Buckwalter and Mankin, 1997a, Yang and Temenoff, 2009). *In vitro*, micromass pelleting and addition of dexamethasone and transforming growth factor–β3 to cell are usually used to differentiate MSCs to chondrocytes (Mackay et al., 1998). Chondrocytes differ according to their function, size and shape based on their position and the cartilage tissue age (see Section 2.2.2) as outlined below.

Chondrocytes

- **Amount:** 1–10% of dry weight of cartilage (Yang and Temenoff, 2009)
- Chondrocytes of different zones differ in shape, size and metabolic activity (Buckwalter and Mankin, 1997a):
    - **Superficial zone:** inactive and elongated
    - **Middle zone:** higher concentrations of synthetic organelles, endoplasmic reticulum and Golgi membranes (Buckwalter and Mankin, 1997a)
    - **Deep zone:** show synthetic activity 10 times greater than the superficial zone (Temenoff and Mikos, 2000b)
    - **Calcified zone:** smaller, with almost no reticulum and very low metabolic activity (Temenoff and Mikos, 2000b)
- **Function:** matrix synthesis; maintains ECM integrity by replacing the degraded matrix component
- **Change with age:** their ability to synthesise some type of proteoglycans and their response to stimuli, including growth factors decrease (Buckwalter and Mankin, 1997a)

2.2.1.2 Extracellular matrix (ECM)

Cartilage ECM comprises collagen, proteoglycans and non-collagenous proteins. Collagen is a natural polymer that characterises the matrix of bone, teeth and connective tissues and can be extracted from animal or human sources (Wahl and Czernuszka, 2006). Articular cartilage has collagen type II as its main type, with a core of collagen type XI and a surface of collagen type IX (Myllyharju and Kivirikko, 2001) (Figure 2.2).

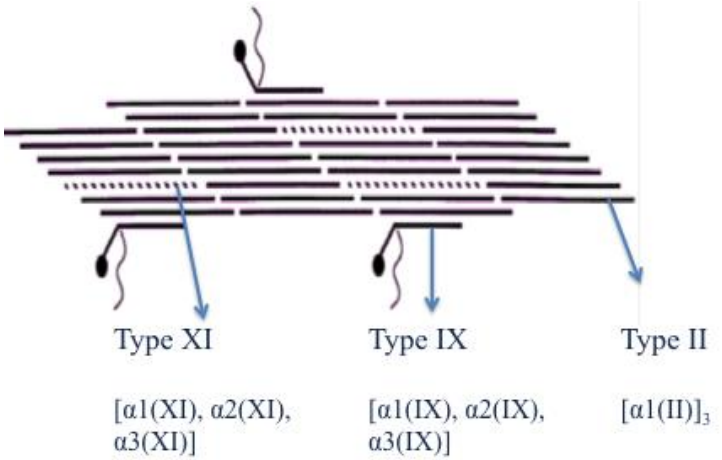


Figure 2.2 Organisation of different collagen types in articular cartilage (Cremer et al., 1998)

The function of cartilage collagen and changes with position and age are summarised below:

Collagen

Amount: 60% of dry weight of cartilage (Buckwalter and Mankin, 1997a), of which 90–95% is collagen type II (Newman, 1998)

Types: Collagen types in cartilage ECM:

- **Type II:** Fibrils of type II are aggregates of tropocollagen molecules, each having an axial periodicity 640–690 Å (Roth and Mow, 1980) . The diameter of microfibres in articular cartilage varies with age, species and depth from 10 to over 100 nm (Lane and Weiss, 1975)
- **Type VI**: Immediate surroundings of chondrocytes
  - → Help them to attach to the matrix (Buckwalter and Mankin, 1998)
- **Type IX:** On the surface of type II fibrils (Eyre, 2002)
- **Type X:** Near calcified zone
  - → Role in mineralisation
  - → Synthesised by terminally differentiating chondrocytes, (i.e. those undergoing hypertrophy) (Morrison et al., 1996)
- **Type XI:** Resembles type II in structure (uninterrupted helices by N-C domains); XI has an extractable α3 (XI) N-propeptide which projects from the fibril (Cremer et al., 1998)

Changes with position: Changes in collagen fibril diameter and orientation according to distance from joint surface (■) and cells (○)

- **Superficial zone:** Fine and parallel to the joint surface
- **Middle zone:** Diameters of fibrils increase, their amount decrease and they are no longer parallel to the joint
- **Deep zone:** Fibrils are thickest, perpendicular to the surface
  - **Pericellular:** Concentration of collagen is very low
  - **Interterritorial:** Highest volume of collagen

Changes with age: Fine fibrils of cartilage (>10% IX, >10%XI, <80% II) transform to the thicker and more varied fibril diameters (~1% IX, ~3%XI, >90%II) (Eyre, 2002). Rates of collagen types II and IX (regulates the size of fibrils) synthesis also decrease with age

Function:

- Collagen gives ECM its tensile strength and stiffness (Martin and Buckwalter, 1996)
- Increases network mechanical integrity
- Provides a restraint for entrapped proteoglycan osmotic swelling pressure (Eyre, 2002)
- Controls the fibrillar diameter (Morrison et al., 1996)
- Type IX acts as a 'spacer' between individual fibrils, 'glue' to bind the type II lattice work and helps interaction of collagen fibrils with proteoglycans (Cremer et al., 1998)

The proteoglycan (PG) monomers comprise a protein core that has multiple sulphated glycosaminoglycans (GAGs), which are long, unbranched polysaccharides (e.g. chondroitin sulfate and keratin sulfate chains) attached to it (see Figure 2.3)(Lynn et al., 2010). The GAGs are negatively charged; therefore, they attract cations and are hydrophilic. Moreover, the negative charges repel each other and keep the molecules in a distended state, which is beneficial to the compression modulus of the tissue (Newman, 1998).

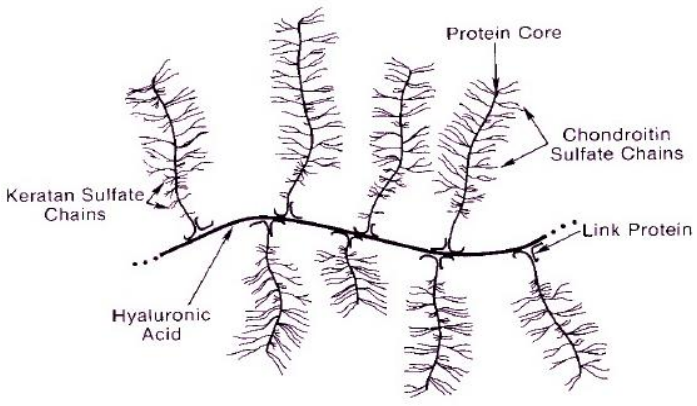


Figure 2.3 Schematic sketch of a proteoglycan monomer (Newman, 1998)

The types, functions and changes of proteoglycan content according to position and age of the tissue are summarised below.

Proteoglycans

Amount: 25–35% of dry weight (Buckwalter and Mankin, 1997a), 95% of which is polysaccharide and 5% proteins (Temenoff and Mikos, 2000b)

Types

- **Aggregating:** Hyaluronic acid, chondroitin sulphate (CS), keratan sulphate, dermatan sulphate (Buckwalter and Mankin, 1997a)
- **Non-aggregating:** decorin, biglycan, fibromodulin

Changes with location

- **Superficial zone:** Lowest concentration
- **Middle zone:** Higher concentration
- **Deep zone:** Highest concentration
  - **Pericellular:** High concentration

Changes with age:

- Decorin and fibromodulin expression increases with age; *in vivo* they are likely to increase fibre diameter
- Biglycan decreases with age (Martin and Buckwalter, 1996)

Function:

- Cell function and organisation of matrix (Pieper et al., 1999):
  - → Binding and modulation of growth factors and cytokines
  - → Inhibition of proteases
  - → Involvement in adhesion, migration, proliferation and differentiation of cells (Pieper et al., 1999, Jackson et al., 1991)
- Mechanical properties of tissue (Temenoff and Mikos, 2000b)

Water (as outlined below) and other fluid containing gases, metabolites and a large amount of cations comprise 60–70% of collagen wet weight to balance the negatively charged proteoglycans in ECM (Temenoff and Mikos, 2000b, Newman, 1998).

Water and tissue fluid

Amount: 60–80% of wet weight (Newman, 1998)

Changes with position:

- **Superficial zone:** Highest concentration
- **Middle zone:** Lower concentration
- **Deep zone:** Lowest concentration

Changes with age: Slight decrease in water concentration with age (Martin and Buckwalter, 1996)

Function: Protection of solid phase under mechanical stresses (Newman, 1998); provision of nutrients and oxygen (Temenoff and Mikos, 2000b)

Non-collagenous proteins (NCPs) comprise a core protein with a few attached monosaccharides and oligosaccharides (Buckwalter and Mankin, 1997a, Temenoff and Mikos, 2000b), including anchorin, fibronectin and tenascin. The proteins promote cell adhesion to the ECM and aid to transmit mechanical forces to the cells as they bind to both the matrix protein and cell receptors (integrin)(Martin and Buckwalter, 1996). The functions, types and changes with tissue age are summarised below.

NCPs

Amount: 10–20% of dry weight (Buckwalter and Mankin, 1997a)

Types: Anchorin CII (collagen-binding chondrocytes surface protein), cartilage oligomeric protein (acidic protein concentrated in territorial region), fibronectin and tenascin (Buckwalter and Mankin, 1997a, Temenoff and Mikos, 2000b)

Changes with age: Fibronectin accumulates in cartilage with age

Function: Stabilise the ECM and aid in chondrocytes–matrix interactions

2.2.2 Structure

The structure and composition of cartilage is organised on two levels, which are determined according to the distance of the cartilage from the surface and in relation to its distance from the cells.

Typically, articular cartilage is divided into four zones based on the distance from the surface: *superficial*, *middle*, *deep* and *calcified zones* (Newman, 1998) (Figure 2.4). The latter is directly below the deep zone, containing hypertrophic chondrocytes embedded in a densely mineralised matrix, which constitutes the osteochondral interface (Lu et al., 2010). The ECM content (collagen and proteoglycans) and chondrocytes' shapes and activities differ in each zone, which is summarised in Table 2.1.

Table 2.1 Structure of articular cartilage according to distance from joint surface

Zone	Description	Collagen content	Proteoglycans content	Chondrocytes shape/activity
Superficial	Thinnest zone (Buckwalter and Mankin, 1997a)	Thin collagen fibrils parallel to the joint surface(Newman, 1998)	-	Inactive and elongated (Newman, 1998)
Middle	Thicker than superficial zone	Thicker collagen fibrils, not parallel (Newman, 1998), lower concentration	Higher concentration (Buckwalter and Mankin, 1997a)	Spherical, higher concentrations of synthetic organelles and Golgi membranes (Newman, 1998)
Deep		Thick fibrils, perpendicular to joint surface (Newman, 1998)	Highest concentration of proteoglycans(Buckwalter and Mankin, 1997a)	Spherical, arranged in columns, high synthetic activity (Temenoff and Mikos, 2000b)
Calcified		Collagen fibrils insert into the calcified cartilage- transition from cartilage to bone (Newman, 1998)	-	Smaller with almost no reticulum, very low metabolic activity (Temenoff and Mikos, 2000b)

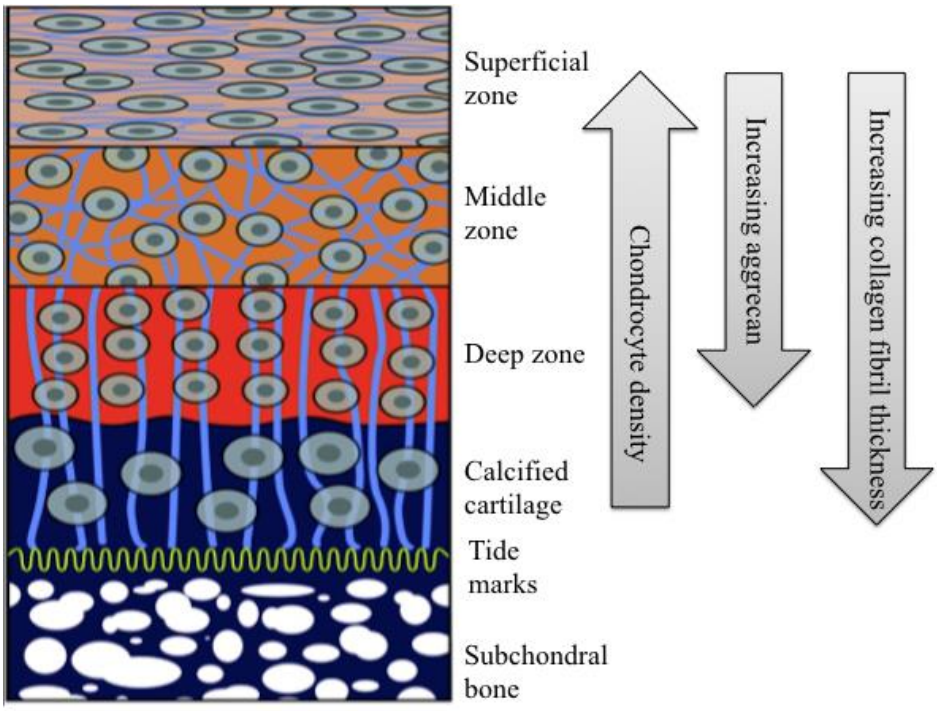


Figure 2.4 Structure of articular cartilage according to the distance of its elements from the joint surface- tidemark denotes a discrete band between mineralized and non-mineralized cartilage (Madry et al., 2010); adapted from (Yang and Temenoff, 2009)

According to its distance from the cells, the articular cartilage can be divided into three regions: *pericellular*, *territorial* and *interterritorial matrix* (see Table 2.2).

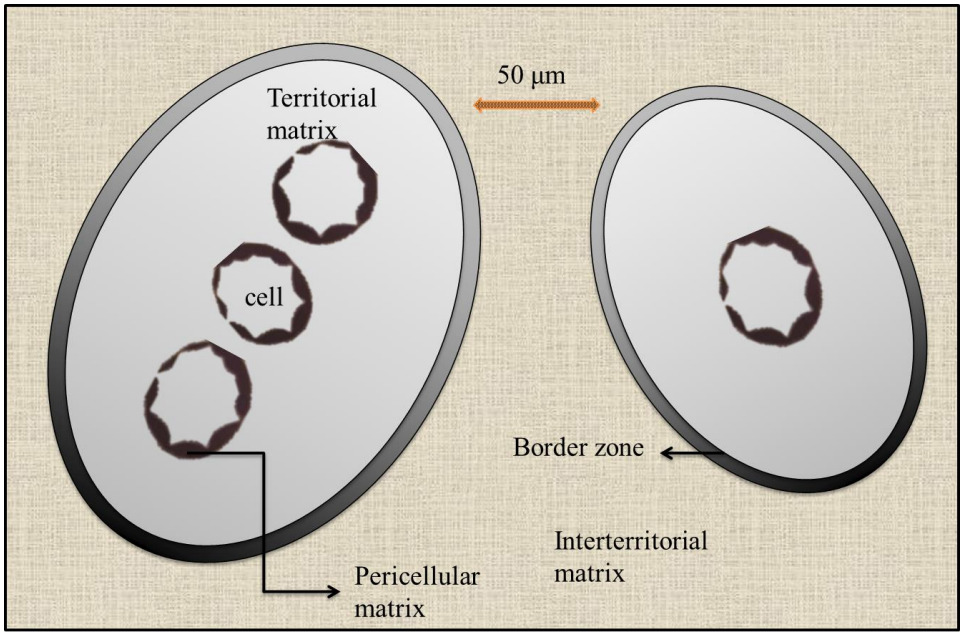


Figure 2.5 Structure of articular cartilage according to its distance from the cells, adapted from (Stockwell, 1979)

The pericellular matrix is the zone immediately around the chondrocytes. The territorial matrix is just outside the pericellular region, and the interterritorial matrix is further away from the cell, which is the largest portion of articular cartilage (Figure 2.5).

Table 2.2 Structure of cartilage according to distance from chondrocytes

Zone	Description	Collagen	Proteoglycans	NC proteins
Pericellular	Immediately around chondrocytes (Newman, 1998)	Very low collagen content (Buckwalter and Mankin, 1997a)	High content (Buckwalter and Mankin, 1997a)	Anchorin CII and non-fibrillar collagen type VI
Territorial	Just outside the pericellular region	Cells and their surroundings are enclosed by thin collagen fibrils (Buckwalter and Mankin, 1997a, Newman, 1998)		
Interterritorial	Farther away from cells; largest portion of articular cartilage (Newman, 1998)	Collagen fibrils are aligned according to their distance from the joint surface (Newman, 1998)		

2.2.3 Mechanical properties

The mechanical function of articular cartilage is to minimise the contact stresses and friction between two sliding bones; this depends on the load distribution in the articular cartilage matrix, which is affected by the mechanical properties of the matrix. Any changes in the matrix (see Section 2.5) can interfere with load transmission and lead to higher contact stresses that are more likely to surpass the tensile strength limits (5–25 MPa)(Martin and Buckwalter, 1996).

The mechanical properties are determined by a number of factors (Roth and Mow, 1980), including the electrostatic interaction and physical entanglement of the major constituents of cartilage (collagen, proteoglycans and interstitial fluid (Mansour, 2003)). The tensile and compressive strength of the matrix originate in the interaction of the collagen network with the proteoglycans. The collagen network hinders the expansion of the proteoglycans, which then attempt to spread out due to mutual repulsion of negative charges (Mansour, 2003). Moreover, the aggrecan-hyaluronan aggregates bind large amounts of intercellular water because of their extensive fixed charges, and are responsible for the elasticity of the tissue. Therefore, the cartilage matrix is compliant under compression but rapidly recovers as water molecules are drawn back into the matrix upon unloading by the strongly hydrophilic aggrecan aggregates (Aigner and Stove, 2003). The native cartilage has an equilibrium compressive modulus of 0.79 MPa (Lu et al., 2000, Armstrong and Mow, 1982), a shear modulus of 0.68 MPa and a tensile modulus of 0.3–10.2 MPa (Lu et al., 2000, Akizuki et al., 1986).

Articular cartilage exhibits biphasic viscoelastic behaviour (Fox et al., 2009) due to flow-independent (intermolecular friction) and flow-dependent (interstitial fluid) mechanisms (Stolz et al., 2004, Mow et al., 1984).

2.2.3.1 Compression

In compression, biphasic behaviour is the dominant mechanism for deformation (Mow et al., 1984). Elastic modulus of articular cartilage matrix can be obtained by dynamic (indentation) (Stolz et al., 2004) or static (confined compression or indentation) (Athanasiou et al., 1991, Hori and Mockros, 1976, Kempson et al., 1971, Hayes and Mockros, 1971, McCutchen, 1962) methods and the values of the obtained properties can vary according to the measurement methods used. Table 2.3 summarises these values for different species according to the measurement method used.

The compressive equilibrium modulus of cartilage decreases with age (Armstrong and Mow, 1982). The compressive stiffness of cartilage is related to the GAG content of native cartilage (CS and keratan sulphate)(Athanasiou et al., 1991, Kempson et al., 1970) and increases as a function of total GAGs, with keratan sulphate having a greater influence on stiffness than does CS (Kempson et al., 1970). Moreover, the compressive modulus decreases with increasing water content; however, no correlation (Mansour, 2003) or a less significant one (Kempson et al., 1970) is observed between collagen content of the tissue and its compressive stiffness, although the significance level was not mentioned in those studies and the linear fit was not presented.

Table 2.3 Mechanical properties under compression using different methods in different species
Note: E=2 G(1+ ν), E short-time>E equilibrium→ 5-11 MPa vs. 0.5–0.7 MPa

Species	Elastic Modulus (MPa)	Shear Modulus (MPa)	Bulk Modulus (MPa)	Poisson's Ratio	Method	Ref.
Human	0.53–0.701			0–0.098	Equilibrium creep indentation	(Athanasiou et al., 1991)
	0.13–1.91 Average: 0.79				Equilibrium confined compression	(Armstrong and Mow, 1982)
	5.06	1.72	31.5	0.47	Short-time confined compression	(Hori and Mockros, 1976)
	8.14–10.15				Short-time (2s) creep indentation	(Kempson et al., 1971)
	11.63	4.1	25	0.42	Short-time (1s) creep indentation	(Hayes and Mockros, 1971)
Bovine	11.1				Short-time between glass plates	(McCutchen, 1962)
	0.58				Equilibrium compression between glass plates	
Canine	0.47–0.89			0.245–0.396	Equilibrium creep indentation	(Athanasiou et al., 1991)
	0.555–0.904			0.093–0.372	Equilibrium creep indentation	(Athanasiou et al., 1991)
Porcine	2.6				Dynamic loading	(Stolz et al., 2004)

2.2.3.2 Tensile

Tensile properties of cartilage are inhomogeneous, anisotropic and age-dependent (Roth and Mow, 1980, Mansour, 2003). At a slow rate of deformation, the collagen network is responsible for tensile strength and stiffness. At higher rates, interaction of the collagen and proteoglycans is more prominent, as proteoglycans restrain the rotation of collagen fibres when tissue is loaded rapidly (Mansour, 2003).

In skeletally mature animals and humans, the tensile strength and stiffness of articular cartilage decreases as the distance from the joint surface increases (Mansour, 2003, Roth and Mow, 1980, Kempson et al., 1973); moreover, low weight-bearing areas have higher tensile moduli than high weight-bearing areas (Akizuki et al., 1986). Tensile strength and stiffness are higher when the tension axis is parallel than when it is perpendicular to the surface cleavage pattern (Table 2.4 and Figure 2.6). This directional dependency of tensile properties diminishes with increasing distance from the articular surface (Roth and Mow, 1980). Using the aggregate modulus values and Poisson's ratio value, Young's modulus is determined as 0.45–0.8 MPa (Mansour, 2003).

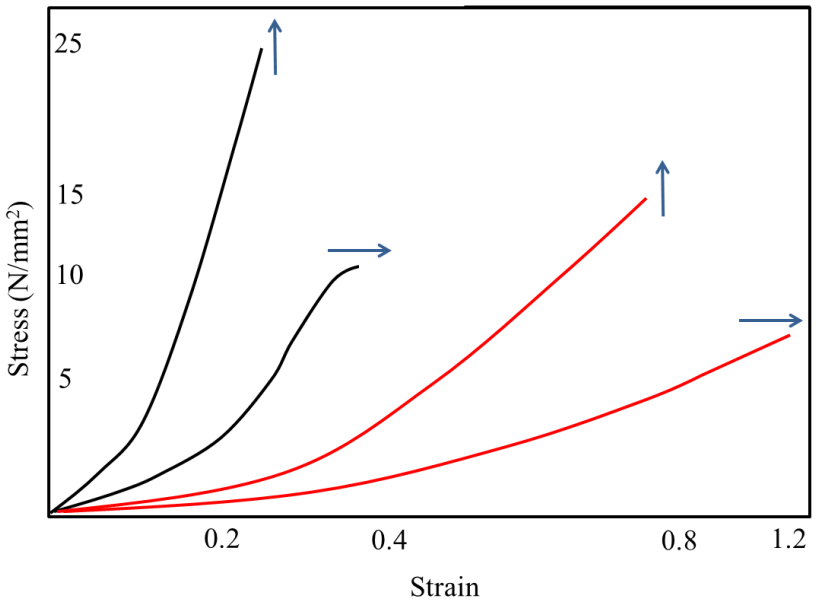


Figure 2.6 Schematic stress-strain curves for samples of human femoral condyle. Vertical arrows (↑) show the stress parallel to surface cleavage and horizontal arrows (→) show the stress perpendicular to surface cleavage. Black lines illustrate the surface of articular cartilage and red lines the deep layer. As seen, surface of articular cartilage has higher tensile strength than deep layer; redrawn from (Kempson et al., 1973)

The tensile stiffness and strength of human cartilage decrease with increasing age; that is, after maturation, the tensile strength properties of the middle and deep zones decrease while those of the superficial zone remain unchanged (Roth and Mow, 1980). Tensile strength and stiffness increase with the increasing collagen content of cartilage, while they are not significantly affected by the amount of GAGs (Kempson et al., 1973).

Table 2.4 Tensile properties of articular cartilage (Roth and Mow, 1980, Akizuki et al., 1986, Kempson et al., 1973); S=Surface, D=Deep

Tensile properties	**Human (Kempson et al., 1973)**				**Bovine (Roth and Mow, 1980)**			
	Parallel		*Perpendicular*		*Parallel*		*Perpendicular*	
	S	*D*	*S*	*D*	*S*	*D*	*S*	*D*
Failure strength (MPa)	25	15	10	5	8	5	5	2.5
Fracture strain (%)	25	85	40	120	30	100	50	115

Tensile modulus (MPa)(Akizuki et al., 1986)	**Human**	**Lateral patella groove**		**Medial femoral condyle**	
		High weight-bearing area	*Low weight-bearing area*	*High weight-bearing area*	*Low weight-bearing area*
	Superficial zone	6.22	20.67	4.98	10.13
	Subsurface	3.4	8.77	3.76	5.94
	Middle zone	3.12	4.14	3.10	4.54
	Middle-deep zone	0.93	1.01	-	-

2.2.4 Healing behaviour

Articular cartilage cannot repair itself (Newman, 1998, Ohno et al., 2004, Pieper et al., 2002). The response of articular cartilage to injury is different from the classic one (as observed in bone) since the tissue is avascular and the second and third phases of the healing process (inflammatory and remodelling) are affected by the vascular system. Moreover, the chondrocytes are surrounded by the ECM, which keeps them from migrating to the injury site from the healthy adjacent tissue (Newman, 1998, Ohno et al., 2004). This is the case if the injury is partial-thickness, where the damage is superficial; however, if the injury penetrates the subchondral bone plate, where there is access to vascular bone, the healing process is more similar to the classic one. Although this first produces a hyaline cartilage (Figure 2.7), the matrix

and cells become more typical of fibrocartilage with inferior mechanical properties later in the process (Newman, 1998, Yaszemski et al., 1996).

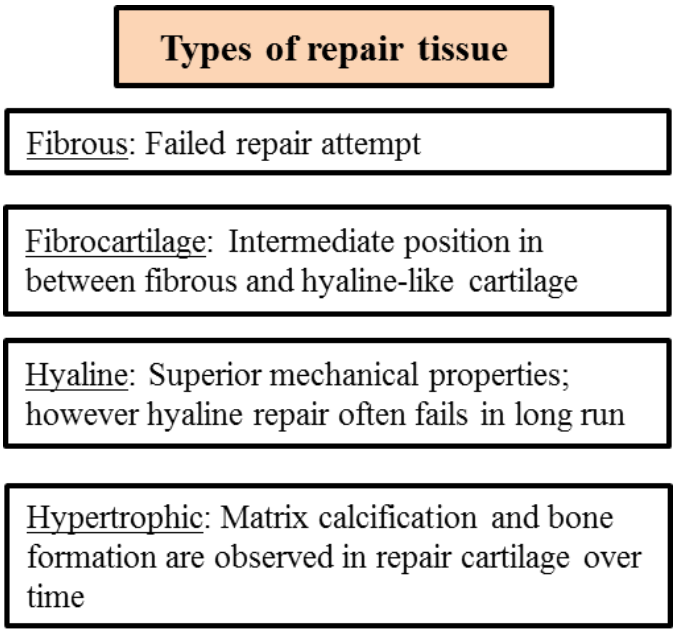


Figure 2.7 Types of repair tissue, from (Aigner and Stove, 2003)

2.3 Biology, anatomy and properties of bone

Bone plays vital roles in the maintenance of body systems, providing protection for critical organs and sites of attachment for the muscles. Bones play mechanical roles by supporting homeostasis and the body tissues (Yaszemski et al., 1996, Sikavitsas et al., 2001) and through the generation of white and red blood cells, oxygenation/nutrition of other tissues, regulation of blood pH, accommodation of progenitor cells (mesenchymal, haemopoetic), and mineral storage of calcium, phosphate and other important ions (Sikavitsas et al., 2001, Yaszemski et al., 1996, Porter et al., 2009).

2.3.1 Composition

Bone consists of cells and ECM. By weight, bone composition is 60% mineral, 10% water and about 30% collagenous matrices (Athanasiou et al., 2000)(Figure 2.8).

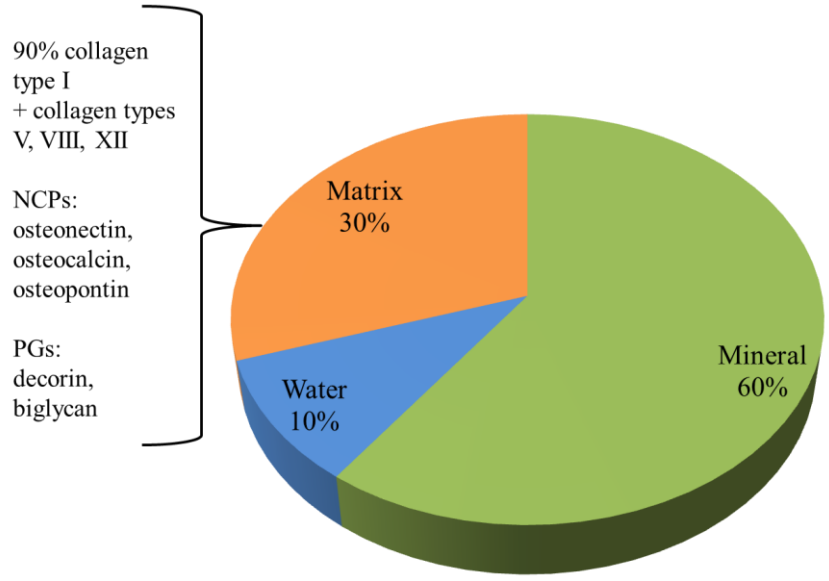


Figure 2.8 Bone matrix components by weight %

2.3.1.1 Cells

Four types of cells are present in bone: osteoblasts, osteoclasts, osteocytes and bone lining cells. Bone is constantly remodelled, with osteoblasts producing and mineralising the matrix, osteocytes maintaining and osteoclasts resorbing the matrix (Karageorgiou and Kaplan, 2005). This process of production and resorption of bone matrix by osteoblasts and osteoclasts plays several important roles in bone physiology, such as bone remodelling. Osteoblasts are originated from MSCs. In order for MSCs to commit towards the osteoprogenitor lineage, specific proteins and transcription factors such bone morphogenetic proteins (BMPs), Runt-related transcription factors (e.g. RUNX2) and osterix (OSX) must be expressed. Once there is a pool of these osteoprogenitor cells expressing RUNX2 and COL1A1, the progenitors show alkaline phosphatase (ALP) activity and are considered pre-osteoblasts. These cells then progress towards mature osteoblasts, shown by an increase in expression of OSX and matrix proteins such as osteocalcin. Osteocytes are stemmed from MSCs through osteoblast differentiation in a four-step process: osteoid-osteocyte, pre-osteocyte, young osteocyte, and mature osteocyte formation. At the end of a bone formation sequence, a subpopulation of osteoblasts becomes osteocytes. Osteoclasts originate from mononuclear cells of the hematopoietic stem cell under the influence of several factors, including macrophage colony-stimulating factor (M-CSF) and RANK ligand, which promote activation of transcription factor and gene expression in osteoclasts (Florencio-Silva et al., 2015).

A summary of cell origin, function and fate in bone are outlined below (Porter et al., 2009):

Osteoblasts

Origin:
Differentiated from MSCs
Function:
- Produce organic and inorganic bone ECM (osteoid)
- Regulate osteoclast activities

Fate:
- Become embedded in their own bone matrix and become osteocytes *or*
- Experience apoptosis (programmed cell death)

Osteocytes

Function:
Key role in mechanotransduction

Fate:
Remain trapped within the matrix and eventually stop generating osteoid

Osteoclasts

Origin:
Multinucleated cells derived from fusion of mononuclear haemopoetic precursors

Function:
Produce acids and proteolytic enzymes, which erode bone ECM

2.3.1.2 ECM

The ECM is a composite of organic (30% (Porter et al., 2009)) and inorganic components. The primary organic component is collagen I (Porter et al., 2009, Athanasiou et al., 2000, Lawson and Czernuszka, 1998) but it also includes collagen types V, VIII, XII, PGs, NCPs (osteocalcin, osteopontin, etc.) bone sialoprotein, thrombospondin and bone growth factors. The main inorganic component is hydroxyapatite, which is a member of the calcium-phosphate family (Athanasiou et al., 2000).

2.3.1.2.1 Collagen

The organic portion of the matrix is mainly collagen type I (90% (Porter et al., 2009)) in the form of microfibres with diameters varying 100–2000 nm (Suchanek and Yoshimura, 1998). The organisation and functions of collagen in bone are summarised below:

Collagen in Bone

Organisation (Lawson and Czernuszka, 1998):

- **Woven bone:** Mineralised collagen fibres express little preferred orientation
- **Lamellar bone:** More ordered, with collagen fibrils' individual lamellae oriented in roughly the same direction, but in adjacent lamellae they are arranged at right angles
- **Parallel-fibred bone:** Parallel arrays of mineralised collagen fibrils, the axes of which are aligned with the bone's long axis

Function: Responsible for tensile properties of bone; contain peptides, which cue bone cells and provide sites for binding of calcium compounds (Porter et al., 2009)

2.3.1.2.2 NCPs and PGs

The NCPs in bone, including osteonectin, osteopontin and osteocalcin, regulate mineral nucleation and deposition and cell migration in the tissue, as outlined below. These NCPs are routinely used as biomarkers for osteoblastic phenotypic behaviour (Porter et al., 2009).

Osteonectin

- Potential nucleator of HAp
- Multiple Ca2+ and collagen binding sites

Osteocalcin

- Role in osteoclast migration
- Ca2+ /HAp affinity
- Biomarkers for mature osteoblast phenotype

Osteopontin

- Cell migration, and regulation of mineral deposition; interfacial adhesion molecule that maintains overall structural integrity of bone
- Biomarker for mature osteoblast phenotype
- Multi-functional extracellular glycoprotein (Porter et al., 2009)

Bone matrix also contains PGs, decorin and biglycan, which influence cell behaviour by blocking adhesion motifs from RGD-containing molecules and binding TGF-b (Porter et al., 2009).

2.3.1.2.3 Hydroxyapatite

The mineral phase of ECM involves a specific calcium-phosphate mineral called hydroxyapatite (HAp), $Ca_{10}(PO_4)_6(OH)_2$ (Porter et al., 2009), with a Ca:P ratio of 1.67. However, this ratio in bone minerals actually ranges 1.37–1.87, indicating the possible existence of additional ions, such as strontium, zinc, hydrogen phosphate and hydrogen carbonate (Wu et al., 2014).

The HAp crystals are present in the form of plates or needles 40–60 nm long, 20 nm wide and 1.5–5 nm thick. They are deposited parallel to the collagen fibres, such that the larger dimension of crystals is along the long axis of the fibre (Suchanek and Yoshimura, 1998). These crystals predominantly occupy the gaps between collagen fibrils; further linking occurs between the apatite and polar groups on the chains (Lawson and Czernuszka, 1998).

2.3.2 Structure

Bone has a hierarchical structure of macro-, micro- and nanoscales (Harley et al., 2010b), as illustrated in Figure 2.9.

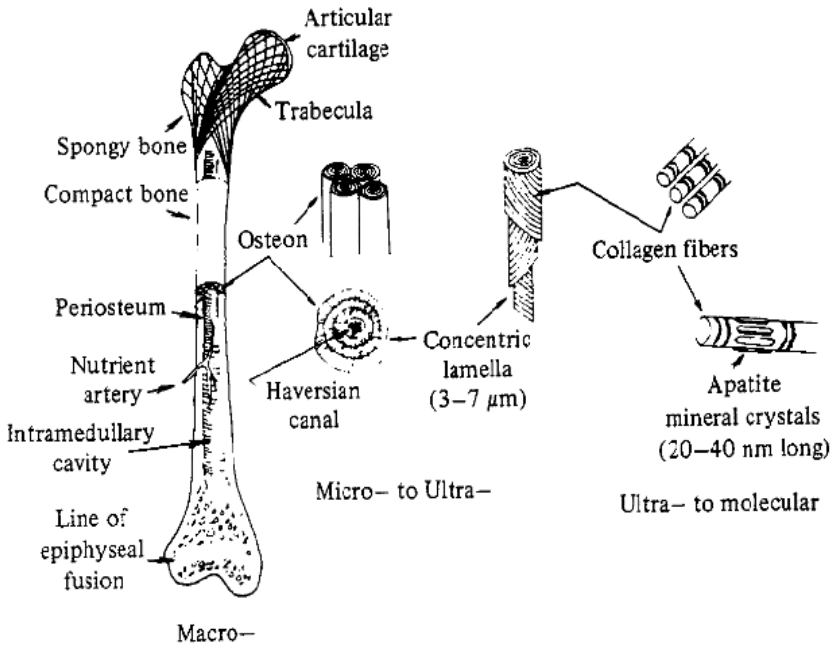


Figure 2.9 Bone hierarchical structure (Suchanek and Yoshimura, 1998)

The macro-scale organisation (of osteons, osteoids and Haversian canals) provides the mechanical anisotropy of long bones. The micro-scale porosity helps with cell migration and vascularisation, and the nanoscale characteristics play a role in cell and mineral binding architecture (Porter et al., 2009).

Mature bone comprises compact or cortical bone and cancellous or trabecular bone (Yaszemski et al., 1996, Buckwalter and Mankin, 1997b). They are different based on structure and location in the body. There is a consensus regarding these; however, whereas Yaszemski et al. (1997) points to the spatial orientations of the mineral and organic elements as one of the

differences between the two (Buckwalter and Mankin, 1997b, Yaszemski et al., 1996), Buckwalter et al. (1995) and Gibson and Ashby (1997) believe that both types have the same matrix composition and structure. The only difference, they say, is higher mass/volume and lower porosity of cortical bone (Buckwalter and Mankin, 1997b, Gibson and Ashby, 1997). The properties of cortical and trabecular bone are summarised below.

Cortical

- **Structure:**
  - Dense (Karageorgiou and Kaplan, 2005) (10% porosity (Yaszemski et al., 1996))
  - Consists of osteon (parallel cylindrical units) oriented in longitudinal direction in long bones (Pieper et al., 2002, Sikavitsas et al., 2001, Lawson and Czernuszka, 1998, Harley et al., 2010b)
- **Pore size:** Haversian canals with a cross-sectional area of 2500–12000 μm^2 (0.028–0.061 mm diameter)(Athanasiou et al., 2000)
- **Main location:**
  - Middle shaft of long bones or shells of other bones (Sikavitsas et al., 2001)
  - Outer surface of small bones and fat bones and diaphysis (Yaszemski et al., 1996)
- **Proportion:** 80% of total mass (Yaszemski et al., 1996)
- **Mechanical properties:** Anisotropic, depends on the orientation of osteons (Athanasiou et al., 2000)

Trabecular

- **Structure:**
  - Highly porous (50–90% porosity (Yaszemski et al., 1996))
  - Honeycomb structure with interconnected bone trusses (trabeculae), oriented along the principal stress directions (Yaszemski et al., 1996)
  - Properties of individual trabeculae are similar to cortical bone (Karageorgiou and Kaplan, 2005)
- **Pore size:** Approx. 1 mm in diameter (Athanasiou et al., 2000)
- **Main location:**
  - Ribs (Sikavitsas et al., 2001) and vertebral column/spine (Sikavitsas et al., 2001)
  - Near the ends of long bones
  - Interior of small bones
  - Between the surfaces of flat bones (Sikavitsas et al., 2001)
  - In metaphysis (Yaszemski et al., 1996) and epiphysis (Sikavitsas et al., 2001)
- **Proportion:** 20%(Yaszemski et al., 1996)
- **Mechanical properties:** Modulus of elasticity and ultimate compressive strength as much as 10 times less than cortical (Yaszemski et al., 1996)

As described above, cortical bone consists of osteons or Haversian systems (parallel cylindrical units about 200 μm in diameter and 10–20 mm long (Athanasiou et al., 2000)), which have a central osteonic (Haversian) canal containing blood vessels surrounded by concentric rings (lamellae, 3–7 μm thick (Athanasiou et al., 2000, Suchanek and Yoshimura, 1998)) of matrix. Osteocytes are located between the rings of matrix in spaces called lacunae. Small channels (canaliculi) extend outward from the lacunae to the Haversian canal to provide microcirculation (Athanasiou et al., 2000, Sikavitsas et al., 2001, Porter et al., 2009). In a Haversian system, cells are not found beyond 200 μm of a blood supply (and therefore oxygen) (Wahl and Czernuszka, 2006).

Trabecular bone consists of plates (trabeculae) 100–300 μm thick with spacing of 300–1500 μm between adjacent trabeculae (Athanasiou et al., 2000)), next to small cavities containing red bone marrow (Porter et al., 2009).

2.3.3 Mechanical properties

As a polymer/ceramic composite of collagen/HAp, bone exhibits high toughness and relatively high modulus (Suchanek and Yoshimura, 1998). In a typical stress-strain curve, there is an initial linear elastic region followed by a flat plastic region. Failure occurs at strains up to 3%. Bone has high toughness at low strain rates, but at high strain rates, the fracture behaviour is more like that of brittle material. The slope of the stress-strain curve (i.e. the stiffness) increases with increasing mineral content. High toughness is mostly due to the interfaces, which stop cracks after little propagation. Therefore, the main toughening mechanisms seem to be microcracks that appear in the plastic region of the stress-strain curve, crack deflection and pull out effects (Suchanek and Yoshimura, 1998).

Factors affecting the mechanical properties of bone are either compositional or organisational (Lawson and Czernuszka, 1998). Compositional factors include the degree of mineralisation and porosity, where increasing mineralisation and decreasing porosity lead to a higher stiffness and tensile/fracture strength (Lawson and Czernuszka, 1998) and lower fracture strain (Suchanek and Yoshimura, 1998).The latter includes the arrangement of the collagen fibrils (anisotropy) and the orientation and spacing of trabeculae (in cancellous bone)(Lawson and Czernuszka, 1998). In cortical bone anisotropy is primarily determined by osteonal orientation. The mechanical properties also vary within a single osteon. The hardness has been shown to increase away from the canal wall and then oscillates between different lamellae due to local differences in mineral content or the lamellar orientation (Lawson and Czernuszka, 1998).

Therefore, as discussed above, the mechanical properties of bone are highly anisotropic and dependent on porosity, mineral content, collagen fibre orientation and crosslinking, which means the mechanical properties vary with species, age, health state, bone type and position within the bone (Lawson and Czernuszka, 1998). As an example, it has been shown that the tensile strength (Suchanek and Yoshimura, 1998) and modulus of femoral cortical bone elasticity decline by approximately 2% per decade (Karageorgiou and Kaplan, 2005), which is primarily because of changes in the structural and molecular integrity of the collagen network (Athanasiou et al., 2000).

As shown in Table 2.5, Young's modulus and compressive strength increase significantly with increasing bone density (cortical vs. cancellous)(Harley et al., 2010b). For instance, strength and moduli of trabecular bone are related to the apparent density by a power law

function. The strength is related to the square of the apparent density. Its modulus can be either the square or cube of the apparent density (Porter et al., 2009, Athanasiou et al., 2000).

Table 2.5 Mechanical properties of cortical and cancellous bone

Bone type	**Cortical**		**Trabecular**
Density (g/cm^3)	1.8 (Athanasiou et al., 2000)		0.2 (Athanasiou et al., 2000)
Test direction	**Parallel**	**Normal**	**Parallel/Normal**
Tensile strength (MPa)	124–174 (Suchanek and Yoshimura, 1998) 80–150 (Roeder et al., 2008)	49 (Suchanek and Yoshimura, 1998) 50–60(Roeder et al., 2008)	10–20 (Lawson and Czernuszka, 1998) 1–6 (Roeder et al., 2008)
Yield strength (MPa)	78–151 MPa in tension, 131–224 MPa in compression (Porter et al., 2009)	51–66 MPa in tension, 106–131 MPa in compression (Porter et al., 2009)	
Compressive strength (MPa)	170–193 (Suchanek and Yoshimura, 1998)	133 (Suchanek and Yoshimura, 1998)	1–100 (no stated direction) (Suchanek and Yoshimura, 1998) 0.5–50 (Lawson and Czernuszka, 1998)
Young's modulus (GPa)	17–20 (Porter et al., 2009) 16–23 (Roeder et al., 2008)	6–13 (Porter et al., 2009, Roeder et al., 2008)	1–2 (in compression, no stated direction) (Suchanek and Yoshimura, 1998) 0.05–1 (in tension, no stated direction) (Athanasiou et al., 2000, Lawson and Czernuszka, 1998, Porter et al., 2009)
Fracture toughness K_{1c} ($MPa^{-1/2}$)	2–7 (Lawson and Czernuszka, 1998) 4–6 (Roeder et al., 2008)	2–4 (Roeder et al., 2008)	
Strain to failure (%)	0.5–4.5 (Lawson and Czernuszka, 1998)		

2.3.4 Bone healing behaviour

When bone is injured, it responds by regenerating bone tissue and remodelling the newly formed bone (Yaszemski et al., 1996) in the direction of shear and tensile stresses (Carter et al., 1998). Regeneration of fractured bone is similar in many ways to embryonic bone formation and involves three stages: inflammation, repair and remodelling (Sikavitsas et al., 2001). The first phase is the shortest. It begins with blood clot formation, which releases signals for phagocytic cells to remove cellular debris from the wound site. The repair process begins when proliferating osteoblasts from the periosteum around the fracture start to cover the blood clot. MSCs migrate to the fracture area and differentiate into osteoblasts if the fracture is mechanically stable. If the fracture is unstable, the MSCs differentiate into chondrocytes that secrete collagen (fracture callus) to act as a temporary bridge. This is then substituted by woven bone via endochondral bone formation. Woven bone is then gradually resorbed and replaced with lamellar bone during remodelling (Sikavitsas et al., 2001).

2.4 Cartilage-bone interface

The osteochondral interface is a tissue-to-tissue interface that acts as a boundary between where the avascular, non-mineralised articular cartilage and vascular, calcified bone meet to form a smooth, stable interface (Lu et al., 2010) with a tidemark of a 2–5-μm basophilic band (Harley et al., 2010a).

As described in 2.2.2, articular cartilage is divided into three regions, namely surface, middle and deep zones. Directly below the deep zone is the calcified cartilage region containing hypertrophic chondrocytes in a highly mineralised matrix. This matrix comprises the osteochondral interface (Lu et al., 2010), a highly complex structure due to its physical, chemical and biological variations, which are a function of the distance from the articulating surface to the subchondral bone (Erisken et al., 2010). However, the transition between cartilage and bone, called a 'soft' interface, is continuous.

Compositionally, calcium phosphate content gradually decreases from the levels found in the subchondral bone plate (75 wt %) across a zone of calcified cartilage to zero in articular cartilage. Over this same transition, type II collagen content significantly increases from zero in the subchondral bone to the levels found in cartilage (Harley et al., 2010a).

The collagen fibrils are arranged vertical to the interface in the calcified cartilage region while they are parallel to it in the regions close to the surface. Similarly, the chondrocytes are organised parallel to the interface at the surface and vertical to it at the calcified region. The calcium particles, rather, are aligned perpendicular to the interface in calcified cartilage and parallel to it in the bone. The cartilage-bone interface contains cells showing a chondrogenic

phenotype on the cartilage side, osteoblastic phenotype on the bone side and multiple phenotypes in a spatially organised fashion in between (Erisken et al., 2010).

This graded soft interface in the native tissue, as well as mimicking it in the design of an osteochondral scaffold, are important from a contact mechanics perspective. As mentioned in Section 2.2, as the joints move, the cartilage layers lining the articular surfaces of the bones slide and roll (Ateshian and Wang, 1995). When two layers of cartilage contact one another, the geometry of contact is equivalent to a rigid sphere indenting a flat articular cartilage layer (Ateshian et al., 1994) as depicted in Figure 2.10.

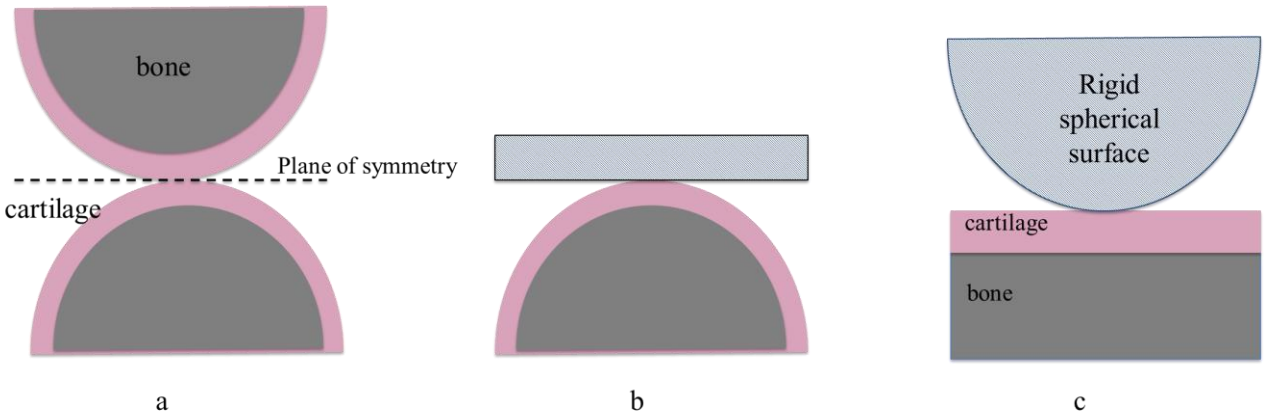


Figure 2.10 Two cartilage layers in contact having a plane of symmetry; (a) the contact problem is equivalent to a rigid plane contacting a bone-cartilage layer or (b) a rigid sphere indenting a flat cartilage-bone layer (Ateshian et al., 1994)

In cases where cartilage and subchondral bone bind with a sharp interface (as Figure 2.11a), the sliding contact in the joint induces tensile and shear stress in the interface and leads to decohesion and delamination between the bone and cartilage (Ochsner et al., 2008). This interface is either continuous, as is the case in native tissue, or it is in fine, discrete steps across the interface between the bone and cartilage, which have dissimilarities in composition, structure

and mechanical properties, and can redistribute the stresses, suppressing interface failure(Suresh, 2001).

Therefore, the significance of following the graded interfacial structure for an osteochondral plug is clear. Following this structure would not only provide biological advantages for the cells as a bio-inspired microenvironment, it would also deliver essential mechanical stability superior to a homogeneous or layered substrate with sharp interfaces.

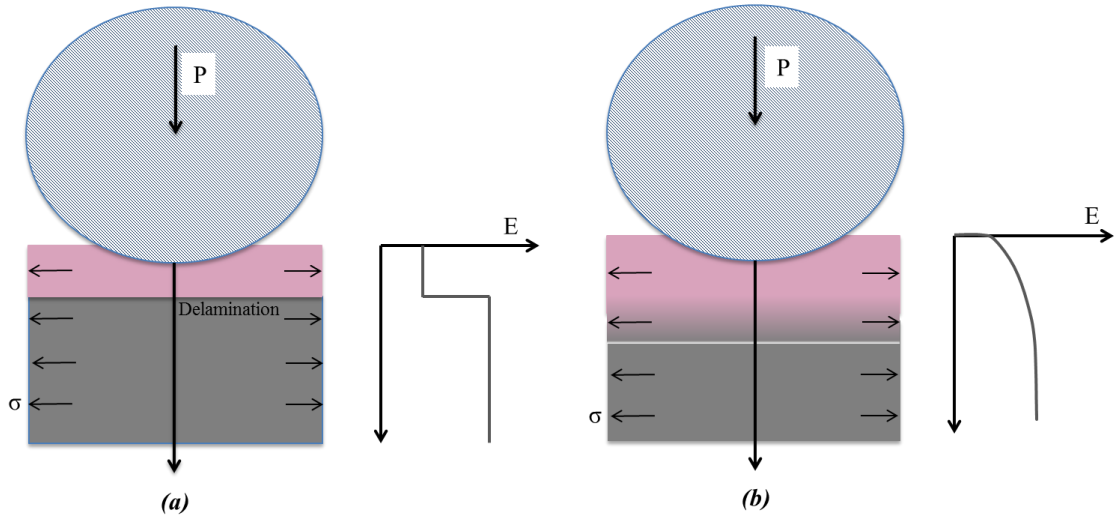


Figure 2.11 Contact with force P between a rigid sphere and two layers with (a) sharp interface, which leads to delamination between the layers caused by the tensile and shear stresses at the interface due to abrupt change in modulus E, (b) graded interface with gradual increase in E, which suppress delamination; diagram from (Giannakopoulos, 1998)

2.5 Bone and cartilage defects

Factors such as osteogenesis imperfections, osteoarthritis, traumatic injury, orthopaedic surgeries (i.e. total joint arthroplasty, spine arthrodesis, implant fixation, etc.) and primary tumour resection can contribute to bone defects (Porter et al., 2009).

Thanks to a spontaneous capacity for regeneration, most bone lesions, such as fractures, repair with conventional therapy. However, in cases of large defects and osseous congenital deformities, bone grafts or substitutes are needed to aid healing (Leng et al., 2013). The process of fracture healing is a sequence that begins with hematoma formation, and then moves to inflammation, destruction of non-vital debris, granulation tissue proliferation, callus formation, conversion of woven bone to lamellar bone, and finally, remodelling of the healed bone (Karageorgiou and Kaplan, 2005).

In the case of articular cartilage, injuries are commonly caused by mechanical, chemical and microbiological means and accompanied by the disabling symptoms of arthritis (Newman, 1998). Articular cartilage, unlike bone, has a poor intrinsic capacity to repair itself, partly due to its avascularity (Puppi et al., 2010).

Defects of articular cartilage that do not penetrate to the subchondral bone (chondral defects/partial-thickness defects) and stay entirely within the cartilage, fail to heal spontaneously since subchondral vessels are not involved. Defects that penetrate to the subchondral bone (Figure 2.12) (subchondral defects/full-thickness defects) promote an intrinsic repair response as mesenchymal chondroprogenitor cells invade the lesion, which produces a fibrocartilaginous repair tissue. Many arthroscopic repair strategies utilise this response to induce repair. However,

the goal is to produce a repair tissue that has the same functional and mechanical properties as hyaline articular cartilage. Indeed, this, along with integration between repair and native tissue, are two major obstacles to tackle (Puppi et al., 2010).

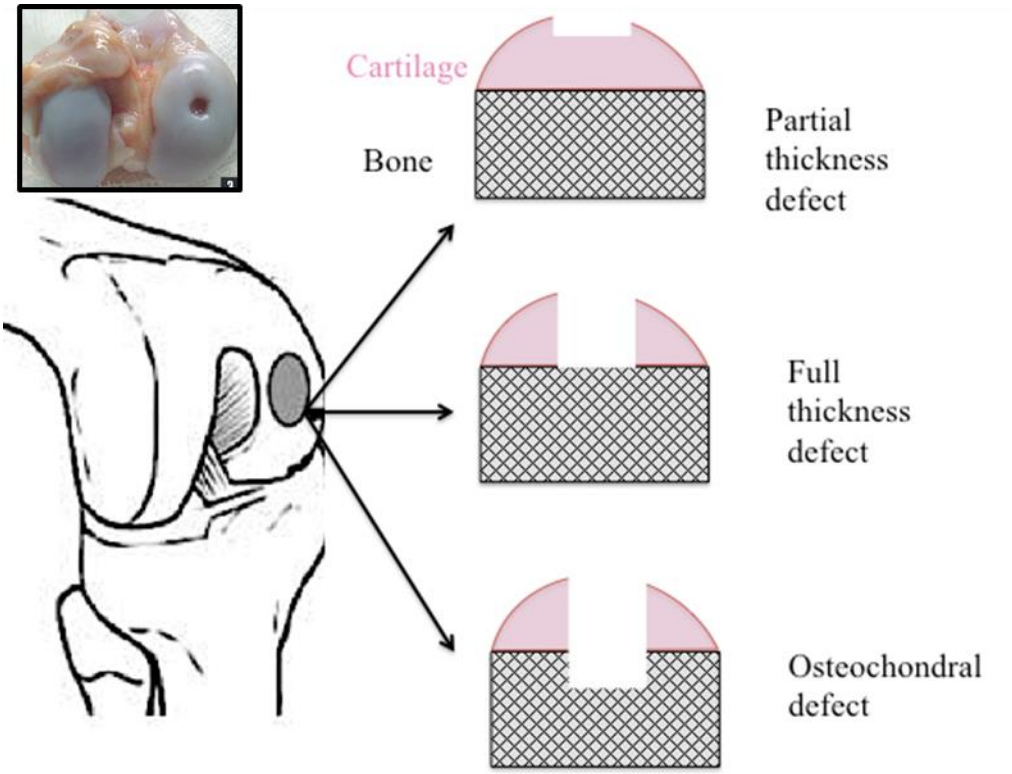


Figure 2.12 Partial-thickness, full-thickness and osteochondral defects; adapted from (O'Shea and Miao, 2008), picture from (Leng et al., 2013)

Osteoarthritis (OA) is a prevalent degenerative joint disease, affecting more people than any other joint syndrome. As shown in Figure 2.13, OA is a progressive loss of articular cartilage (Martin and Buckwalter, 1996) and can occur in the absence of a known cause (primary OA) by destruction and failure of the cartilage ECM (O'Shea and Miao, 2008, Aigner and Stove, 2003). It can also be the result of joint injury, infection or metabolic or developmental disorder (Temenoff and Mikos, 2000a).

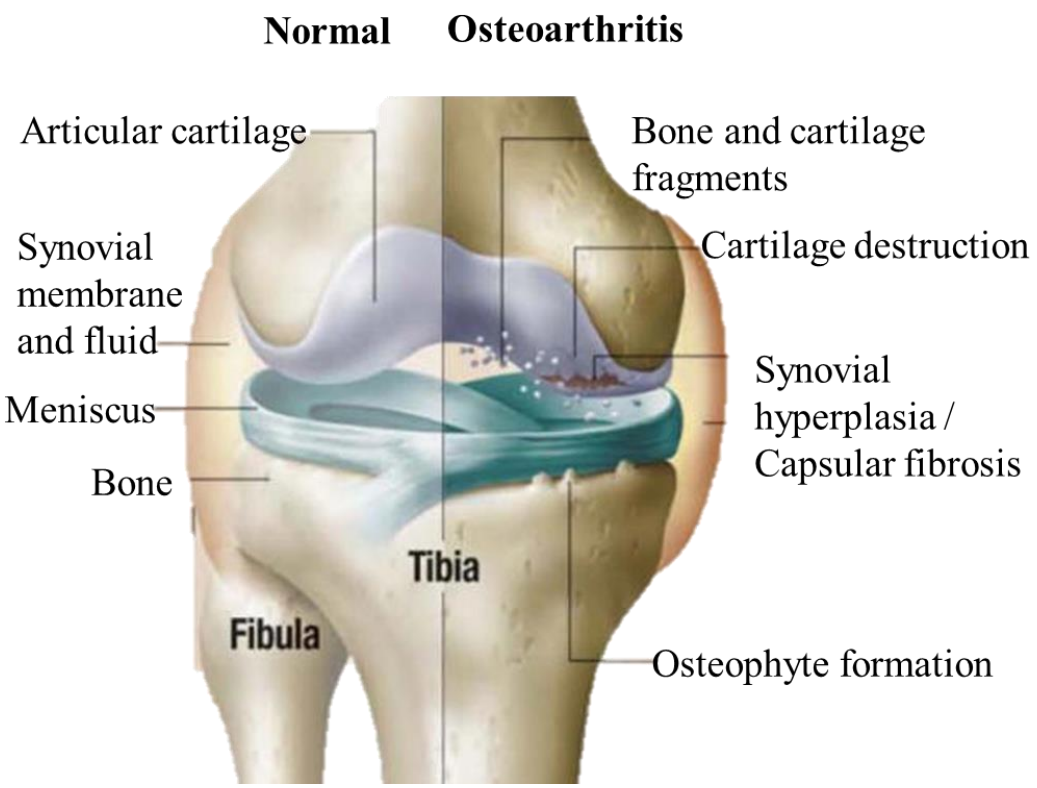


Figure 2.13 Schematic representation of the main structures of a healthy (left) and degenerated (right) joint; modified from (Aigner and Stove, 2003), picture modified from http://thinkloud65.files.wordpress.com/2012/05/oa2.jpg

ECM failure may be due to the destruction and loss of the interterritorial or pericellular cartilage matrix. The former is caused by an imbalance between degradation and de novo synthesis of matrix components. This leads to changes in the two major components of the interterritorial matrix: the collagen network and the PG aggregates. Collagen-network loosening leads to the loss of PGs, which then leads to a mechanical overload, thereby inducing the damage and further loosening of the collagen network. In OA, the composition of the PGs seems to change, and molecules, such as tenascin and collagen types IIA and III, which are normally absent in healthy cartilage, seem to emerge (Aigner and Stove, 2003). In osteoarthritic cartilage *pericellular* matrix is also severely altered. Synthesis and/or degradation of collagen type VI increases and the collagen aggregates become 'long-spaced'. Since this matrix is supposed to act

as a protective network for cells, these changes might hinder proper cell–matrix interaction and the cell might lose its protective net against compression forces. Changes in the *pericellular* microenvironment can play a role in chondrocyte clustering typical of osteoarthritic cartilage (Aigner and Stove, 2003). Thus, it has been suggested that repairing of articular cartilage may be an appropriate strategy to prevent the progression of OA (O'Shea and Miao, 2008).

2.6 Current treatments

In the field of hard tissue repair and replacement, the biomaterials industry has a worldwide annual turnover of $2.3 billion (Li, 2000). Each year, more than 2.2 million bone grafting and 1 million articular cartilage repair procedures take place (Place et al., 2009).

Lost bone can be replaced by bone grafts, including xeno-, allo- and autografts (Table 2.6). The current gold standard (Porter et al., 2009) is autograft where host bone is removed from another site to fill the defect. However, the complication rate is as high as 30% due to donor site morbidity, pain, hematoma and inflammation. Moreover, in many cases, critical-sized defects in bone have proved challenging to this treatment (Porter et al., 2009, Sikavitsas et al., 2001). Novel materials, cell transplantation and bioactive molecule delivery are being explored as alternatives. The goal of these strategies is to use the body's natural ability to repair injured bone with new bone tissue, and to remodel that new bone in response to the local stresses it experiences (Sikavitsas et al., 2001).

Table 2.6 Bone graft methods comparison (Porter et al., 2009, Wahl and Czernuszka, 2006, Puppi et al., 2010, Tenhuisen et al., 1995).

Bone grafts			
Xenograft		**Allograft**	**Autograft**
Def.	Uses bone tissue from other species	Uses tissue from other humans (typically cadavers), which may derive from viable or sterilized non-viable sources	Host bone is removed from another site (typically from the pelvis or iliac crest) and used to fill the defect
Disadv.	Associated with infection and inflammation and has perceived ethical disadvantages	Risk of infection (as high as 13%), disease transmission, poor mechanical properties, reduced osteogenic capacity and host immune response	Complication rate is as high as 30% in this treatment due to donor site morbidity, pain, hematoma and inflammation

As discussed earlier, due to the lack of cells capable of entering the defect (Erisken et al., 2010, Hunziker, 2002) cartilage cannot be adequately replaced with de novo synthesised, normal articular cartilage (O'Shea and Miao, 2008). Chondrocytes are embedded in the lacunae and have limited abilities to migrate within the matrix. No stem or reserve cells are available within the adult articular cartilage (Aigner and Stove, 2003). Therefore, surgical interventions are usually required to repair a damaged cartilage.

Selection of the appropriate treatment method depends on the size, cause and depth of a defect. Large defects or advanced OA are usually treated with total knee arthroplasty (TKA), whereas smaller defects can be treated with limited arthroscopic methods. The full-thickness defects have temporary spontaneous capacities for healing, whereas partial-thickness lesions have no such capacity. Marrow stimulation techniques can be used to treat the intermediate-sized

defects. These techniques include abrasion arthroplasty, subchondral drilling and microfracture, which may provide temporary pain relief and can delay the need for TKA for several years (Lynn et al., 2004a). These techniques create a full-thickness defect penetrating the subchondral bone by either abrasion or drilling. A clot forms over the bone surface, which, if left unloaded, can provide a scaffold for migration of MSCs and their eventual differentiation into chondrocytes and osteocytes (Leng et al., 2013). Other surgical strategies include marrow stimulation techniques (including autologous chondrocyte implantation (ACI)), arthroscopic repair procedures, soft tissue grafts and osteochondral transplantation (Sharma and Elisseeff, 2004).

Currently, there is no gold standard for repairing cartilage defects (Slynarski and Deszczynski, 2006), and all of the abovementioned strategies have disadvantages. The shortage of donor organs and the need for lifelong immunosuppression remain the main obstacles to allografts. Furthermore, transferred tissue does not possess all the functions of the native tissue and can involve donor site complications. Non-biological materials may have limited durability and lack biocompatibility. For these reasons, stem cells, TE and organogenesis are promising alternatives (Leng et al., 2013, Lynn et al., 2004a).

2.7 Tissue engineering (TE)

The major goal of TE is to regenerate tissues, including skin, cartilage, bone, nerve and liver. A porous scaffold or matrix that mimics the tissue ECM is fabricated; cells attach to this matrix, where they then multiply and function. Typically, donor tissue is harvested from the patient and dissociated into individual cells using enzymes. The cells (osteoblasts, chondrocytes and MSCs in this case (Martino et al., 2012)) are then seeded onto the scaffold (or *in vitro*) in a cell culture medium. The damaged tissue is removed, and the matrix and attached cells are then implanted in the patient. Over time, the synthetic matrix resorbs and the cells produce their own natural ECM (Livingston et al., 2003).

As illustrated in Figure 2.14, there are three key ingredients necessary in TE: a scaffold, which may be either natural or synthetic, cells (Petite et al., 2011) and inductive signals (i.e. growth factors or proteins)(Lynn et al., 2004a).

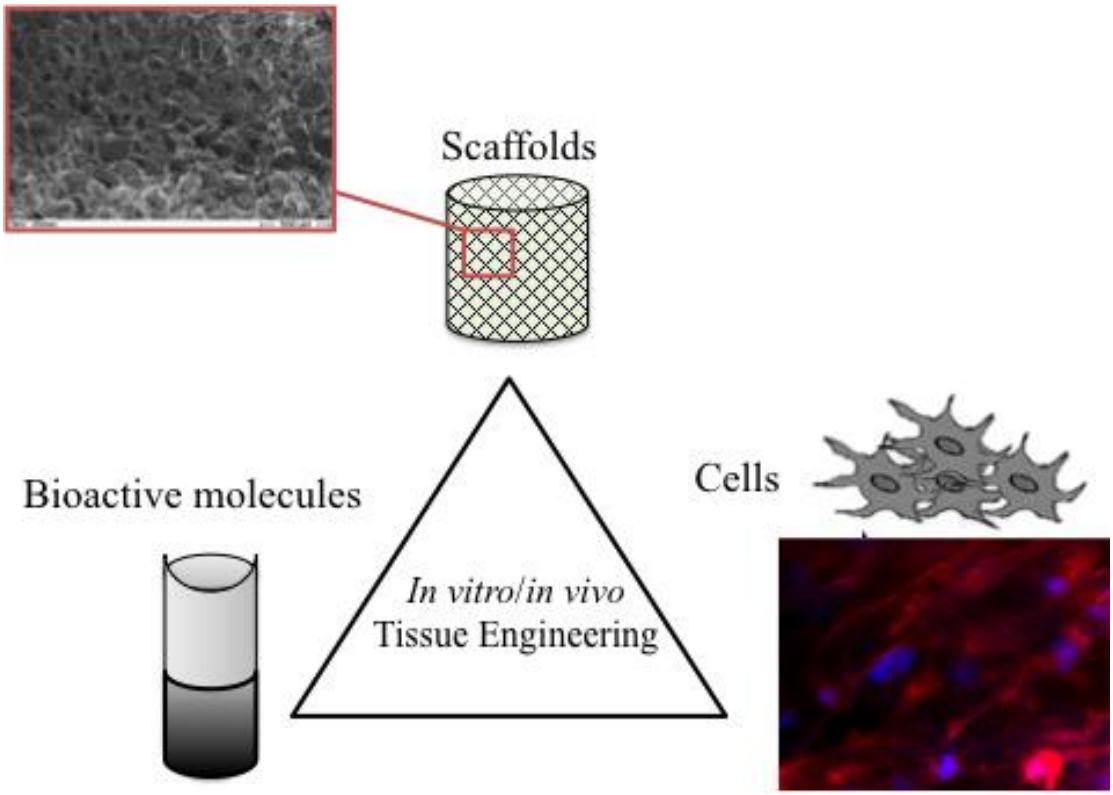


Figure 2.14 Three key ingredients of TE; adapted from (O'Shea and Miao, 2008)

2.7.1 Scaffolds

Some research suggests that cells might be unable to establish themselves properly within a defect without matrix guidance (Aigner and Stove, 2003). Therefore, a scaffold must be developed to provide a three-dimensional structure to support the cells, aid their proliferation and help them maintain their differentiated functions, while its architecture defines the ultimate shape of the new bone and cartilage (Leng et al., 2013, Hunziker, 2002, Martino et al., 2012).

There are several requirements for the development of an orthopaedic biomaterial. First, a scaffold must be biocompatible and bioactive, meaning it must not elicit an inflammatory response, extreme immunogenicity or cytotoxicity (Porter et al., 2009, Leng et al., 2013, Hunziker, 2002, Martino et al., 2012, Livingston et al., 2003, Cui et al., 2011), and must be

either osteoinductive/osteoconductive or chondroinductive/chondroconductive, depending on bone or cartilage (Porter et al., 2009, O'Shea and Miao, 2008, Lawson and Czernuszka, 1998, Place et al., 2009).

Moreover, the scaffold must be porous (Porter et al., 2009, O'Shea and Miao, 2008, Leng et al., 2013, Cui et al., 2011) and possess an interconnected pore structure (porosity exceeding 90%) (Leng et al., 2013, Livingston et al., 2003) to allow in vitro cell adhesion and ingrowth. Pore interconnectivity influences the diffusion of nutrients and gases to cells as well as the removal of metabolic waste from cells. Additionally, a good distribution of a large number of cells requires high internal surface-area-to-volume ratios. Since increased pore size decreases internal surface area, a compromise must always be found (Leng et al., 2013). The pore size must be within a critical range, the lower bound of which is controlled by the size of the cells, while the upper bound is related to the specific surface area through the availability of binding sites (Livingston et al., 2003). In addition, a porous surface improves mechanical interlocking between the implant and the surrounding natural bone, providing greater mechanical stability (Lawson and Czernuszka, 1998). It has been suggested that a pore size greater than 300 μm and a significantly interconnected porosity are needed for new bone formation (O'Shea and Miao, 2008) (this is discussed in Section 6.4.5). In vitro, lower porosity stimulates osteogenesis by suppressing cell proliferation and forcing cell aggregation. In contrast, in vivo, higher porosity and pore size result in greater bone ingrowth. The preferred pore size of the matrices for cartilage TE is controversial. Some give preference to small pore sizes of less than 50 μm, whereas others do not find any significant difference between 20 and 80 μm pore diameters (Aigner and Stove, 2003).

However, mechanical integrity and porosity are conflicting requirements(Freyman et al., 2001a); an increase in scaffold porosity greatly diminishes the mechanical properties, thereby setting an upper functional limit for pore size and porosity (Lawson and Czernuszka, 1998, O'Shea and Miao, 2008). The most common techniques used to create porosity in a biomaterial are salt leaching, gas foaming, phase separation, freeze-drying and sintering, depending on the material used to fabricate the scaffold (Lawson and Czernuszka, 1998). These are further discussed in Section 2.9.

Although macroporosity (pore size 450 μm) strongly affects osteogenic outcomes, microporosity (pore size 10 μm) and pore wall roughness play important roles as well. Microporosity results in a larger surface area that contributes to higher bone-inducing protein adsorption as well as to ion exchange and bone-like apatite formation by dissolution and re-precipitation. Surface roughness enhances attachment, proliferation and differentiation of osteoblasts (Lawson and Czernuszka, 1998). Surface properties of scaffolds include morphology, hydrophilicity, surface energy and charge affect in vitro cell adhesion, migration, phenotype maintenance and intracellular signalling, as well as in vivo cell recruitment and healing at the tissue-scaffold interface (Leng et al., 2013).

Mechanical properties (Puppi et al., 2010, Porter et al., 2009) are especially important in scaffolds for orthopaedics (Temenoff and Mikos, 2000a) because the scaffolds must also interact with their mechanical surroundings to transmit mechanical signals to cells and modify cell behaviour (i.e. differentiation, motility and contractility). The stiffness of ECM can have effects at a transcriptional level, determining whether stem cells make the decision to become cells as functionally diverse as nerve and bone (Place et al., 2009). It has been said that compressive

properties are the most relevant for the replacement of cancellous bone and tensile properties are important for cortical bone (Temenoff and Mikos, 2000a), however, this cannot be entirely true. If the human femur is considered as a hollow tube, it is subjected to bending forces, which means that the forces vary from tension to compression from one side to the other (Figure 2.15). Therefore, it can be seen that both tensile and compressive properties are important for cortical bone.

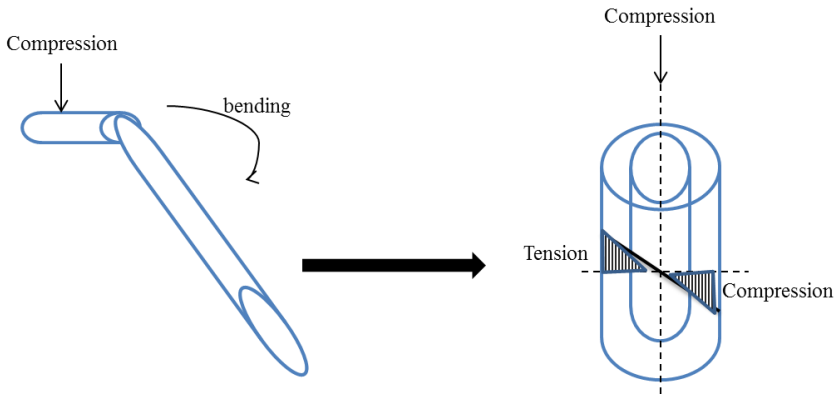


Figure 2.15 Schematic of forces on femur bone; the center represents the cancellous bone and the outer represents the cortical bone. Cancellous bone is subjected predominantly to compression while cortical bone is exposed to both tensile and compressive forces

It is also desirable that scaffolds degrade controllably (Porter et al., 2009, O'Shea, Miao, 2008 and Freyman et al., 2001a) and are sterilized without altering the chemical composition (Porter et al., 2009, Temenoff and Mikos, 2000a). Additionally, materials that are readily available, comparatively inexpensive, easy to manufacture and FDA approved for clinical applications (O'Shea and Miao, 2008) are preferred. The matrix scaffold requirements are summarised in Table 2.7.

Table 2.7 Scaffold matrix properties, modified after (Sharma and Elisseeff, 2004)

Matrix properties	**Biological basis**
1. Porosity	Cell migration, nutrient, oxygen and waste transfer
2. Surface roughness	Cell attachment
3. Biodegradability	Physiological remodelling
4. Biocompatibility and bonding	Good contact and integration with contact tissue
5. Internal cohesiveness	Prevention of matrix outflow
6. Elasticity and sufficient mechanical properties	Due to dynamic and static deformation, acts as a temporary support for the cells
7. Structural anisotropy	Promotion of native anisotropic tissue structure

TE scaffolds can be designed to interact with cells by mimicking key molecular features of the ECM. As described in previous Sections 2.2.1.2 and 2.3.1.2, ECM contains many macromolecules, such as PGs, collagens, laminins, fibronectin and sequestered growth factors. It is primarily this molecular information that confers its bioactivity, and these components are believed to be critical in determining how cells behave within tissue (Place et al., 2009).

Synthetic or natural polymers can be used as scaffolds for TE. The most widely used synthetic and natural polymers include collagen, gelatine (denatured collagen), fibrin, alginate, agarose, polyglycolic and polylactic acids and hyaluronan (Aigner and Stove, 2003). While synthetic polymers are widely used in TE, the chemicals (additives, traces of catalysts, inhibitors) or monomers (glycolic acid, lactic acid) released from polymer degradation may induce local and systemic host reactions that cause clinical complications (Wahl and Czernuszka, 2006). However, natural polymers have the advantage of biocompatibility and biodegradability (Karageorgiou and Kaplan, 2005), and are therefore the preferred material source in this study.

2.7.2 Cells

Cells can be obtained from a number of sources at varying stages of differentiation. When selecting the optimal cell type, the proliferative capacity of the cells *ex vivo* and their phenotypic stability and immunogenicity must be considered. For instance, fully differentiated autologous cells may serve as a reliable cell source with no concern of an immune response; however, their proliferative capacity is limited. In the case of stem cells, the legal, political and ethical questions regarding the use of embryonic stem cells has driven researchers to investigate alternative stem cell sources from adult bone marrow, muscle, fat and brain (Sharma and Elisseeff, 2004).

2.7.2.1.1 Embryonic stem cells (ES)

These cells show endless proliferation *in vitro* and the ability to differentiate into any cell type in the human body (Sharma and Elisseeff, 2004). For the purposes of cartilage and bone TE, alternate sources such as bone marrow-derived cells, mature chondrocytes or periosteal cells could be sufficient, thereby avoiding many of the controversial issues surrounding the use of ES cells.

2.7.2.1.2 Mesenchymal stem cells

Adult bone marrow is a source of hematopoietic and non-hematopoietic stem cells. The former is responsible for renewing circulating blood components and the latter are MSCs (Sharma and Elisseeff, 2004). Stem cells reside in a microenvironment called a niche, and their number is maintained by the balance between quiescent and active cells, where cell division can result in a daughter that remains a stem cell and a progenitor daughter (asymmetric division), or in two stem cell daughters (symmetric division) (Martino et al., 2012). MSCs are multipotent

cells and capable of differentiating along several lineage pathways (Livingston et al., 2003), such as bone, cartilage, muscle, ligament, tendon, adipose and stroma (Sharma and Elisseeff, 2004), whereas progenitor cells tend to differentiate into specific lineages. Bone marrow-derived stem cells are potentially an autologous cell source. The challenge lies in designing a microenvironment to bring these cells to the desired functional state to create structurally organised tissues (Sharma and Elisseeff, 2004).

To this point, the choice of the cell type for cartilage TE is empirically based: already-differentiated chondrocytes or MSCs/chondroprogenitor cells with the potential to differentiate into chondrocytes are used (Aigner and Stove, 2003). For use in bone TE, MSCs combined with biphasic calcium-phosphate ceramics have been shown to promote bone regeneration (Livingston et al., 2003, Petite et al., 2011). To increase their clinical performance, current investigations focus on exploiting the osteogenic potential of MSCs, and further development of scaffold material (Petite et al., 2011).

2.7.3 Growth factors

Growth and transcription factors are large polypeptides that are synthesised and expressed in very low physiological concentrations to act as local regulators of cell behaviour (Porter et al., 2009).

Growth factors, including bone morphogenetic proteins (BMPs), transforming growth factors beta (TGF), insulin-like growth factors (IGF), fibroblastic growth factors (FGF), platelet-derived growth factor (PDGF) and vascular endothelial growth factor (VEGF), have the ability to instruct the cells. They can be attached to scaffold by either covalent or non-covalent binding.

The latter can be achieved by physical entrapment of the growth factor into the scaffold, through its adsorption on the scaffold surface or through the formation of ionic complexes between the growth factor and the scaffold (Puppi et al., 2010).

More natural mechanisms of growth factor binding and release are also being pursued. *In vivo*, GAGs affect growth factor activity by sequestering them, preventing their degradation and presenting them to cell-surface receptors. CS in commercial products may perform a similar function, including modulating the activity of cell-derived signalling factors (Place et al., 2009). TE has produced success in a number of soft/hard tissue applications, as can be seen in Table 2.8.

Table 2.8 Commercial scaffolds currently available (Place et al., 2009).

Tissue	Product	Description	Use	Form
Bone	INFUSE bone graft, Medtronic (2002)	Bovine type I collagen sponge soaked in rh-BMP-2 in LT-CAGE lumbar, tapered fusion device	Spinal fusion	Solid
	OP1-Stryker (2001)	Bovine type I collagen with rh-BMP-7	Bone injury	Paste
	Vitoss® Scaffold FOAM™, Orthovita (2004)	Composite foam of b-TCP and collagen I	Bone injury	Foam
	BioSet™ IC, Pioneer surgical (2008)	Human demineralised bone matrix with bovine bone chips in type I collagen carrier	Bone injury	Paste
	FortrOss™, Pioneer™ surgical (2008)	Nanocrystalline HAp and E-matrix (porcine collagen co-polymerised with dextran)	Bone injury	Paste
	Regenafil®, Regeneration Technologies/Exatech (2005)	Human mineralised bone matrix in porcine gelatine carrier	Bone injury	Paste
	GEM 21S®, BioMimetic Therapeutics (2005)	b-TCP particles and recombinant human platelet-derived growth factor-BB (PDGF-BB)	Dental bone/gum defects	Paste
	BCT001, BioCeramic Therapeutics (preclinic)	Strontium releasing bioactive glasses	Bone defects	Granules, paste
Cartilage	SYNVISC®, Genzyme (1997)	Hyaluronic acid (Hylan GF-20 and Hylan B) from chicken combs	Synovial fluid replacement	Gel
	CaReS®, Arthro-Kinetics (2007)	Rat-tail type I collagen matrix seeded with chondrocytes	Articular cartilage injury	3D disc
	BioSeed®-C, BioTissue Technologies (clinic 2001)	Polyglycolic/polylactic acid and polydioxanone scaffold containing chondrocytes	Articular cartilage injury	3D disc
	Menaflex®, ReGen Biologics (2008)	Bovine type I collagen with hyaluronic acid and glycosaminoglycans, hydrated	Meniscus cartilage injury	Mesh
	Hyalograft® Autograft, Fidia Advanced Biopolymers (2008 EU)	HYAFF (esterified derivative of hyaluronic acid) scaffold with autologous chondrocytes	Articular cartilage injury	3D disc
	MACI®, Genzyme (unregulated EU)	Type I collagen membrane seeded with chondrocytes	Articular cartilage injury	Sheet

2.8 Osteochondral tissue engineering

TE repair of articular cartilage represents a potential OA treatment strategy superior to current surgical techniques. In particular, osteochondral TE promotes the simultaneous regeneration of articular cartilage and underlining subchondral bone and may be a clinically relevant approach to preventing OA progression (Schaefer et al., 2000, O'Shea and Miao, 2008).

More recently, the concept of osteochondral TE, a hybrid of bone and cartilage regeneration, has drawn considerable attention, especially as a technique for promoting superior cartilage integration (Cui et al., 2011) and a treatment for osteochondral defects (O'Shea and Miao, 2008).

There are some problems associated with engineering cartilage tissues, such as fixing tissue-engineered cartilage onto the recipient site (Cui et al., 2011). Cartilage-to-cartilage interfaces do not integrate well because of the dense, non-adhesive matrix and scarcity of cells at the interface; however, host bone integrates well with grafted bone tissue and other implant materials. Therefore, to better integrate engineered cartilage tissue with host tissue, an osteochondral implant can be used where the bony region can serve as an anchor for the implant. The cartilage and bone regions of the osteochondral composite scaffold may require different physical and mechanical properties as well as different culture conditions (Lynn et al., 2004a). A major challenge is generating the natural gradation in porosity, composition and biomechanical properties associated with both tissues (i.e. bone and cartilage) as well as the interface between the two (Erisken et al., 2010), as discussed in Section 2.4

2.8.1 Osteochondral scaffold materials

Recently, the focus of TE has shifted towards the development of biomimetic scaffolds. The ability of a scaffold to succeed as a template for cells depends on its microenvironment and how closely this environment can match the structure of the target tissue (Tamaddon and Czernuszka, 2013). Consequently, scaffold materials that resemble the actual ECM of the target tissue have significant potential for repair and regeneration of damaged tissues (Davidenko et al., 2012). Therefore, considering the composition and structure of bone and cartilage tissue, promising scaffolds candidates are collagen, which is the main structural macromolecule in bone and cartilage ECM, CS, which is the major GAG component of native cartilage, and hydroxyapatite, which is the main inorganic constituent of bone (Buckwalter and Mankin, 1997a, Harley et al., 2010b, Sharma and Elisseeff, 2004).

2.8.1.1 Collagen

Collagen is the fundamental structural protein in the body. Twenty-eight different types of collagen are known, differing by amino acid composition (Shoulders and Raines, 2009).

Collagen has a hierarchy of primary, secondary and tertiary structures (Yannas, 1972). The primary structure of collagen denotes a sequence of amino acids residues (X-Y-Gly), where frequently *X* is proline, *Y* is hydroxyproline and *Gly* is glycine. The position of glycine as the smallest amino acid residue at every third position allows close package of the chains into a helix (Cremer et al., 1998, Cen et al., 2008). The amino acids in collagen molecules contain the amine (-NH2), acids (-COOH) and hydroxyls (-OH) groups (Khor, 1997). These blocks of amino acids form a helical polypeptide chain called the α-chain. The secondary structure refers to the local configuration of these individual chains. The tertiary structure signifies the large-

scale folding and helicity of the chains, which form the fundamental unit of the collagen molecule, tropocollagen (Yannas, 1972). These tropocollagen molecules are bundled into microfibrils. The molecules are not linked end-to-end, and there are overlaps and gap regions in the structure creating a quarter staggered array pattern with a periodicity of 67 nm called *d-banding* (Ottani et al., 2002) (Figure 2.16). Bundles of microfibrils form larger fibrils, which then form even larger fibres. The ordered structure rises from the interactions of the hydrophobic and polar groups of the molecules. These forces are enough to assemble the fibrils; however, they do not give the structure much mechanical stability. This is achieved by the formation of covalent crosslinks, which can be intramolecular (within a tropocollagen unit) or intermolecular (between tropocollagen units) (Lawson and Czernuszka, 1998).

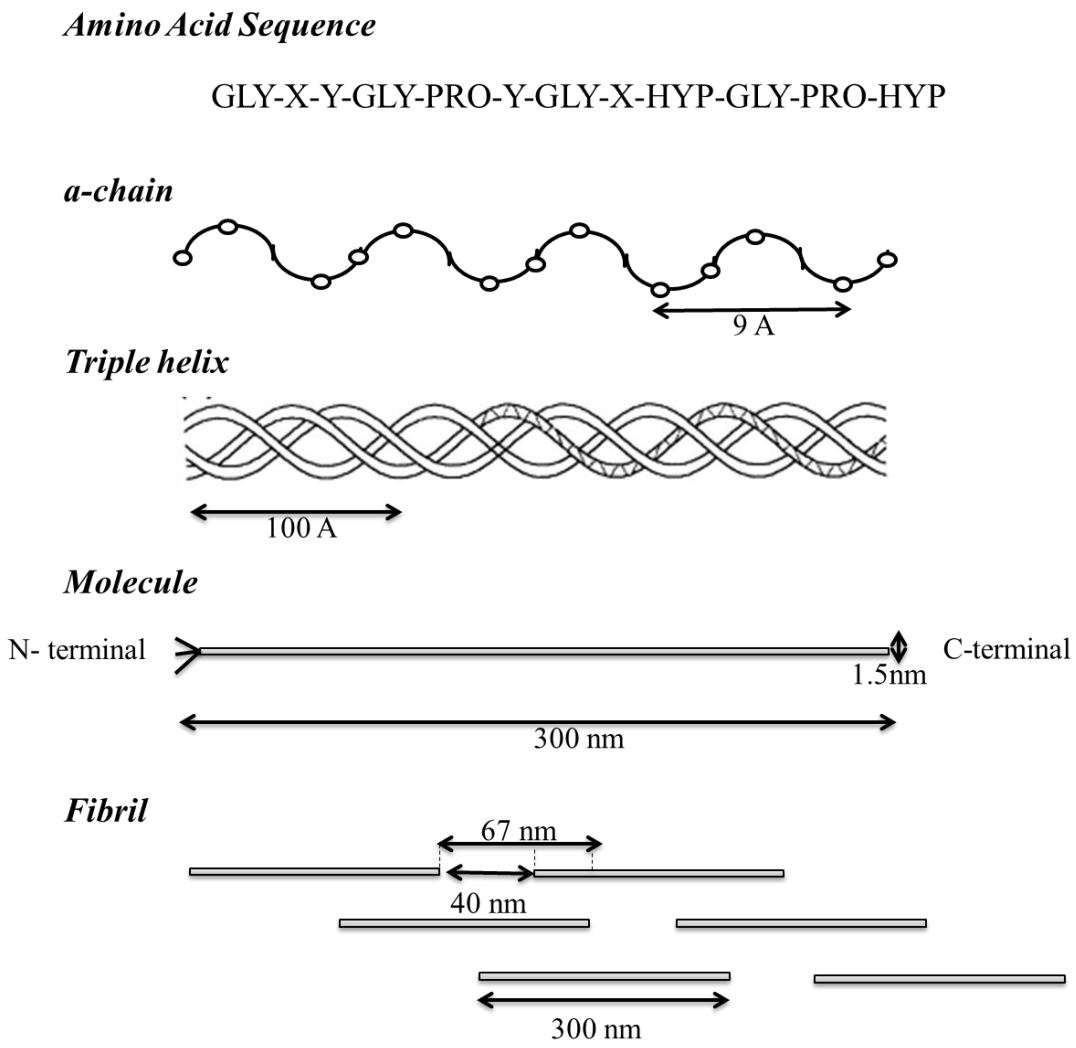


Figure 2.16 Hierarchical structure of collagen, showing the amino acid sequence, alpha-chain, triple helix and molecular structures and assembly into fibrils of quarter staggered pattern (67nm) consisting of gap (40nm) and overlap regions; redrawn from (Tamaddon and Czernuszka, 2013, Lane and Weiss, 1975)

Collagen molecules can be divided into eight families (Myllyharju and Kivirikko, 2001), as summarised in Table 2.9.

Table 2.9 Collagen molecules families.

1. Fibril-forming collagens → Type I, II, III, V and XI	2. Fibril-associated collagens with interrupted triple helices, which are located on the surfaces of fibrils → Type IX, XII, XIV, VXI and XIX
3. Collagens that form hexagonal networks → Type VIII and X	4. Family of Type IV collagens found in base membrane
5. Type VI collagen that forms beaded filaments	6. Type VII that forms anchoring fibrils for basement membrane
7. Collagens with transmembrane domains (Type XIII and XVII)	8. The family of Type XV and XVIII

The fibril-forming collagen molecules (as in articular cartilage and bone) comprise an uninterrupted triple helix approximately 300 nm long and 1.5 nm in diameter, flanked by short extrahelical telopeptides. These telopeptides do not have a repeating Gly-X-Y structure and triple-helical conformation. They account for 2% of the molecules (Kadler et al., 1996) and are believed to contribute to most of the antigenic properties of collagen (Khor, 1997).

Collagens may be extracted from tissues rich in the desired collagen type. An extraction of isolated collagen triple helices may be referred to as 'monomeric' and 'soluble', whereas extractions of collagen with a retained fibrillar structure may be referred to as 'polymeric' and 'insoluble'. The monomeric form may be pepsin-digested, telopeptide-deficient (atelocollagen) or acid-soluble telopeptide-intact (tropocollagen), and the polymeric form is insoluble and naturally crosslinked tropocollagen.

Currently, the majority of collagen materials are extracted from animal tissue derivatives, which brings the concern of collagen antigenicity. Antigenic determinants of collagen may be

helical, central or terminal; the latter can exhibit great interspecies variation, which may be the major antigenic determinant for certain donors and recipients (Lynn et al., 2004b).

Thus, atelocollagens devoid of these p-determinants (a region sensitive to antibodies near the C-terminus of both α-chain types) are usually preferred forms of collagen. However, it must be noted that the location of major antigenic determinants on the collagen molecule varies depending on the donor and recipient species (Lynn et al., 2004b). The telopeptides are usually eliminated by enzymatic digestion using pepsin (Wahl and Czernuszka, 2006, Yin Hsu et al., 1999, Kikuchi et al., 2004).

These monomeric soluble atelocollagen can be induced under certain physiological conditions to form fibrils *in vitro* through fibrillogenesis. The extent of fibril formation and fibril diameter depend partly on the type of collagen (Birk and Silver, 1984) and method of extraction (Williams et al., 1978). It has been shown that type I collagen fibrils extracted from dermal tissue have diameters ranging from 50–100 nm, whereas type II collagen fibrils from nasal cartilage are much thinner with diameters ranging from 10–20 nm (Birk and Silver, 1984).

Spontaneous self-assembly of collagen monomers *in vitro*, which is usually studied using turbidity-time curves, is compared by many authors (Comper and Veis, 1977, Gelman et al., 1979) to the nucleation-growth process of a crystal, and is suggested to show two distinct phases: 1) a lag phase, including initiation and linear growth, and 2) a lateral growth phase(Gelman et al., 1979, Silver and Trelstad, 1979). The initiation/lag phase is temperature-dependent, and nuclei may form by thermal fluctuations of atoms; however, the solution does not show any turbidity. In the next stage, which is temperature independent, intermediate aggregates form in the shape of long thin filaments with sizes ranging from 3–15 nm (Na and

Philips, 1983). They form mainly by electrostatic forces, which are undetected by light scattering. However, in the lateral growth phase, which is temperature-dependent, these microfilaments associate laterally by hydrophobic forces and covalent crosslinks to form fibrils, increasing the turbidity in a sigmoidal manner (Na and Philips, 1983, Gelman et al., 1979, Walton, 2010). Collagen molecules possess numerous hydrophobic amino acid side chains that are exposed to the solvent. Their hydrophobic bonding contributes majorly to fibrillogenesis in this stage (Wallace, 1985). The factors affecting the self-assembly of collagen include the temperature and the pH and ionic strength of the solution (Hayashi and Nagai, 1973).

Collagen is osteoconductive (Tenhuisen et al., 1995) providing a large number of ligands suitable to promote cell attachment and growth and delivery of growth factors, genes and other biologically active agents. It is also haemostatic, playing an important role in coagulation and thrombin formation: when collagen becomes exposed to flowing blood, platelets rapidly adhere to it, spread, become activated and begin to form an aggregate (Farndale et al., 2004).

The mechanical properties and degradation rates of collagen-based materials can be tailored by altering crosslink density, while their high porosity, characterised by an open network of interconnecting pores, provides binding sites for cellular invasion, attachment and proliferation (Lynn et al., 2010).

Different types of collagen elicit different responses from cells. Chondrocytes embedded in collagen types I and II matrices show different behaviours: cells in type I collagen show a more fibroblastic cellular phenotype, whereas cells in type II collagen are more chondrocytic. The mean deposition of GAGs in the type II collagen-seeded matrix exceeded that found in the type I collagen matrix (Aigner and Stove, 2003). The special sites within the collagen type II,

which are thought to be important mediators of cell–matrix interaction in articular cartilage and very likely important in the homeostasis of the cartilage tissue (Aigner and Stove, 2003) are thought to be the integrin α2β1 in native collagen and α5β1-fibronectin bridge in denatured collagen (Tuckwell et al., 1994).

Another study showed that type I collagen-based matrices efficiently recruited osteoprogenitor cells from the subchondral bone, whereas type II collagen-based matrices were more efficient at directing cells into a chondrogenic phenotype. Based on these observations, the authors proposed the concept of a composite cell-free matrix consisting of a deep layer of collagen type I and a superficial layer of collagen type II (Buma et al., 2003, Martin et al., 2007).

2.8.1.2 Chondroitin sulphate (CS)

Chondroitin sulphate is a polymeric carbohydrate with a molecular weight of 5–50 kDa (Gandhi and Mancera, 2008). It consists of sulphated, negatively charged, repeating disaccharide units. These units contain N-galactosamine (which is characteristic for CS) and D-glucuronate or L-iduronate. Several CS types have been identified, depending on the source organism, age, tissue type and location within the tissue. CS-A, also known as chondroitin-4-sulphate, is mostly isolated from tracheal cartilage and contains D-glucuronic acid and N-galactosamine sulphated at the C4 position (Lauder, 2009, Douglas et al., 2007). The behaviour of all the GAGs is the same in terms of aggregation, hydration and stability, but there are certain differences in their affinities to bind ions and proteins; CS-A is believed to have a lesser capacity to bond with collagen fibrils (Arias et al., 1998).

CS is non-immunogenic and can affect cell function, including adhesion, migration, differentiation (Tierney et al., 2009b) and organisation of the matrix(Pieper et al., 1999), as well

as the mechanical properties of the tissue (Temenoff and Mikos, 2000b). The addition of CS to collagen fibrils has been shown to enhance osteoblast adhesion, promote the differentiation of human MSCs and stimulate the proliferation of fibroblasts and chondrocytes *in vitro* while increasing cellular ingrowth and reducing foreign body response *in vivo*. Furthermore, growth factors (GFs) have maintained their bioactivity when immobilized on scaffolds containing CS. It has also been suggested that CS may apply a stabilising influence on GFs (Douglas et al., 2007).

2.8.1.3 Collagen-chondroitin sulphate composites

Given the nature and composition of native cartilage ECM architecture, collagen type II and hybrid collagen type II/CS scaffolds could be promising materials. Today, collagen-GAG porous scaffolds made by freeze-drying are being used to regenerate skin; this material received FDA approval for clinical use in 1996 (Freyman et al., 2001a). Copolymerization of collagen with GAGs and subsequent crosslinking can increase the compressive stiffness from 0.145–1.117 kPa (Lee et al., 2001). This influences not only the mechanical stability, but also the cell proliferation and matrix synthesis of cells (Aigner and Stove, 2003).

A number of studies have been done on types I and II collagen-CS scaffolds (Table 2.10) produced either by co-precipitation of collagen and CS, or by covalent attachment of CS to the collagen matrix, with the ratios of collagen to CS ranging 1.5:1–44:1. Mainly polymerised naturally crosslinked collagens were used in these studies.

Table 2.10 Currently investigated collagen-CS scaffolds; DHT=dehydrothermal crosslinking, EDC=1-ethyl-3-(3-dimethylaminopropyl) carbodiimide, GTA=Glutaraldehyde crosslinking; FD= freeze-drying

Scaffold	Collagen/CS concentration	Preparation methods	Crosslinking	Application	Reference
Type I collagen					
Type I—CS(6)	Co-precipitation, Fibrillar, 10:1	FD	DHT	Bone and cartilage	(Farrell et al., 2006)
Type I—CS (6)	Co-precipitation, Fibrillar, 10:1	Centrifugation / FD	DHT	-	(Liang et al., 2010)
Mineralised Type I—CS (6)	Co-precipitation, Fibrillar, ~10:1	Vacuum filtration and FD	DHT	Tendon and ligament	(Kanungo and Gibson, 2010)
Type I—CS	Co-precipitation, 10:1	FD	DHT	Tendon and ligament	(Kinneberg et al., 2010)
Type I—CS	Co-precipitation, Fibrillar, 10:1	FD	DHT	-	(O'Brien et al., 2004)
Type I—CS	Co-precipitation	FD	GTA	Skin	(Dagalakis et al., 1980)
Type I—CS	Co-precipitation, ~10:1	FD	DHT—EDC/NHS	Cartilage	(Mullen et al., 2010)
Type I—CS	Covalent attachment of CS using crosslinking, 0.8w/v% collagen, 0.125g/g matrix CS → 7:1	FD	EDC/NHS	Cartilage	(van Susante et al., 2001)
Type I—CS	Covalent attachment of CS using crosslinking, ~44:1–7:1	FD	DHT—EDC/NHS	-	(Pieper et al., 1999)
	Covalent attachment of CS using crosslinking, ~20:1–5:1	FD	EDC/NHS	-	(Pieper et al., 2000)
Type I—CS	Co-precipitation, 10:1	FD	DHT—EDAC/NHS		(Harley et al., 2007)
Type II collagen					
Type II—CS	Covalent attachment, ~5:1	FD	EDC/NHS	Cartilage	(Pieper et al., 2002)
Type II—CS /HA	Covalent attachment, 1w/v% of collagen, 17.8 ug/scaffold CS	FD	Genipin	-	(Ko et al., 2009)
Type II—CS	Reconstituted fibrillar, co-precipitation during fibrillogenesis, ~ 1.5:1–6:1	Air drying on titanium implant surface	EDC/NHS on titanium surface	Implant coating	(Douglas et al., 2007, Douglas et al., 2006)
	Covalent attachment using crosslinking, 5mg/ml collagen, 2w/v% CS	FD	EDC/NHS	Cartilage	(Cao and Xu, 2008)

2.8.1.4 Hydroxyapatite (HAp)

The most common types of calcium-phosphate materials for synthetic bone (Amjad et al., 1978) scaffolds are hydroxyapatite ($Ca_{10}(PO_4)_6(OH)_{2)}$, tricalcium phosphate (TCP), $Ca_3(PO_4)_2$, biphasic calcium phosphates (BCP) and multiphasic bio-glasses. The physical properties of the calcium-phosphate ceramics, such as degradation rate, modulus and processability, can be changed by altering the composition and stoichiometry (Porter et al., 2009).

Calcium phosphates exist commercially as HAp extracted from bone (Wahl and Czernuszka, 2006, Rodrigues et al., 2003) or they can be prepared by *in vitro* precipitation of calcium and phosphate ions (Wahl and Czernuszka, 2006), the sol-gel route, combustion synthesis, plasma, etc. (Singh, 2012). Synthetic HAp is biocompatible and bioactive, promotes osteoblast adhesion and migration/infiltration *in vitro* and has demonstrated excellent cellular and tissue responses *in vivo* (Porter et al., 2009, Suchanek and Yoshimura, 1998). For example, microspheres comprised of particulate hydroxyapatites dispersed in fibrous collagen matrices have been shown to support osteoblast cell growth (Yin Hsu et al., 1999).

However, the cellular response to HAp particles depends on properties such as particle size and morphology (needle like, spherical or irregular plates), chemical composition, crystallinity and sintering temperatures (Wahl and Czernuszka, 2006). For example, smaller, nano-sized particles are associated with a higher resorption rate than micro-sized particles (Filova et al., 2014). Therefore, although the dense HAp disc is not biodegradable, particulate HAp can be removed and remodelled by cells in the host (Yin Hsu et al., 1999).

2.8.1.5 Collagen-hydroxyapatite composites

Hydroxyapatite can be made into scaffolds in the forms of coatings, sintered powders, dense and porous ceramics, HAp-based ceramic and bioactive glass composites and HAp/polymer composites (Suchanek and Yoshimura, 1998). However, the ceramic form of HAp is brittle and its direct implantation can dislocate material within the tissue (Yin Hsu et al., 1999). To avoid these complications, HAp is often incorporated into a polymer matrix to form a composite that imparts high stiffness and compressive strength and better integration with the surrounding tissue (Yin Hsu et al., 1999, Lynn et al., 2010).

Following a biomimetic approach to scaffold fabrication, the composite of natural polymer collagen and HAp surpasses the bone-growth-enhancing abilities of each component alone (Wahl and Czernuszka, 2006).

Figure 2.17 shows a typical stress-strain curve of a collagen-HAp composite. The value of the modulus is dependent on the amount of precipitate and the sizes of the crystals, increasing from 0.44–2.82 GPa by increasing the mineral content and strain rate of the test (Lawson and Czernuszka, 1998). The mechanical properties of fabricated composites in this study are discussed in Chapter 7.

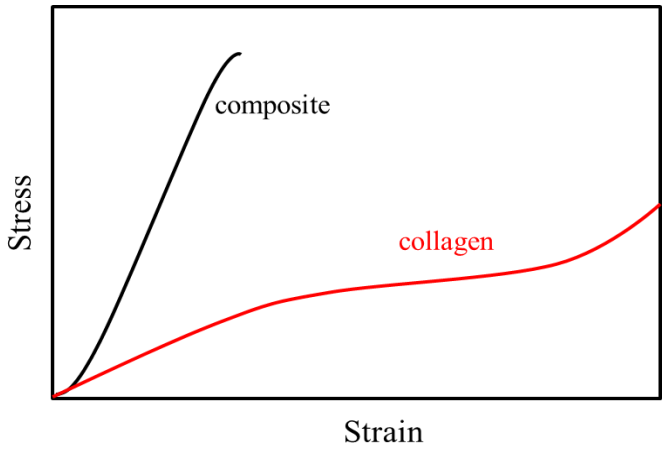


Figure 2.17 Typical stress-strain curve for collagen and calcium-phosphate-collagen composites; redrawn from (Lawson and Czernuszka, 1998)

Collagenous material can be mineralised by co-suspension with pre-synthesised or commercially available HAp (Wahl and Czernuszka, 2006). Cunniffe et al. (2010) produced collagen-HAp scaffolds by fabricating nano-hydroxyapatite and co-suspending it with naturally fibrillar collagen (Cunniffe et al., 2010). Collagen fibrils can also co-precipitate with calcium-phosphate crystallites having a preferred orientation. However, due to difficulties in controlling the calcium-phosphate-to-collagen ratio, the exact composition of bone cannot be mimicked (Lynn et al., 2010). Another way to fabricate a collagen-HAp matrix is by direct mineralisation, where collagen is fixed as a solid film through which calcium and phosphate ions diffuse into the fibrils (Lawson and Czernuszka, 1998) or a phosphate-containing/acidic calcium-containing collagen solution (Bradt et al., 1999). The advantage of using the first method is that the orientation of the collagen fibres can be controlled (Wahl and Czernuszka, 2006). In addition to abovementioned routes, immersion techniques using simulated body fluids (SBF) have also been used to produce mineralised matrices (Al-Munajjed et al., 2009). A number of collagen-HAp scaffolds have been developed by different methods and starting materials, which are shown in Table 2.11.

Table 2.11 Currently researched collagen-HAp scaffolds. GTA =glutaraldehyde , DDPA=glutaraldehyde. Diphenylphosphorylazide, EDC/NHS =carbodiimide/N-hydroxy succinimide.

Collagen	HAp	Mechanical	Biological	Crosslinking	Fabrication method	Ref.
0.5 w/v% naturally fibrillar	Co-suspension with pre-synthesised nHAp	Compression: 5.5±1.70 kPa	Good distribution of cells; equivalent cell no. to collagen	N/A	Freeze-dry	(Cunniffe et al., 2010)
1–2% naturally fibrillar	Co-Precipitation	1.3 GPa young's modulus	N/A	GTA - DDPA	N/A	(Gotora and Czernuszka)
1% naturally fibrillar	Commercial co-suspension (5 um avg. diameter), up to 200%	0.4–1.2 kPa compression	*In vitro*: increase in cell no. *In vivo*: healing critical size defect	±DHT and EDC/NHS	Freeze-dry	(Gleeson et al., 2010)
~1.1% naturally fibrillar	Commercial nHAp co-suspension (70:30, 50:50, 30:70 wt%)	N/A	*In vitro*: cell proliferation; identical gene expression to collagen	EDC/NHS Cryogel	Freeze-dry	(Rodrigues et al., 2013)
1–2% insoluble collagen	Co-suspension, commercial nHAp	23.3–671.7 kPa	N/A	EDC/NHS DHT	Freeze-dry	(Sionkowska and KozÅ‚owska, 2013)

According to Villa et al., several collagen–HAp materials are currently FDA approved for use as void fillers with bone marrow extracts. These materials include HEALOS® (DePuy), Collagraft® (Zimmer), OssiMend® (Collagen Matrix) and Mozaik™ (Integra LifeSciences)(Villa et al., 2014).

2.9 Scaffold fabrication techniques

There are a number of techniques available to produce porous scaffolds. However, those used to fabricate synthetic porous networks differ from those appropriate for natural polymers such as collagen.

Pore-inducing techniques for synthetic polymers include solvent casting in conjunction with particulate leaching, phase separation, gas foaming, melt-moulding, fibre bonding and direct 3D printing (Sachlos and Czernuszka, 2003, Hutmacher, 2001), all of which involve high temperatures, the use of chemicals or pH levels unsuitable for protein-based natural polymers. Consequently, the number of methods to generate pores in natural polymer is quite limited.

In one highly studied and common technique, the natural polymer suspension is frozen to produce an interconnecting network of ice crystals. These ice particulates are then removed by freeze-drying (Davidenko et al., 2012, Sachlos and Czernuszka, 2003) or critical point drying. In the former, the ice crystals are sublimated by low heat and low pressure in a vacuum chamber. In critical point drying, the suspension is dehydrated through flushing with a supercritical fluid, such as ethanol, at high pressure. The liquid is then taken to its supercritical point at high temperature.

Both methods are suitable for collagen scaffold fabrication; however, which technique is superior is controversial (Sachlos and Czernuszka, 2003, Walton, 2010, Schoof et al., 2001). Based on some preliminary studies (data not shown), there is a high degree of shrinkage in collagen scaffolds produced by critical point drying; therefore, the method of choice for

subsequent experiments was freeze-drying. Figure 2.18 shows a schematic of the freeze-drying technique.

The pore size, shape and interconnectivity produced by this method can be regulated by controlling ice crystal nucleation and growth (Yunoki et al., 2006).

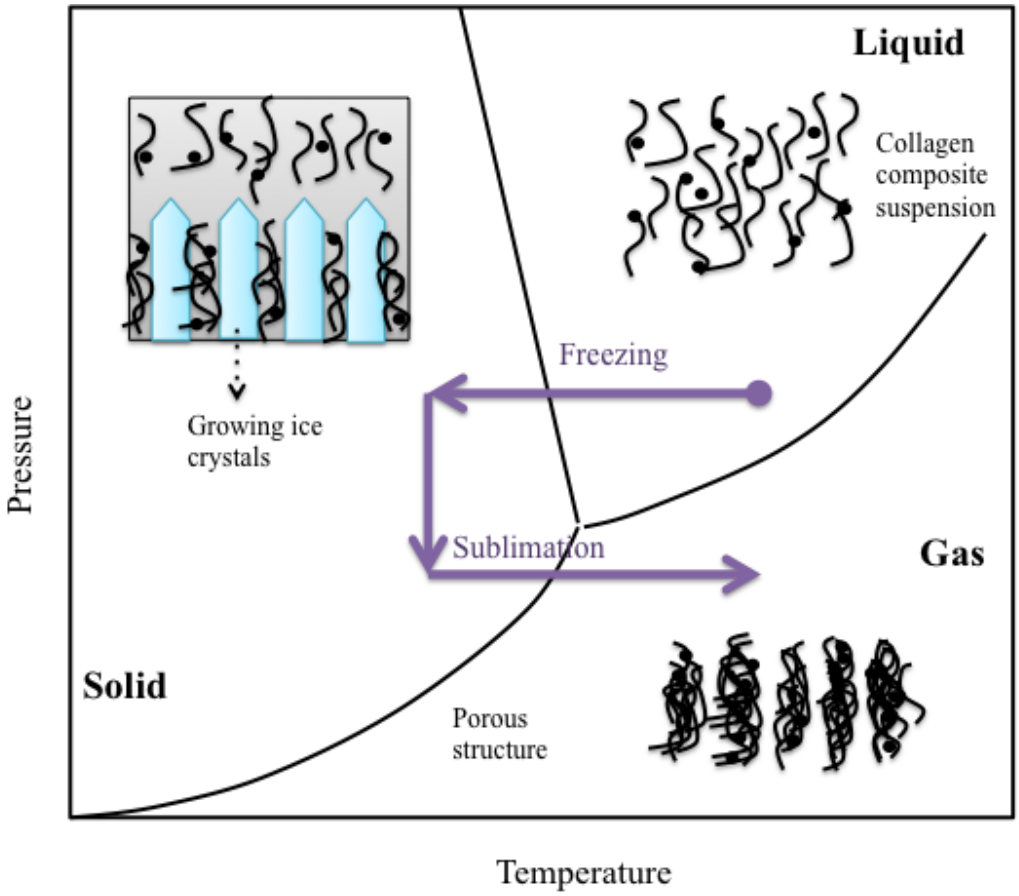


Figure 2.18 Freeze-drying principle to produce porous structures; adapted from (Deville, 2008)

2.10 Scaffold-cell interaction

To understand the behaviour of cells on a scaffold, it is important to first study the molecular mechanism of cell adhesion on biomaterials (illustrated in Figure 2.19). When an anchorage-dependent cell contacts a surface, it must adhere to the surface to remain viable, proliferate or differentiate. Adhesion can be non-receptor-mediated via weak chemical bonding, such as electrostatic, hydrogen or ionic bonding; however, this type of adhesion does not guarantee the transmission of signals from the microenvironment to the cells that is necessary to prompt the secretion of ECM molecules from cells; therefore, the cells may go into apoptosis. Another form of adhesion is receptor-mediated adhesion through ECM molecules, such as fibronectin or collagen. These molecules adsorb onto the surface of biomaterial from the surrounding environment and then bind cell integrins through their specific amino acid sequences. These specific amino acids are called ligands, and the minimum adhesion motif on ECM molecules should contain at least three amino acids, which are often symbolised by Arg-Gly-Asp (RGD). On the other hand, integrins are glycoproteins comprising one α and one β chain. There are about 16 recognised subunits and eight subunits with various combinations, which results in receptors with preferential binding affinity to certain ECM molecules (Bacakova et al., 2004, Anselme, 2000).

After ligand binding, integrins are formed into dot-like or streak-like regions called 'focal adhesions'. In these regions, integrins communicate with structural and signalling molecules, such as talin, α-actinin, filamin, paxillin or vinculin, which link integrin receptors to cytoplasmatic actin cytoskeleton. External signals are then transmitted from the microenvironment to the nuclei of cells (Zhao et al., 2013), thereby influencing intracellular

transport processes and the secretion of various molecules and determining whether there is cell proliferation and differentiation or apoptosis (Bacakova et al., 2004).

The microenvironmental factors affecting cell behaviour include scaffold stiffness, porosity, pore size and shape and the surface characteristics of the biomaterial (e.g. wettability, roughness, crystallinity and charge) (Singh et al., 2008).

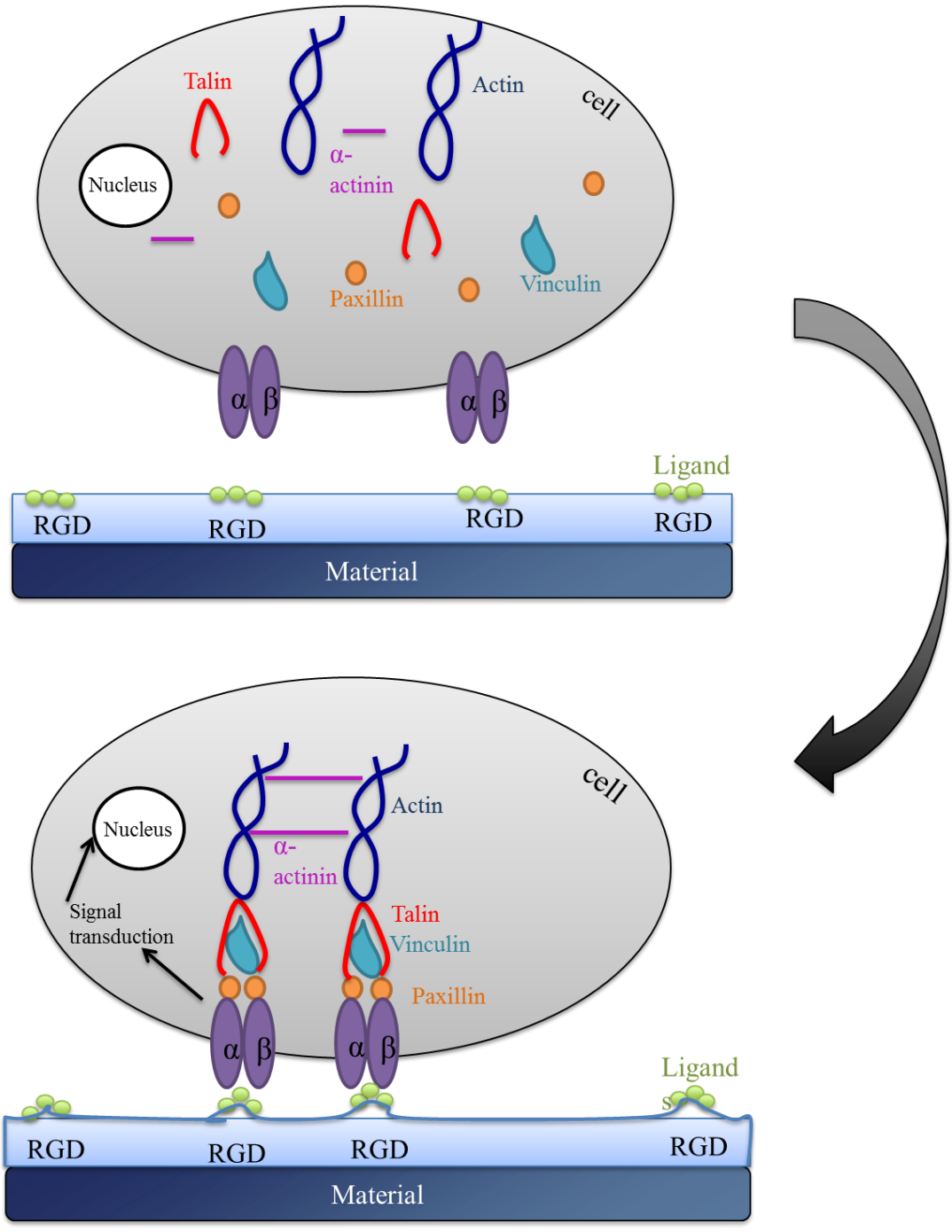


Figure 2.19 Cell and material interaction; adapted from (Martino et al., 2012, Anselme, 2000)

The extent and strength of cell adhesion to a surface affects its migration and its decision to switch between proliferation and differentiation behaviour (Bacakova et al., 2004, Zhao et al.,

2013, Bacakova et al., 2011) (Figure 2.20). For example, cells with large adhesion are usually dormant concerning migration and proliferation and more active in the expression of differentiation markers (Bacakova et al., 2011). The optimum adhesion of cells generally occurs on a moderately hydrophilic and positively charged scaffold because the adhesion molecules are adsorbed in a favourable geometric conformation, making ligands available to bind with cell receptors (Bacakova et al., 2011).

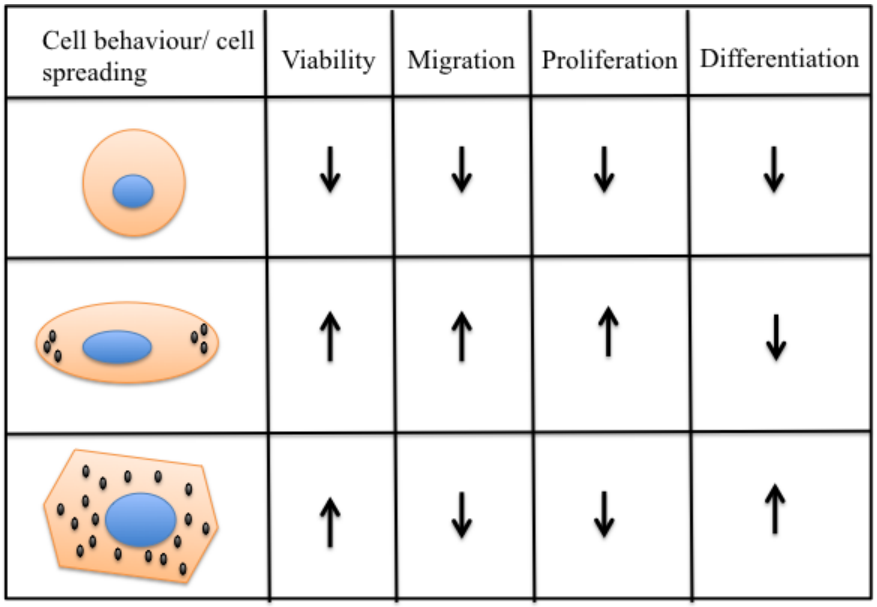


Figure 2.20 Effect of cell spreading/adhesion on subsequent cell behaviour. Blue refers to cell nuclei and black dots represent focal adhesions; redrawn from (Bacakova et al., 2004)

Cells use a bridging mechanism when migrating through a porous scaffold; that is, they use neighbouring cells as support to bridge across pores larger than their diameters. Thus, a cell can only spread along the walls of a pore if the pore dimension greatly exceeds the size of the cell, a phenomenon that influences cells' migration ability and speed in general (Murphy et al., 2013). Similarly, the matrix stiffness can affect cell migration. The contact between fibroblasts,

epithelial cells, smooth muscle and the matrix reduces on softer substrates, and cells migrate from softer regions to stiffer regions when subjected to gradient stiffness (Singh et al., 2008).

To conclude, the control of biomaterial surface properties, availability of ligands for cell adhesion and microenvironments where cells interact with the substrate are vital factors in cell behaviours, including attachment, proliferation and differentiation.

2.11 Basis and aims of this research

In addition to the literature presented above, this research was founded on the scaffold preparation and characterisation techniques developed at the Biomaterials Group, Department of Materials, University of Oxford (Wahl and Czernuszka, 2006, Gotora and Czernuszka, Liu et al., 2009, Dawson et al., 2007a, Dawson et al., 2007b, Dawson et al., 2008, Lawson and Czernuszka, 1999, Sachlos et al., 2003, Wahl et al., 2007, Walton et al., 2010), and the extraction and preparation techniques used by the Collagen Research Group of the Veterans Affairs Medical Centre Research Service, University of Tennessee (Brand et al., 2003, Brand et al., 2007, Brand et al., 2002).

The relevant literature revealed that following the natural structure, composition and biology of the target tissue, in this case cartilage, is one way to engineer tissue; however, due to the poor capacity of renewed cartilage to integrate biologically and mechanically with surrounding tissue, scaffold/implant loosening is a major limitation of this method. Moreover, the regenerated tissue usually has inferior mechanical properties. Therefore, fabricating an osteochondral scaffold, which includes both cartilage and subchondral bone, could be a potential solution for both integration with the host tissue and recruitment of MSCs residing in subchondral bone. Figure 2.21 shows a schematic illustration of the proposed design of a multilayered scaffold mimicking the structure/composition of cartilage and subchondral bone. This is based on the biomimetic approach to osteochondral regeneration as well as the incorporation of layers to simulate the interface between bone and cartilage (see Section 2.4)

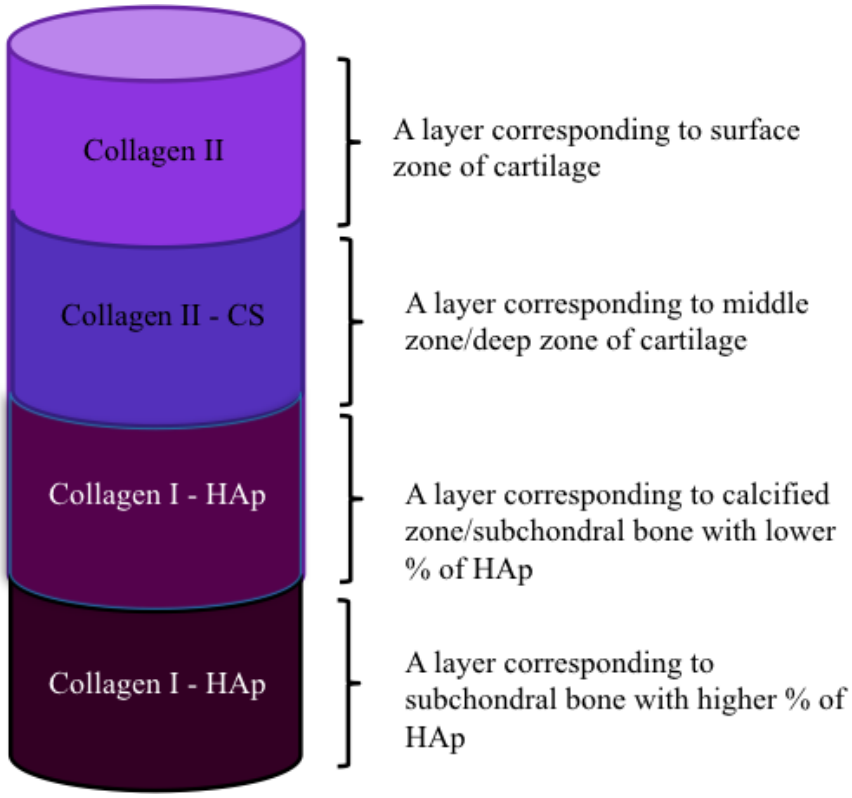


Figure 2.21 Proposed scaffold for osteochondral TE

It is apparent from the literature on the scaffold material for bone and cartilage TE (see Section 2.8.1) that the most commonly used natural material (i.e. collagen) is utilised in its insoluble, naturally fibrillar form. Due to existing crosslinks, this may lead to batch variation. In addition, an antigenic response is usually connected with the existence of telopeptides. Consequently, the soluble form of collagen 'atelocollagen' is proposed as an alternative material. To the author's knowledge, no previous studies have produced atelocollagen afibrillar and reconstituted fibrillar types I and II scaffolds with the incorporation of CS and hydroxyapatite, systematically characterising both in terms of their properties.

Therefore, the development of novel conjugated atelocollagen types I and II collagen scaffolds for bone and cartilage TE appeared to be the logical step to address this gap in the literature.

Thus, the principal aims of this research are as follows:

1) Develop layers of an osteochondral scaffold comprising a layer corresponding to bone and a layer corresponding to cartilage by following the natural composition of the bone and cartilage interface, using different types of collagen (types I and II), and other major components of these tissue (i.e. hydroxyapatite and CS)
2) Investigate the properties of such porous composite scaffolds fabricated from telopeptides-free collagens in afibrillar and reconstituted fibrillar form, in terms of their structures, microstructures, mechanical properties and rheological properties, and evaluate the stem cell response to these scaffolds

Chapter 3. Experimental Procedures: Scaffolds Fabrication

3.1 Introduction

Collagen-based scaffolds in tissue engineering have the potential to become a viable extracellular matrix for bone, cartilage and osteochondral regeneration.

In this chapter, monomeric type-I and type-II collagen-based preparations and scaffolds were fabricated (Section 3.2). The first section (Section 3.2.2) describes the preparation of collagen-based suspensions, while dialysis and *in vitro* fibrillogenesis procedures are described in Section 3.2.3. Scaffold fabrication by freeze drying is explained in Section 3.2.4.

3.2 Preparation of collagen-based scaffolds

This section explains the synthesis of afibrillar and reconstituted fibrillar collagen type-I with/without hydroxyapatite and afibrillar and reconstituted fibrillar collagen type-II with/without chondroitin sulphate in suspension and scaffold forms.

3.2.1 Materials

All the consumables and reagents were purchased from Sigma Aldrich or Fischer Scientific, unless otherwise stated. Hydroxyapatite (nano powder, <200nm) and chondroitin sulphate A (from bovine trachea) were supplied from Sigma-Aldrich (Poole, Dorset, UK). Type I pepsin-digested atelocollagen monomers extracted from foetal calf skin, and type II pepsin digested atelocollagen acid extracted from foetal calf cartilage were in lypholised form provided by Dr. David Brand, Veterans Affairs Medical Center, Tennessee.

3.2.2 Collagen solutions

Pure afibrillar collagen solutions (type I and II) were produced by adding lypholised monomers to dilute acetic acid (pH 3.2) to achieve the target concentration of 0.5% (v/w) (0.5 g of collagen in 100ml of solution). The preparations were then homogenised three times for 1 min in a glass beaker surrounded by ice to keep the temperature at 4 °C, using a hand-held blender (Braun 400W). The air bubbles were removed using centrifugation (IEC CL10, Thermo Electron Corporation) at 5000 rpm for 5 minutes.

To produce afibrillar type I-HAp (1:1 and 1:3 wt) solutions, 0.5g and 1.5g of HAp, and to produce afibrillar type II-CS solution (1:1 wt) 0.5g of CS, were dissolved in acetic acid (pH: 3.2) respectively, and added drop-wise during homogenisation of collagen to prevent sharp changes

in pH. Air bubbles were removed through vacuum degassing to preserve homogeneity of the suspensions. Collagen solutions were stored in centrifuge tubes at 4 °C, until required.

3.2.3 Dialysis and Fibrillogenesis

Monomeric collagen solutions were induced to form reconstituted fibrillar structure under certain conditions. In order to provide the suitable ionic strength and pH conditions, monomers were moved to a neutral salt solution via dialysis. Then, in order to prompt fibrillogenesis, the temperature of the dialysed monomeric solutions were raised- in this case to 37°C as a representation of human body temperature.

10-15ml of collagen solutions/suspensions (as prepared in Section 3.1.2) were syringed in dialysis tubing (Spectra/Por 4 dialysis tubing, 12-14K MWCO, 45mm flat-width) and dialysed at 4°C twice against 1L of *Tris*-buffered saline (TBS) solution (50mM tris-(hydroxymethyl)-aminomethane, 150mM sodium chloride, pH 7.4). At the end of this period, the monomers were collected from the tubing and syringed in centrifuged tubes and kept at 4°C until required.

The dialysed monomers were placed in an incubator at 37°C for 4hrs to allow formation of fibrillar gels or precipitation in solution. They were kept at 4°C, until required. Scaffold combinations are summarised in Table 3.1.

Table 3.1 Collagen solution types and acronyms used throughout the text.

Collagen type		**Hydroxyapatite (collagen:HAp weight ratio)**	**Chondroitin sulphate (collagen:CS weight ratio)**	**Acronym**
Type-I	Afibrillar	0		*1af*
		1:1		*1af-HAp 1:1*
		1:3		*1af-HAp 1:3*
	Reconstituted fibrillar	0		*1rf*
		1:1		*1rf-HAp 1:1*
		1:3		*1rf-HAp 1:3*
Type-II	Afibrillar		0	*2af*
			1:1	*2af-CS*
	Reconstituted fibrillar		0	*2rf*
			1:1	*2rf-CS*

This procedure was used by Walton (2010) for pure collagens of the same type and source, and fibril formation was confimed by turbidity measurements, Atomic Force Microscopy and Transmission Electron Microscopy (TEM) (Walton, 2010), as shown in Figure 3.1.

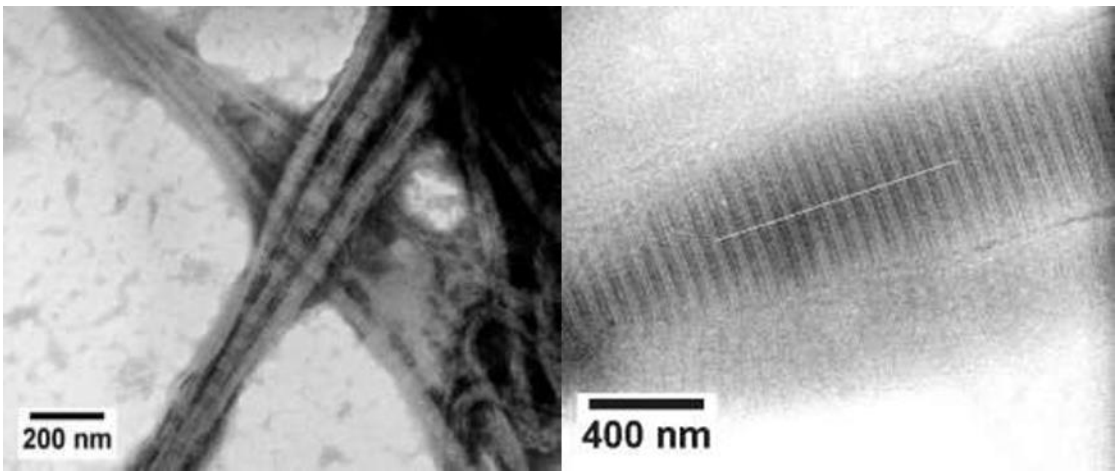


Figure 3.1 TEM micrographs of reconstituted fibrillar type-I atelocollagen (left) and of reconstituted fibrillar type-II atelocollagen (right) (Walton, 2010)

3.2.4 Casting and Freeze-drying

Two different types of casting moulds were made to produce appropriate scaffold sizes for characterisation and cell work as illustrated in Figure 3.2 and Figure 3.3. For the former, moulds were made from plastic tubing with dimensions of 1.5mm wall thickness, 8mm diameter and 12mm length) and for the latter, they were made from PTFE, 6mm inner diameter and 4mm length. The reason for smaller moulds for cell work was the large number of samples required with a limited supply of collagen. Moulds were sealed at one end with PTFE tapes.

Collagen solutions/suspensions (as described in Section 3.2.2) were syringed into the prepared moulds and were then transferred to a freezer set to -20°C and left to freeze overnight.

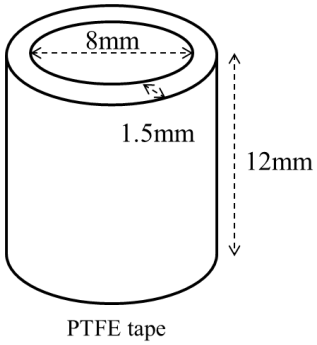


Figure 3.2 Plastic tubing mould to produce samples for characterisation

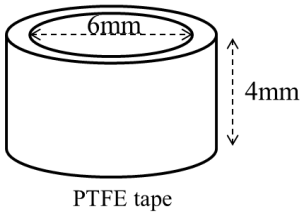


Figure 3.3 PTFE mould to produce samples for cell study

Freeze-drying or lypholisation is a process of removing water from frozen samples via sublimation, which creates a porous three-dimensional structure. The freeze-dryer used was an

Ehriss (Alpha I-5) equipped with an Edwards vacuum pump (Edwards Limited, UK). The frozen samples were moved to the freeze-drying chamber quickly and freeze-dried for 24 hrs. After that, samples were removed from the machine and their respective moulds.

Chapter 4. Fourier Transform Infrared Spectroscopy

4.1 Introduction

The interaction between constituents of scaffolds as well as changes in their molecular structure can have significant effects on the behaviour of preparations (e.g. viscosity) and subsequently properties of scaffolds (e.g. mechanical, microstructure, cell behaviour, etc.). This chapter studies the molecular structure and chemical bonding between collagen type-I with hydroxyapatite and collagen type-II with chondroitin sulphate as well as changes in the systems by fibrillogenesis.

The objective of this chapter is to develop an understanding of scaffold structure at molecular levels using *Fourier Transform Infrared Spectroscopy*. The first section (Section 4.2) explains the experimental procedure for performing Fourier Transform Spectroscopy on samples. The results are presented in Section 4.3 and discussed in Section 4.4. A summary of findings are presented in Section 4.5

The hypothesis of this chapter is that the molecular interactions between chondroitin sulfate, collagen type-II, hydroxyapatite and collagen type-I occur within the synthesised composite scaffolds.

4.2 Experimental Procedures

FTIR spectroscopy is a technique in which transmission of infrared (IR) light through a thin sample section is measured as a function of wavelength. The transmitted IR light is detected, which states how much energy was absorbed at each wavelength. Each wavelength is characteristic of a specific molecular vibration, which makes the IR spectra useful for determining these chemical bonds. Infrared absorption at specific wavelength (A) is related to the concentration of the different molecular species (c) in a sample according to Beer-Lambert:

$$A = log\frac{I}{I_0} = \varepsilon bc$$

Where ε is the wavelength-dependent absorptivity coefficient, b is the optical path length of light, i.e. thickness of the sample section, and I and I_0 are intensities of sample and reference, respectively (Saarakkala et al., 2010).

FTIR spectroscopic imaging is one of the well-established experimental techniques for the analysis of secondary structure of polypeptides and proteins. However, analysis of FTIR spectroscopic data is complicated since absorption peaks of different components often overlap with each other (Rieppo et al., 2012).

In this case, collagen and chondroitin sulphate show significant absorption in same regions of the spectrum. To resolve this problem, second derivative spectroscopy was used which enhanced the separation of overlapping peaks. Here, the registered raw spectrum is numerically differentiated twice. The peak frequency is identical to the original one and intensity of the second derivative is proportional to the original peak intensity (Susi and Byler, 1983). The

second derivative spectra are calculated by using Savizky–Golay algorithm (smoothing polynominal order: 2, points window: 20) in OriginPro 8.1. The samples were analysed in absorbance mode at 4 cm^{-1} (cm^{-1} refers to the wavenumber) resolution 64 times over the range of 500–4,000 cm^{-1} using an Agilent FTS 3500 Excalibur.

4.2.1 Statistical Analysis

Three samples per group were tested (n=3), and the average spectra was calculated and used for all the analysis. There were no shifts in peak frequencies across triplicates. The changes greater than 4 cm^{-1} in peak frequencies across groups were considered as significant.

4.3 Results

The FTIR spectra of all collagen containing samples showed characteristic collagen amide I, II and III bands. Figure 4.1 and Figure 4.2 show the averaged (n = 3) FTIR spectra of collagen type-I and II scaffolds, respectively. Figure 4.3 and Figure 4.4 show the second derivative of the spectra. Band assignments for the second derivate spectra of collagen, HAp and CS are shown in Table 4.1 and Table 4.2. CH_2 side chain vibration peak at 1338 cm^{-1} is an important characteristic feature of collagen, which was determined in all of the collagen-containing samples.

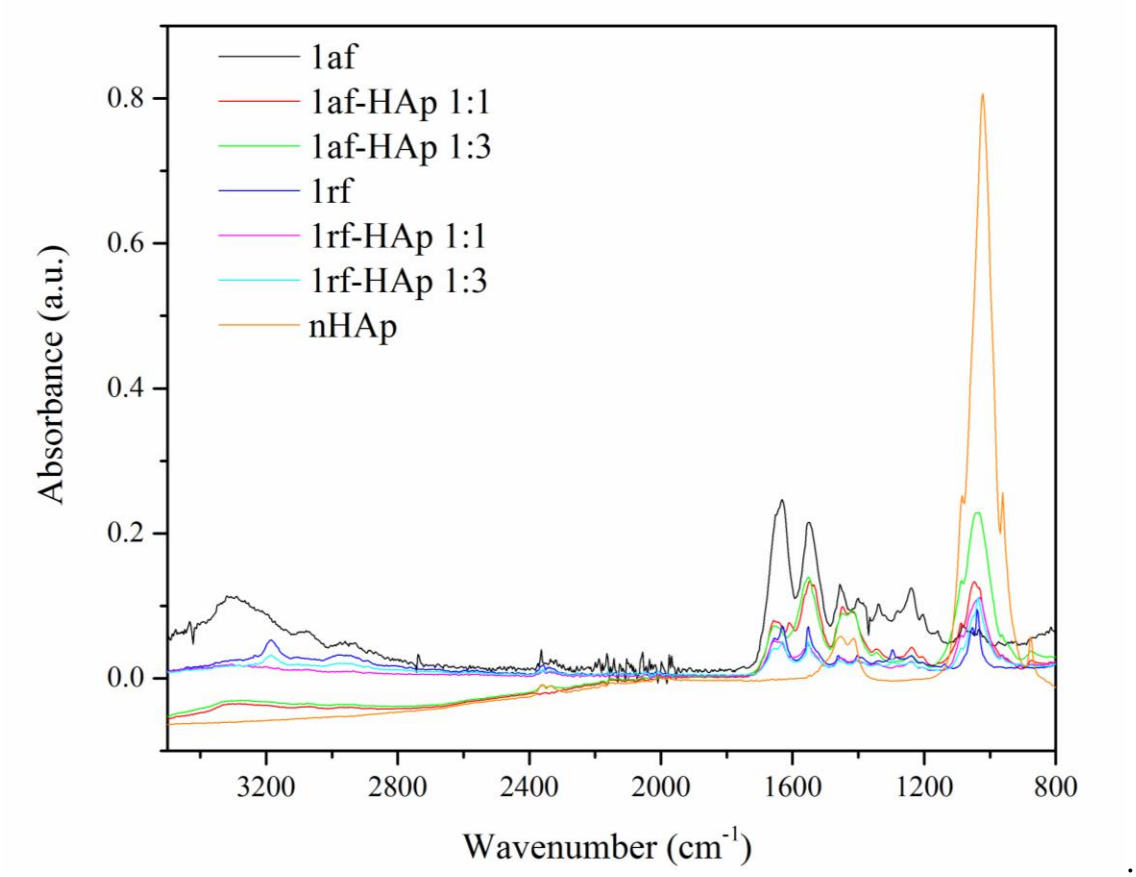


Figure 4.1 FTIR spectra of type-I composite scaffolds (n=3) in 800-3500cm^{-1} range

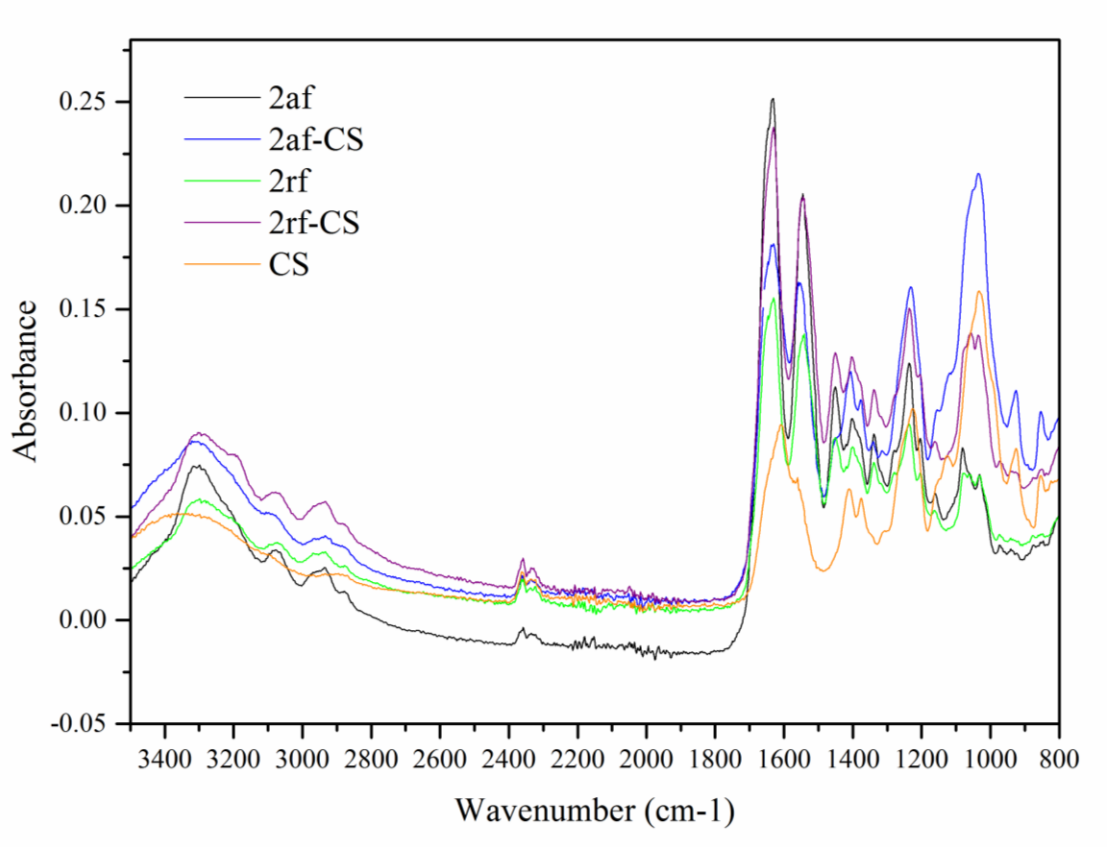


Figure 4.2 FTIR spectra of type-I composite scaffolds (n=3) in 800-3500cm^{-1} range

Table 4.1 FTIR second derivative band assignment in type-I composite scaffolds; # denotes a shoulder rather than peak. The unit is cm^{-1} and refers to the wavenumber

Band Assignment	***1af***	***1af-HAp 1:1***	***1af-HAp 1:3***	***1rf***	***1rf-HAp 1:1***	***1rf-HAp 1:3***	***nHAp***	***Ref***
Amide A	3331	3326	3326	3306	3303	3303		(Doyle et al., 1975)
Amide I	1640	1655, 1620#	1655	1640, 1673#	1648, 1616#	1641, 1673#		
Amide II	1547	1544	1552	1547	1549	1545		
Amide III	1243	1240	1240	1240	1240	1240		
Carboxyl group with wagging of proline	1334, 1327#	1331	1331	1339	1331	1339		
P-O stretching in PO^{-3}_4	-	941, 1043	941, 1038	-	941, 1037	941, 1037	955, 1021	(Slosarczyk et al., 1997)

Table 4.2 FTIR second derivative band assignment in type-II composite scaffolds; the unit is cm^{-1} and refers to the wavenumber

Band Assignment	*2af*	*2af-CS*	*2rf*	*2rf-CS*	*CS*	*Ref*
Amide A	3321	3321	3323	3323	-	(Doyle et al., 1975)
Amide I	1628, 1656	1633, 1657	1628, 1657	1628, 1657	1606, 1651	(Doyle et al., 1975)
Amide II	1549	1553	1549	1550	1554	(Doyle et al., 1975)
C-H deformation in collagen/ C-O stretching in CS/ COO- stretch of amino side chain	1397 1379	1409 1374	1398 1377	1402 1376	1412 (C-O) 1373 (C=O)	(Rieppo et al., 2012)
C-O stretching/asymetric of hydroxyl in CS and collagen	1079/ 1120	1073/ 1124	1078 1123	1078/ 1125	1066/ 1126	(Rieppo et al., 2012, Tian et al., 2013)
Amide III in collagen / S=O	1237	1231	1237	1237	1220	(Saarakkala et al., 2010, Tian et al., 2013, Foot and Mulholland, 2005)
-O-SO3 stretching and C-O-S stretching	845	853	846	846	854	(Tian et al., 2013)

In type-I scaffolds, addition of HAp to *1af* and *1rf* significantly downshifted the Amide A bands. In afibrillar scaffolds, Amide I peak shifted from 1640 cm^{-1} to higher wavenumber of 1655 cm^{-1} in *1af-HAp 1:1* and *1:3* and in *1rf* from 1640 cm^{-1} to 1648 cm^{-1} (*1rf-HAp 1:1*), Amide II peak from 1547 cm^{-1} in *1af* to higher wavenumber of 1552 cm^{-1}, and CH_2 from 1340 cm^{-1} to 1333 cm^{-1} in *1rf-HAp 1:1*. Peaks of PO^{-3}_4 appeared in all of HAp-containing samples with a shift from 955 cm^{-1} in pure HAp to lower wavenumbers of 941 cm^{-1}.

Fibrillogenesis shifted the Amide A and I peaks in HAp containing samples to lower wavenumbers, Amide II peaks of HAp containing sample *1af-HAp 1:1* to higher wavenumbers

and *1af-HAp 1:3* to lower wavenumbers, CH_2 bands shifted to higher wavenumbers in *1af* compared to *1rf* and *1af-HAp 1:3* compared to *1rf-HAp 1:3*, PO^3_4 to lower wavenumbers in *1af-HAp 1:1* compared to *1rf-HAp 1:1*.

In case of type-II scaffolds, the afibrillar (*2af*) and fibrillar (*2rf*) collagen spectra closely match, with no significant changes (<4 cm^{-1}) in frequency of the characteristic peaks. There were no significant changes in Amide A bands. Amide III peaks (1200, 1237 and 1280 cm^{-1}) shifted significantly in *2af-CS* sample compared to *2af* and CS.

All of the samples showed Amide I, II and III peaks, while there is a significant shift in their frequencies in *2af-CS*. In *2af-CS*, other significant changes were at 1079 cm^{-1} (C–O) stretching of carbohydrate residues in collagen and PGs), 845 cm^{-1} and 1120 cm^{-1} (C–O-S stretching) and 1397 cm^{-1} (COO- stretching of amino side chains). These shifts were not observed in *2rf -CS* scaffolds.

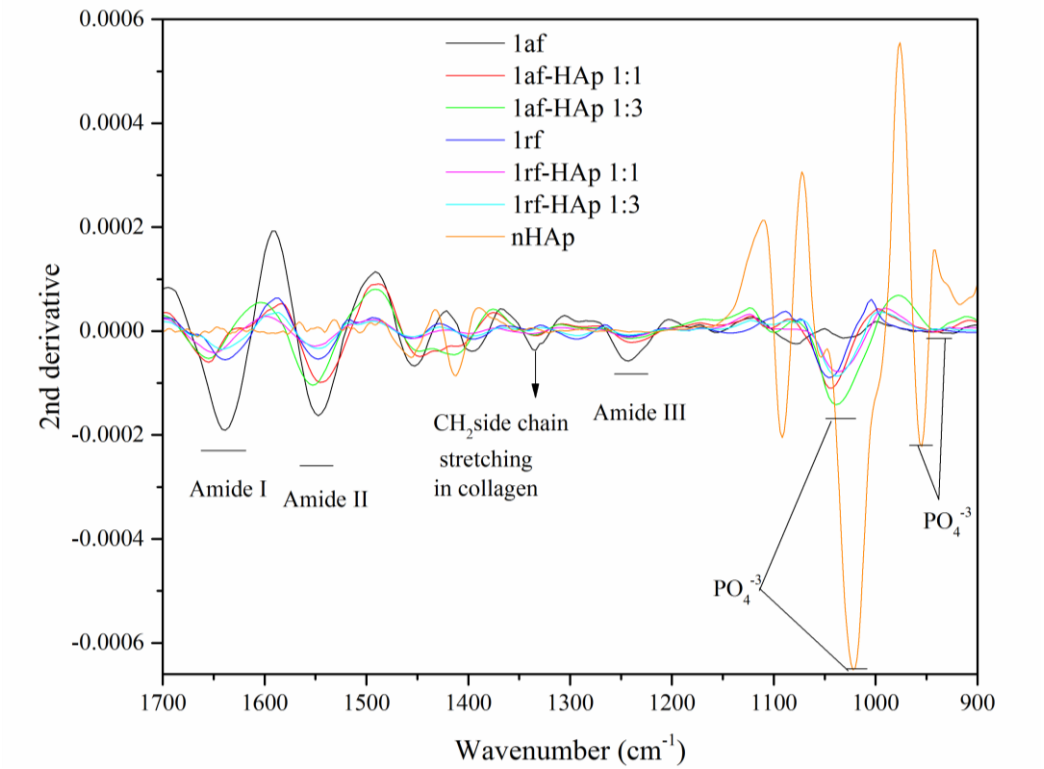


Figure 4.3 Second derivative spectra (900-1700 cm-1) of type-I composite scaffolds

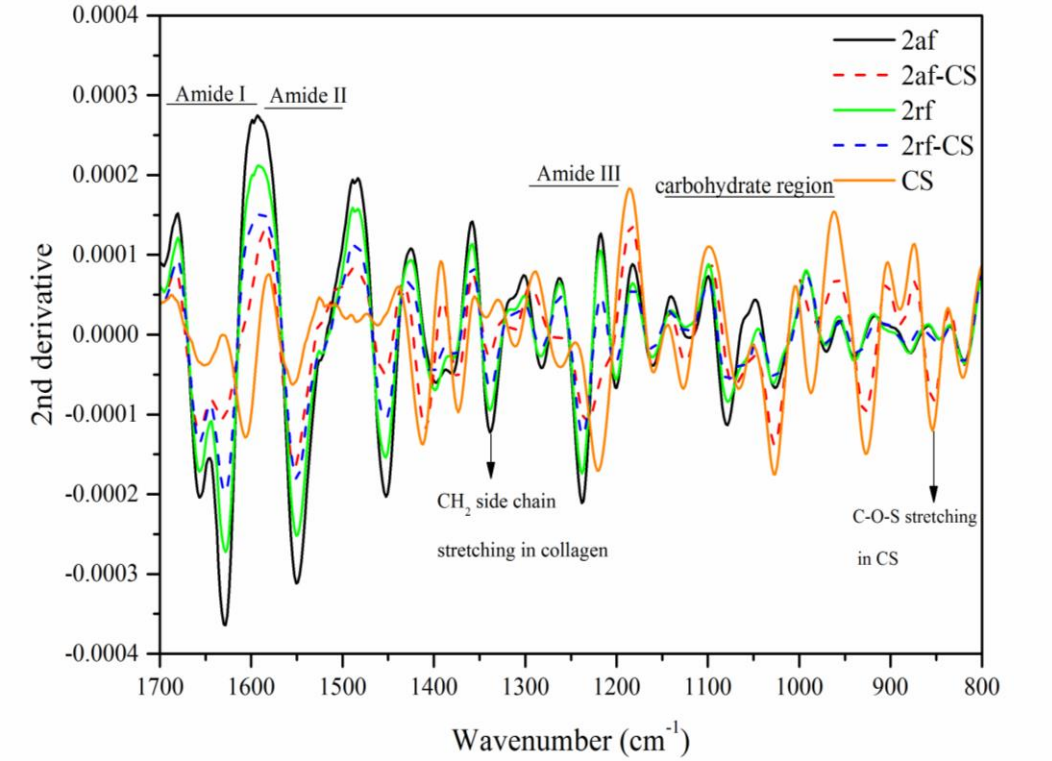


Figure 4.4 Second derivative spectra (800-1700 cm-1) of type-II composite scaffolds

4.4 Discussion

All samples containing collagen disclosed the Amide A, I, II and III bands. These bands are assigned according to the literature as indicated in George & Veis, (1991), confirming that the primary structures were maintained during scaffold fabrication (George and Veis, 1991). The FTIR spectra for all polypeptides and proteins also yields bands that are very sensitive to conformational changes in the polypeptide backbone and hence may serve as markers for the integrity of the secondary structure (Bandekar, 1992, Kong and Yu, 2007, Barth, 2007, Chang and Tanaka, 2002). For most of the proteins the marker is the Amide I band, where its frequency is found to be independent of the underlying amino acid sequence. However, for a triple-helical polypeptide such as collagen, such independence is not observed, as both the amino acid composition and protein secondary conformation contribute to this band (Doyle et al., 1975). Therefore, this band was not selected as a determinant of the secondary structure of the preparations. The observed band frequencies do however serve as indicators of bond strength, as higher wavenumbers correspond to stronger bonds and lower wavenumbers indicate weaker bonds.

Collagen type-I and type-II both possess a secondary helical structure that is stabilized by hydrogen bonds arising between carboxyl and hydroxyl groups of three strand (2 [αI] and 1[αII] in the case of type-I, and 3[αII] in case of type-II), forming a supercoiled triple helical conformation as shown by the Amide A (N-H stretching of the core polypeptide and also basic amino acid side chains, *e.g.* lysine and arginine) band (Chang and Tanaka, 2002); the frequency of which determines the extent of supercoiling, as this leads to an angular distortion or

'lengthening' of hydrogen bonds. Amide A occurs with a frequency of around 3325-3330 cm^{-1} in collagen, about 25 cm^{-1} higher than in other polypeptides (Doyle et al., 1975).

In type-I preparations, the shift of this band to lower frequencies with mineralization (~5 cm^{-1}) and fibrillogenesis (~25 cm^{-1}) implies a decrease in the extent of supercoiling within helices (*i.e.* a less densely coiled or 'packed' triple helix). In the case of mineralization of collagen, the formation of a new bond between the amine group and PO^{-3}_4 on HAp (as detailed in Section 4.4.1), may serve to explain the less tightly coiled triple helix and the resultant weakening of the N-H bond and a shift to lower frequencies. As for reconstituted fibrillar scaffolds it is possible, owing to the subjection of resulting suspensions to temperatures of 37°C during the process of fibrillogenesis, that a partial denaturation of the collagen occurs and hence there is an accompanying reduction in the degree of supercoiling, as was seen in the gelatin spectra published by Doyle et al. (1975). Alternatively, this phenomenon may arise due to the hydrogen bond formation engendered by fibrillogenesis.

Regardless of the tested sample no substantial changes were observed in Amide A band of type-II. This observation indicated that the collagen triple helix structure was not affected by CS addition and fibrillogenesis. However, the ~10cm^{-1} difference between type-I to type-II may point out to the formation of a stronger hydrogen bond in type-II collagen. According to Grynpas et al., 1980, type II collagen due to its unique amino acid sequence and high content of glycosylated hydroxylysines possesses at least 2A higher lateral separation between its molecules compared to type-I collagen (Grynpas et al., 1980). This difference in 3D structures may contribute to higher wavenumber of Amide A in *2rf* compared to *1rf*.

Amide I bands arise from C=O (carbonyl) vibrational stretching along the polypeptide backbone are observed between 1600 and 1700 cm^{-1}, with minor C-N stretching vibrations and N-H bending (Chang and Tanaka, 2002). In contrast, Amide II bands are more complex, arising mainly from an out-of phase combination of N–H in-plane bending (60%) combined with C–N stretching vibrations (40%) of the peptide bonds (Chang and Tanaka, 2002). Finally, amide III bands mainly result from C–N stretching and N–H deformation vibrations (Chang and Tanaka, 2002), while the peaks between 1331-1339 cm^{-1} are due to the presence of a dissociated carboxyl group (COO^-) from the proline side chain.

4.4.1 Changes in molecular structure of Type-I scaffolds

Collagen telopeptides provide a catalytic role during fibrillogenesis and may stabilise the quaternary structure via formation of covalent cross–links. However, all the information required for self-assembly during fibrillogenesis is encoded in the collagen triple helix itself. In turn, the triple helix directs the fibrils organisation through hydrophobic and Van der Waals interactions between non-polar side chains or hydrogen bonding (Kuznetsova and Leikin, 1999). Distinct changes in Amide I bands resulting from the fibrillogenesis of the mineralised scaffolds are manifested by lower frequencies observed during FTIR investigations. This observation may be associated with the formation of hydrogen bonds upon fibrillogenesis in composite scaffolds, which in turn may change the local conformation of the polypeptide backbone (Arrondo and Goni, 1999).

It can be speculated that in pure *1af* scaffold intermolecular interactions, involving N-H bonds have a more pronounced effect on the fibril formation, rather than hydrogen bonds involving the C=O groups, shifting Amide A peak to lower frequencies, while having no effect

on the position of the Amide I band. In composite scaffolds, however, the bonds between triple helices are considered to be represented by C=O···H hydrogen bonds, shifting Amide I bands to lower wavenumbers in *1rf-HAp 1:1* and *1rf-HAp 1:3*.

In type-I composite scaffolds, the interaction and bond formation between collagen and HAp was established by the observed changes in the position and magnitude of specific peaks frequencies. The carboxyl and amino groups are responsible for the approximately 20% of the amino acid residue on a collagen molecule what makes them ideal targets for calcium and phosphate ions originated from HAp (Kikuchi et al., 2001). For this reason, the carboxyl peak shifted to lower wavenumbers in afibrillar scaffolds upon addition of both HAp (*1af-HAp 1:1* and *1af-HAp 1:3)* and reconstituted fibrillar *1rf-HAp 1:1*, while Amide I peaks shifted to higher wavenumbers. This observation can be explained by an electrostatic interaction and formation of a covalent bond between Ca^{2+} ions and carboxylate groups (C=O and C-O) as well as stabilisation of the carboxylate mezomeric form as represented in the Figure 4.5 (Chang and Tanaka, 2002, Wang et al., 2006, Ficai et al., 2009). As it is clear from Figure 4.5, without HAp, the two CO bonds are cvasi double, while the addition of this reagent strengthen the double bond (C=O) and weaken the single bond (C-O) (Grynpas et al., 1980, Ficai et al., 2009) thus shifting the amide I and carboxyl bands to higher and lower wavenumbers, respectively, as observed in the corresponding spectra (Ficai et al., 2009) .

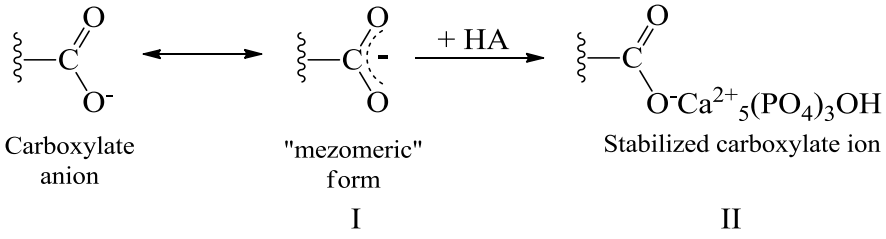


Figure 4.5 Collagen and HAp interaction and bond formation, redrawn from (Ficai et al., 2009)

It was also observed that the non-degenerate P-O symmetric stretching (*v1*) of PO^{-3}_4, shifted from nHAp to lower wavenumbers (14 cm^{-1}) in composite scaffolds, showing the formation of a new chemical bond between the phosphate ion in HAp and the amino groups (NH^{3+}) in collagen (Brand et al., 2002).

4.4.2 Changes in molecular structure of Type-II scaffold

As it was manifested by Figure 4.4 the Amide I region of collagen showed two distinct peaks in the spectra of the second derivative. The observed band complexity is explained by the coupling between similar carbonyl groups or the heterogeneity between different carbonyls located in the same backbone having dissimilar intrinsic basicity or conformational distinctions due to strength of hydrogen bonding (Kuznetsova and Leikin, 1999). In general, the peaks in the amide I region are associated with three carbonyl groups of Gly-X-Y, where Gly and Y are almost always in contact with the solvent, while X (proline), which is considered to be responsible for the formation of a 1660 cm^{-1} band, is susceptible to conformational changes due to internal H-bond (Susi and Byler, 1983). Using the second derivative method it was possible to detect two of three amide groups at ~1630 and ~1657cm^{-1}, where the former amide group showed a considerable upshift from *2af* → *2af-CS* while the latter group remained constant through all of the preparation. Based on the observations above it can be stated that

fibrillogenesis and CS-addition did not have any effect on carbonyl groups of proline, pointing out to the preservation of the internal H-bonds during interaction with CS or other triple helices during fibrillogenesis and preservation of triple helix conformation. The band at 1628 cm^{-1}, however, has been associated with the hydroxyproline carbonyl group, which shifted towards higher wavenumbers, indicating an interaction with CS, disturbed by fibrillogenesis and the shift of the peak back to 1628 cm^{-1}.

It has been shown that addition of PGs and GAGs may hinder lateral fibril growth by sterically hindering the approach of additional collagen molecules or through anionic repulsion when the indicated glycans are attached to collagen(van Susante et al., 2001). Moreover, Öbrink et al. (1975) found out that there are at least three binding sites on each collagen molecule, able to interact with CS-4. The number of these sites remains constant, however, with increasing ionic strength the binding affinity decreases due to the fact that some of the bonds between collagen and CS in acidic environment are weakened and abolished during fibrillogenesis (Obrink et al., 1975, Obrink, 1973). Therefore, the combined obstruction effect during fibril formation, as well as the effect of increasing pH and ionic strength in physiological conditions, resulted in lesser proportion of collagen incorporating into fibrils and lower amount of CS attaching to collagen. This conclusion was supported by the fact that no significant changes were observed in spectra of *2rf-CS*.

Figure 4.6 shows the molecular structure of collagen and CS, with potential sites for their interaction. Since CS is an anionic polymer, it is expected to interact with cationic regions of collagen. However, the chemical binding of CS to collagen is still not fully understood and yet to be investigated (Tian et al., 2013). However, it is generally accepted that the interaction between

collagen and CS is of electrostatic nature (Snowden and Swann, 1980, Gelman and Blackwell, 1973, Tian et al., 2013, Lindahl and Hook, 1978) under physiological condition or outside of the isoelectric point of collagen and CS. It was also revealed that this interaction was not only electrostatic, but also could be of other types such as hydrogen bonding (Tian et al., 2013). For instance, in neutral pH, close to the isoelectric point of collagen, the net charge of collagen is very small; therefore, the interaction mechanism is expected to be mainly dictated by hydrogen bonding. This deduction can explain lack of any sulfate group shifts in *2rf-CS*, and the appearance of only one peak at 1398 cm^{-1}, assigned to carboxyl C-O group, shifted towards higher wavenumbers.

Tian et al. (2013) also showed that the interaction between collagen and CS could be of electrostatic origin (Tian et al., 2013). The corresponding groups could be sulfate or carboxyl group of CS and positively charged collagen side-chains such as arginine and lysine, since they are both cationic in the acidic and the physiological environment. Additionally, the hydrogen bond between hydroxyl (C-O) of CS and C=O of collagen could also take part in the investigated interactions. This can explain the shift in wavenumber of the band assigned to S=O stretching, carboxyl C-O and C=O stretching, and hydroxyl C-O stretching in *2af-CS*, which indicate interaction between collagen and CS.

However, variation in collagen source, pH, ionic concentration, GAG molecular weight, and collagen to GAG ratios can affect the interaction between collagen and CS and is the reason for some of the contradicting results in literature (Stuart and Panitch, 2008).

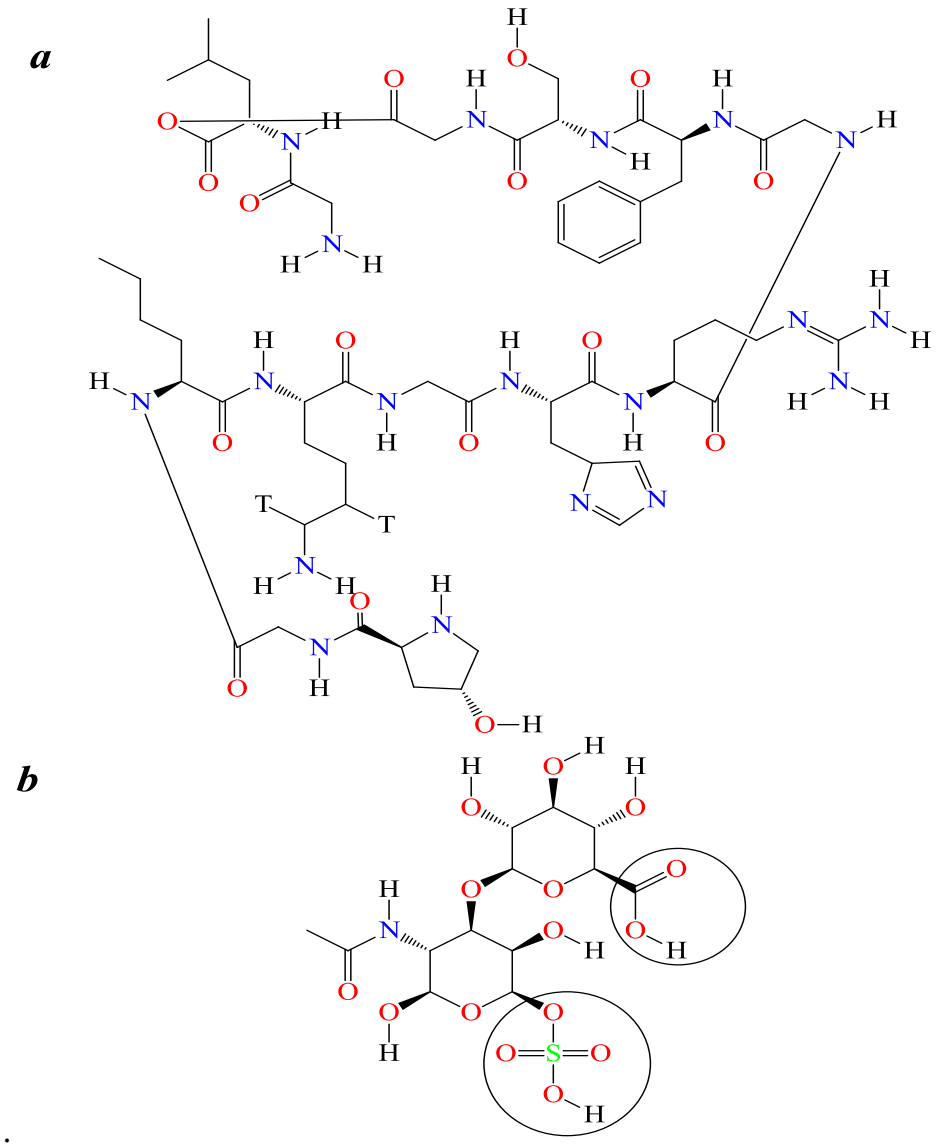


Figure 4.6 Proposed bonding between a) collagen and b) chondroitin sulphate. Circles indicate the sulphate and hydroxyl/carboxyl groups; drawings from (National Center for Biotechnology Information)

4.5 Summary

Mineralisation and fibrillogenesis lead to weakening of N-H bond and a less coiled triple helix in type-I scaffolds, but no such changes were observed in type-II scaffolds. It was shown that fibrillogenesis of pure type-I scaffolds involves N-H groups between triple helices, while fibril formation in composite scaffolds is most likely a result of hydrogen bonding involving C=O groups of collagen triple helices. The interaction between collagen type-I and HAp was confirmed by shifts in carboxyl and phosphate groups.

The adverse effect of CS on fibrillogenesis of collagen was confirmed by the FTIR spectra of *2rf-CS*. It was stipulated that the interaction between hydroxyproline carbonyl groups and CS is disturbed by fibrillogenesis. Moreover, the electrostatic interactions between negatively charged CS and positively charged side chains of collagen are weakened in physiological conditions. Therefore, it is concluded that addition of CS hindered fibrillogenesis, and although some side chains such as arginine stay cationic in physiological conditions and may contribute to some local binding of CS to reconstituted fibrillar collagen, fibrillogenesis destabilised most of the bonds between the two.

4.6 Conclusion

The goal of this chapter was to evaluate the molecular interactions between collagen type-I and HAp, and collagen type-II and CS. The hypothesized bonding between these constituents was confirmed by the observed shifts in the FTIR spectra of composite scaffolds as summarised in Section 4.5. It is thought that these molecular interactions can affect the viscosity,

which has further implications for the microstructure and mechanical properties of scaffolds. This will be examined in the next chapter (Chapter 5).

Chapter 5. Rheological properties of preparations

5.1 Introduction

Rheological properties of suspensions can aid to clarify the molecular state of collagen-CS and collagen-HAp systems. This is an extension to the chemical bonding studied in the previous chapter (Chapter 4), and will help to explain the microstructure and mechanical properties in the subsequent chapters (Chapter 6 and Chapter 7). The first section explains the experimental procedures (Section 5.2). The results are shown in Section 5.3, which are later discussed (Section 5.4) in terms of suspension behaviour during rotational (Section 5.4.1) and oscillatory shear (Section 5.4.2). A summary of findings are presented in (Section 5.5). It is hypothesized that molecular interactions between different constituents of scaffolds examined in Chapter 4, leads to differences in viscosity and rheological properties, which can in turn affect their microstructure (Chapter 6).

5.2 Experimental Procedures

The study of rheological properties attempts to determine the flow behaviour of a solution/suspension, which is responsive to the molecular structure of the fluid. The study of their viscoelastic behaviour can shed light on the freezing process of the solution/suspension and therefore has implications for the final scaffold pore structure.

A rheometer assesses the rheological properties of a complex fluid as a function of rate or frequency of deformation. The device either produces a shearing flow and measures the resulting stresses (strain controlled) or imposes a shearing stress and computes the resulting shearing rates (stress controlled) in rotational or oscillatory conditions. Strain controlled tests are usually the preferred method, especially in suspensions and weak gels, as the system inertia in a

stress-controlled tests can lead to unrealistic values (Baravian et al., 2006, Klemuk and Titze, 2009). First, flow behaviours of solutions/suspensions were examined by performing strain controlled rotational tests, then the viscoelastic properties of solutions, including storage modulus (G'), loss modulus (G"), complex modulus (G*) complex viscosity (η*), and loss tangent (tanδ) were determined in strain controlled oscillatory tests, both using an Anton Paar 301 with plate-plate geometry according to Equation 5.1, Equation 5.2, Equation 5.3 and Equation 5.4:

$$\sigma(t) = \gamma_0[G'(\omega)sin(\omega t) + G"(\omega)cos(\omega t)] \qquad \text{Equation 5.1}$$

Where shear stress (σ) produced by a small amplitude deformation is proportional to the amplitude of the applied strain (γ_0), which is sinusoidally varying in time (t). The regime of small amplitude straining in which stress can be represented by this equation is called the linear viscoelastic region (Larson, 1999).

$$\tan\delta = {G"(\omega)}/{G'(\omega)} \qquad \text{Equation 5.2}$$

Where tanδ is the loss tangent based on loss (G'') and storage (G') moduli.

$$G* \equiv G' + iG" \text{ and therefore, } |G^*| = \sqrt{G'^2 + G''^2} \qquad \text{Equation 5.3}$$

Where G* is the complex modulus of a viscoelastic material based on storage (G') and loss (G'') moduli.

$$\eta * = \eta' + i\eta"$$ Equation 5.4

Where $\eta *$ is the complex viscosity, $\eta' = {G''}/{\omega}$ and $\eta'' = {G'}/{\omega}$, and therefore, $|\eta^*| = \sqrt{\eta'^2 + \eta''^2}$.

The measuring head for the Toolmaster © was 50mm and the gap between the cylinder head and the base was set to 1mm. Approximately 0.7ml of the pure collagen solution or composite suspension was pipetted into the gap, the head was lowered and its surrounding was trimmed. Temperature was controlled at 20°C with a Peltier temperature control with accuracy of ±0.1°C. Each test was repeated 3 times and since they were similar, only the results from one test is shown and used in analysis.

Based on the physiological oscillatory motion in joints (<10 rad s−1) and angular frequency of ω=0.7 rad s−1, corresponding to joint movements at ordinary walking speed (Nishimura et al., 1998), it was decided to determine the Linear Viscoelastic Region (LVR) at angular frequency (ω) 10 rad/s, with strain amplitude (γ) of 0.1 to 100%.

Rotational sweeps were conducted within the LVR with shear rates ranging from 0.1-100 1/s and from 100 to 0.1 1/s to examine any possible changes in the system by subjecting to ascending and descending shears. Dynamic frequency sweeps were conducted within LVR, at 1% strain with angular frequency of 0.1 to 100%.

5.3 Results

The collagen preparations were analysed for their rheological properties and the results are shown in this section. The first part (Section 5.3.1), determines the Linear Viscoelastic Region of each suspension. All of the subsequent measurements must be performed within this linear region. The change of viscosity with shear rate, and also time-dependency of samples when subjected to ascending and descending shear rates are shown in Section 5.3.2. The third section (Section 5.3.3) evaluates the complex viscosity and modulus of preparations in a dynamic frequency sweep test.

5.3.1 Linear Viscoelastic Region (LVR)

In this section, the suspension response to increasing deformation amplitude (strain) is monitored at a constant frequency and temperature. The linear viscoelastic regions of different collagen preparations are shown in Figure 5.1 and Figure 5.2. While the sample is within the strain range for maintaining its structure, the storage modulus (G') is remained constant, which is also a measure of sample's stability. Beyond a critical strain (γ_c) the storage modulus will be a function of strain and declines.

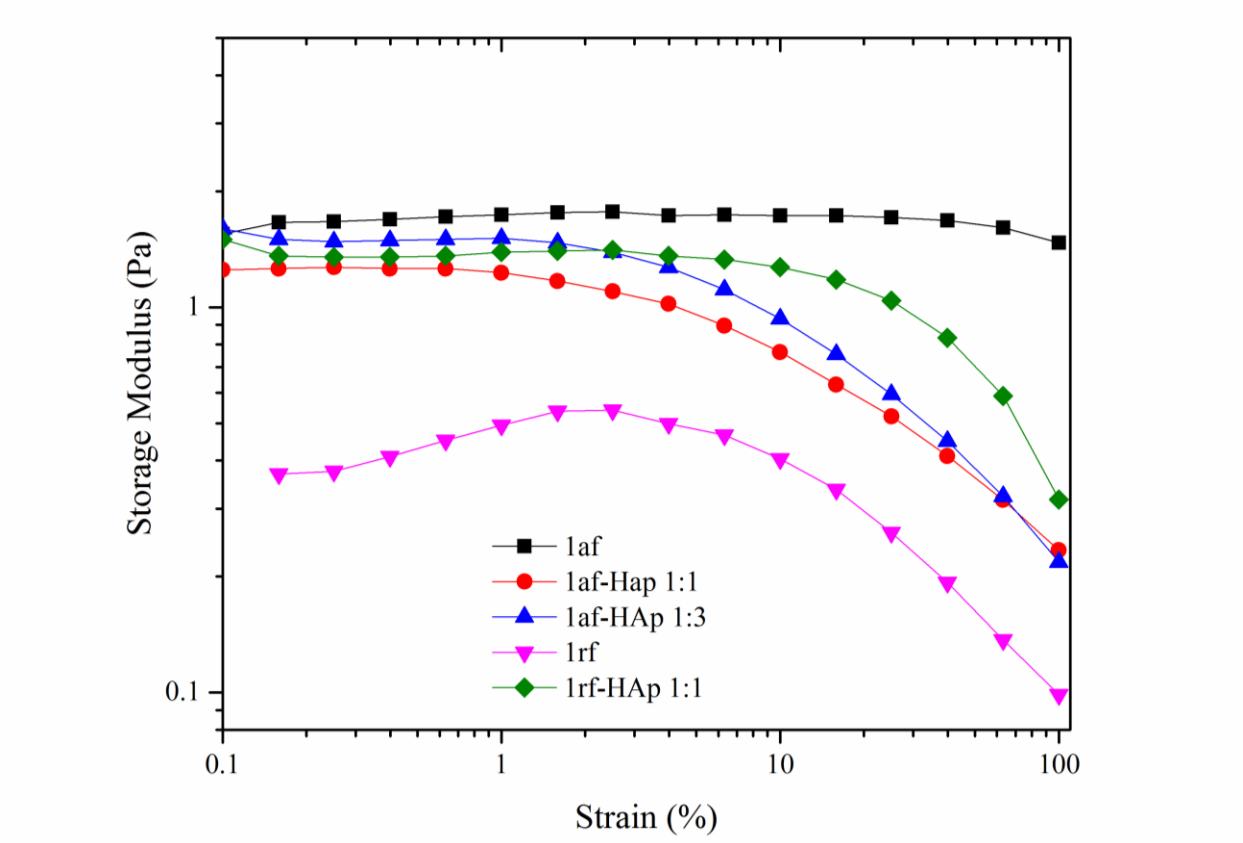


Figure 5.1 Storage modulus G' vs. strain of type-I collagen composite preparations in a strain sweep (0.1-100%) mode of an oscillatory shear test (strain=0.1-100%, T=20C)

From Figure 5.1 and Figure 5.2, it can be seen that the strain level of 1%, which was used for all of further examinations is within the LVR for all of the type-I and II preparations. It was observed that pure afibrillar collagen solutions *1af* and *2af* showed the highest stability according to the length of their LVR, compared to their reconstituted fibrillar counterparts and composite solutions.

The graphs in these two figures are rearranged in Figure 5.3 and Figure 5.4 in a way that show the effect of fibrillogenesis and particle/solute incorporation, respectively, on stability of suspensions.

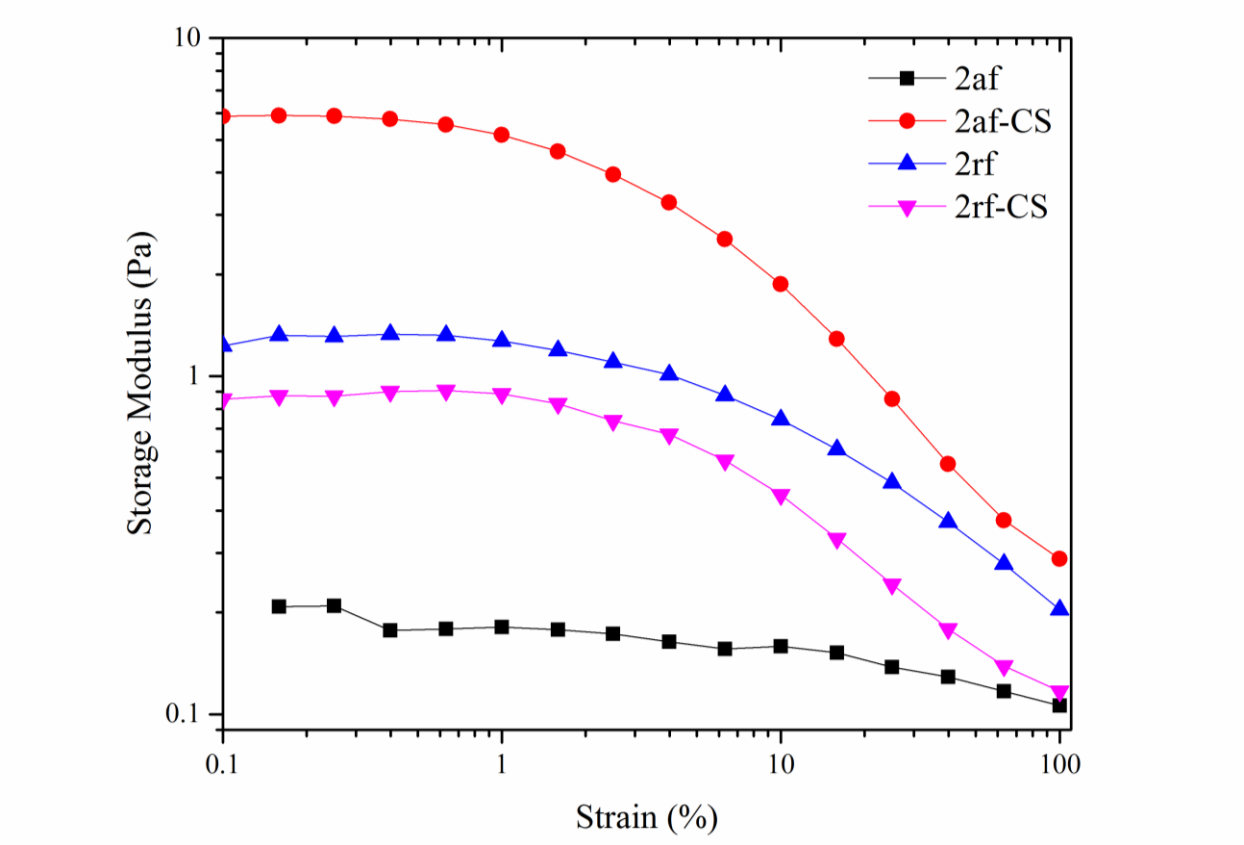
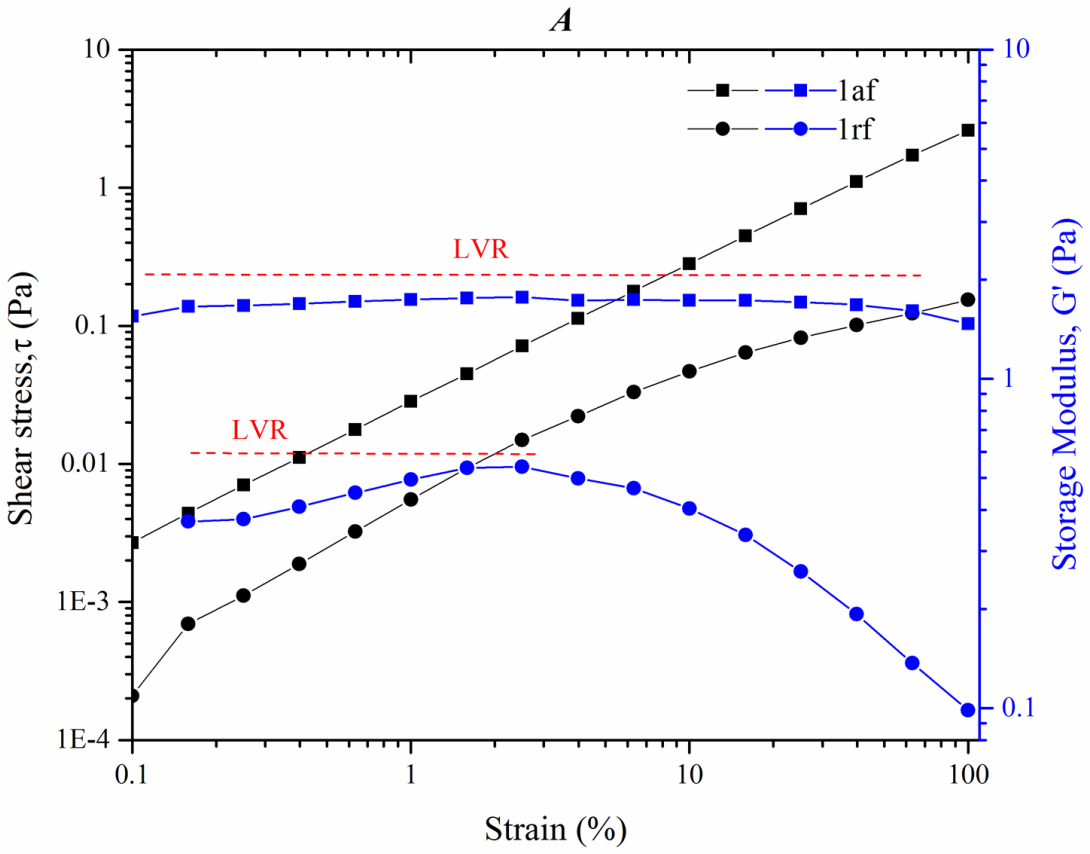
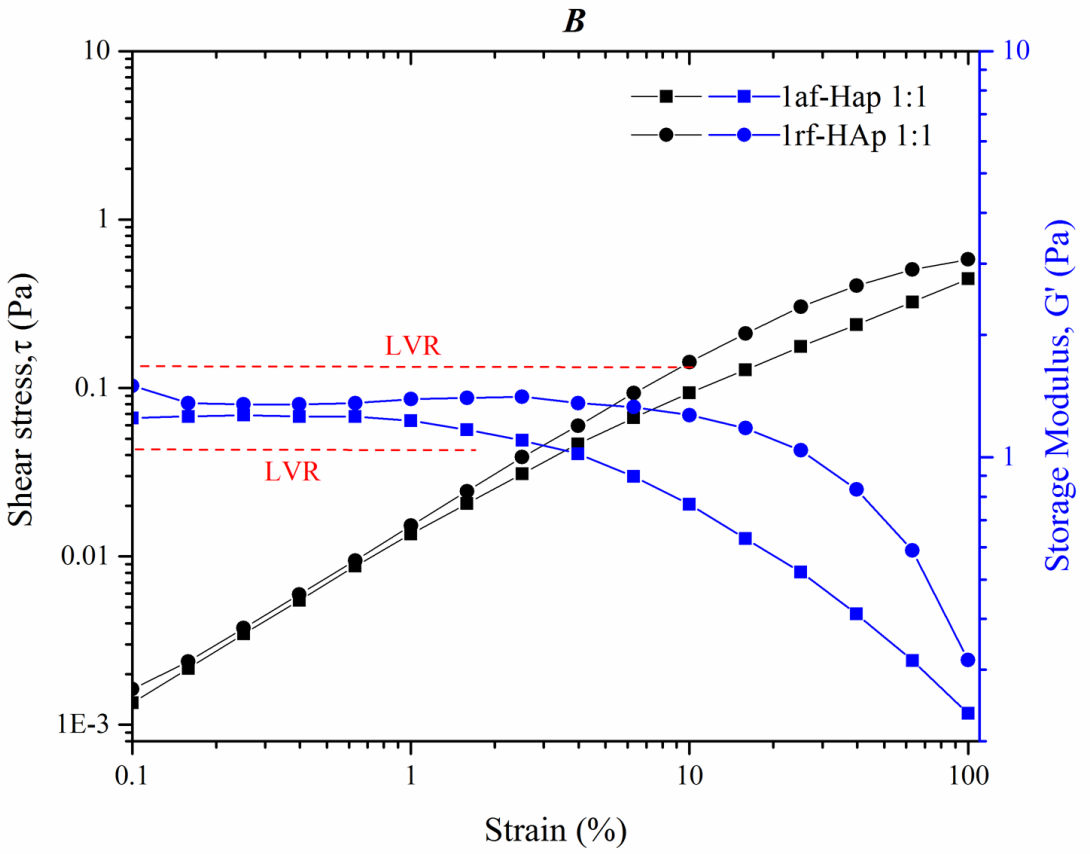
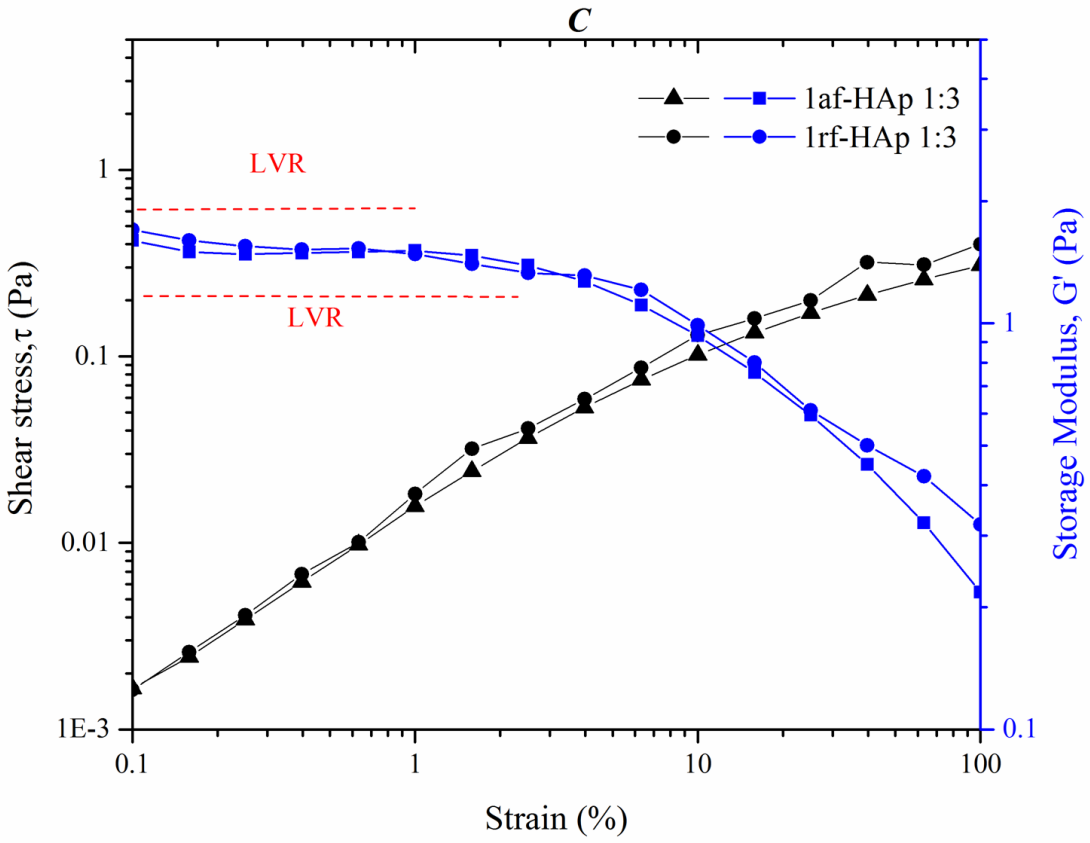


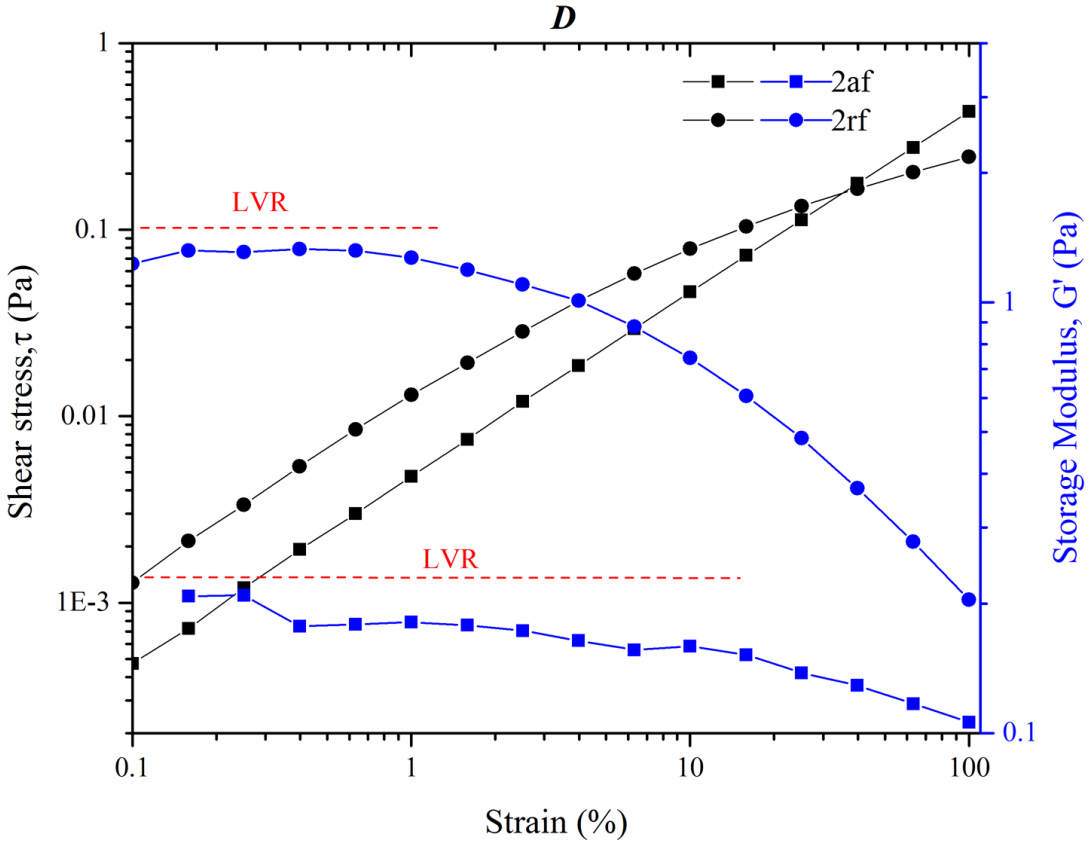
Figure 5.2 Storage modulus G' vs. strain of type-II collagen composite preparations in a strain sweep (0.1-100%) mode of an oscillatory shear test (strain=0.1-100%, T=20ºC)

Figure 5.3 examines the influence of fibrillogenesis on stability and stress/strain behaviour of suspensions. It can be seen that in case of pure collagen suspensions, fibrillogenesis (*1rf*, *2rf*) shortened the LVR and stability of suspension compared to afibrillar counterparts (*1af*, *2af*), while it stabilised *1rf-HAp 1:1* compared to *1af-HAp 1:1*. No changes were observed in other preparations with fibrillogenesis. In terms of stress-strain behaviour, *1af* and *2af* displayed linear curves over the examined strain range.


A
1af
1rf
LVR
LVR
Shear stress,τ (Pa)
Storage Modulus, G' (Pa)
Strain (%)
10
1
0.1
0.01
1E-3
1E-4
0.1
1
10
100


B
1af-Hap 1:1
1rf-HAp 1:1
LVR
LVR
Shear stress,τ (Pa)
Storage Modulus, G' (Pa)
Strain (%)
10
1
0.1
0.01
1E-3
0.1
1
10
100


C
1af-HAp 1:3
1rf-HAp 1:3
LVR
LVR
Shear stress,τ (Pa)
Storage Modulus, G' (Pa)
Strain (%)
1
0.1
0.01
1E-3
0.1
1
10
100


D
2af
2rf
LVR
LVR
Shear stress,τ (Pa)
Storage Modulus, G' (Pa)
Strain (%)
1
0.1
0.01
1E-3
0.1
1
10
100

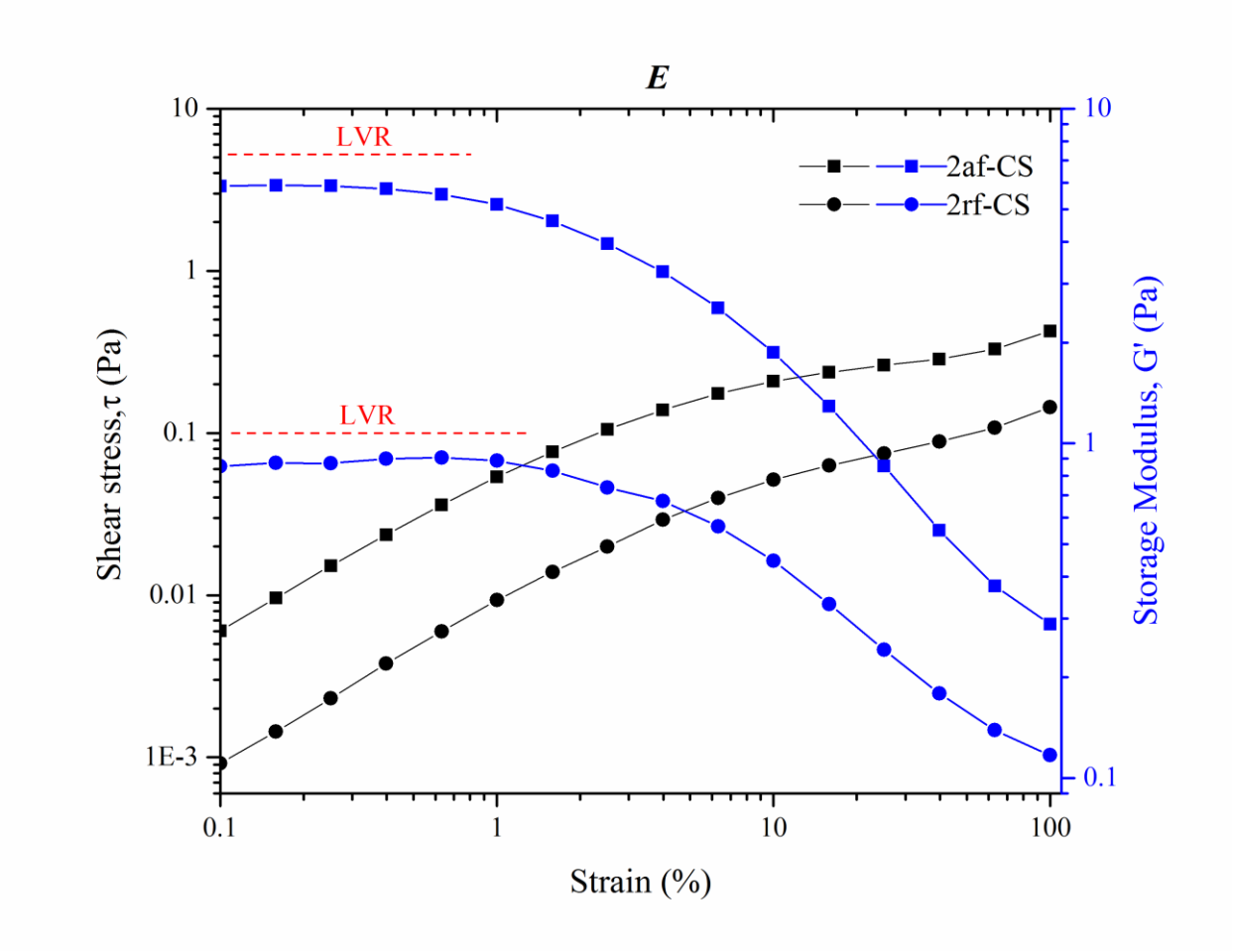
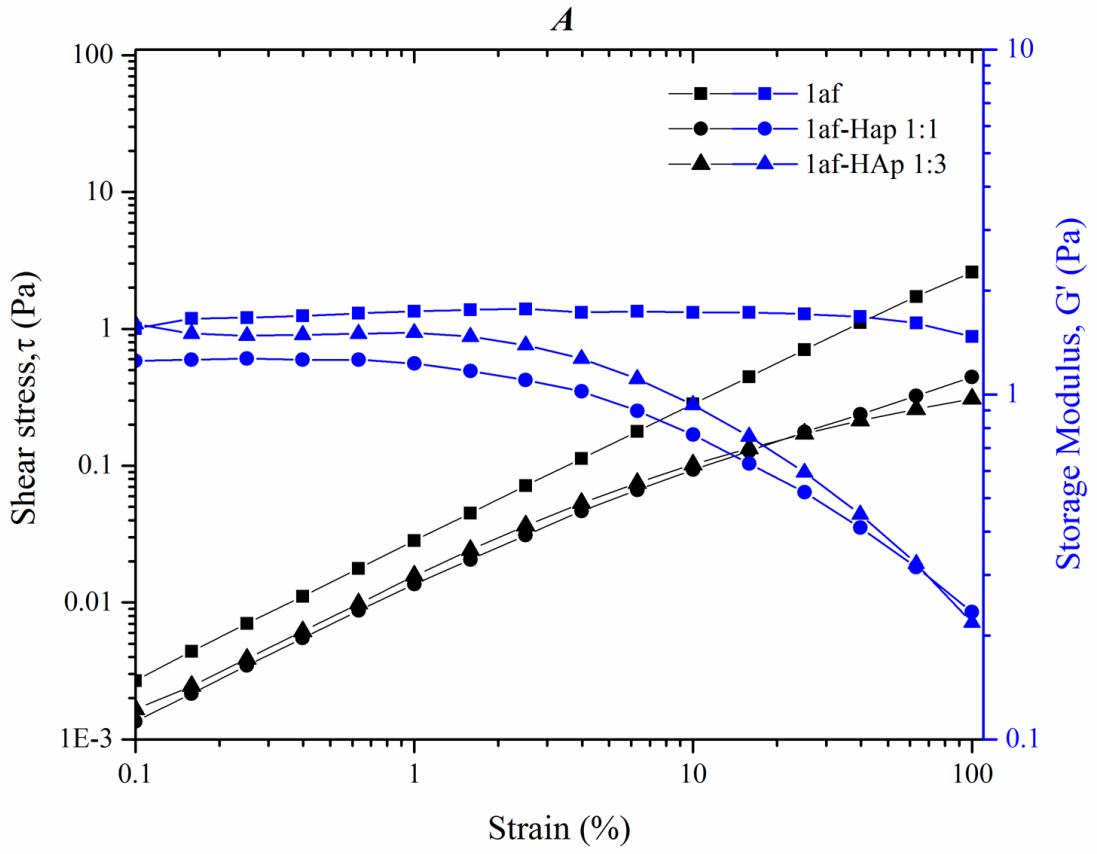
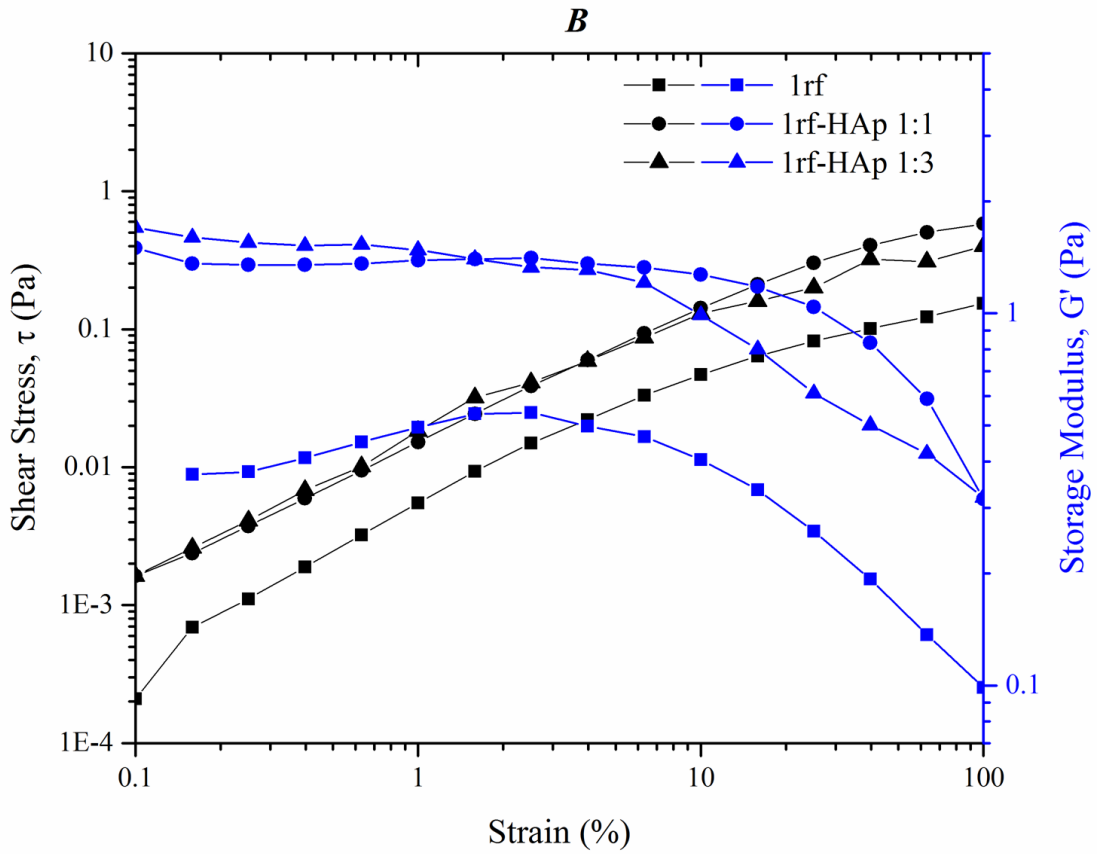


Figure 5.3 The effect of fibrillogenesis on Linear Viscoelastic Region of the preparations: A) 1af, 1rf B)1af-HAp1:1, 1rf-HAp 1:1 C)1af-HAp 1:3, 1rf-HAp 1:3 D)2af, 2rf E) 2af-CS, 2rf-CS. The red line indicaes the flat part of the curve corresponding to the LVR. Strain=0.1-100%, T=20ºC


A
1af
1af-Hap 1:1
1af-HAp 1:3
Shear stress,τ (Pa)
Storage Modulus, G' (Pa)
Strain (%)
100
10
1
0.1
0.01
1E-3
0.1
1
10
100


B
1rf
1rf-HAp 1:1
1rf-HAp 1:3
Shear Stress, τ (Pa)
Storage Modulus, G' (Pa)
Strain (%)
10
1
0.1
0.01
1E-3
1E-4
0.1
1
10
100

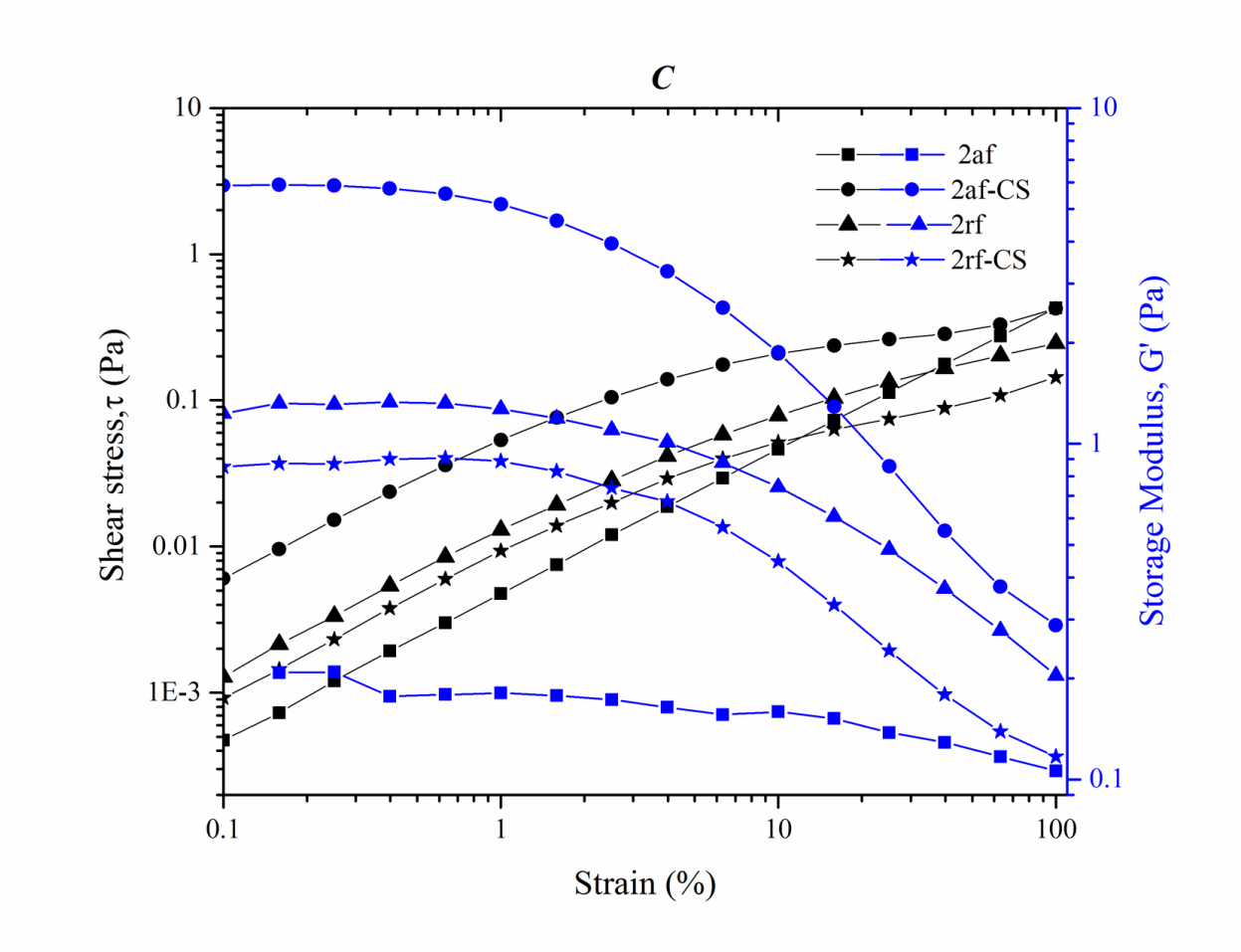


Figure 5.4 The effect of HAp and CS addition on LVR of different preparations: A)1af, 1af-HAp 1:1, 1af-HAp 1:3 B)1rf, 1rf-HAp 1:1, 1rf-HAp 1:3 C)2af, 2af-CS, 2rf, 2rf-CS; shear stress versus strain and storage modulus versus strain shown. Strain=0.1-100%, T=20ºC

Figure 5.4 demonstrates the impact of adding particles/solutes to preparations on LVR. Addition of HAp to type-I afibrillar and reconstituted fibrillar suspensions shortened LVR. It was observed that although incorporating CS in type-II afibrillar suspensions (*2af*) shortened LVR, it had no effect on the reconstituted fibrillar preparations.

5.3.2 Shear rate dependency

In this section, shear viscosity and stress were measured as a function of shear rate. Figure 5.5 and Figure 5.6 show that the viscosity of all preparations decreases with increasing shear rates; this is called shear-thinning and is a characteristic of pseudoplastic behaviour. Upon removing the shear, the viscosity increases back either instantaneously or after a delay; the latter is called thixotropy, as is shown by a hysteresis loop in these figures.

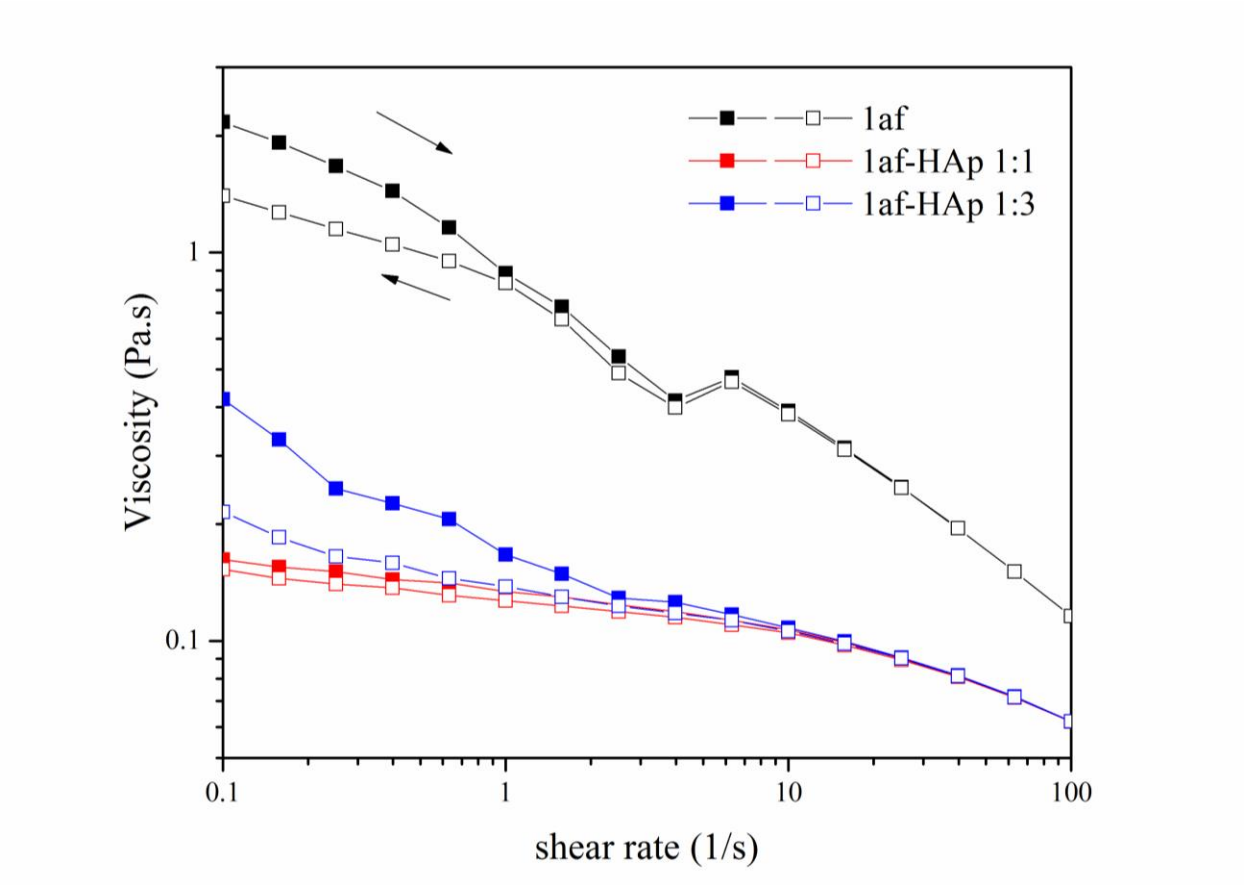


Figure 5.5 Flow curves and hysteresis loops of preparations showing the effect of particle addition to type-I preparations; shear rate=0.1-100 1/s. T=20C. Filled symbols (■) and downward arrow show increasing shear rate, while open symbols (□) and upward arrow show decreasing of shear rate

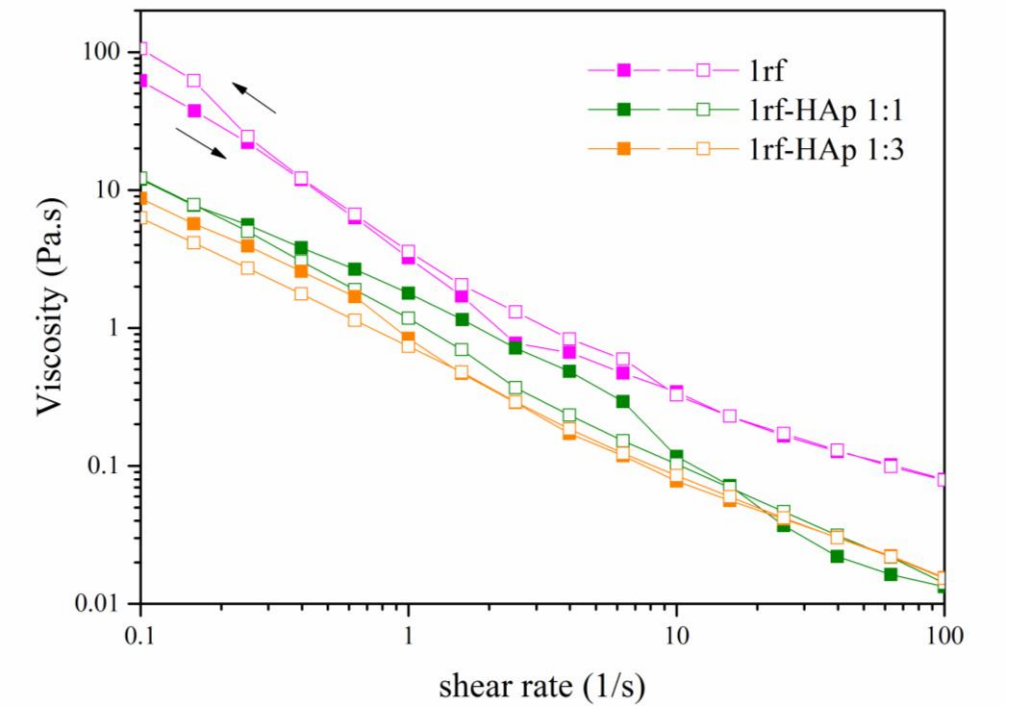


Figure 5.6 Flow curves and hysteresis loops of preparations showing the effect of fibrillogenesis of type-I preparations; shear rate = 0.1 – 100 1/s, T= 20C. Filled symbols (■) and downward arrow show increasing shear rate, while open symbols (□) and upward arrows show decreasing of shear rate

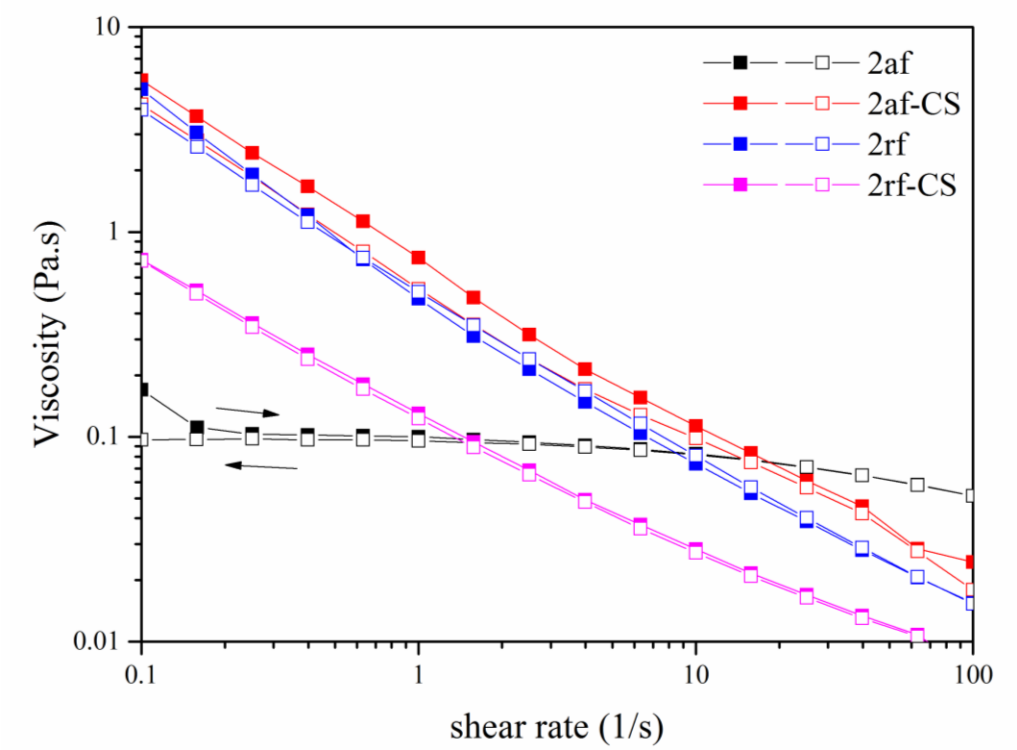


Figure 5.7 Flow curves and hysteresis loops of preparations showing the effect of shear rate on viscosity of type-II preparations; shear rate = 0.1 – 100 1/s, T= 20ºC. Filled symbols (■) and downward arrow show increasing shear rate, while open symbols (□) and upward arrows show decreasing of shear rate

Figure 5.6 shows the effect of fibrillogenesis on shear rate dependency of viscosity in different type-I preparations. It has been observed that fibrillogenesis increased the low shear viscosity of *1rf* by a factor of 100, while the effect on high shear viscosity was much less significant, with *1af* having a slightly higher viscosity.

Also, the same effect was detected in the low shear viscosity of *1rf-HAp 1:1* and *1rf-HAp 1:3*, which were 10 and 100 times higher than *1af-HAp 1:1* and *1af-HAp 1:3*, respectively; however, fibrillogenesis reduced the high shear viscosity of both type-I composite preparations.

2af showed the highest viscosity at high shear rates and the lowest viscosity at low shear rates. At low shear rates, *2af-CS* and *2rf-CS* displayed the highest viscosity. Incorporation of CS in afibrillar solution (*2af-CS*) and fibrillogenesis (*2rf*) decreased the high shear viscosity to the same extent, where addition of CS to *2rf*, decreased the high shear viscosity even further. Besides, it can be seen that increasing shear rate had a less pronounced effect on viscosity of *2af*, compared to other type-II preparations, where viscosity decreased to nearly the same extent.

The shear stress path upon increasing and decreasing of shear rate may lag, forming a hysteresis loop, which can be seen in Figure 5.5, Figure 5.6 and Figure 5.7. All of the preparations showed some degree of hysteresis loop, except for *2af-CS* and *2rf*, where this effect was not observed.

5.3.3 Dynamic Frequency Sweep

In this section the material response to increasing frequency is examined at a constant amplitude strain and temperature, and is presented in terms of cross-over frequency, phase angle, complex modulus- including storage and loss moduli- and complex viscosity.

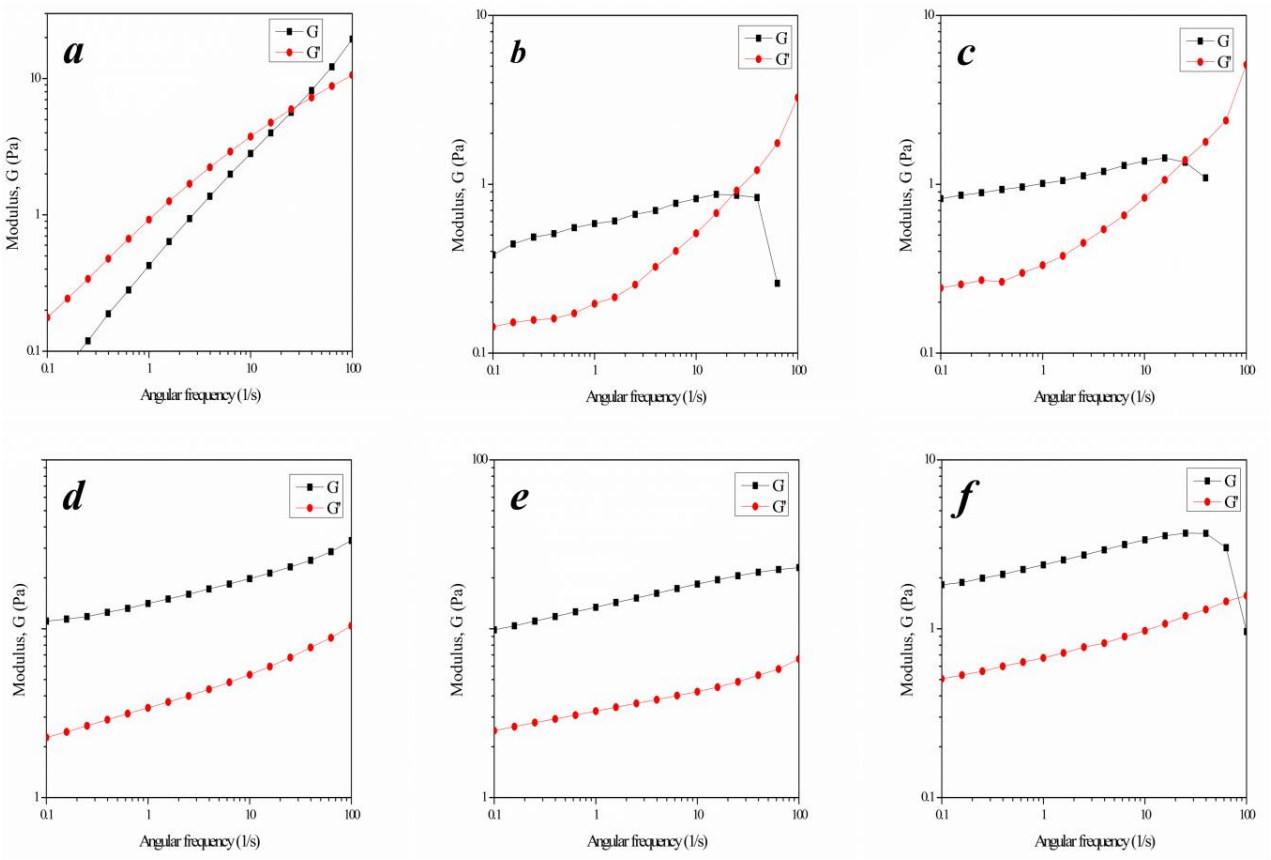


Figure 5.8 Storage (G') and loss (G'') modulus cross-over of a) 1af, b) 1af-HAp 1:1, c) 1af-HAp 1:3, d)1rf, e)1rf-HAp 1:1, f)1rf-HAp 1:3 in frequency sweep test; angular frequency = 100-0.1 rad/s , strain amplitude γ = 1%, T =20ºC

It can be seen from Figure 5.8 in all of preparations that G' was more prominent, except for *1af*, where G'' exceeded G'' up to the crossover point. Addition of HAp (1:1 and 1:3) to afibrillar type-I, produced a reverse effect, where elastic characteristics (G') is a dominant factor at low frequencies.

From Figure 5.8 it becomes evident that fibrillogenesis of pure type-I collagen led to a G'>G'' over the entire range of tested frequencies, which means that the storage and loss moduli did not intersect; the same applies to fibrillogenesis of *1rf-HAp 1:1*, but not *1rf-HAp 1:3*, where the cross-over modulus remained nearly the same, but the cross-over frequency increased more than three times

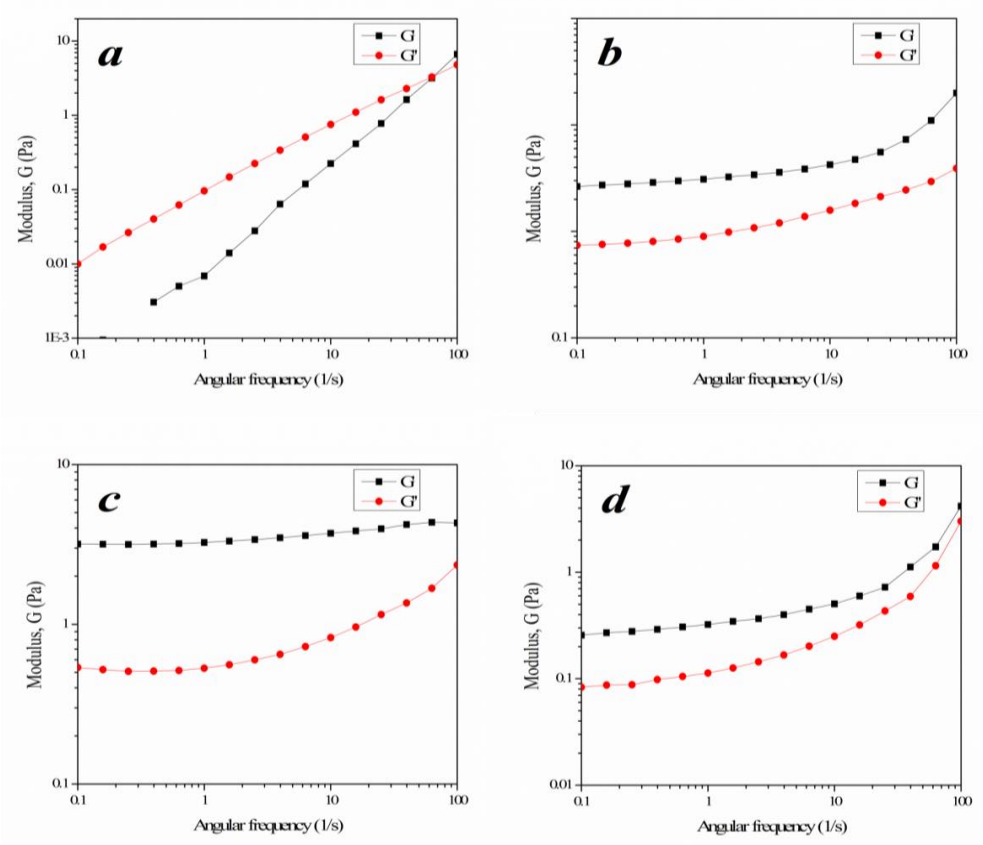


Figure 5.9 Storage (G') and loss (G'') modulus of a) 2af, b) 2af-CS, c) 2rf and d) 2rf-CS in frequency sweep test; angular frequency = 100-0.1 rad/s , strain amplitude γ = 1%, T =20ºC

In type-II samples G' and G'' only intersected in *2af* preparations (Figure 5.9), where G'' was more pronounced up to the cross-over point; G' was higher in all other preparations.

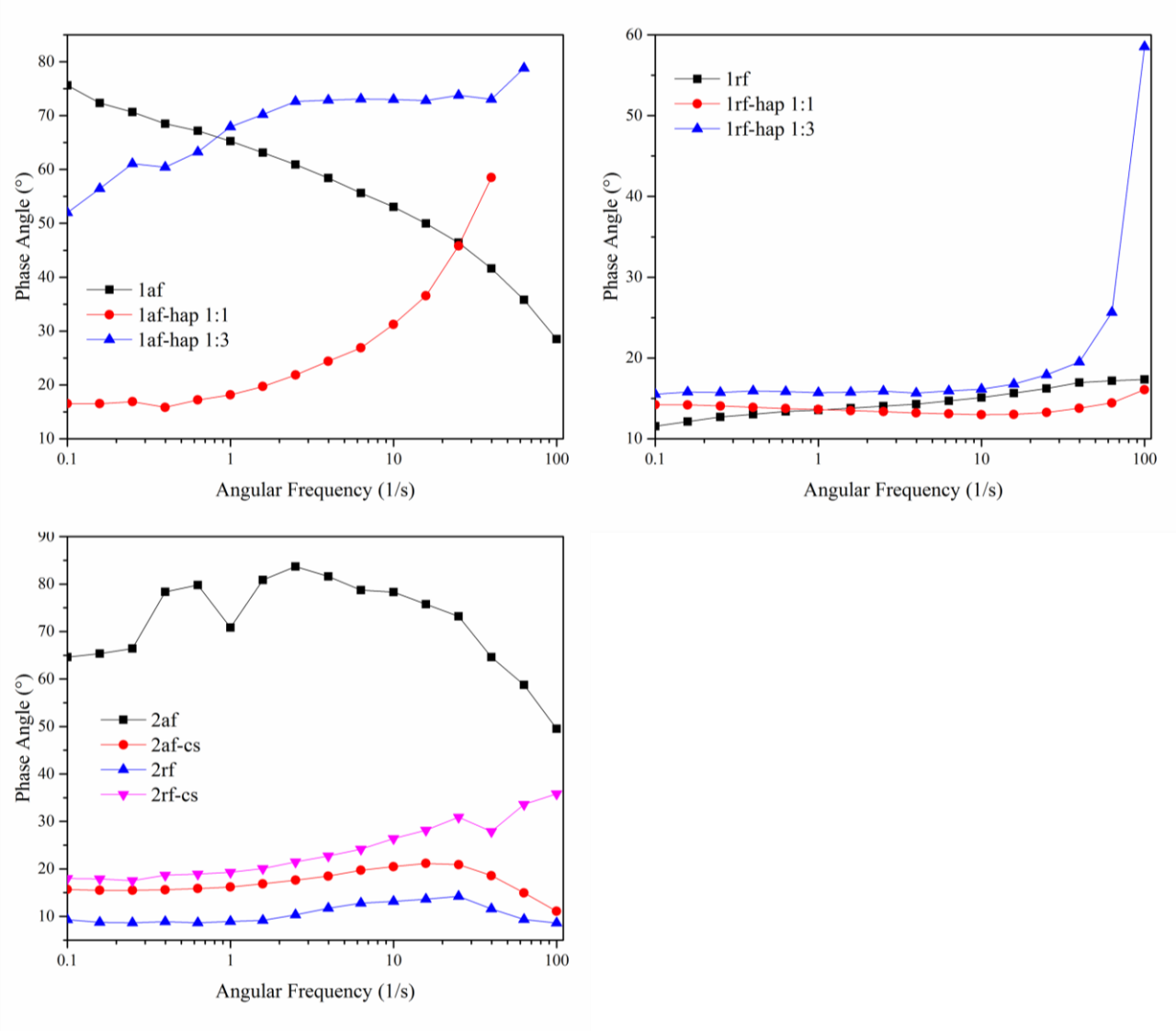


Figure 5.10 Phase angle between shear stress and strain in oscillatory shear test in frequency sweep (angular frequency = 100-0.1 rad/s , strain amplitude γ = 1%, T =20ºC)

It is observed in Figure 5.10 that the phase angle (δ) of all type-I preparations except for *1af* increased with raising the angular frequency. At low frequency of 0.1 (1/s), *1af* showed the highest phase angle while its reconstituted fibrillar counterpart (*1rf*) had the lowest phase angle. Among type-II preparations, there was a large gap between the phase angle of *2af* and other samples, with *2af* showing the highest δ at low and high angular frequency. Table 5.1 shows the phase angle of preparations at low and high frequencies.

Table 5.1 Phase angle of different preparations.

Sample	**δ at low frequency (°)**	**δ at high frequency (°)**
1af	75	30
1af-HAp 1:1	15	60
1af-HAp 1:3	50	80
1rf	11	17
1rf-HAp 1:1	14	14
1rf-HAp 1:3	15	58
2af	80	50
2af-CS	15	11
2rf	9	8
2rf-CS	18	36

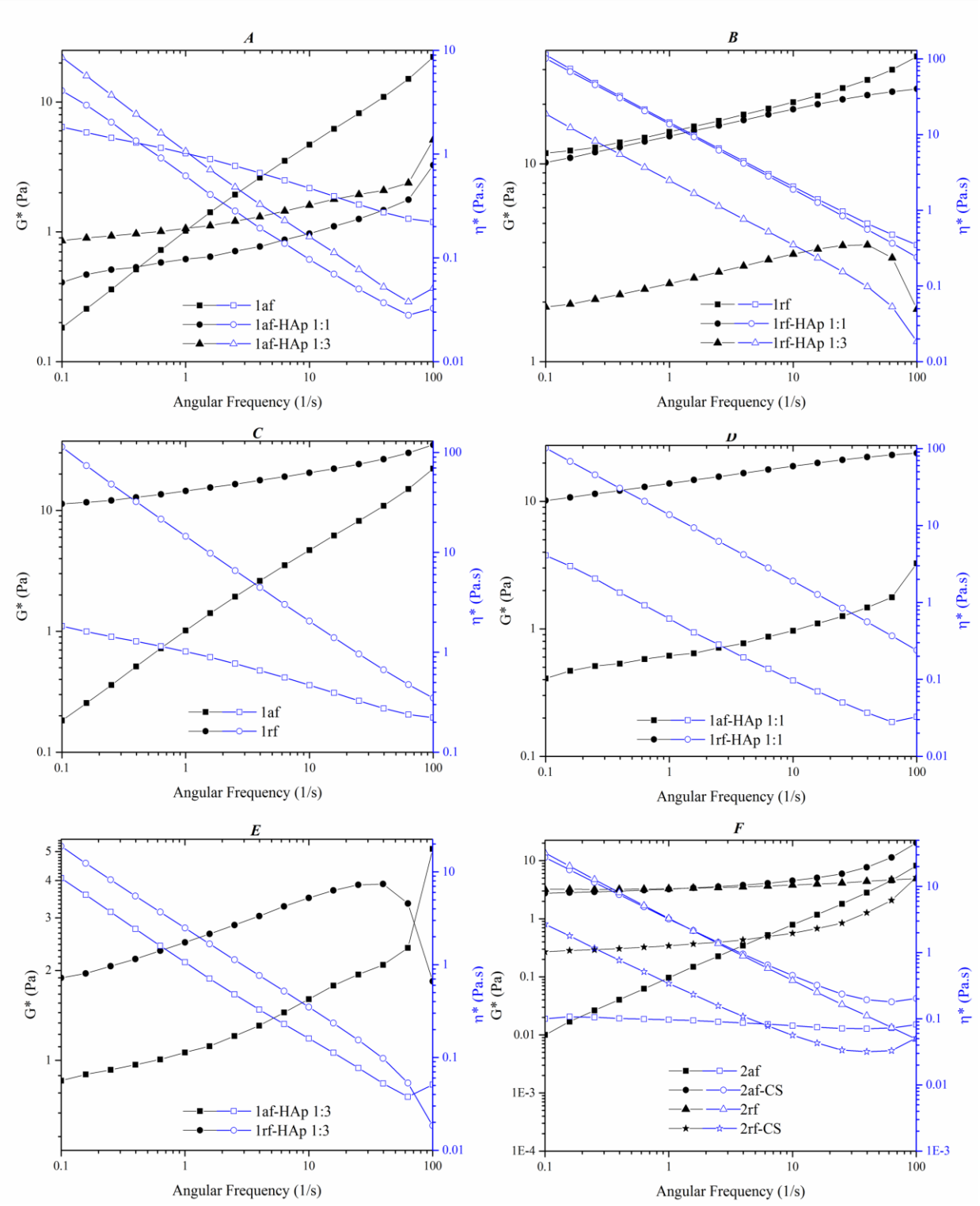


Figure 5.11 Complex modulus (G*) and complex viscosity (η*) in oscillatory shear test; frequency sweep (angular frequency = 100-0.1 rad/s , strain amplitude γ = 1%, T =20C). Effect of HAp addition on type-I preparations (A) and (B); effect of fibrillogenesis on type-I preparations (C), (D) and (E); type-II preparations (F)

As it is observed in Figure 5.11, the complex viscosity of all preparations decreased with increasing the angular frequency. In type-I samples, mineralised *1af-HAp 1:3* showed the lowest complex modulus and η* at low angular frequency, while *1rf* and *1rf-HAp 1:1* showed the highest G* and η*.

Adding HAp to *1af* sample (*1af-HAp 1:1*) did not change the G* and η* significantly, however increasing it to 3:1, decreased the complex modulus and viscosity considerably. At high frequency *1af* had the highest G* and η*, while *1af-HAp 1:1* and *1:3*, both came to the same value. The complex modulus of reconstituted fibrillar samples remained stable over the tested frequency range. Addition of HAp in 1:1 ratio, did not alter the low frequency G*, while decreased the high frequency G*. Increasing the amount of HAp to 3:1 decreased both low and high frequency complex modulus significantly.

In type-II samples, at low frequencies, *2af* showed the lowest G*, rising significantly with increasing the angular frequency. Its complex viscosity was the lowest but decreased only slightly over the frequency range. By addition of CS to *2af*, both G* and η* increased significantly, while incorporation of CS in *2rf*, decreased G* and η*.

As it can be seen from Figure 5.11, fibrillogenesis of *1af* to *1rf* increased G* and η* considerably, raising G* from 2.5 Pa to 47.5 Pa at low frequency, and from 30 Pa to 42.5 Pa at high frequency, while η* was increased from 0.1 to 1800 Pa.s at low frequency and 0.3 to 0.4 at high frequency. The same trend was observed in fibrillogenesis of *1af-HAp 1:1* to *1rf-HAp 1:1*, with G* escalating from 5 to 50 at low frequency, and from 5 to 30 at high frequency, whereas η* increased from 190 to 1000 Pa.s at low frequency and from 0.05 to 0.3 Pa.s at high

frequency. Fibrillogenesis of *1af-HAp 1:3* to *1rf-HAp 1:3* increased G* and η* at low frequency. G* increased 10 times and η* increased from 0.1 to 300, while at high frequency both declined.

5.4 Discussion

To understand the behavior of solutions/suspensions/gels under shear, an insight into their molecular structure, state of the preparation and the defects in the system is required.

It has been shown that soluble collagen monomers, which are rodlike and assume a triple-helical configuration, are neither flexible, nor completely rigid, but show partial flexibility (Yang and Kaufman, 2009, MacKintosh et al., 1995, Levental et al., 2007). This semiflexibility is thought to be originated from either the hinge-like flexible domain on the molecule where the triple-helical structure is interrupted, or the gradual bending of the helical structure itself (Amis et al., 1985, Chow et al., 1985, Doi and Edwards, 1986), which can be depicted by Kuhn chain and "worm-like" chain models, respectively (Larson, 1999) as illustrated by Figure 5.12.

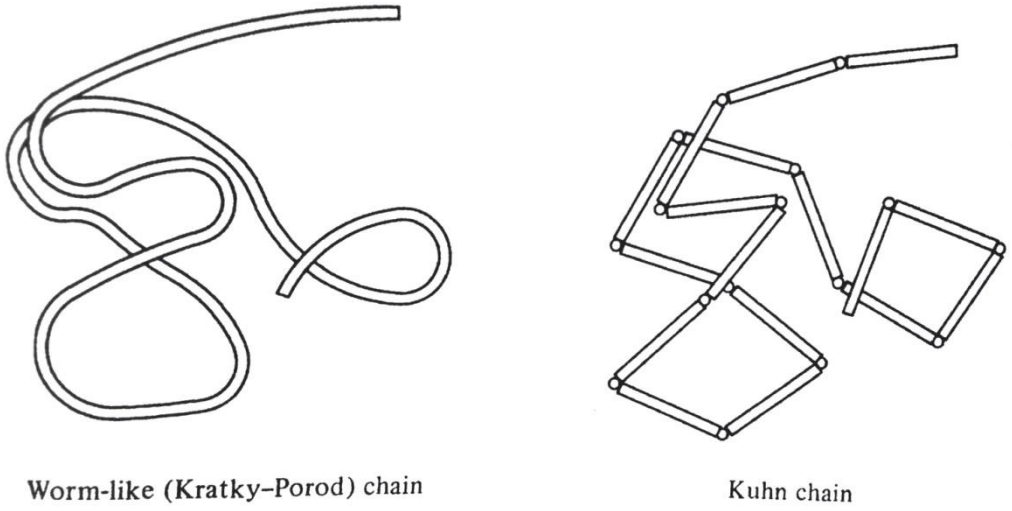


Figure 5.12 Schematic illustration of worm-like polymer chains with continuous flexibility and Kuhn chains with rigid and flexible domains (Larson, 1999)

A collagen monomer typically has a chain length (L) of 300nm and diameter (d) of 1.4nm and its resistant to bending can be characterized by a persistent length λ_p of 170nm, where

$\lambda_p = {\kappa}/{k_B T}$ with κ being the bending rigidity of the chain and T the temperature (Larson, 1999, Amis et al., 1985, Chow et al., 1985). Since the chain length is larger than the persistent length, the monomer is not completely rigid and exhibits the semiflixibility seen in collagen.

It is also important to understand the state of the mixtures in terms of their concentration, i.e. dilute, semi-dilute, isotropic concentrated or nematic (see Figure 5.13), since this has an impact on the behavior and interaction between molecules/particles in the solution. For solutions/suspensions of rodlike molecules with a high aspect ratio (${L}/{d}$), as is the case in collagen molecules (${L}/{d} = {300}/{1.4} = 214$), diluteness is only achieved when the concentration/volume fraction of molecules ($\emptyset_0$) are low enough that a single rod can rotate freely without inhibition from other rods. The transition boundaries are calculated based on the following equations:

$$\emptyset_0 = 24({d}/{L})^2 \sim 0.05\% \qquad \text{Equation 5.5}$$

$$\emptyset_0' = {\pi d}/{4L} \sim 0.6\%\text{-}1\% \qquad \text{Equation 5.6}$$

$$\emptyset_1 = 3.3\,{d}/{L} \sim 1.5\text{-}2.5\% \qquad \text{Equation 5.7}$$

Where ϕ_0, ϕ'_0 and ϕ_1 mark the transition from dilute to semidilute, semidilute to concentrated and concentrated to nematic solution.

The above equations (Larson, 1999) are for rigid rods; hence an upper limit can be calculated if L is substituted for the persistent length λ_p.

Calculating the volume fraction of collagen monomers based on $\emptyset = {\pi d^2 L v}/{4}$, where v is the monomer concentration, which can be calculated to be around 10^{16} molecules/ml, having the molecular weight of 300kDa and initial collagen concentration of 0.5g/ml, will give a value around 0.7%. Therefore, it can be concluded (see Equation 5.6 (Larson, 1999)) that the state of pure collagen solutions is semidilute.

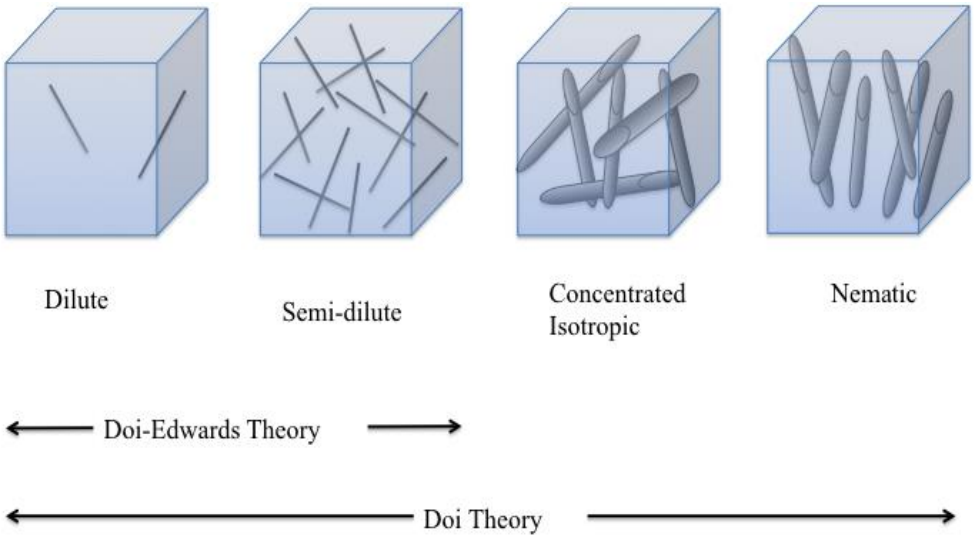


Figure 5.13 Concentration regimes for rodlike rigid molecules, redrawn from (Larson, 1999, Doi and Edwards, 1986)

In addition to the molecular structure and system state, basic forces, defects in monomers and polydispersity can also affect the rheological properties of mixtures as will be explained later in this chapter.

In rotational and oscillatory measurements all of the samples showed shear-thinning behaviour, where their viscosity decreased with increasing shear rate/angular frequency, hence, they may be classified as pseudo-plastic fluids. In fact, this shear thinning has been observed in collagen and HAp suspensions (Monmaturapoj et al., 2012, Moritz and Richter, 2007).

The reason for this shear thinning behaviour can be explained as follows: There is equilibrium of forces between collagen/particles in solution/suspension and shear is likely to disturb this equilibrium, so that the arrangements of molecules/particles are pushed toward an unfavourable state of lower entropy, weakening intermolecular / interparticulate forces. These basic forces include the following:

Based on *excluded volume repulsion*, if two molecules or two parts of one molecule are pushed together so that their electron cloud collide, a repulsive force is experienced (Larson, 1999); therefore, it is possible that shear forces the collagen molecule into a conformation that is unfavourable in terms of excluded volume (Nicholson, 1991), or aligns the molecules/fibrils and bring them to close proximity, hence producing a repulsive force.

The same repulsive force can be generated between the molecules due to *electrostatic forces*, where shear-induced breaking of water-bridge bonds between molecules can lead to production of like-charged groups (Nicholson, 1991). These groups may repel each other when they are forced together during shear, so the intermolecular bonds may be weakened (Vasilev et al., 1973). Moreover, the electrostatic interaction and *covalent bonding* between collagen and CS/HAp (Sections 4.4.1 and 4.4.2) may be disrupted due to shear. The dipole-dipole interaction between the molecules can lead to an attractive *Van der Waals force* (Larson, 1999), which, again, can be affected during shear.

The combined effect of the repulsive forces and interruption of attractive forces can lead to less cohesive forces between molecules, fibrils, and particles, and therefore a reduced viscosity by increasing shear.

Moreover, as explained above, collagen molecules are anisotropic but have random distribution in the solution in semidilute state, giving a large cross-section and more resistance to movement; so that overall effect is that the solution is isotropic at rest and low shear rates. However, as the shear rate increases, the molecules/fibrils align with the direction of flow, giving much smaller effective cross-sections, therefore reducing the resistance to flow.

5.4.1 Rheological behaviour during rotational shear measurements

Rotational shear measurements were performed to shed light on the flow behaviour of mixtures. It is known that by applying and increasing shear reversible and irreversible changes can occur in the microstructure of suspensions (Mewis and Wagner, 2009), while by decreasing and removal of this shear the microstructure can recover to its initial state. Here, the mixture were subjected to ascending shear rates and during the descent, the corresponding shear stress and viscosity curves lagged behind in all of type-I preparations except for *1af-HAp 1:1*, creating a small area between up and down curves. This can be considered as reflection of a weak thixotropy in the mixtures, where the network recovery after shear is not instantaneous and requires time.

In *1af*, the mixture is a semidilute solution of collagen monomers, suspended in acidic aqueous environment by aid of hydrogen bonding and water-bridges. At rest the solution is entangled network of collagen monomers; as shear is applied and increased the chains begin to untangle and align with the motion (Barnes, 1997), breaking the structure, rebuilding of which takes slightly more time as indicated by the small area in the curve (see Figure 5.5).

1af-HAp 1:3 is a suspension of entangled collagen monomers with fractions of HAp particles attached to them by electrostatic interactions and covalent bonds (see Section 4.4.1) and the rest of particles are thought to be mechanically locked in the entanglement network, forming different sizes of agglomerates. Here by application of shear collagen network untangles releasing HAp particles, therefore, the rate of viscosity decrease is lower than that of *1af*, and it takes longer for the network to recover, hence the slightly higher area in the curve (Figure 5.5).

Interestingly, *1af-HAp 1:1* did not show any thixotropy and the decrease in viscosity was minimal. This is suggested to be due to a more stable structure network, as shown by a complete recovery of stress/viscosity after decreasing shear rate to 0.1 (1/s), as opposed to *1af* and *1af-HAp 1:3*. This can imply that no irreversible changes were induced in the structure of *1af-HAp 1:1* and the shear-induced network rearrangements were not significant and the recovery was instantaneous. One of the reasons for this could be the concentration of HAp particles, which were 3 times lower meaning less potential of agglomerates being present and breaking down during shear, contributing to lower a viscosity decrease and higher stability.

A similar principle is applied to reconstituted fibrillar suspensions (*1rf*, *1rf-HAp 1:1* and *1:3*). For instance, in *1rf* collagen monomers self-assemble into a fibrillar form. Thixotropy seen in these suspensions may occur due to the movement of fibrils and constituting monomers relative to each other, as well as the movement of interfibrillar and intrafibrillar water molecules; at low shear the molecules have enough time to rearrange themselves, which becomes increasingly difficult as the shear rises. At this stage slippage inside and between fibrils may occur (Silver et al., 2002), recovery of which may not be immediate.

In type-II collagen, a very slight thixotropy was observed in all of the preparations, with *2af-CS* showing a more pronounced effect. This is thought to be due to disruption of electrostatic forces between collagen and CS during shear. Re-establishing these forces seemed not to be instantaneous. This was not the case in *2rf-CS*, since it was suggested that in the alkaline environment many of the interactions between collagen and CS were abolished (see 4.4.2), thus the effect on thixotropy was not the same.

5.4.2 Rheological behaviour during oscillatory measurements

During oscillatory rheological testing, it is important that all of the measurements are conducted in the LVR of the modulus versus strain curve, where the topology of network structure is not significantly changed (Kurniawan et al., 2012). Drastic decrease in storage modulus with increasing strain may indicate a network fracture (Xu and Craig, 2011); therefore, the length of the LVR can point to the stability of network before it undergoes a permanent change. This can be linked to the phase angle measurements where zero represents purely elastic and $\pi/2$ purely viscous responses (Kurniawan et al., 2012), showing that the more viscous the preparation (see Figure 5.10), the longer is its LVR and higher is its critical strain (Figure 5.1 and Figure 5.2). *1af* and *2af* showed the highest phase angle as well as the longest LVR. This can be explained by the fact that in these pure afibrillar preparations, although the network is in semidilute state where some transient entanglements exist, however, no *real* bonding or crosslinking occurs between the molecules, enabling them to rearrange themselves more easily when necessary, so the network does not break. Whereas in composite and reconstituted fibrillar states, actual covalent and hydrogen bonding as well as cross-linking take place, thus extensive molecular rearrangement is not possible and instead network failure occurs.

All of the samples showed reduced viscosity with increasing angular frequency. In afibrillar type-I at low frequencies (0.1 1/s), *1af-HAp 1:3* showed the highest complex viscosity, which is in agreement with the statements above. That is, presence of HAp, which is attached covalently/electrostatically or is locked in the network mechanically, leads to a higher initial viscosity. However, this means that at higher frequencies (1-100 1/s), once the unbound HAp is freed from the network, the agglomerates break down and give a less effective resistance to flow; hence the higher rate of drop in viscosity compared to *1af*.

Interestingly, in reconstituted fibrillar suspensions *1rf-HAp 1:3* showed the least complex viscosity in both low and high shear rates. It is proposed that the high amount of HAp has either reduced available interaction sites for collagen-collagen binding during fibrillogenesis or physically prevented extensive fibril formation and inhibiting growth. Since *1rf-HAp 1:1* showed a similar viscosity to *1rf*, it is suggested that probably the latter is responsible for the lower complex viscosity observed in *1rf-HAp 1:3*.

The effect of fibrillogenesis on complex viscosity of suspensions can be explained by the higher molecular weights attained by fibril formation (Chow et al., 1985), increasing the complex viscosity of reconstituted fibrillar suspensions compared to afibrillar preparations.

In type-II preparations, afibrillar monomeric *2af* showed the lowest complex viscosity at low angular frequencies (<10 1/s), due to the same reason explained for *1af*. However, the three-fold increase in viscosity of *2af-CS* and *2rf* compared to *2af* can be explained as follow: CS is a flexible extended linear molecule CS (molecular weight 5-50 kDa (Gandhi and Mancera, 2008)), with a high viscosity itself (Arias et al., 1998), presence of it alone in the suspension may increase the viscosity; moreover, due to its extended flexible nature an effective networks of

entanglements may be produced, combining with possible electrostatic/hydrogen bonding with collagen, it contribute to increasing the complex viscosity of *2af-CS*. In fact, a similar effect was observed by addition of CS to Hyaluronan, which raised the viscosity of solution 2-3 fold (Nishimura et al., 1998).

Monomeric *2af* solution is a uniform distribution of relatively low weight molecules with narrow distribution, whereas fibrillogenesis has produced a system of large macromolecules containing crosslinks and a large distribution in molecular weight. This is an effective hindrance to flow at low frequencies; however, based on theory by Marrucci and Grizzuti (1983), a long molecule among shorter ones can reorient itself more quickly, due to dissolution of the cage produced by motion of short rods, so it can slide many times out of a fixed cage (Chow et al., 1985), therefore at high frequencies (>10 1/s) this polydispersity (Rosenblatt et al., 1993) may be the reason for lower viscosity of *2rf* compared to *2af-CS*. The lower viscosity of *2rf* -CS may be explained by the fact that there is no bonding between CS and collagen fibrils, and it has been shown that the CS actually disrupts fibril (Douglas et al., 2006, Scott, 1988), so the resulting final structure is a combination of afibrillar collagen, fibrillar collagen and CS molecules without any bonding to collagen.

The difference in rheological behaviour of type-I and –II preparations can be explained in light of their amino acid sequence, which affects the rigidity of the molecules. It has been shown that the rigid amino acid residues of collagen are proline and hydroxyproline(Silver et al., 2002, Zhang et al., 2010), thus a collagen type rich in these amino acids will show different viscosity behaviour compared to a collagen type with lower amount of these amino acid residues.

5.4.2.1 Storage (G') and loss (G'') moduli

The technique of dynamic oscillation is capable of resolving the structural properties of a suspension into its elastic (G') and viscous (G'') components(Kasapis and Mitchell, 2001). Thus any variation in G' or G" must reflect some changes in the intermolecular interaction in collagen containing solution (Yoshimura et al., 1999).

The behaviour of G' and G'' as a function of frequency could be explained by three-zone model(Ferry, 1980), where the viscoelasticity can be characterized by two sets of relaxation times where G' and G'' intersect (see Figure 5.14). The region where G''>G' at lower frequencies is "terminal" zone which is attributed to long relaxation times characterized by long range configurational rearrangements of chains beyond entanglements. Whereas the region where G'>G'', "transition" zone is related to configurational rearrangements between chain entanglements. In the "plateau" region the chains are rigid and characterized by a strong interaction between them.

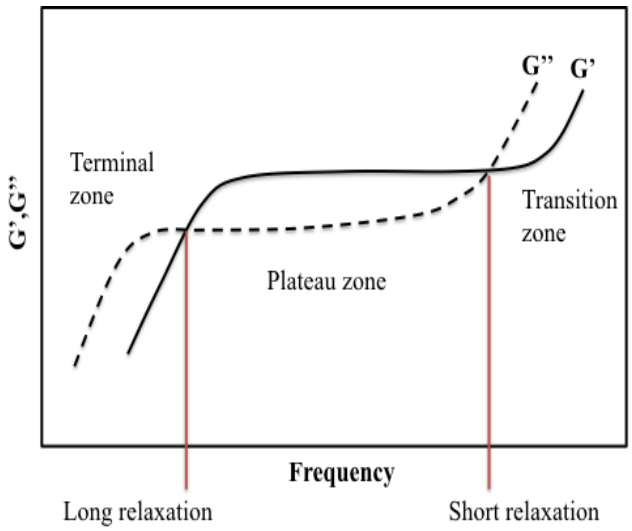


Figure 5.14 Schematic illustration of three zone model in dynamic rheological measurements; G' and G'' vs angular frequency. Adapted from (Ferry, 1980, Larson, 1999)

1af and *2af* suspensions received a greater contribution from the viscosity (G'') than elasticity (G')(Chen et al., 2011), due to a more non-restricted molecular motion (Zhang et al., 2010, Hsieh et al., 1999), hence it appears to be in the terminal zone; however, with addition of HAp and CS the suspension moves into plateau region, implying that the changeover from terminal zone to plateau zone appeared at lower frequencies, which may point to much slower long-range relaxation characteristics consistent with the presence and attachment of HAp/CS to collagen chains and the expectation for the less flexibility of collagen chains (Lai et al., 2008).

All of reconstituted fibrillar suspensions remained in plateau region over the measured angular frequencies; domination of G' in fibrillar suspensions has been previously observed in literature, e.g. Chen et al. (2011) or Piechocka et al. (2011), who showed that G' is weakly dependent on frequency which is typical for biopolymer gels (Piechocka et al., 2011). Such behaviour is thought to arise from the rigidity of chains due to presence of HAp/CS and strong interactions between collagen molecules due to fibrillogenesis.

Now an image about the molecular structure and viscoelastic behaviour of suspensions begins to emerge. Monomeric collagen solutions composing of semiflexible molecules show a dominantly viscous performance, showing although some entanglements may be present, but the chains have retained their mobility and can move relatively freely upon applying strain, thus showing the longest linear viscoelastic region. Upon adding CS, HAp or fibrillogenesis, suspensions move to a plateau region, showing much slower long-range relaxation times, which indicates extensive rigidity of networks compared to monomeric solutions.

It seemed that overall fibrillogenesis (hence higher molecular weights) had a more pronounced effect on increasing the storage modulus of suspensions than addition of HAp.

5.5 Summary

In this chapter the state of collagen suspensions, their shear thinning, thixotropy and behaviour under oscillatory measurements were discussed. It was shown that based on a combination of Worm-like-chain/Kuhn models and Doi-Edwards theory, monomeric collagen suspensions were in a semi-dilute state. This affected their thixotropy, as well as their stability shown by length of LVR. Thixotropy was observed to some degree in all of the samples (except *1af-HAp 1:1*). This was explained by the disturbance of collagen entanglements and attached/mechanically locked HAp in case of type-I and CS in case of type-II preparations. The effect of fibrillogenesis was also discussed. The shear thinning of suspensions was explained based on the excluded volume repulsion, Van der Waals, electrostatic and covalent interactions between molecules. Based on the three-zone model, it was shown that fibrillogenesis and addition of HAp and CS increased collagen chain rigidity. The structures of suspensions were

explained by considering the effect of HAp/CS addition and fibrillogenesis of collagen on complex viscosities and moduli.

5.6 Conclusion

The aim of this chapter was to assess the rheological properties of different collagenous suspensions. It was hypothesized that the molecular interactions between collagen and HAp/CS – which was shown in the previous chapter – would affect their viscosity. This was confirmed by an increase in the complex viscosities obtained from oscillatory measurements, and was explained by three-zone models of different suspensions as summarised in Section 5.5. The importance of rheological properties is associated with their effect on final scaffolds microstructures: it is assumed that the viscosity of preparations would affect the ice crystal growth during freezing and subsequent pores after freeze-drying. This hypothesis is examined in the next chapter (Chapter 6).

Chapter 6. Microstructural Evaluations

6.1 Introduction

The aim of this chapter was to evaluate the microstructure, including pore structures, pore sizes and shapes of type-I and II composite scaffolds. *Scanning Electron Microscopy* was used to examine the microstructure of fabricated scaffolds, as explained in Section 6.2, and the results are presented in Section 6.3. The formation of scaffolds is discussed in Section 6.4.1 and their pore structure is explained in Section 6.4.2. Pore sizes and shapes are elucidated and measured in Sections 6.4.3, 6.4.4 and 6.4.5, respectively. It is hypothesized that the differences in viscosity of preparations shown in Chapter 5 would affect scaffolds microstructures.

6.2 Experimental Procedures

To examine the microstructure and pore sizes of scaffolds, SEM was the method of choice. Scanning electron microscopy with a field emission gun (FEG) was used to produce topographical images of the scaffolds. Collagen scaffolds are unstable at high accelerating voltages and this type of electron gun allows high primary electrons and small spot size even at low accelerating potentials due to release of electrons from a sharply pointed tungsten tip by applying a strong electric field.

Specimens were cut horizontally and vertically by a sharp medical scalpel, mounted on SEM stubs and coated by 4 nm of platinum using Cressington 208HR sputter coater. A JEOL FEG-SEM (JSM-840F) was operated at 5 kV and images of different magnifications were taken in order to discern any hierarchical microstructure.

One hundred pores (n=100) in each sample group were measured by using the image processing software ImageJ. Images were converted to binary and the threshold was manually

set so that the collagen was white and the pores were black. As it will be discussed in Section 6.4.5, the pores are best described by ellipses, therefore based on the set thresholds, ellipse axes dimensions were measured. Dimensions were then used to calculate the pore areas, A, and isoperimetric quotients of circularity, Q, based on Equations 6.1-6.4. Using major (b) and minor (a) ellipse axes, the cross-sectional area (A) can be defined as:

$$A = \pi({}^{a}/_{2})({}^{b}/_{2}) \qquad \text{Equation 6.1}$$

If the pores are considered as perfect circles instead of ellipses, then from Equation 6.1 the circularised pore diameter (d) is defined as:

$$d = 2\sqrt{{}^{A}/_{\pi}} \qquad \text{Equation 6.2}$$

Using Equation 6.1 the quotient of circularity (Q) is expressed as:

$$Q = {}^{4\pi A}/_{L^2} \qquad \text{Equation 6.3}$$

Where L is the ellipse circumference (pore perimeter), which can be adequately described (Walton, 2010) by:

$$L = 2\pi\sqrt{\frac{({}^{a}/_{2})^2+({}^{b}/_{2})^2}{2}} \qquad \text{Equation 6.4}$$

Means of these parameters were then calculated for each scaffold

6.2.1 Statistical Analysis

Hundred pores (n=100) in each sample group were measured as described before. The means of the studied parameters were calculated. The pore areas and quotients of circularity data were not distributed normally, hence a non-parametric Mann-Whitney test was used to statistically analyse the data at significant level of 0.05.

6.3 Results

SEM micrographs of type-I and-II composite scaffolds are qualitatively described in Section 6.3.1 and quantitatively analysed in Section 6.3.2.

6.3.1 Microstructure evaluation

SEM micrographs were obtained to assess the internal features of scaffolds showing a microstructure of interconnected pores where the pore boundaries are defined by sheet-like structures of dense afibrillar or fibrillar collagen.

6.3.1.1 Type-I composite scaffolds

From Figure 6.1, it can be seen that 1af has a nearly uniform/circular pore structure, while by addition of HAp, as observed in Figure 6.2 and Figure 6.3, pore shapes have been transformed towards a more elongated form. Secondary pores – perforations/holes in the pore walls- are frequently seen in *1af,* while they occur less with addition of HAp.

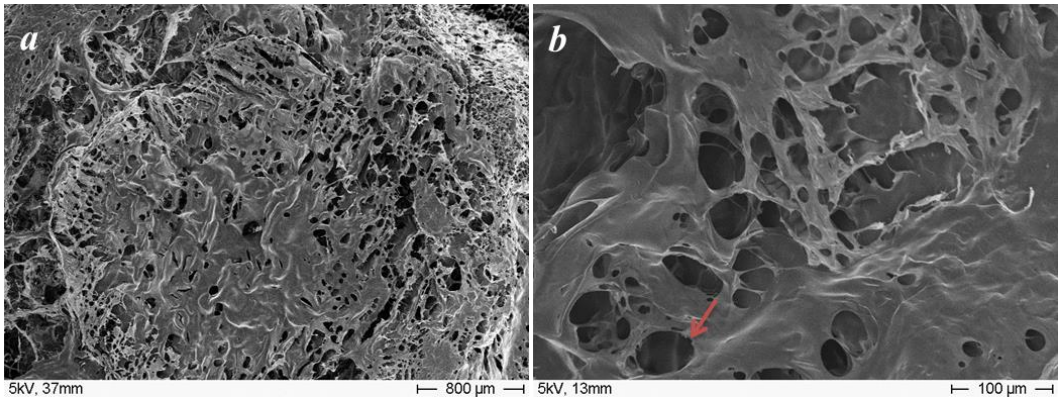


Figure 6.1 SEM images of *1af* at a) low magnification, b) high magnification with the red arrow indicating a secondary pore

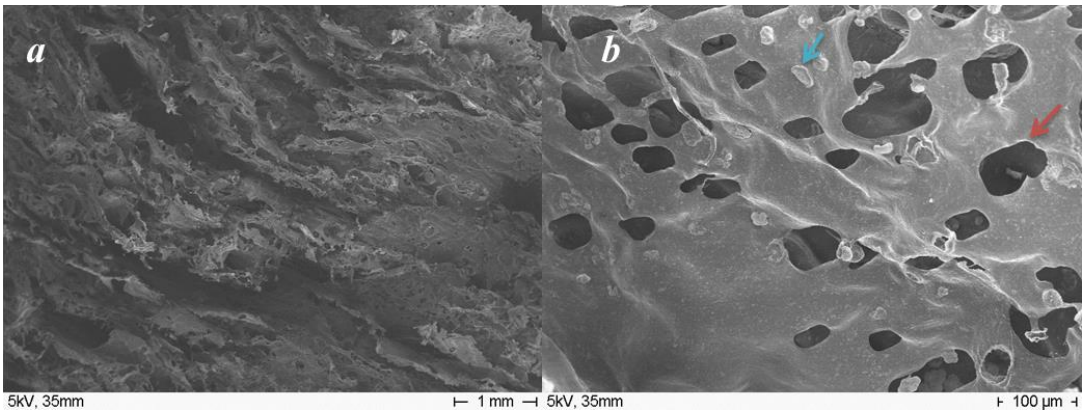


Figure 6.2 SEM images of *1af-HAp 1:1* at a) low magnification, b) high magnification with red arrow indicating a secondary pore and blue arrow a colony of HAp deposit on collagen sheet

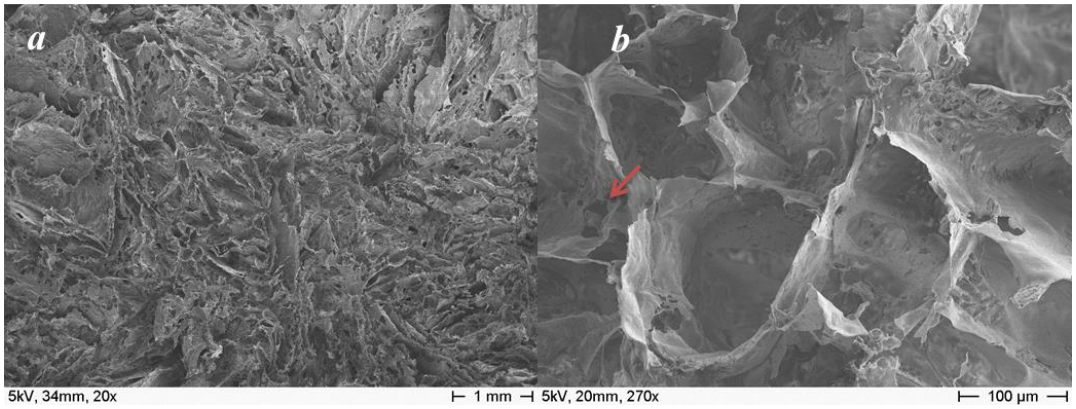


Figure 6.3 SEM images of *1af-HAp 1:3* a) low magnification, b) high magnification with red arrow indicating a secondary pore

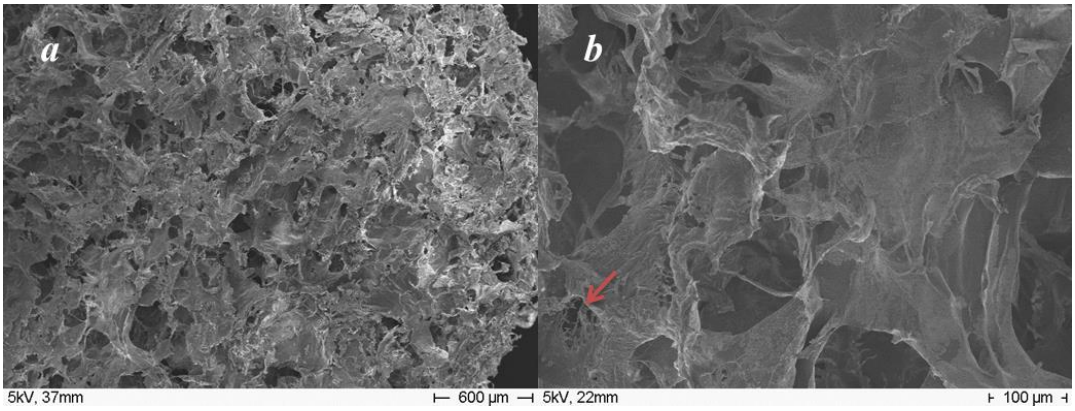


Figure 6.4 SEM images of *1rf* at a) low magnification, b) high magnification with red arrow indicating a secondary pore

From Figure 6.4, it can be seen that fibrillogenesis (*1rf*) of pure collagen-I scaffold seems to have created a less defined pore structure compared to *1af*. The pores became more circular in reconstituted fibrillar HAp-containing scaffolds, and smaller, with a relatively large variation in their size in *1rf-HAp 1:1* (Figure 6.5a) compared to *1af-HAp 1:1* (Figure 6.2a). Secondary pores were observed and clusters of HAp were detectable on collagen sheets and pore walls.

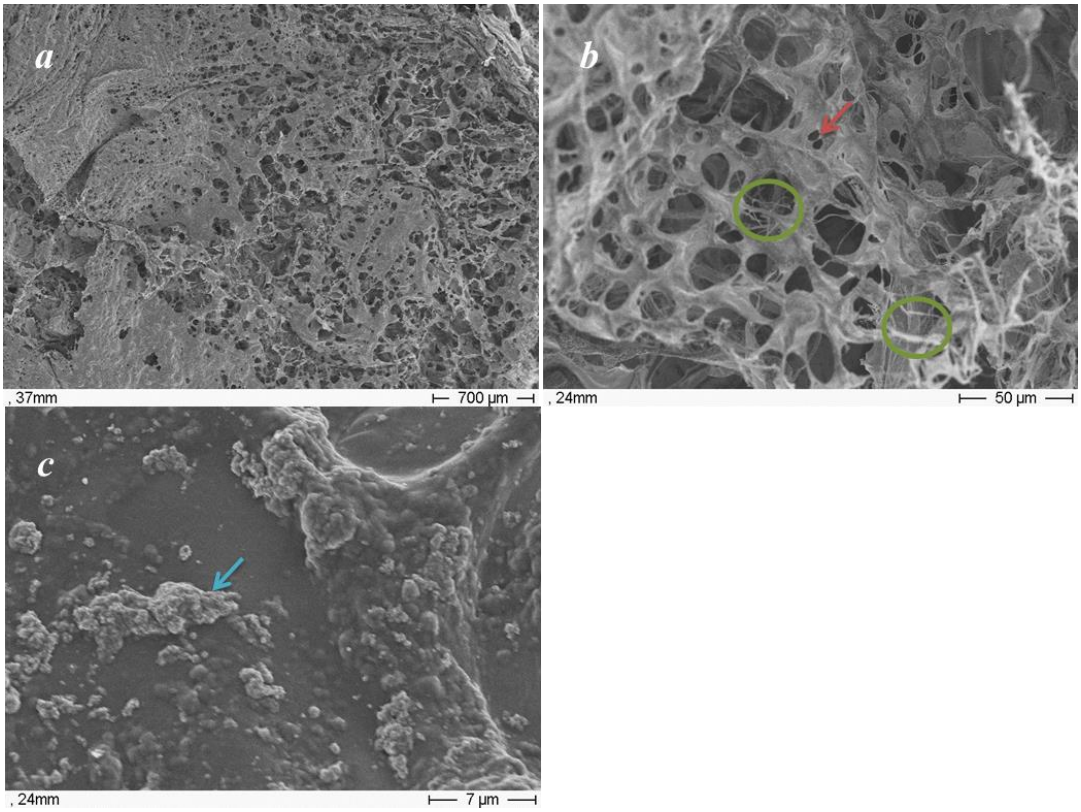


Figure 6.5 SEM images of *1rf-HAp 1:1* at a) low magnification, b) higher magnification with the red arrow indicating a secondary pore and green circles fibrous struts and c) high magnification with the blue arrows showing clusters of HAp deposit on collagen sheet

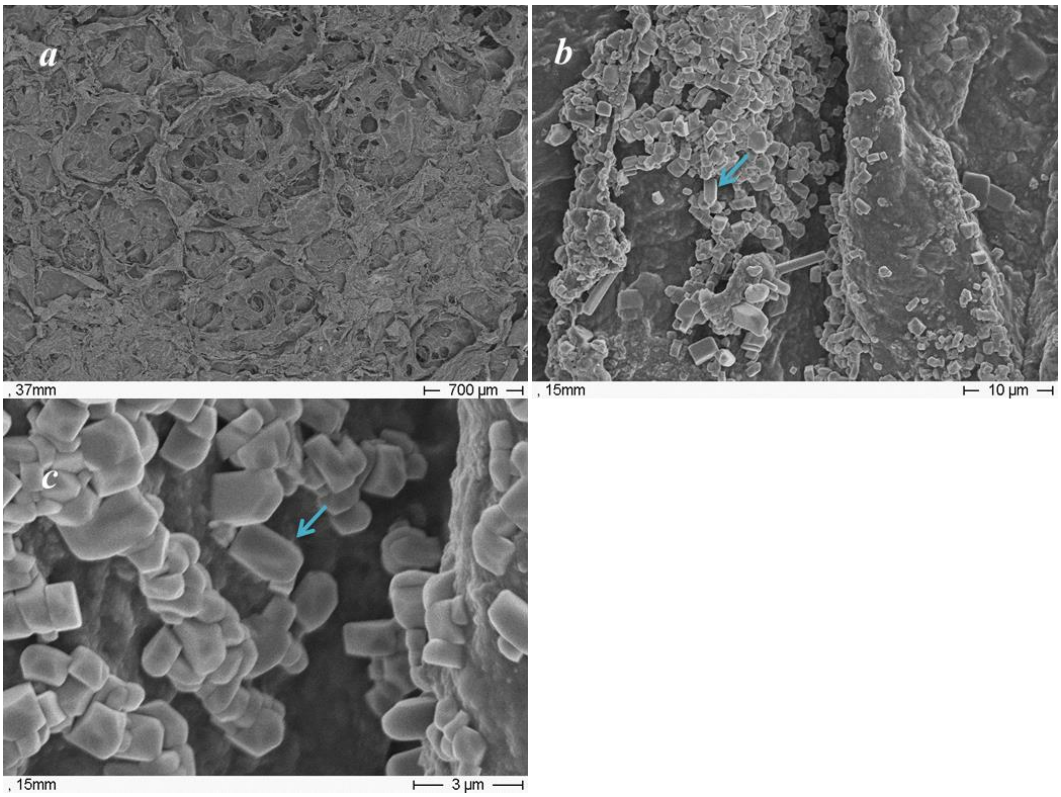


Figure 6.6 SEM images of 1rf-HAp 1:3 at a) low magnification, b) and c) high magnifications with the blue arrows showing clusters of HAp deposit on collagen sheet

6.3.1.2 Type-II composite scaffolds

The reconstituted fibrillar scaffolds (*2rf* and *2rf -CS*) (Figure 6.9 and Figure 6.10) appear to have a similar pore size distribution to afibrillar scaffolds (*2af* and *2af-CS*) (Figure 6.7 and Figure 6.8), with secondary pores present, while fibrous struts are also observed between pores. It was evident that the reconstituted fibrillar scaffolds possessed a less defined pore structure and pore directionality compared to their afibrillar counterparts.

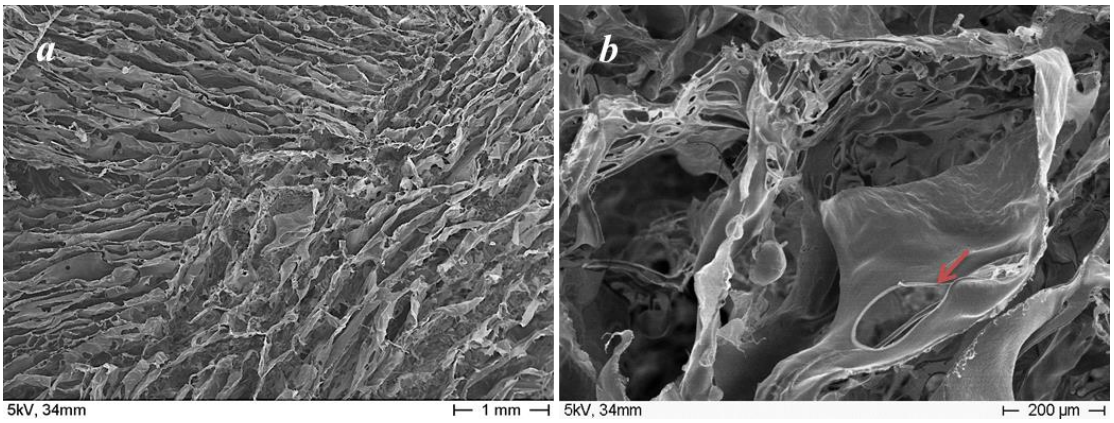


Figure 6.7 SEM images of *2af* at a) low magnification, b) high magnification with red arrow indicating a secondary pore

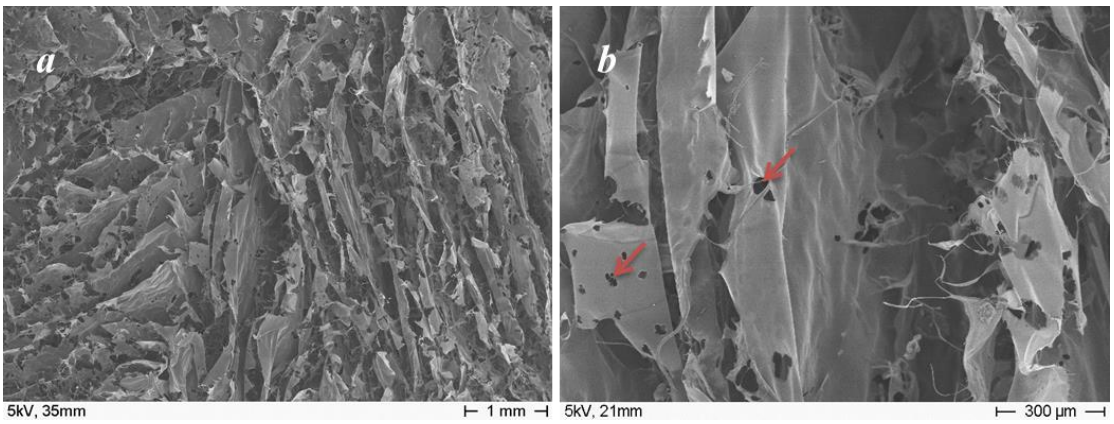


Figure 6.8 SEM images of *2af –CS* at a) low magnification, b) high magnification with red arrow indicating a secondary pore

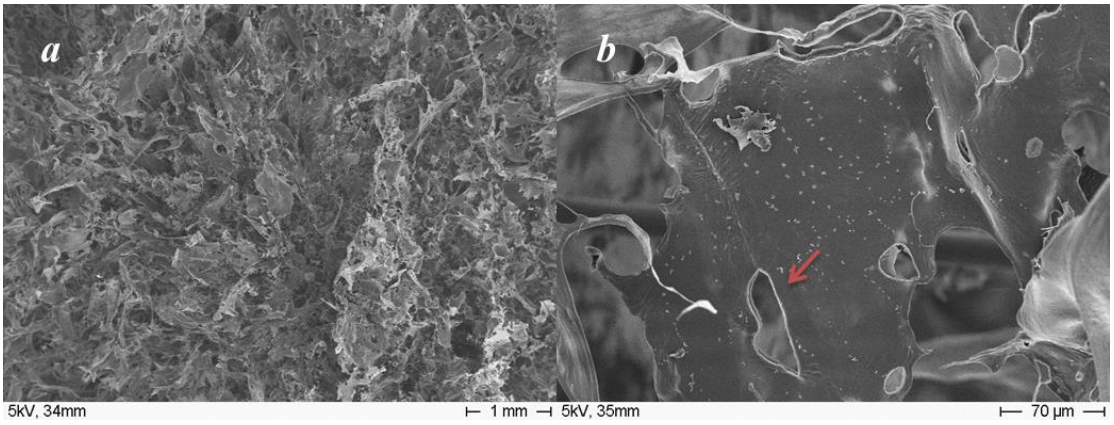


Figure 6.9 SEM images of *2rf* at a) low magnification, b) high magnification with red arrow indicating a secondary pore

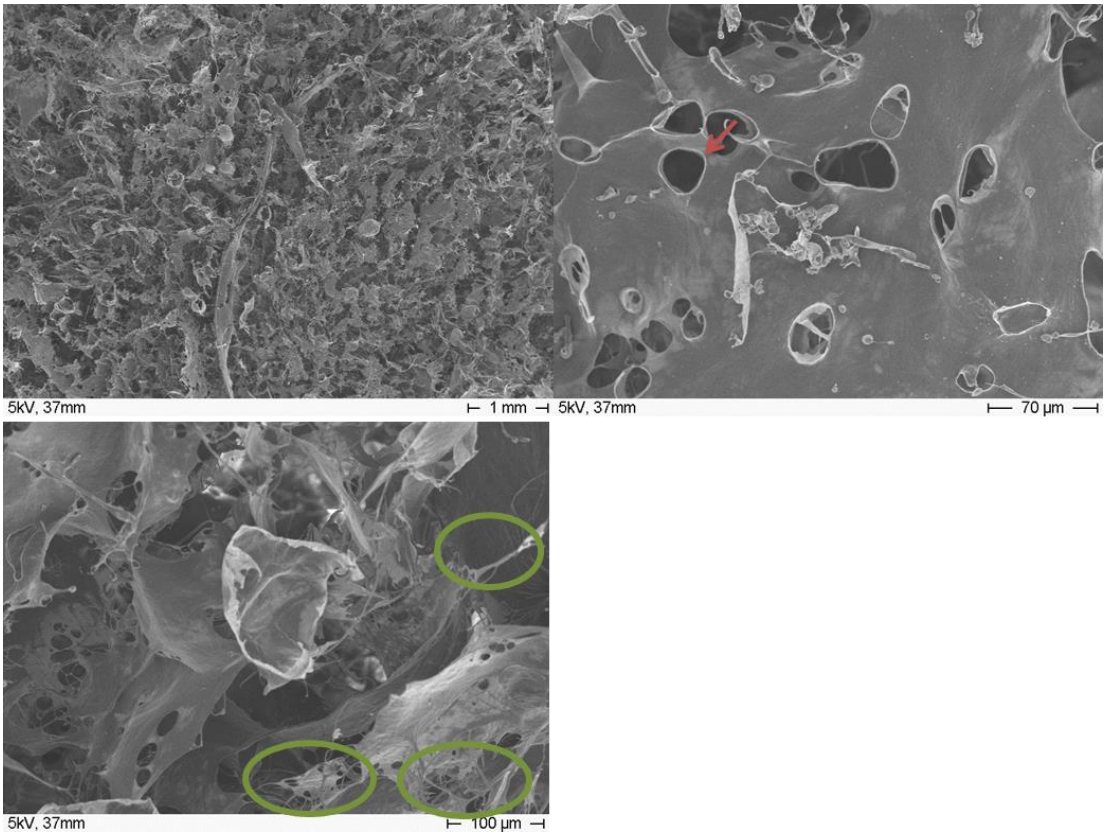


Figure 6.10 SEM images of *2rf –CS* at a) low magnification, b) high magnification the red arrow indicating a secondary pore and c) high magnification with green circles showing fibrous struts

6.3.2 Pore size analysis

In this section, pore structures of type-I and II composite scaffolds were quantitatively analysed. The pores are considered, first as ellipses with major and minor axes, *a* and *b*, cross-sectional pore areas, *A*, (Equation 6.1) and isoperimetric quotient of circularity, *Q*, (Equation 6.3) and second as circles with circularized pore diameter, *d*, (Equation 6.2) shown in Figure 6.11 and Figure 6.12. The former was considered as the principal method of pore quantification and was shown in Figure 6.13, Figure 6.14 and Figure 6.15 with the relevant frequency plots.

For type-I collagen scaffolds, in terms of circularized pore diameter, the afibrillar atelocollagen scaffold, *1af*, gave the smallest size of 61um (Figure 6.11), followed by

reconstituted fibrillar scaffolds *1rf-HAp 1:3*, *1rf* and *1rf-HAp 1:1*, with insignificant difference in their values. In terms of mean pore area the same trend was observed with *1af* showing the smallest area of 0.0034 mm^2 with 97% of pores between 0 and 0.01 mm^2. In mineralized afibrillar scaffolds (*1af-HAp 1:1* and *1af-HAp 1:3)*, 69% and 68% of pores were observed to be in that range and in reconstituted fibrillar scaffolds, these values were between 85% and 87% (see Table 6.1).

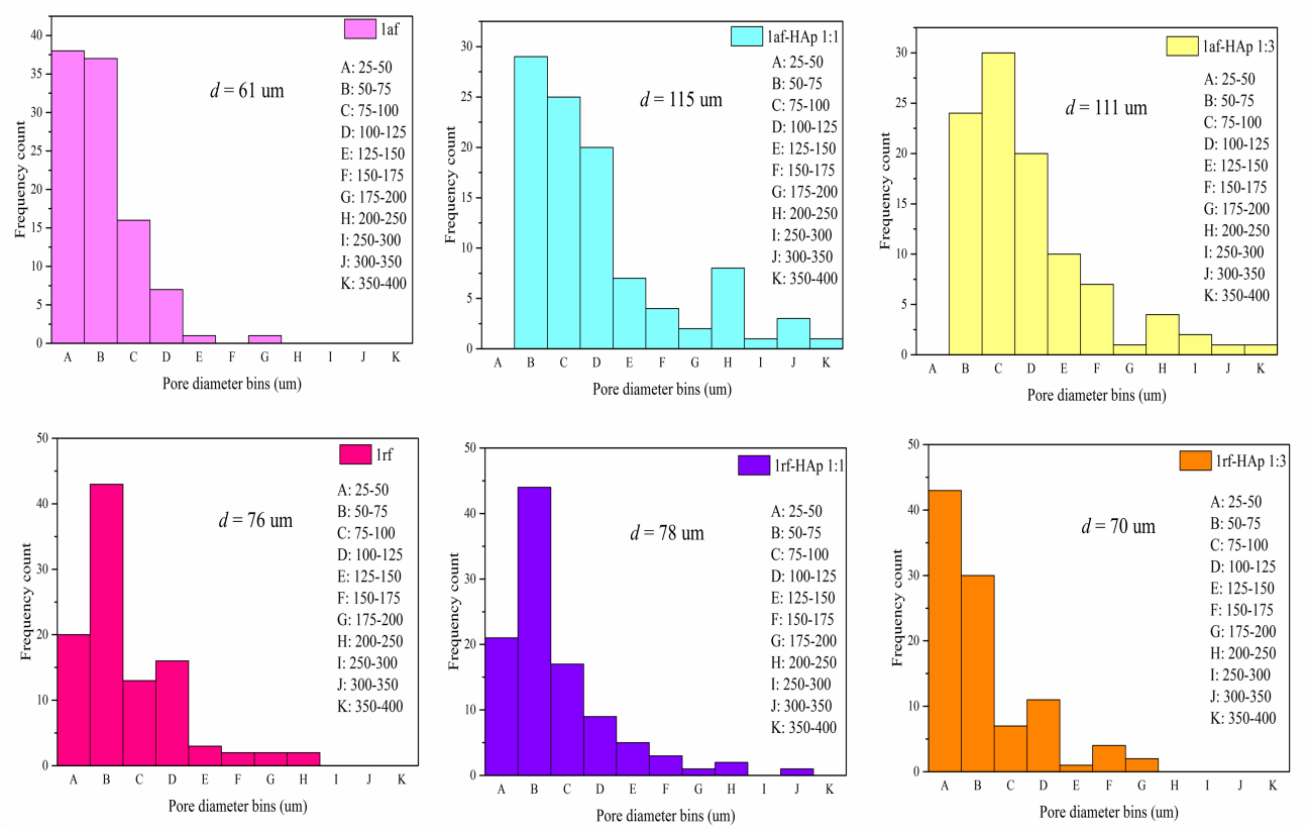


Figure 6.11 Frequency plots of circularised pore diameters Type I collagen composite scaffolds (number of measured pores, n = 100)

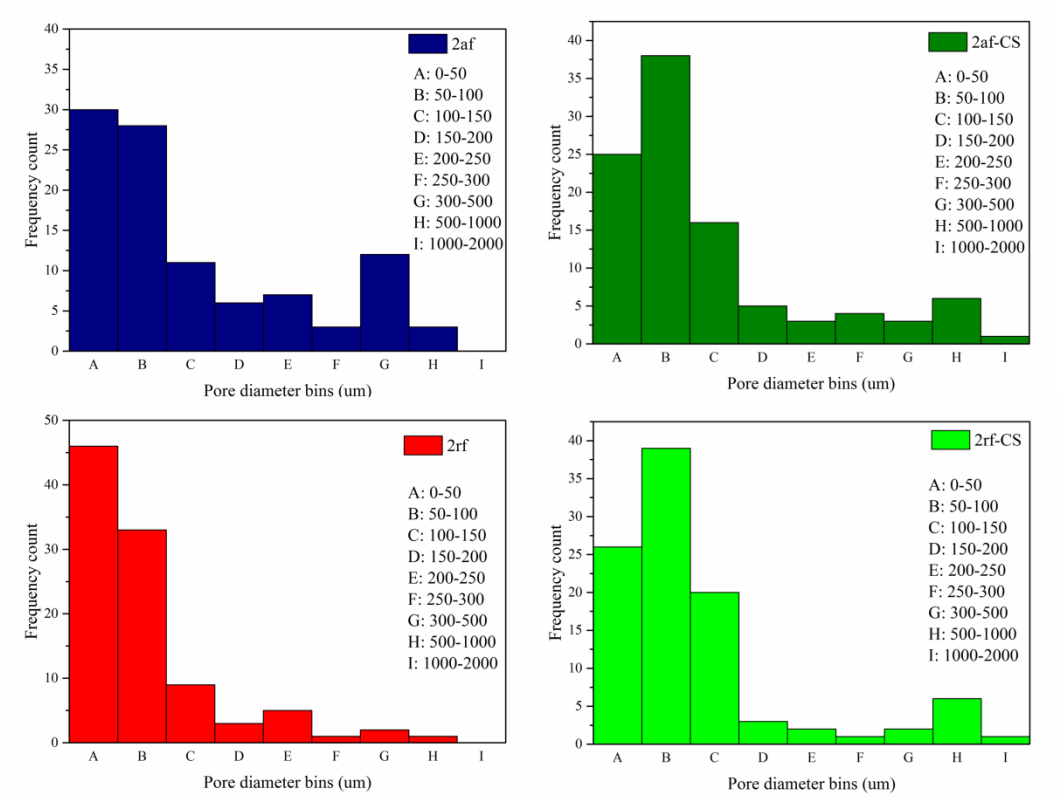


Figure 6.12 Frequency plots of circularised pore diameters for Type II collagen composite scaffolds (number of measured pores, n = 100)

Table 6.1 Mean pore areas, distribution of pore area sizes (% of pores between x and y mm^2), and isoperimetric quotient of circularity *Q*. Symbol * denotes significant difference from 1af, ● denotes significant difference from *1rf*, + denotes significant difference from *1rf-HAp 1:1*, ■ denotes significant difference from 2af and # from *2rf*; symbol ♦ indicates significant difference with all other scaffolds in type-II. Significant level is at 0.05 using Mann-Witney test.

Type-I scaffolds			
	Mean pore area, *A* (mm^2)	**Distribution between 0 and 0.01 (mm^2)**	***Q***
1af	0.0034■	97%	0.8
1af-HAp 1:1	0.0137*	69%	0.71*●+
1af-HAp 1:3	0.0112*	68%	0.73*●+
1rf	0.0056*	87%	0.8
1rf-HAp 1:1	0.0062	87%	0.81
1rf-HAp 1:3	0.0055+●	85%	0.77
Type-II scaffolds			
	Mean pore area, *A* (mm^2)	**Distribution between 0 and 0.05 (mm^2)**	***Q***
2af	0.034	82	0.62 ♦
2af-CS	0.054	87	0.76
2rf	0.011●■	96	0.79
2rf-CS	0.057#	90	0.78

As can be seen in Figure 6.13 and Figure 6.14, fibrillogenesis decreased the pore area size of mineralized afibrillar *1af-HAp 1:1* significantly from 0.0137 mm^2 to 0.0062 mm^2 in *1rf-HAp 1:1*, while significantly increasing the circularity of the pores from *Q*=0.71 to 0.81.

Addition of HAp (1:1) to afibrillar scaffold significantly increased the pore area size, while no significant changes were observed in reconstituted fibrillar scaffolds. Mineralisation

also affected the circularity of pores in a way that they became more elliptical in *1af-HAp 1:1* and *1af-Hap 1:3* when HAp was added to afibrillar scaffold *1af*. Again, this did not have an influence on reconstituted fibrillar scaffolds.

In summary, for type-I collagen scaffolds, *1af-HAp 1:1* had the largest mean pore size area and lowest isoperimetric quotient of circularity, *Q*, while *1af* had the smallest mean pore size area and *1rf-HAp 1:1* had the highest *Q*. Table 6.1 shows these parameters for different type-I scaffolds with statistical differences.

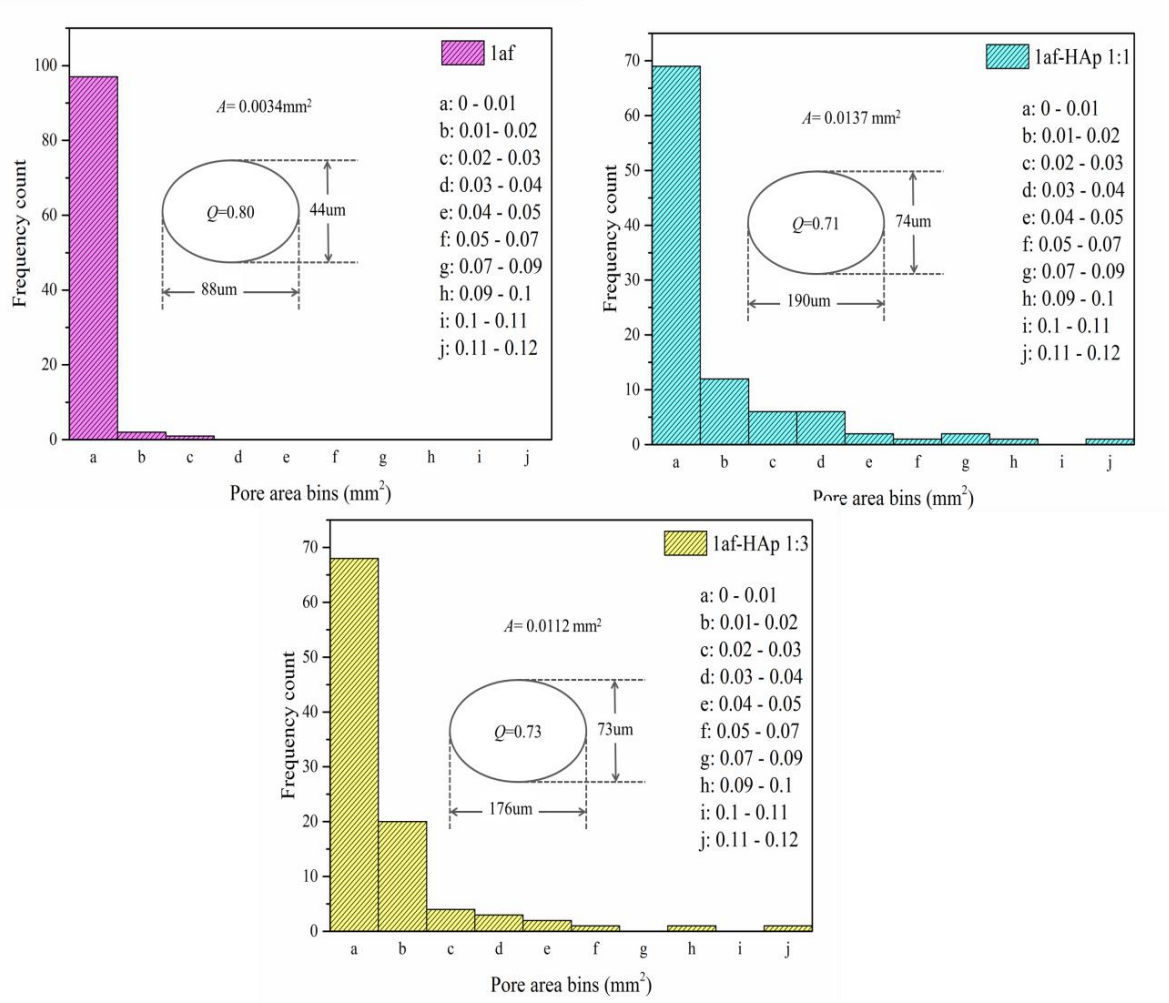


Figure 6.13 Frequency plots of cross-sectional elliptical pore areas for afibrillar Type I collagen. Ellipses represent proportioned, averaged pores, with mean major and minor axis dimensions, (A = mean cross-sectional area of pores, Q = mean isoperimetric quotient of circularity), (n = 100)

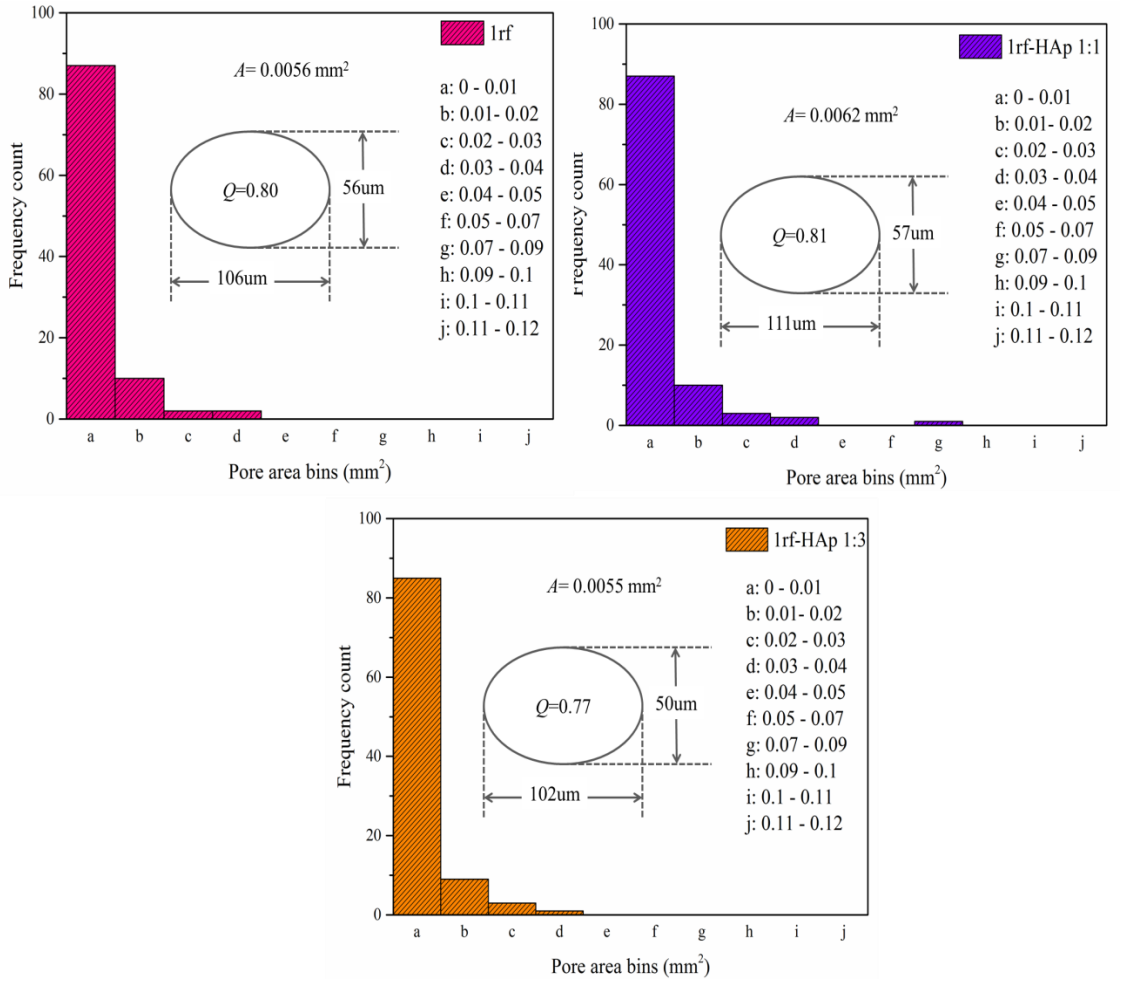


Figure 6.14 Frequency plots of cross-sectional elliptical pore areas for reconstituted fibrillar Type I collagen. Ellipses represent proportioned, averaged pores, with mean major and minor axis dimensions, (A = mean cross-sectional area of pores, Q = mean isoperimetric quotient of circularity), (n = 100)

For type-II collagen scaffolds, in terms of circularized pore diameter, the reconstituted fibrillar scaffold, *2rf*, gave the smallest diameter of 82 µm. In terms of mean pore area the same trend was observed with *2rf* showing the smallest area of 0.011mm^2 with 96% of pores between 0 and 0.05 mm^2, followed by *2af* with the area of 0.034 mm^2 and 82% of pores being smaller than 0.05 mm^2 (see Table 6.1). The averaged pore dimensions showed that there is a large skew within this sample towards elongated pores—this is quantified by a low mean circularity quotient, Q = 0.61.

Addition of CS increased both the average pore area (not significantly) and the circularity of afibrillar scaffolds (significantly). Average pore area of reconstituted fibrillar scaffold increased by adding CS. Fibrillogenesis of *2af* decreased the average pore area, while increasing circularity. This did not have an effect on CS-containing scaffold *2af-CS*.

In summary, the statistical analysis showed that the average pore areas are not significantly different ($p < 0.05$), however, addition of CS and fibrillogenesis of *2af*, i.e. *2af-CS* and *2rf*, shifted the pores towards more circular shapes from Q=0.62 to Q=0.76 and 0.79, respectively.

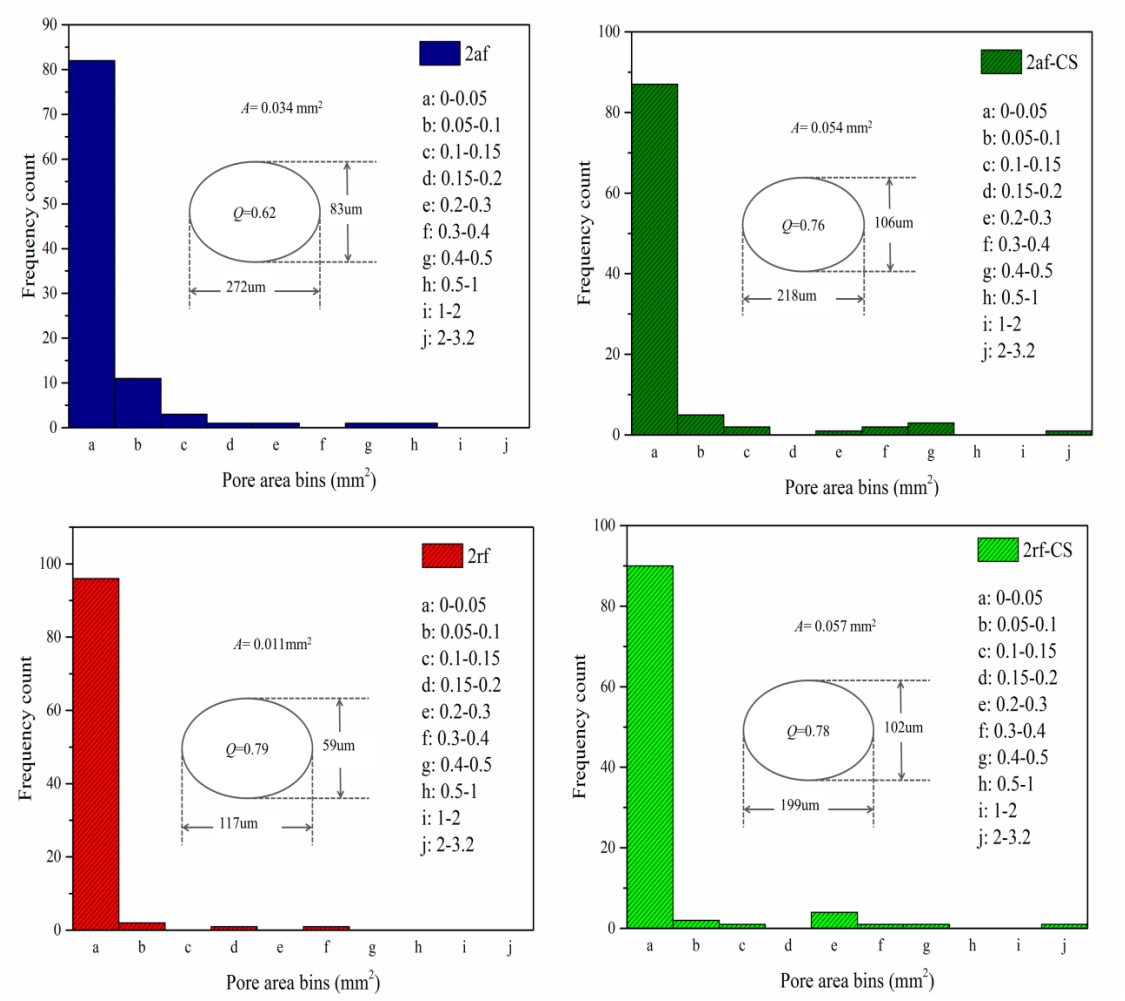


Figure 6.15 Frequency plots of cross-sectional elliptical pore areas for Type II collagen. Ellipses represent proportioned, averaged pores, with mean major and minor axis dimensions, (A = mean cross-sectional area of pores, Q = mean isoperimetric quotient of circularity), (n = 100)

6.4 Discussion

This section discusses the formation of collagen suspensions and subsequently scaffolds during freeze-drying (Section 6.4.1). It also explains the microstructural features of different type-I and II scaffolds (Section 6.4.2) and analyses their pore sizes (Section 6.4.3).

6.4.1 Scaffold formation

To explain the formation of scaffolds from collagen suspension/solution, it is important to first look at the formation of this suspension by understanding the molecular interaction between collagen triple helix and the aqueous environment, and then at how this suspension is processed by freeze-drying to produce porous scaffolds.

6.4.1.1 Mechanism of formation of collagen suspensions

An isolated collagen triple-helix is stabilized by the formation of hydrogen bonds (Myllyharju and Kivirikko, 2001) between three strands, and further by formation of a "hydration shell" around collagen triple helices in an aqueous environment, which also supports the macromolecular assembly of collagen molecules (Bella et al., 1995). Therefore, a homogenous solution will form when the amino acids interact with water. However, this does not occur in deionized water at room temperature. Since deionized water at room temperature has a pH very close to isoelectric point of collagen, where the molecules are amphoteric - containing both amine and carboxylic groups on each amino acid – amino acids have no net charge to be able to associate with water. Therefore, an acidic or alkaline environment is required to produce positively or negatively charged ions, respectively, which enables them to interact with water. It has been shown that the alkaline environment necessary to dissolve collagen can change the native structure of the molecules (Bowes and Kenten, 1950); therefore,

collagen was subjected to an acidic environment to produce homogenous solutions. It was experimentally observed that the collagen monomers were surrounded by "hydration shells" and were readily soluble in the dilute acetic acid solution. Blending, however, was essential to produce a uniform solution. This was due to the fact that the swelling of collagen in acidic environment is directed by, firstly, the osmotic pressure difference between the protein and the external solution as a result of protein salt formation [$CH_3CO^{2-}NH^{3}+$] causing a Donnan membrane effect (Donnan, 1924, Bear, 1952), and secondly, by the cohesion of collagen due to intermolecular forces, which oppose swelling (Bear, 1952). The blending of material is likely to reduce such cohesive forces, and to increase the protonation of COO- through more exposure to acetic acid solution, and creation of repulsive electrostatic forces between now similarly charged ions on the amino acids in the materials, which partially opens the structure and allows for further association with water. The same principles are applied in composite suspension formation, as an acidic environment is needed to produce positively charged collagen and negatively charged CS to initiate interaction between them, and blending is crucial, also to disperse CS and HAp homogenously in collagen suspension.

6.4.1.2 Scaffold synthesis from collagen suspensions

The porous structure of scaffolds after freeze-drying arises from ice crystal formation during freezing and their removal upon lypholisation; therefore, the pores are negative replica of the ice crystal morphology (Schoof et al., 2000)This process utilizes the principle of solidification of a liquid medium such as water and is therefore also known as 'ice-templating' (Wegst et al., 2010). The freezing process starts by heterogeneous nucleation of ice crystals from the particles or the uncovered ends of the solution/suspension in the cylindrical mould, which are in contact with the cold air. The rate of nucleation, which can be controlled by freezing

temperature as well the available nucleation sites, determines the number and size of ice crystals. Lower temperatures means a larger undercooling of the freezing front, resulting in an increased rate of nucleation and hence more numerous, smaller ice crystals. The freezing-front, which is the interface between the newly formed solid and the liquid, then travels through the sample. The velocity of this freezing-front, and the manner in which the liquid carrier, in this case water solidifies, determine the sample pore structure. Collagen, HAp and CS suspended in water during freezing, may either be trapped and captured in the ice area or repelled by the moving freezing front into the liquid region (Azouni et al., 1990). In order for a definable porous structure to form these particles need to be rejected from the ice crystal and trapped between adjacent ones. The thermodynamic criterion for this particle repulsion is described by Equation 6.5 (Li et al., 2012):

$$\Delta\sigma = \sigma_{ps} - \left(\sigma_{pl} + \sigma_{sl}\right) > 0 \qquad \text{Equation 6.5}$$

Where the interfacial free energy between particles and solidification front σ_{ps} should be larger than the sum of interfacial energies of solid–liquid σ_{pl} and particle–liquid σ_{sl} .

If the thermodynamic criterion is satisfied, then the velocity of the freezing-front and also the balance of two opposing forces (attractive viscous drag and repulsive Van der Waals) on each particle become relevant. At low velocities, there is a net repulsive force (F_σ) on particles, which repels them into the liquid phase; however, as the velocity increases and reaches a critical value (v_{cr}) (Equation 6.7), the attractive force (F_n) becomes dominant and the particles are encapsulated into the growing ice crystals (Wegst et al., 2010, Schoof et al., 2000).

$$v_{cr} = \frac{\Delta\sigma_0 a_0}{12\eta\mu R} \qquad \text{Equation 6.6}$$

Where $\Delta\sigma_0$=free energy, η=liquid viscosity, R=particle radius, a_0=mean distance between the molecules in the liquid layer, $\mu = \frac{\lambda_p}{\lambda_l}$ is the thermal conductivity ratio of particle to liquid (Wegst et al., 2010).

The same principle is applied to monomeric and composite collagen preparations, where larger particles (R↑) and higher viscosities (η↑) favour particle entrapment by increasing the attractive drag force (F_n) on particles, according to Equation 6.7and Equation 6.8:

$$F_\sigma = 2\pi R\Delta\sigma_0(\frac{a_0}{t})^n \quad \text{Equation 6.7}$$

$$F_n = 6\pi\eta\upsilon R^2/_t \quad \text{Equation 6.8}$$

Where *R* is the particle radius, *a* is mean distance between the molecules in the liquid layer, *n* is a constant between 1 and 4, *t* is liquid film thickness, η is viscosity of suspension and υ is the velocity of the ice front (Wegst et al., 2010).

The behaviour of freezing front in colloidal suspension and migration of particles depends on several factors, including the interface velocity and particle size (Deville et al., 2009). When the particles are small (e.g. <0.1 um) or the freezing front velocity is slow (e.g. < 20um/s), the Brownian motion of particles ahead of the interface is dominant, whereas when the particles are larger or the front velocity is high (e.g. 20-40um/s), particle motion mainly occurs by physical redistribution, where diffusion of particles is not possible due to lack of enough time for Brownian motion, so particles are physically pushed by the moving interface (Deville et al., 2009) or are engulfed in the ice front (Li et al., 2012). In fact considering the Stokes-Einstein

equation (Equation 6.10) for diffusivity of an isolated particle (Peppin et al., 2008), it can be seen that by increasing the particle radius (R) or dynamic viscosity of the liquid (μ), which in turn depends partly on particle concentration (see Section 5.4), the diffusivity of particles may decreases to a point that it becomes irrelevant.

$$D_0 = \frac{K_B T_m}{6\pi R\mu} \qquad \text{Equation 6.9}$$

Where D_0 is Stokes-Einstein diffusivity, K_B is Boltzmann's constant and T_m is the freezing temperature.

By increasing the viscosity of suspension (μ) and particle radius with fibrillogenesis, and also increasing the concentration of particles (Darcy's law for closed pack suspension, Equation 6.11), diffusivity of particles decreases and it is more likely that diffusion plays an increasingly less important role and collagen/CS/HAp are being physically repelled by the growing ice crystal.

$$D = n\,\frac{k}{\mu}\frac{\partial \prod}{\partial n} \qquad \text{Equation 6.10}$$

Where $\prod$ is osmotic pressure, n is the number of particles per unit volume (particle-particle interaction/friction) and k is permeability coefficient.

Whether the collagen-particles are physically pushed or move by diffusion, they have to be repelled from the ice front in order for a defined pore structure to form, as detailed in Section 6.4.2.

6.4.2 Microstructure

SEM micrographs show a microstructure of interconnected pores, where the pore walls are defined by sheet-like structures of dense afibrillar or fibrillar collagen with/without CS/HAp. The gaps in the pore walls, which can be expressed as "secondary pores" are arguably present in all of the scaffolds.

The final microstructure of a freeze-dried scaffold is determined by a number of factors: The break of planar ice front (by undercooling due to composition/solute and viscosity of solution) as well as the interaction between the growing ice front and collagen/particles (Li et al., 2012) determine whether a definable pore structure is formed by their rejection into the solidifying liquid (Section 6.4.2). The ice nucleation and growth affects the number and size of the pores, respectively, which are discussed in Section 6.4.3. These together with the mode of freezing (homogenous or directional) will control the overall shape of the pores.

6.4.2.1 Type-I collagen scaffolds

Primary pores

As described in 6.4.1.2, in order to produce well defined pore structure, the planar ice-front needs to be broken down by either pinning the ice front by particles or constitutional undercooling at the tip of ice crystal due to solute rejection. Ice crystal structure has very low solubility for impurities; therefore, when ice crystal is formed any soluble molecule/particle initially present in water is separated from the ice crystal, which causes increase in local concentration of solutes leading to a lower freezing point and constitutional undercooling at the head of the ice crystal. This eventually leads to breaking of planar ice front and formation of a columnar interface, also known as Mullins–Serkerka instability (Deville et al., 2007). This needs

to be controlled in a way that collagen is rejected from the ice-front during freezing and concentrated in regions between the growing ice crystals (Schoof et al., 2000). Therefore, the solute concentration and based on Equation 6.6, Equation 6.7 and Equation 6.8, the cohesion of the suspension play parts in the manner in which the ice crystals grow and the final microstructure. Type-I and II composite scaffolds showed different microstructural features, which are explained below.

The relatively well-defined pore structure of *1af* can be explained by Equation 6.7 and Equation 6.8, in light of its relatively low cohesion during freezing, as the growing ice crystal can more easily reject collagen monomers into the liquid ($F_\sigma > F_n$), hence it is less likely to get random particle entrapment. Conversely, *1af-HAp 1:1* showed a less defined structure compared to *1af* and *1af-HAp 1:3*. The viscosity of this solution is moderate, higher than *1af* and lower than *1af-HAp 1:3*, hence it is expected that the pore structure reflects this. The particle phase now includes both collagen and HAp, which can affect the critical velocity of the ice front, by influencing not only the viscosity but also the thermal conductivity of the suspension(Caliari et al., 2011), according to Equation 6.6, where $\mu = \frac{\lambda_p}{\lambda_l}$ is the thermal conductivity ratio of particle to liquid (Wegst et al., 2010). At a qualitative level, adding HAp (λ_p =0.77 W/mK, λ_l=0.56 W/mK (Wegst et al., 2010)) increases μ and η, thereby decreasing the critical ice front velocity, which needs to be surpassed for particles to become encapsulated within the ice crystals. Therefore, a less defined structure is observed in *1af-HAp 1:1* compared to *1af*. Following this line of reasoning, it was expected to see an even less defined pore structure in *1af-HAp 1:3*; however, it is possible that the higher solid volume fraction led to mechanical interlocking of collagen monomers and the particles and increase rigidity of them; therefore, it was less likely

for the invading ice crystal to separate collagen/particles and move them into the growing dendrite. Moreover, due to the high concentration of HAp, the pore walls were more compact and defined. Fibrous struts are argued to form due to entrapment of collagen/particles within the growing ice crystal. They were not observed in afibrillar scaffolds due to the abovementioned reasons.

In reconstituted fibrillar scaffolds, there was no definitive evidence of fibrous struts within the primary pores of reconstituted fibrillar scaffolds. The reason for this is thought to be due to the presence of residual salts from the dialysis step and their rejection into the liquid, the local freezing temperature of ahead of the growing ice tip increases, which causes a decrease in ice front velocity (Panday and Corapcioglu, 1991), therefore, it is more likely that fibrils/particles are rejected and not engulfed by the ice crystals. The dense microstructure of type-I fibrillar scaffolds with 75% HAp (Figure 6.6), is believed to be due to the high particle concentration which means less water is available in the system for ice formation, thus a denser final structure (Li et al., 2012).

Secondary pores

Secondary pores, as defined by Walton (Walton, 2010) as perforations within the primary pore walls due to the growth and fusion of adjacent ice crystals, enhance the interconnectivity of the porous structure (Hutmacher, 2001, Hutmacher, 2000, Zhang et al., 2014), which is important for enhanced cell infiltration and nutrient transfer within the scaffold leading to sustained cell growth. In afibrillar scaffolds, *1af* and *1af-HAp 1:1* showed noticeably more evidence of secondary pores compared to *1af-HAp 1:3*, which is thought to be related to the

lower cohesion and rigidity of the interstitial collagen/collagen composite suspensions (see Section 5.4.2.1), allowing for an easier penetration of growing ice crystals.

6.4.2.2 Type-II collagen scaffolds

Primary pores

In type-II scaffolds, the solute used was acetic acid for the afibrillar collagen *2af* and *2af-CS* and CS for CS containing samples (*2af-CS* and *2rf-CS*); however, it has been shown in FTIR results that CS interacts with collagen, and according to Schoof (Schoof et al., 2001, Schoof et al., 2000, Ryan and Macklin, 1968) in order to achieve the well-defined pore structure, a non-interacting solute is required. This is why *2rf* and *2rf-CS* both gave rise to a less defined pore structure.

The reconstituted fibrillar scaffolds (*2rf* and *2rf-CS*) appear to have a similar pore size distribution to afibrillar scaffolds (*2af* and *2af-CS*), however, fibrous struts are observed between pores in *2rf-CS*. The reason is thought to lie in the structure of the suspension, which is believed to be a mixture of collagen monomers, collagen fibrils, collagen-CS and fibrils-CS, having different molecular weights. The larger agglomerates require higher force to be pushed to the liquid (see Equation 6.7 and Equation 6.8); combining this with the low cohesion of the suspension, means that the higher molecular weight bundles can more easily be separated and are more likely to be trapped in the growing ice crystal, producing fibrous struts.

Secondary pores

All of the scaffolds showed evidence of secondary pores to some extent. However, it was difficult to qualitatively compare the afibrillar and reconstituted fibrillar scaffolds, the reason being the relatively non-definable pore structure in the latter.

6.4.3 Pore sizes

The different pore sizes can be explained by the differences in nucleation and growth across the scaffolds. Freezing of collagen composite suspension comprises two consecutive steps: nucleation of ice crystals and their subsequent growth. In this system, the nucleation is thought to be heterogeneous, initiating on mould walls and bottom, uncovered ends of suspension in contact with cold air and particles (Fu et al., 2008, Moritz and Richter, 2007) (i.e. HAp and reconstituted fibrillar collagen). Growth rate is influenced by the velocity of the ice-front movement, which depends on the heat conductivity of the frozen potion (Ryan and Macklin, 1968) and the viscosity of the remaining suspension. The viscosity of the suspension can act as a mechanical force opposing the growing ice, especially when macromolecules are present in the system, allowing for larger ice crystal formation. This relationship holds up to a certain viscosity above which growth ceases altogether (Blond, 1988).

While Type-I afibrillar scaffolds show pore dimensions which correlate well with the observed viscosity at low angular frequencies (0.1 s^{-1}) and thermal conductivity of samples, the presence of higher nucleation sites and hence higher nucleation rates seemed to not have the same pronounced effect.

Higher cohesion of *1af-HAp 1:1* and *1af-HAp 1:3* is expected to provide a greater opposing force to growth of the ice crystals, hindering the ice front velocity. The growth is slowed down allowing for formation of larger ice crystals and hence larger pore sizes, which were observed in these scaffolds, compare to *1af*.

Moreover, the ability of the sample to conduct the heat away decreases with increasing the amount of hydroxyapatite according to Equation 6.11, consequently reducing the rate of ice crystal growth. This again allows for larger crystals to form and corroborates the larger pores observed in mineralized scaffolds.

$$\lambda_s = \psi\lambda_I + (1-\psi)\lambda_P \qquad \text{Equation 6.11}$$

Where λ_s is the thermal conductivity of the formed solid according to the rule of mixture, $\boldsymbol{\psi}$ is the volume fraction of pure ice lamellae, λ_I is the thermal conductivity of formed ice crystals (λ_I=2.14 W/mK) and λ_P is thermal conductivity of HAp particles (λ_P=0.77 W/mK) (Wegst et al., 2010).

It is probable that, while the collagen/particle is rejected into the interstitial areas between growing ice crystals in *1af-HAp 1:3*, the local viscosity was increased in a way that the critical value of viscosity was reached and growth was ceased, which can explain similar pore sizes compared to *1af-HAp 1:1*. Following the same reasoning, in reconstituted fibrillar scaffolds, due to their very high cohesion, the opposing force on the growing crystals was so high that they did not grow to the same extent as their afibrillar counterparts.

The fact that the final pore sizes are controlled by growth and nucleation can be explained by the competitive relationship between them. Indeed according to Figure 6.16, it can be seen that at higher temperatures (e.g. -20ºC), growth of ice crystals is favourable and dominates the structure (Xie et al., 2013, Li et al., 2012).

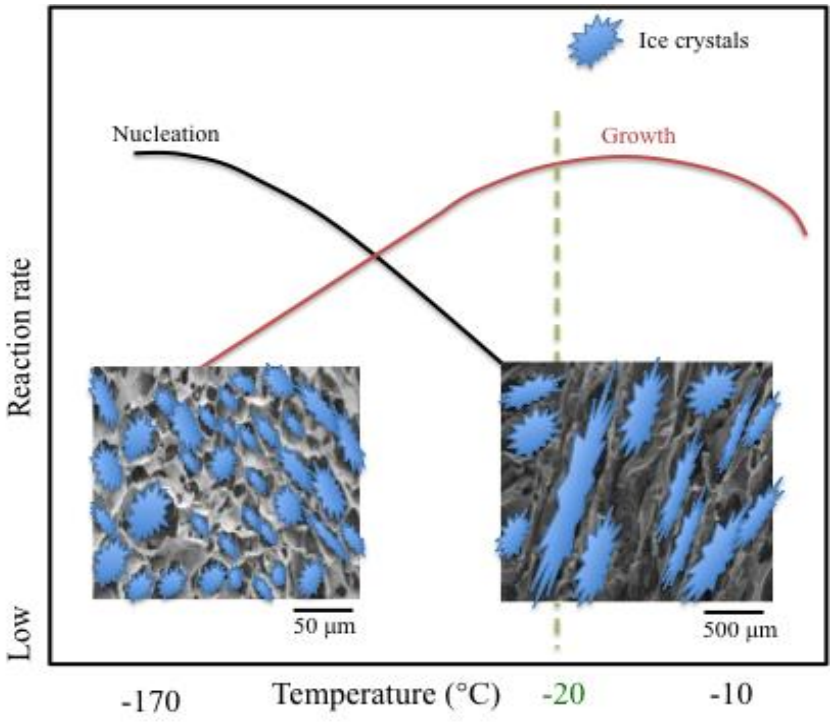


Figure 6.16 Temperature dependency of nucleation and growth rates; it can be seen that at -20C growth rate is dominant in determining the microstructure. Adapted from (Xie et al., 2013)

Remarkably, the type-II scaffolds do not show the same degree of correlation with viscosity compared to type-I scaffolds. One reason for this was suggested by Walton (2010) to be the high degree of α-chain glycosylation in type-II collagen, hence showing a weakly pseudo-plastic behaviour. Therefore, it was stated that the relationship between viscosity and pore sizes in type-II collagen might not be directly comparable to that of type-I collagen (Walton, 2010).

Although cohesions of preparations were not similar across different type-II scaffolds, pore sizes were not significantly different. In afibrillar preparations it is possible that the effects of higher viscosity of *2af-CS* (deterring growth) is cancelled out with the effects of higher constitutional undercooling due to higher solute (CS) volume (increasing growth), giving the same pore sizes as *2af*.

6.4.4 Pore circularity

The pores are negative replica of ice crystals; hence, due to the use of plastic moulds, differences in thermal diffusion gradient lead to some degree of directionality in pores in both type-I and type-II scaffolds, as illustrated by Figure 6.17, creating an anisotropic pore structure, with the orientation of anisotropy in the direction of heat transfer in the mould.

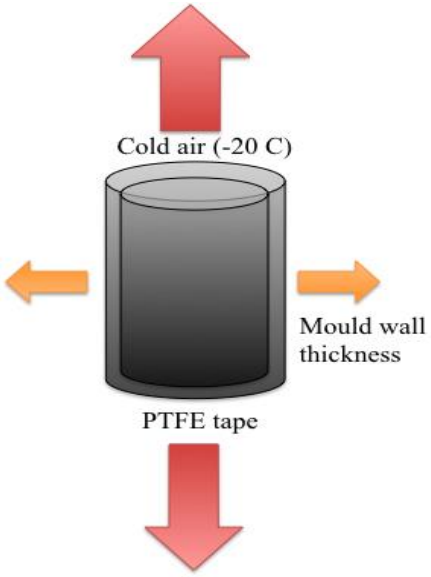


Figure 6.17 Thermal gradient across the scaffold leads to pore anisotropy in the direction of the heat transfer; red arrows show high thermal gradient while orange arrows show lower gradient due to the thickness of the mould wall

Fibrillogenesis of *1af-HAp 1:1* significantly increased the pore circularity. Higher number of nucleation sites, larger crystal sizes and slower growth may have prompted a more equiaxed growth, leading the neighbouring ice crystals to apply more force on each other and arrange themselves in a more circular arrangement. *Q* values show that type-II reconstituted fibrillar scaffolds and CS-containing scaffolds have a higher mean circularity than the afibrillar scaffold (*2af*). These changes in circularity could be explained by the differences nucleation and growth rates of ice crystals during freezing.

The greater number of nucleation sites in *2rf* and *2rf-CS* may have promoted a more equiaxed growth response. Moreover, higher cohesion in *2af-CS, 2rf* and *2rf-CS* products than *2af*, showed by viscosity results, retards the ice front growth by providing an opposing force. Slower ice crystal formation allows neighbouring crystals to exert a compressive force on each other and can compact themselves into a more circular arrangement (Tamaddon et al., 2013).

6.4.5 Measurement method

Assuming that the primary pores adopt a circular arrangement they are often quantified in the literature by taking a single diameter measurement to give an ‘‘average pore size’’ (e.g. (Griffon et al., 2006, Wahl, 2007, Nehrer et al., 1997b)) However, from the observed morphologies of pores in this study, it is suggested that one diameter is insufficient to describe the observed pore morphology and that they could be better quantified as ellipses. Indeed, this need has been recognized in the work of some researchers, such as Zehbe et al. (2010) using Feret’s diameter (Zehbe et al., 2010), Kanungo (2009, 2010), Caliari (2011) and Yunoki (2006) who defined an anisotropy ratio of minor to major axis of best-fit ellipse(Kanungo and Gibson, 2010, Kanungo and Gibson, 2009, Caliari et al., 2011, Yunoki et al., 2006). However, as Walton

(2010) argued, pores are often circularized, either to the minor axis of ellipse, to mean of ellipse axes, to ellipse area or parameter, none of which is an accurate reflection of pore sizes. Therefore, it was decided in this study to fit the pores with ellipses and to state both major and minor axes, cross-sectional pore areas and measure of circularity. Moreover, presenting the data by filtering for desired pore sizes/shapes, which was pioneered by Walton (2010), can be a useful way of communicating the proportion of pores that have the necessary dimensions to support a specific cell type and/or to promote a specific cell activity. The same method was applied to type-I and II scaffolds to categorise the percentage of pores that have the acceptable pore size range for bone and cartilage cell growth, respectively.

It is often shown that the acceptable pore size range for cartilage cell growth in Type II collagen is 50–300 μm (Buckwalter and Mankin, 1997a, Schoof et al., 2001). Bone cells are 10–20 μm in size and many researchers have established that pore sizes between 100 and 1000 μm are suitable for bone growth (Kanungo and Gibson, 2009, Wahl and Czernuszka, 2006, Nehrer et al., 1997b, Klawitter and Hulbert, 1971). The minimum recommended pore size for osteogenesis was said to be 100 μm. Later it was shown that scaffolds with larger pores (>300 μm) favour direct osteogenesis since they allow vascularization and oxygenation while smaller pores result in osteochondral ossification (Karageorgiou and Kaplan, 2005). On the other hand, Itala et al. (2001) showed in a study in rabbits that bone growth occurred in pores as small as 50 μm. Similar results were later obtained for pores in range of 15-40 μm (Itala et al., 2001, Roy et al., 2003, Deville et al., 2006).

Considering the size of bone cells (10-20 μm) it was decided that pore range of 50-600 μm would be a suitable range for type-I scaffolds.

Table 6.2 filtering of pore sizes for type-I scaffolds, % pores with both axes between 50-600um and with the circularised pore diameter between 50-600um.

Sample	% Pores with both axes	% Pores with circularized diameter
1af	28	68
1af-HAp 1:1	67	98
1af-HAp 1:3	77	95
1rf	41	57
1rf-HAp 1:1	44	73
1rf-HAp 1:3	34	62

It is apparent that a relatively low number of pores have the suitable size for osteogenesis in pure *1af* scaffolds (Table 6.2), where the majority of pores on average have both axes below 50 μm. In mineralized afibrillar scaffolds, the numbers were much higher; the limiting factor was the minor axis of ellipse fitted to the pores, since on average pores had their major axis in the desired range, but the minor axis below the threshold.

The same was applied to reconstituted fibrillar scaffolds, where the major axis met the lower limit, but not the minor axis. A similar results were observed by Yunoki (2006), where the "length of the long-axes reached the range that is necessary to bone tissue penetration, whereas that of the short-axes was still small"(Yunoki et al., 2006). Which axis plays a predominant role in bone tissue ingrowth still needs to be determined.

Considering another method of filtration with circularized pore diameters, it can be seen that mineralized afibrillar scaffolds showed a very high percentage of pores with appropriate

sizes. Comparing the results, it becomes clear why it is important to clearly communicate the employed method in order to avoid misleading assessments.

Table 6.3 filtering of pore sizes for type-II scaffolds; % pores with both axes between 30-500um.

Sample	% Pores with both axes	% Pores with circularized diameter
2af	35	55
2af-CS	31	64
2rf	22	54
2rf-CS	37	48

Type II scaffolds, especially with addition of CS, have a moderate percentage of pores (Table 6.3) that should be able to support the growth of chondrocytes, and a relatively high level of circularity which may be desirable for the growth of chondrocytes, because the cells adopt a circular shape in situ and hence the surrounding ECM accommodates this shape around the cell (Wahl, 2007). Thus, these scaffolds may well be suitable to support cartilage cells.

6.5 Summary

The viscosity of suspensions, particle radius as well as changes in the thermal conductivity determined whether a defined pore structure in type-I scaffolds will form. Increasing the viscosity and particle radius by fibrillogenesis, as well as the thermal conductivity by addition of hydroxyapatite ensured the dominance of an attractive force on collagen/particles and therefore a less defined pore structure. However, increasing viscosity also meant higher rigidity of reconstituted fibrillar collagen/composites, thus it is less likely for them to be separated by the growing ice crystal; this also affected the probability of secondary pores

presence. Therefore, the final pore structure is affected by a combination of the abovementioned factors. The same was applied to collagen type-II scaffolds, where differential molecular weight of components also played a part in the final pore structure.

The pore sizes, especially in type-I scaffolds, were explained by growth rate and viscosity of suspensions. The pores were anisotropic and described by major and minor axes of ellipse. A filtering method was applied to measure the proportion of pores with both dimensions in the desired range: a high proportion of pores in type-I and a moderate proportion of pores in type-II scaffolds were suitable for osteoblast and chondrocyte ingrowth, respectively.

6.6 Conclusion

The goal of this chapter was to evaluate the microstructure, including pore sizes and shapes of different scaffold types. The hypothesis regarding the effect of suspension's viscosity on scaffold microstructure was confirmed. However, this was only true for type-I collagenous scaffolds; type-II scaffolds did not show the same degree of correlation between viscosity and pore size. Moreover, it was shown that in type-I scaffolds *1af-HAp 1:1* and *1:3* and in type-II scaffolds *2af-CS* and *2rf-CS* had the highest proportion of pores suitable for osteoblasts and chondrocytes ingrowth, respectively. It is thought that the microstructure evaluated in this chapter, as well as scaffolds chemical compositions examined previously would affect their mechanical properties, which are assessed in the next chapter (Chapter 7).

Chapter 7. Mechanical Properties of Scaffolds

7.1 Introduction

In order to evaluate the suitability of scaffolds for clinical applications, it is important to study their mechanical behaviour. This parameter is especially important when the scaffold is implanted into a defect site, since it must withstand the forces generated by a surgeon during press-fitting. Additionally, the mechanical properties of scaffolds can affect the behaviour of cells *in vitro* and *in vivo*, as will be discussed in Chapter 8. The behaviour of scaffolds in dry state under compression is examined in this chapter. The first section (Section 7.2) describes the experimental procedure of mechanical testing, while the results are presented in Section 7.3, and are discussed in Section 7.4 It is hypothesized that differences in molecular structures (Chapter 4 and 5) and microstructures (Chapter 6) of composite scaffolds affect their compressive modulus.

7.2 Experimental Procedure

The compression test has been widely accepted for measuring the mechanical strength of porous scaffolds and in case of collagen scaffolds for bone and cartilage, compression testing is the most physiologically relevant technique.

Compressive modulus and stress-strain behaviour of scaffolds were determined using Perkin Elmer Dynamic Mechanical Analyzer 7e equipped with a 5N cell load operated at the crosshead speed of 1 mm min^{-1}. All compression tests were performed perpendicular to the plane of the scaffold disc in dry state between two impermeable platens. The indenter was disc-shaped with a size larger than the diameter of the scaffold. Stress-strain curves were plotted and used to calculate the compressive modulus: a line was fitted to the first linear region of stress-strain curve using OriginPro 8.1, and the slope of this line was considered as the compressive modulus.

7.2.1 Statistical Analysis

Tests were repeated on average 5 times for each sample group to achieve mean data (n=5). One-way ANOVA was used to determine any statistical difference between samples with post-hoc Fisher LSD test at level of 0.05.

7.3 Results

The stress-strain curves of scaffolds under compression were obtained as shown in Figure 7.1 and Figure 7.3 for type-I and II composite scaffolds, respectively. Compressive modulus (E*) of cellular solids can be obtained by linear regression of the initial elastic region of the stress-strain curve, which appears in Figure 7.2 and Figure 7.4. In most of the scaffolds it was difficult to distinguish the linear elastic region of the curves. The results are presented in Table 7.1.

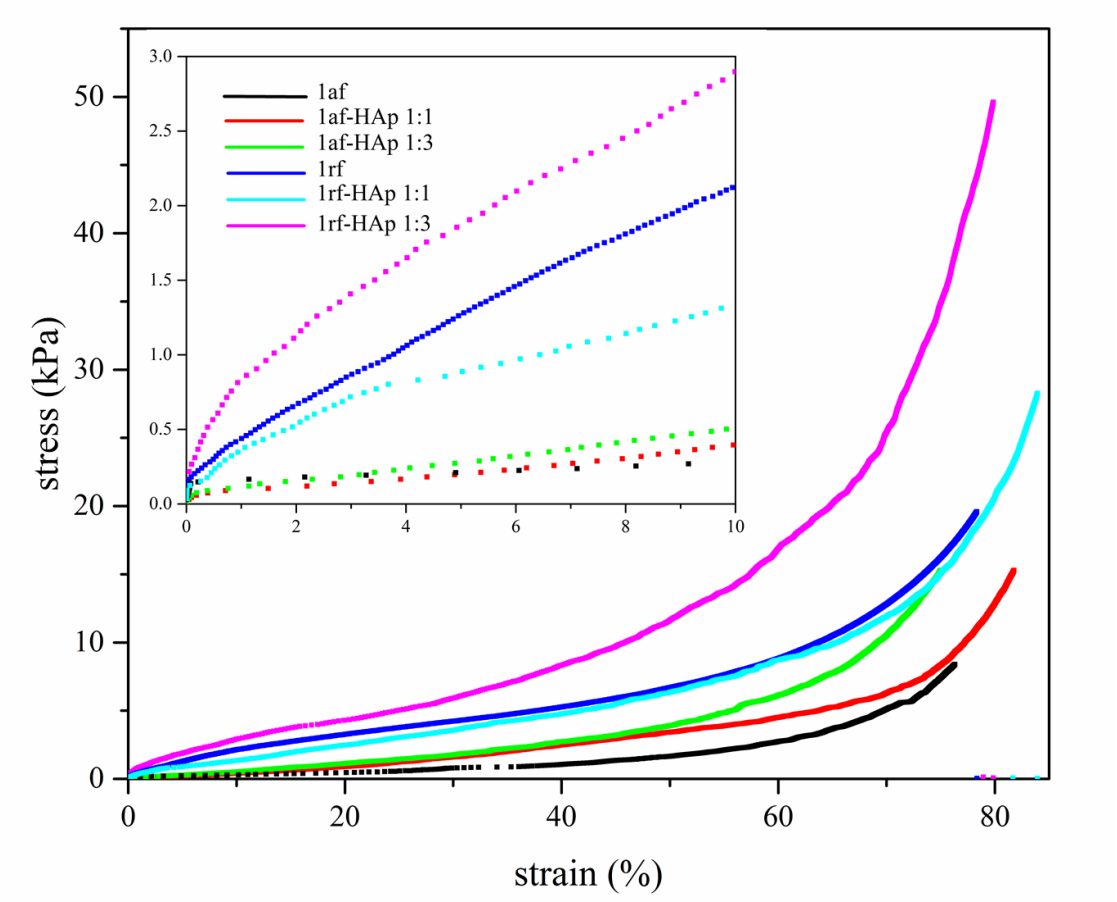


Figure 7.1 Stress-strain curves of type-I collagen composite scaffold under compression (n=5). The inset shows the linear portion of the curve, through which a line was fitted (ending points for *1rf-HAp 1:1* and *1:3* were 20%, for the rest 10% strain); the slope of this line was considered as the compressive modulus

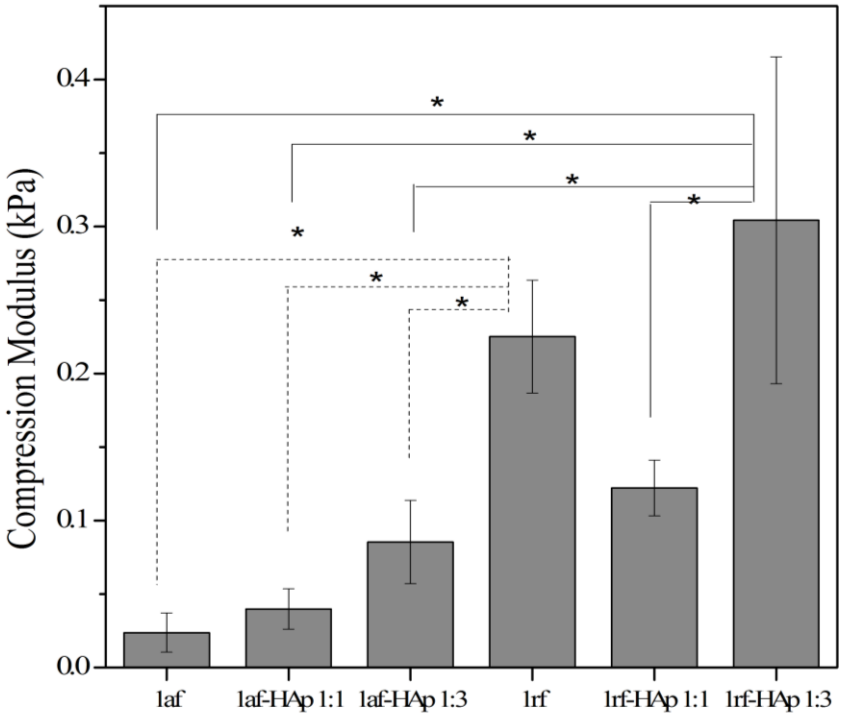


Figure 7.2 Compressive modulus (E*) of type-I composite scaffolds (n=3); * indicates a significant difference at p=0.05

From Figure 7.2, it can be seen that fibrillogenesis significantly increased the compressive modulus of *1af* and *1af-HAp 1:3* nearly 10-fold and 3.5 times, respectively. While addition of HAp had no significant effect on afibrillar scaffolds, trebling the amount of HAp in fibrillar scaffolds increased the E* 3 times.

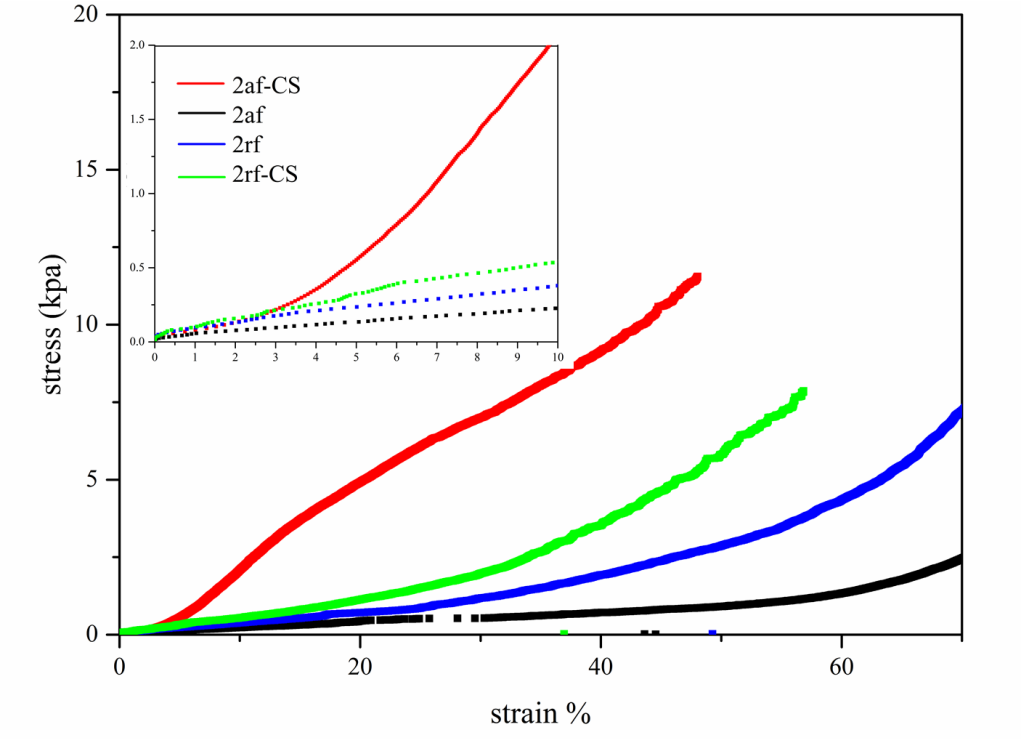


Figure 7.3 Stress-strain curves of type-II collagen composite scaffold under compression (n=5). The inset shows the linear portion of the curve, through which a line was fitted (ending points 10% strain); the slope of this line was considered as the compressive modulus

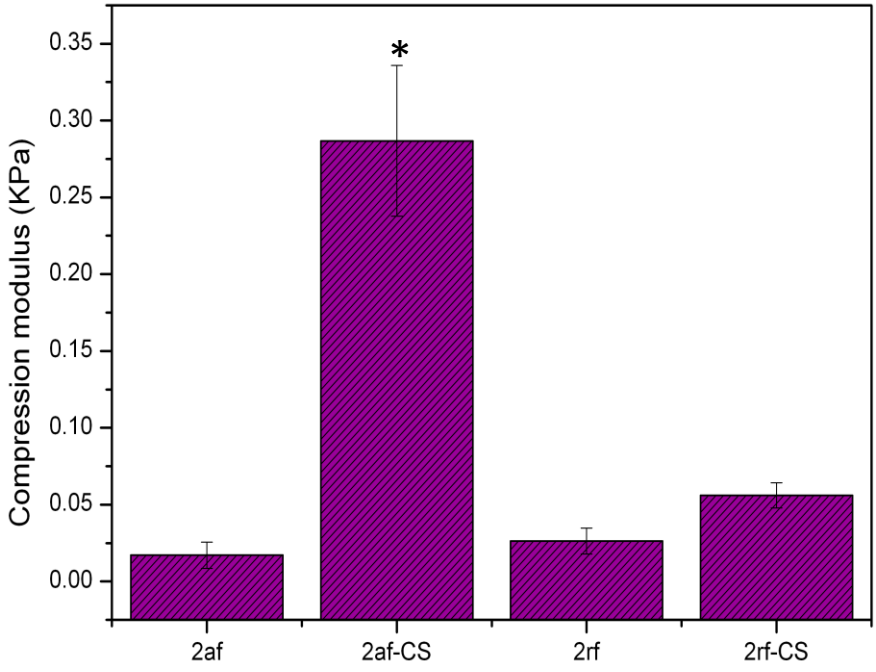


Figure 7.4 Compressive modulus (E) of type-II composite scaffolds (n=5); * indicates a significant difference at p=0.05

As illustrated in Figure 7.4, there was no significant difference in compressive modulus of afibrillar scaffold (*2af*) with fibrillogenesis, while this had a negative effect on the E* of CS-containing scaffolds. Addition of CS to afibrillar scaffold increased the modulus 10-fold while it had no significant effect on reconstituted fibrillar scaffolds.

Table 7.1 Compression modulus of type-I and II composite scaffolds (n=5), SD= standard deviation.

Sample	**Compression Modulus (kPa)**	**SD**
	Type-I	
1af	0.023	± 0.013
1af-HAp 1:1	0.040	± 0.013
1af-HAp 1:3	0.085	± 0.028
1rf	0.225	± 0.038
1rf-HAp 1:1	0.122	± 0.019
1rf-HAp 1:3	0.304	± 0.111
	Type-II	
2af	0.017	± 0.008
2af-CS	0.287	± 0.049
2rf	0.026	± 0.008
2rf-CS	0.056	± 0.008

7.4 Discussion

The mechanical behaviour of collagen composite scaffolds in compression was evaluated and the results were presented in the form of a compressive modulus (E*). In order to explain the differences in the compressive moduli of scaffolds, the mechanism of deformation as well as the parameters affecting it should be clarified.

It has been shown that scaffolds exhibit behaviours typical of low-density foams (Gibson and Ashby, 1997). As can be seen from Figure 7.5, according to cellular solid mechanics the stress-strain curve is characterised by three distinct regions: a linear elastic regime (controlled by pore-edge bending) occurring at approximately 5% strain, a collapse plateau (controlled by pore wall buckling) and a densification regime (controlled by complete pore collapse) occurring at around 80% strain, when pore walls are forced into contact and further buckling is not possible (Gibson and Ashby, 1997, Harley et al., 2007, Chen et al., 2012, Ashby, 2006). This is similar to classifications made by Gibson and Ashby (1997) for an open-cell elastomeric foam, where the collapse plateau was influenced by the pore edge buckling; however, based on microstructural evaluations, the scaffolds in this study, although possessing interconnected porosity, exhibit not only pore edges but also pore walls. It is worth mentioning that the deformation mechanism of most foams, whether open-cell or closed-cell is bending-dominated (Ashby, 2006).

A schematic diagram of the stress-strain curve for low-density foam under compression is shown in Figure 7.5, depicting linear, collapse and plateau regions.

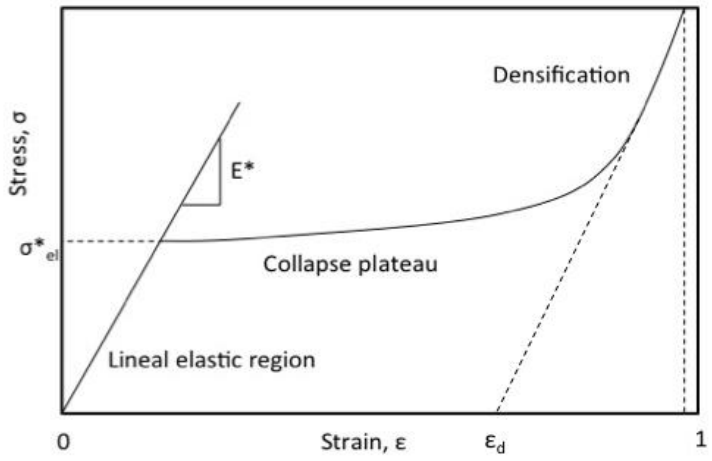


Figure 7.5 Schematic stress-strain curve of a low density foam under compression; σ*is collapse stress and ε_d is densification strain. Adapted from (Ashby, 2006, Gibson and Ashby, 1997)

In some cases, the initial linear elastic region was hard to distinguish, especially in afibrillar type-I scaffolds (Figure 7.1) and pure afibrillar type-II scaffold (Figure 7.3). The reason is likely to be that the pore edge bending and pore wall buckling occurred at the same time.

The mechanical properties of these cellular solids are a function of the relative density (density of scaffold ρ^* /density of solid ρ_s), their topology (connectivity and shape of the pores) and the solid material from which they are made (Ashby, 2006).

If the solid behaves similar to an elastomer (in this work collagen/collagen-CS) its compression modulus is buckling-dominated (Figure 7.6) and is described by Equation 7.1 and Equation 7.2, where C_1 is an empirical constant (~1) and E_s is the solid modulus (Gibson and Ashby, 1997, Harley et al., 2007, Kanungo and Gibson, 2010):

$$E^* = C_1.(\frac{\rho^*}{\rho_s})^2.E_s$$ Equation 7.1

Substituting E_s by its equivalent from rule of mixture, we will have:

$$E^* = C_1.\left(\frac{\rho^*}{\rho_s}\right)^2.(v_{col}.E_{col} + v_{CS}.E_{CS})$$ Equation 7.2

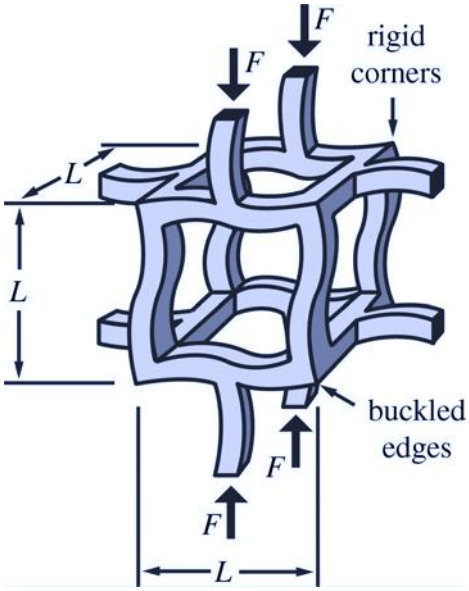


Figure 7.6 Buckling dominated behaviour of a pore (Ashby, 2006)

If the solid is brittle then its deformation is fracture-dominated and can be depicted by Figure 7.7; the behaviour of *1af-HAp 1:3* and *1rf-HAp 1:3* might be in part controlled by this mechanism due to the high amount of HAp.

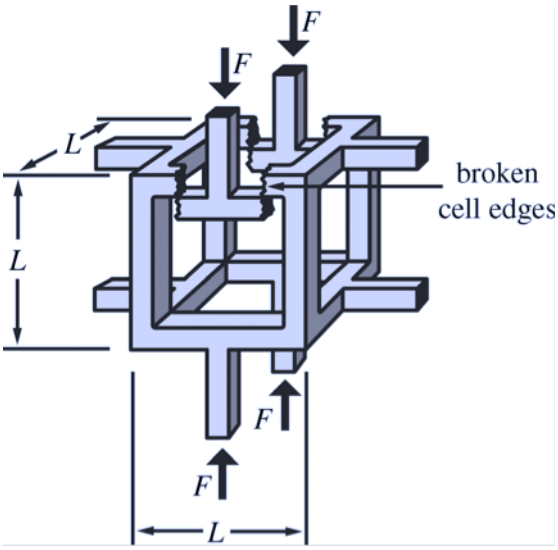


Figure 7.7 Fracture-dominated behaviour of a pore (Ashby, 2006)

The relative densities of scaffolds (Table 7.2 and 7.3) were determined to be not significantly different (p<0.05), using the measurements of scaffold weight and dimensions, and density of solid material (ρ_{col}=1.3 g/cm3, ρ_{CS}=5.5 g/cm3, ρ_{HAp}=3.16 g/cm3)(Harley et al., 2007, Monmaturapoj et al., 2012, Kanungo and Gibson, 2010). In fact, Tiernery et al. (2008) also reported that addition of GAG to their collagen scaffold had little effect on porosity (Tierney et al., 2009a). Therefore, other parameters, explained below, are more likely to be influential in determining the compressive modulus.

Table 7.2 relative density of type-I scaffolds; no significant difference at level of 0.05 between afibrillar scaffolds; significant difference between 1rf and afibrillar scaffolds, and between 1rf and 1rf-HAp 1:1, and between 1rf-HAp 1:3 and all other scaffolds.

Scaffold	***1af***	***1af-HAp 1:1***	***1af-HAp 1:3***	***1rf***	***1rf-HAp 1:1***	***1rf-HAp 1:3***
Relative density $(\frac{\rho}{\rho_s}^*)$	0.00769	0.00791	0.0111	0.04511	0.01014	0.12504

Table 7.3 Relative density of type-II scaffolds; no significant difference at level of 0.05 was observed

Scaffold	***2af***	***2af-CS***	***2rf***	***2rf-CS***
Relative density ($\frac{\boldsymbol{\rho}^*}{\boldsymbol{\rho_s}}$)	0.00501	0.00523	0.00564	0.00479

Another factor affecting mechanical behaviour is pore anisotropy. Caliari et al. (2011) described modulus E_a^*, when the pores are anisotropic, as (Caliari and Harley, 2011):

$$E_a^* = E_i^*\left(\frac{2R^2}{1+\left(\frac{1}{R}\right)^3}\right) \qquad \text{Equation 7.3}$$

Where E_i^* is the modulus of the isotropic foam, and R is the aspect ratio of pores.

Based on the results from Section 6.3.1, it can be seen that in general, pores in afibrillar type-I and type-II scaffolds were more anisotropic than their reconstituted fibrillar scaffolds in the transverse direction. Since the thermal gradient during freezing of suspensions is in the longitudinal direction, it is therefore expected that even more anisotropy will be observed in this direction, which is also the loading direction in compression testing. It is thus hypothesised that the anisotropy in the transverse direction can be indicative of anisotropy in the longitudinal direction, yielding more or less the same relationship between the R of different scaffolds (see Table 7.4). Caliari et al. (2012) (Caliari et al., 2012) observed that the anisotropy of pores was larger in the longitudinal direction and followed the same trend as in the transverse direction.

Table 7.4 Anisotropy ratio, R, of different scaffolds.

Scaffold	Aspect ratio, R	Scaffold	Aspect Ratio, R
1af	2	***2af***	3.2
1af-HAp 1:1	2.56	***2af-CS***	2.05
1af-HAp 1:3	2.4	***2rf***	1.98
1rf	1.89	***2rf-CS***	1.95
1rf-HAp 1:1	1.94		
1rf-HAp 1:3	2.04		

The last parameter to consider is the modulus of the solid pore wall. For type-I composite scaffolds Equation 7.4 applies, which shows that according to the rule of mixture the modulus of a solid would increase when increasing the volume of HAp (constituent with the higher modulus, $E_{HAp} > E_{col}$).

$$E_{comp} = E_{col}V_{col} + E_{HAp}V_{HAp} \qquad \text{Equation 7.4}$$

$$E_{comp} = E_{col}V_{col} + E_{CS}V_{CS}$$

Where V_{col}=volume fraction of collagen, V_{HAp}=volume fraction of HAp, V_{CS}=volume fraction of CS.

Overall, in this study composite scaffolds (both type-I and type-II) contained a higher amount of solid material in the starting suspension compared to pure scaffolds, which is expected to render a denser scaffold (Wahl et al., 2007) and thicker pore walls and edges that contribute to their higher compression modulus. Harley et al. (2007) postulated that an increase in the size and therefore flexural rigidity of struts would increase the macroscopic compressive

and tensile moduli (Harley et al., 2007, Caliari et al., 2012). An attempt was made to measure the thickness of the walls; however, it proved to be very subjective and therefore was not pursued.

7.4.1 Mechanical behaviour of type-I scaffolds

The increase in the compressive modulus of afibrillar scaffolds with addition of hydroxyapatite can be attributed to a combination of the factors mentioned above. The relative densities of the scaffolds were not significantly different; however, the pore anisotropy of mineralised scaffolds was higher than that of pure collagen scaffold. Moreover, the solid modulus of the scaffolds increased by adding and increasing the amount of HAp as described by Equation 7.4. Further, the pore walls and edges are expected to be thicker because the density of the starting suspension is 0.5% wt/v in *1af*, 1%wt/v in *1af-HAp 1:1* and 2% wt/v in *1af-HAp 1:3*, which led to the continual increase in the compressive modulus with the addition of HAp.

In reconstituted fibrillar scaffolds, it is possible that the fibrillar structure of collagen, which is brought about by fibrillogenesis, has increased the modulus of the solid pore wall. In rheology results (Figure 5.11 in Section 5.4.2) an increase in the complex modulus of reconstituted fibrillar suspensions was observed compared to afibrillar mixtures; moreover, it is possible that crosslinks that formed during freeze-drying, stabilised the structure and subsequently increased the modulus. It has been shown that local heterogeneity in the structure can adversely affect the modulus of the scaffold (Harley et al., 2007, Kanungo and Gibson, 2009); however, no such heterogeneity was observed in SEM pictures of *1rf-HAp 1:1* (Figure 6.5) to explain the lower modulus compared to *1rf*.

7.4.2 Mechanical behaviour of type-II scaffolds

In type-II scaffolds, there are a number of factors involved in significantly increasing the compressive modulus of *2af-CS* compared to other scaffolds. The pore anisotropy was intermediate; however, following a same line of reasoning regarding the pore wall and edge thickness, *2af-CS* is expected to be superior to *2af* and *2rf*. Yet, it is suggested that the 10-fold increase in the modulus mainly originates from the elastic modulus of the solid and the interaction of collagen and CS at molecular level as explained in Section 4.4.2. Indeed it has been shown that GAG chains play an important role in stabilising the structure of collagen networks and transferring stress efficiently (Liang et al., 2010, Redaelli et al., 2003). The bonding between afibrillar collagen and CS in *2af-CS* scaffolds, observed in FTIR results (Figure 4.3), may therefore be corroborated by the improved mechanical properties.

However, fibrillogenesis does not seem to have had any significant ($p<0.05$) effect on compressive modulus. Type-II collagen, by itself, is incapable of forming fibrils of extensive lengths (Brinckmann et al., 2005) and it has been shown (Douglas et al., 2006) that the proportion of collagen incorporated into fibrils, as well as fibril length and thickness, decreases with addition of CS. Once bound to fibrils, CS may prevent further fibril growth, resulting in less collagen being incorporated into fibrils; the more CS present, the greater the hindrance. This may explain the significantly lower E* for *2rf* -CS compared to *2af* -CS. Another hypothesis is that the loss of some CS occurred as the reconstituted fibrillar scaffolds were subjected to dialysis and subsequent washing; however, Liang et al. (Liang et al., 2010) produced concentrated collagen-CS scaffolds using the same method utilised for washing the scaffolds and reported no loss of CS during the process.

In order to evaluate the mechanical properties of these scaffolds at a practical level, one question is how they behave when they subject to loads similar to those during the press fit implantation of bone plugs, which is approximately 100kPa (Harley et al., 2010b).

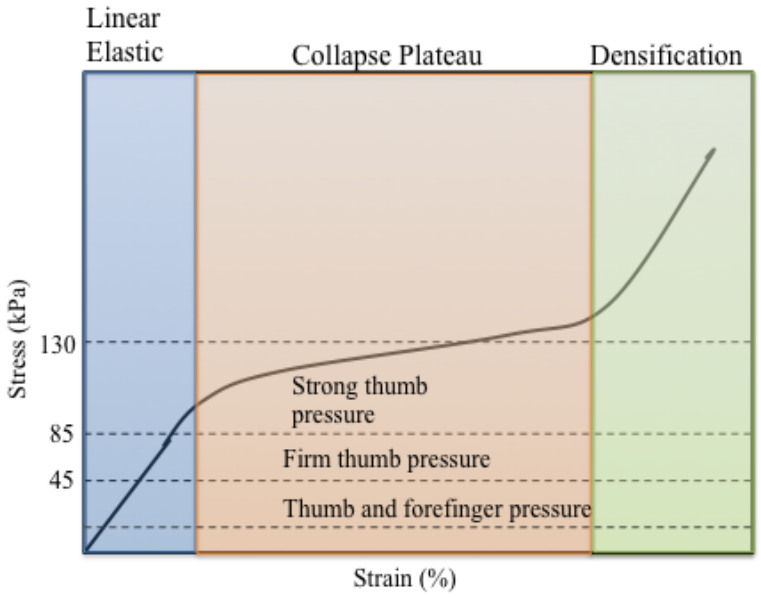


Figure 7.8 Schematic diagram of stress-strain curve of a hypothetical scaffold with regions marked for typical loads generated by thumb, firm thumb and strong thumb pressures. Adapted from (Harley et al., 2010b)

Comparing the stress-strain curve of type-I and II scaffolds (see Figure 7.1 and Figure 7.3), it can be seen that all of the scaffolds will be in densification region (Figure 7.8) if subjected to the thumb pressure during implantation. Therefore, alternative implantation techniques should be explored. An example is to use tweezers for placing the scaffold in the defect site. The low compressive modulus of these scaffolds is one of the limitations of using monomeric collagen compared to microfibrillar collagen. One way of overcoming this restriction is crosslinking, which has been used extensively to produce scaffolds with improved mechanical properties (e.g. in (Walton, 2010, Harley et al., 2010b)). Other options may include –as

mentioned in this section- increasing the concentrations of starting materials and controlling the relative density of scaffolds.

7.5 Summary

In type-I scaffolds, the combination of the increasing solid wall modulus/density by addition of HAp as well as pore anisotropy led to higher compressive moduli, while in type-II, the change in solid wall modulus by bond formation between CS and collagen is thought to be the main reason for the 10-fold increase in compressive modulus of *2af-CS*.

It should be noted that by press-fitting the scaffolds in defects, scaffolds would be in densification region, thus a mechanism for increasing the compressive modulus, either by increasing the percentage of starting materials or cross-linking could be beneficial.

7.6 Conclusion

The aim of this chapter was to measure the compressive modulus of the synthesised scaffolds and evaluate their suitability for clinical applications. The hypothesis that differences in molecular and microstructures of composite scaffolds affect their compressive modulus was confirmed: In case of molecular structure, addition/interaction of HAp/CS with collagen, as well as fibrillogenesis, increased the solid wall modulus of samples and was determined to be a significant contributor to the increased compressive modulus. In terms of microstructure, pore shape (anisotropy) had the most effect on the mechanical properties of scaffolds. Considering the results of this chapter, in type-I scaffolds *1rf* and *1rf-HAp 1:3* and in type-II scaffolds *2af-CS* are the most suitable groups. It is thought that scaffolds chemical/molecular structure (as discussed

in Chapter 4), microstructure (as discussed in Chapter 6) and mechanical properties (as discussed in this chapter) would affect cellular behaviour. This hypothesis is examined in Chapter 8.

Chapter 8. Biological Properties of composite scaffolds

8.1 Introduction

The first step in evaluation of scaffold interaction with cells is usually an *in vitro* cell culture. The cell culture work and analysis were carried out with the kind collaboration of Dr. Eileen Gentleman and her group at Craniofacial Development & Stem Cell Biology, King's College London. The scaffolds were prepared as described in Section 3.2and sterilised (Section 8.2.1). The protocols for examination of scaffolds biocompatibility, cell morphology, and proliferation are presented in Sections 8.2.3, 8.2.4 and 8.2.5, respectively. The procedures for histological and immunohistochemistry are explained in Sections 8.2.6 and 8.2.7. The results are given in Section 8.3 and are discussed in Section 8.4. A summary of findings is shown in Section 8.5.The objectives of this chapter were to determine the biocompatibility of scaffolds and examine scaffold-cell interactions, and it is hypothesized that the scaffold characteristics determined in earlier chapters, would affect cellular response in terms of proliferation and differentiation.

8.2 Experimental Procedure

8.2.1 Scaffold sterilization

Gamma irradiation is commonly used for sterilisation of medical devices and pharmaceuticals. Here, gamma rays are produced by self-disintegration of Cobalt 60 or Cesium 137, generating ionization throughout a sample (da Silva Aquino, 2012). The changes induced by these photons at the molecular level cause the death of the organisms and sources of contamination. This was the sterilisation method of choice because it does not create any

residuals and it does not involve the detrimental washing process of using ethanol as sterilant as described elsewhere (Walton, 2010).

The samples were placed in suitable containers (clear vials, Sigma Aldrich, UK) and exposed to radiation at a dose of 18 kRads per hour for 1 hour.

The industry standards for sterilisation of implants by gamma is 2.5Mrads (Cheung et al., 1990), however, collagen is susceptible to damage at such high dosages. Therefore, a much lower dose was chosen and the effect on collagen structure was studied. Also, it was investigated whether this dosage was enough to sterilise the samples.

8.2.1.1 Sterilisation effectiveness

Six types of gamma-irradiated scaffolds (*1af, 1af-HAp 1:1*, *1rf-HAp 1:1*, *2af*, *2af-CS* and *2rf-CS*) were chosen as representative, and one of each was placed in α-MEM (negative Ribonucleosides) containing 10% Fetal Bovine Serum (FBS), for 3 days and any changes in the media (cloudy appearance, sudden drops in pH and moving granules/bacteria) was observed. After that, human bone marrow mesenchymal stem cells (hBMMSCs) passage 6 were seeded on *1af* and *2af-CS* in order to see if any infection occurs.

8.2.2 Cells and Media

The response of hBMMSCs to the scaffolds was examined. These types of cells were selected because they are capable of differentiating along several lineage pathways including mesenchymal tissues such as bone and cartilage (Pittenger et al., 1999, Sharma and Elisseeff, 2004, Livingston et al., 2003). Hence, the following assays were designed to assess whether the scaffolds of different types have the ability to differentiate cells into bone and cartilage lineage.

The cells were isolated from bone marrow of young adults, cryopreserved and thawed when required. To prepare the cells, they were thawed at 37°C in a water bath, and then resuspended in α-MEM medium (Gibco, UK) containing 10% or 15% FBS. When the tissue culture flasks were near confluent, the cells were passaged until sufficient number of cells was achieved.

Hundred microliter of expansion medium containing either 450,000 or 160,000 cells per well was placed on top of each scaffold in a 24-well suspension plate, and cells were allowed to adhere for 1 h before adding 500ul of medium supplemented with 1% antibiotics, and were incubated at 37°C and 5% CO_2. The medium was changed every other day until the time point for each assay (up to 28 days).

hBMMSCs viability, morphology, infiltration, proliferation, GAG production and differentiation on scaffolds were assessed using the following assays as illustrated in Figure 8.1.

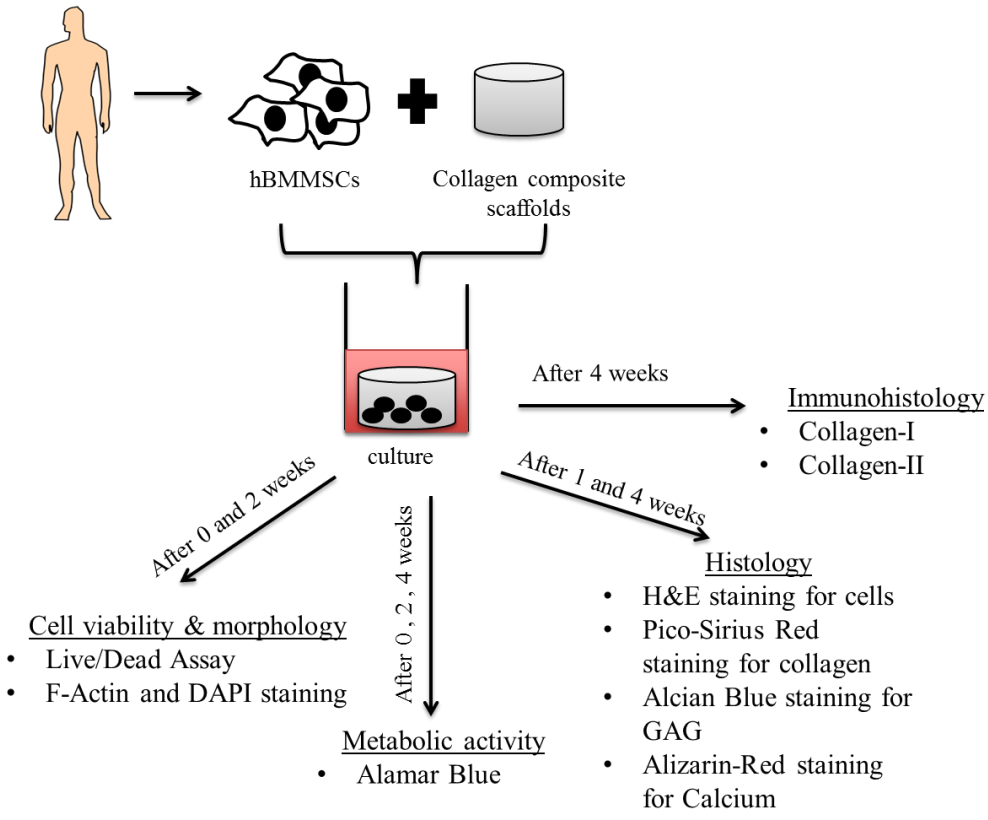


Figure 8.1 Cell culture and characterisation assays

8.2.3 Live/Dead assay (cell viability)

BMMSCs viability on scaffolds (160,000 cells per scaffold) was assessed using the Live/Dead Cell Viability assay (Invitrogen) after 0 and 2 weeks in culture. Scaffolds were rinsed twice with PBS and incubated with 4 mM Calcein AM and 4 mM ethidium homodimer-1 in PBS for 15 mins, which stain live and dead cells green and red, respectively.

Cells were imaged using an Olympus IX51 fluorescence microscope equipped with an Olympus DP70 camera. After imaging, scaffolds were rinsed with sterile PBS and incubated with cell culture media until next screening.

8.2.4 Cytoskeletal immunostaining (cell morphology)

Cell cytoskeletal organization, which is an indication of cell morphology, was assessed by immunostaining for cell nuclei using DAPI (4',6-diamidino-2-phenylindole, dihydrochloride) and for cytoskeleton using Alexa Fluor Phalloidin which is a high-affinity F-actin probe conjugated to Alexa Fluor dye.

The primary solution was produced by adding 1.5ul of Alexa Fluor 568 phalloidin (Invitrogen; 1:160) to 100ul of 1%BSA in PBS and DAPI solution was prepared by adding 2ul of DAPI (Sigma, UK; 1:1000) to 100ul of deionized water for each sample.

Scaffolds (160,000 cells per scaffold) at 0 and 2 weeks, were fixed in 4% w/v paraformaldehyde (PFA) for 20 min, washed twice with PBS, and permeabilized with 0.1% v/v Triton X-100 in PBS for 30 min. 3% Bovine Serum Albumin (BSA) in PBS was then added to the samples for 30 min. Actin cytoskeleton was stained with the primary solution for 1 hour, and nuclei were stained with DAPI solution for 1min. The samples were then rinsed with PBS, and cells were imaged on an Olympus IX51 epifluorescence microscope equipped with an Olympus DP70 camera.

8.2.5 Cell Proliferation

Cell proliferation is a critical feature of cell study when developing a TE scaffold. To measure cell proliferation and number, there are various assays available, including Alamar Blue and DNA quantification. Alamar Blue is a water-soluble tetrazolium salt, based on measuring the metabolic activity of cells. After 1, 7, 14 and 28 days, scaffolds were transferred to a new well-plate, imaged with an HP scanner to determine the size of scaffolds and then cell culture

media containing 10% Alamar Blue (Invitrogen) was added to each well. The scaffolds were incubated for 4 hours and 200 µl of supernatant was transferred to a 96 micro well-plate. The plate was read by a fluorescent plate reader at 530-560 nm excitation and 590 nm emission. Two sets of Alamar Blue experiments were conducted with cells from two different donors. In the first experiment, the metabolic activity of cells decreased monotonically over 28 days. The reason for the unusual behaviour of cells in the first experiment is thought to be due to the quiescent nature of first donor cells; in the Alamar Blue experiment, it is assumed that all live cells are metabolically active, as opposed to quiescent. Therefore, in results and subsequent analysis only data from the second experiment are presented and used.

8.2.6 Histological examination

At week 1 and 4, the samples (450,000 cells per scaffold) were fixed in 4% PFA and stored in PBS. To embed the samples in wax, they were first moved to 70% v/v and then 90%v/v ethanol solution, each time for 10 min. 100% ethanol was then added three times, each time for 10 min, removed and replaced by three rounds of histoclear and finally paraffin. The embedded samples were then sectioned at a thickness of 10um.

The sections were stained to distinguish different elements using the following stains:

Pico-Sirius Red was used to mark the collagenous structure, where under bright-field light, it appears red. Sirius Red is a strong elongated anionic dye, which reacts with collagen via its sulphonic acid groups, with basic groups present in the collagen (Junqueira et al., 1979).

Alcian blue is one of the most widely used dyes for GAGs staining. It is mainly positively charged and therefore, is thought to work by forming electrostatic bonds with negative sites on the polysaccharide staining them blue.

The sections were first deparaffinised using two rounds of histoclear (10 min each), rehydrated in industrial methylated spirit (IMS) 100%, 90%, 70% and 50% each for 2 min, washed with deionised water and placed in Alcian Blue (pH 2.5) for 10 min, washed with running and deionised water, stained with haematoxylin for 2 min and washed again with running and deionised water. The sections were then transferred to phosphomolybdic acid 2.5% (Fisher Scientific, UK) for 10 min. They were washed with deionised water and incubated with Sirius Red F3B 0.5% (Direct Red 80, Sial) in saturated picric acid for 1 hour. The sections were then rinsed with acetic acid 0.5% twice, placed in 100% IMS and histoclear three times each for 5 min, and finally permanently mounted with Neo-Mount glue (Merck) and dried before observation with a Zeiss Axioskop 2 Plus microscope in conjunction with a Zeiss AxioCam HR camera and the AxioVision software.

Alizarin Red (pH 4.3) is used to specify calcium-rich deposits by cells for hydroxyapatite screening, where calcium forms an Alizarin Red S-calcium complex in a chelation process, coloured red/orange and the end product is birefringent (Gregory et al., 2004).

The sections were deparaffinised with two rounds of histoclear each for 10 min, and rehydrated in 100% and 90% IMS for 2 min. The sections were then transferred to Alizarin Red solution for 2 min. They were washed with acetone, acetone-xylene 1:1 solution and xylene, and mounted with DPX and coverslip and dried in a Unitemp Incubator (B&T, UK) set at 42°C before microscopy.

Hematoxylin and Eosin (H&E) is the most commonly used technique for nuclei and cytoplasm staining, where basophilic structures (nucleic proteins) are shown blue, black, purple or grey by haematoxylin and acidophilic structures (cytoplasmic proteins) are pink and red by Eosin.

The sections were deparaffinised and rehydrated as stated before. They were then washed with deionised water, stained with Ehrlich's Haematoxylin (Solmedia) for 10 min, washed with running water, deionised water, acid alcohol (1% HCL in 95% IMS), and another round of running and deionised water, and stained with 0.5% Eosin Y (Sigma Aldrich, UK) in 2mM acetic acid. The sections were washed and dehydrated and mounted with Neo-Mount (Merck) and dried before microscopy.

8.2.7 Immunohistochemistry

Immunohistochemistry (IHC) is a technique employed to localise and visualise proteins in a tissue section using specific antibodies (Chi and Chandy, 2007). Although it is less sensitive for a quantitative analysis of protein expression than methods such as ELISA, it nevertheless enables the observation of such proteins.

The primary antibodies are raised in another species against a target of interest, and a secondary antibody is raised against the immunoglobulins of the primary antibody species conjugated to a dye or fluorophore facilitating its visualization.

In order to detect any collagen type-I and -II, the primary antibodies used were mouse monoclonal to collagen-I (ABCAM ab 90395) and mouse monoclonal to collagen-II (ABCAM

ab 3092), respectively. They react only with collagen-I and II in human. The secondary antibody used was goat anti-mouse conjugated to Alexa488 (ab150117) in both cases.

The PFA-fixed, paraffin-embedded samples were sectioned at 10 μm and deparaffinised with two rounds of histoclear each 10mins, and rehydrated by 100%, 90%, 70% and 50% of IMS, and kept in water to avoid non-specific binding. In order to unmask antigens and epitopes in formalin-fixed and paraffin-embedded sections, enzymatic antigen retrieval with pepsin solution was performed. Basically, formalin forms protein cross-links, masking the antigenic sites in tissue specimens, thereby giving weak staining for detection. The pepsin-based enzymatic solution disrupts these cross-links, hence enhancing staining intensity of antibodies.

Pepsin equilibration solution (0.02N HCl) was added for 10 mins to slides and then the slides were incubated at 37°C with pepsin digestion solution (10mg/ml in 0.02N HCl) for 45 mins in a humidified chamber and washed with PBS following antigen retrieval. Blocking solution (5% Goat serum in 0.01% Triton-PBS) was added for 60 mins, after which the primary antibody (1:200 dilution) was applied and samples were incubated at 4°C overnight. On day two, the samples were washed with PBS, and incubated for 1 hour at room temperature with the secondary antibody (1:200 dilution). The samples were then counterstained with DAPI, mounted and stored at 4°C in the dark until microscopy.

8.2.8 Statistical Analysis

For qualitative assays, including Live/Dead, cytoskeletal imaging, histology and immunohistochemistry, one sample per group per time point was used (n=1). For quantitative assays, including Alamar Blue and scaffold size measurements, three scaffolds per group per

time point were used (n=3). In addition to that, one control sample (no cells) for Alamar Blue, and 3 control samples (no cells) for size measurements per time point were utilised. Significant difference was determined by one-way ANOVA with post-hoc Fisher LSD test at level of 0.05.

8.3 Results

This section described the outcomes of the cell study. Firstly, the scaffold size changes in cell culture media and by the cells are presented. Then the assays results including Live/Dead assay, cytoskeletal immunostaining, AlamarBlue proliferation, histology and immunohistochemistry are reviewed.

8.3.1 Scaffold size evaluation and cell mediated contraction

The sizes of the scaffolds were measured after 1 and 28 days of culture and their reduction relative to the original size is shown in Figure 8.2.

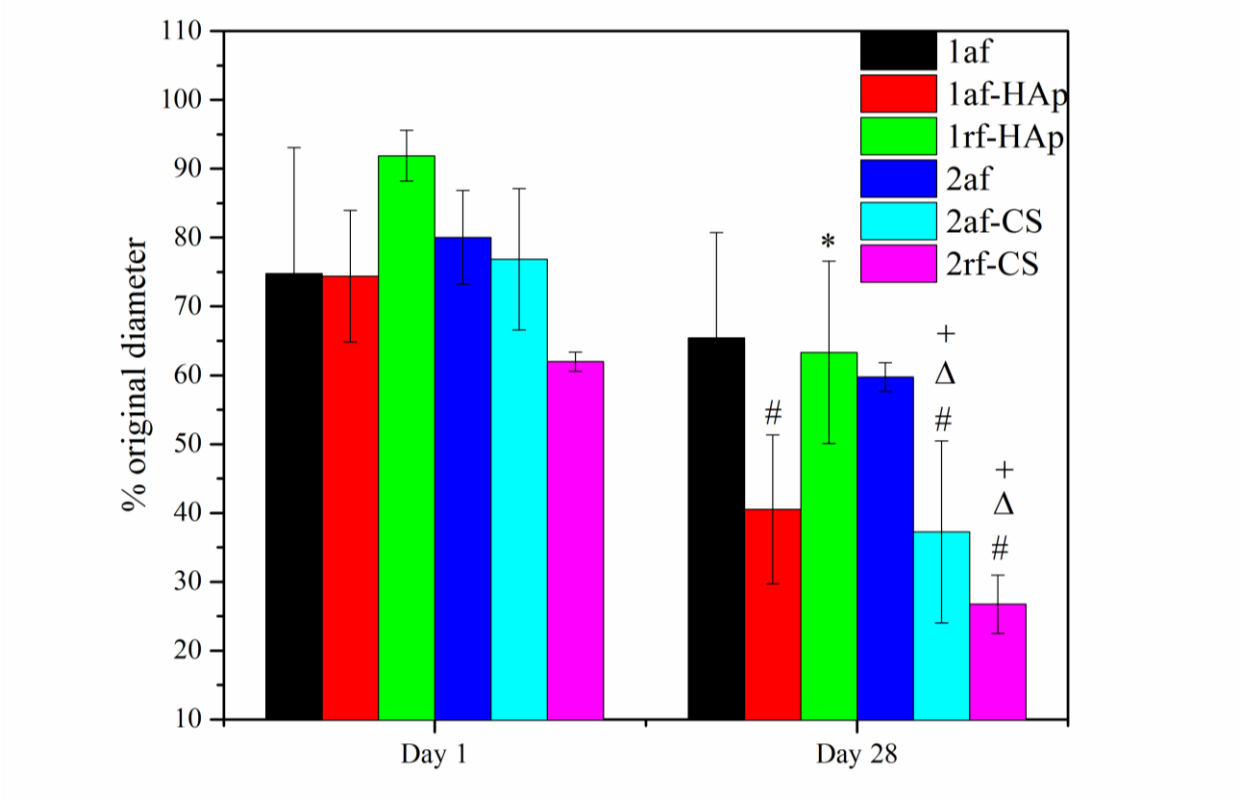


Figure 8.2 Percentage of change in scaffold diameter before cell seeding and after 1 and 28 days of culture. Symbols show significant difference at $p<0.05$: # significantly different from *1af*; * significantly different from *1af-HAp*; Δ significantly different from *1rf-HAp*; + significantly different from *2af*. No significant difference between groups at day 1 ($p<0.05$)

After 28 days *1af*, *1rf-HAp* and *2af* decreased to 60-70% of their original size, while *1af-HAp*, *2af-CS* decreased to 35-45% of the original size. It was observed that *2rf-CS* exhibited a more dramatic drop to only 10% of its size before culture.

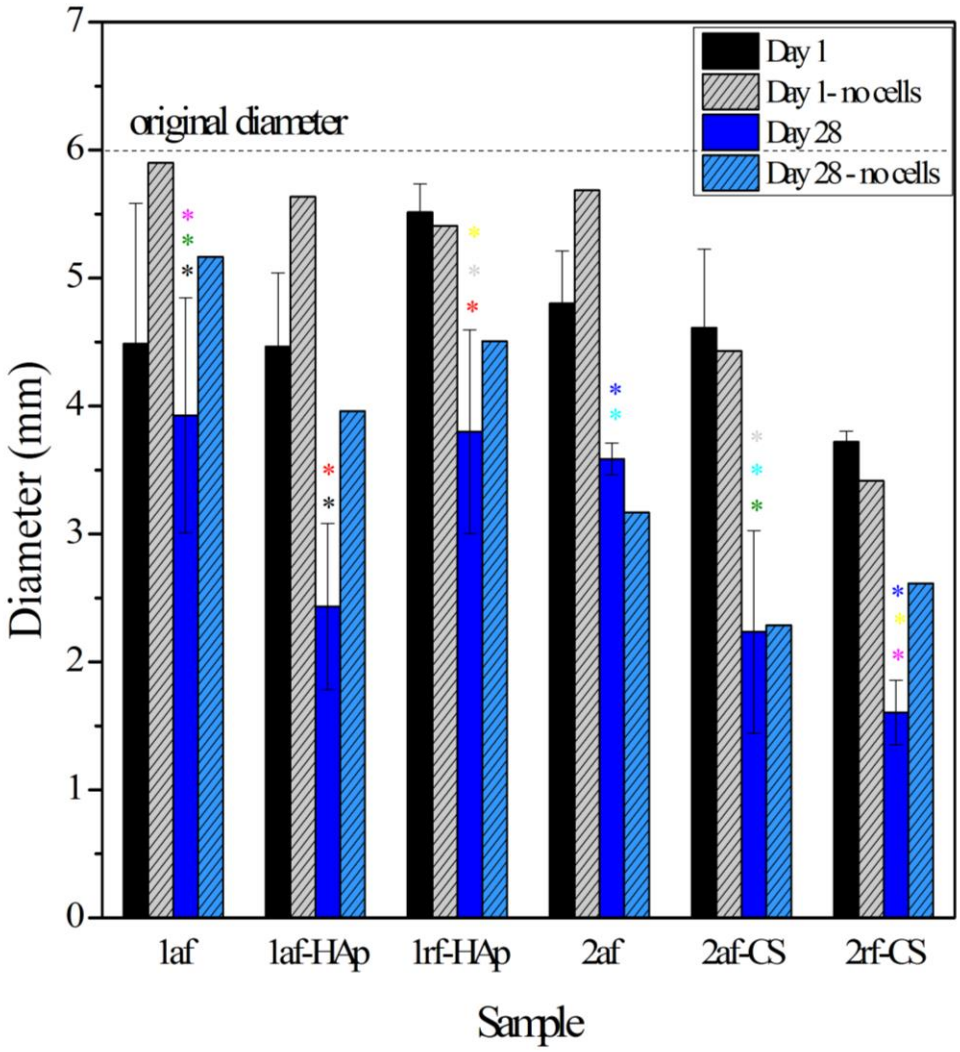


Figure 8.3 Scaffold sizes after 1 day (black column) and 28 days (blue column) of cell seeding in culture media. The dashed columns represent scaffold diameter after 1 day (gray) and 28 days (light blue) in media only (no cells). The diameter of scaffolds before cell seeding is denoted by dashed line. The "*" of different colours demonstrates significant difference between groups at day 28. There was no significant difference at day 1 (p<0.05) (n=3)

As it can be seen in Figure 8.3, after 1 day of culture, all of the cell-seeded scaffolds except *1af*, *1af-HAp* and *2af* showed a greater reduction in diameter than unseeded scaffold. After 28 days, only *2af* showed a slightly lower reduction in diameter in cell-seeded compared to

unseeded scaffold. Also, it was noted that the diameter of all of the unseeded scaffolds decreased over time.

In order to show the cell-mediated changes in size the readings from the control scaffold and cell-seeded scaffolds were used in Equation 8.1 (Lee et al., 2001). The results are shown in Table 8.1 and Table 8.2.

$$Cell\ mediated\ change\ in\ size = \left(\frac{original\ diameter - diameter}{original\ diameter}\right)_{seeded} - \left(\frac{original\ diameter - diameter}{original\ diameter}\right)_{unseeded} \quad \text{Equation 8.1}$$

Table 8.1 The overall, cell-mediated and solution-mediated changes in scaffold diameter at day 1. The overall reduction was calculated as (original diameter-diameter at day1)/original diameter; SD= standard deviation (n=3).

Scaffold	% overall reduction in size	% solution-mediated changes	% cell-mediated changes	SD
1af	25.22	1.63	23.59	± 18.28
1af-HAp	25.58	6.07	19.51	± 9.56
1rf-HAp	8.1	9.87	-1.77	± 3.68
2af	19.97	5.26	14.71	± 6.81
2af-CS	23.14	26.17	-3.03	± 10.26
2rf-CS	38.02	43.07	-5.05	± 1.41

Table 8.1 shows that at day 1 the diameter of *2rf-CS* scaffold decreased to a higher extent compared to other samples, followed by *1af* and *1af-HAp* . Cell-mediated changes were greatest in *1af* (although a large standard deviation was observed).

Table 8.2 cell-mediated and overall reduction in scaffold diameter at day 28; SD= standard deviation (n=3).

Scaffold	% overall reduction in size	% solution-mediated changes	% cell-mediated changes	SD
1af	34.55	13.9	20.65	± 15.30
1af-HAp	59.46	34.01	25.45	± 10.82
1rf-HAp	36.67	24.9	11.77	± 13.25
2af	40.23	47.2	-6.97	± 2.06
2af-CS	62.75	61.58	0.87	± 13.20
2rf-CS	73.26	56.41	16.85	± 4.22

Over time, it can be seen that *2rf-CS* showed the highest overal reduction (73%) in size while only 16% of it was cell-mediated. On the other hand *1af-HAp* showed the highest cell-mediated contraction (25%), with the overal 59% decrease in diameter. The lowest overal change in size was observed in *1af* followed by *1rf-HAp* (Table 8.2). It has to be noted that after 28 days some scaffolds were disintegrated to pieces or they were deformed or elongated; therefore establishing the overall diameter was somewhat subjective in those cases.

8.3.2 Live/Dead assay (cell viability)

The cell viability has been examined by Live/Dead assay, where viable cells are shown as bright green regions and dead cells as red regions, as can be seen in Figure 8.4 and Figure 8.5. The staining showed that cells remained viable in scaffolds over 14 days. However, more cells stained red in day 14, indicating the number of dead cells increased (e.g. in *2af* and *1rf-HAp)*.

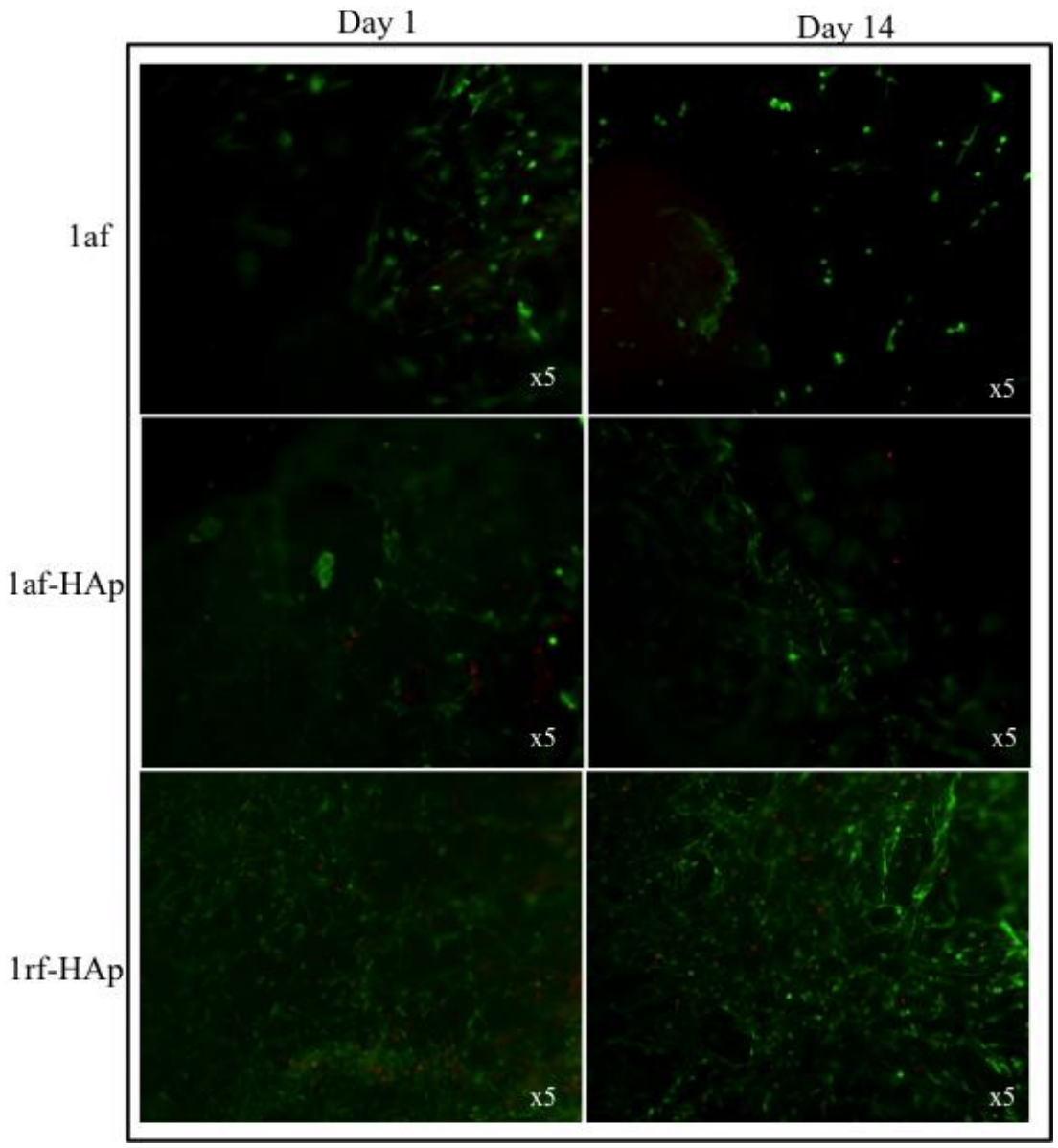


Figure 8.4 Live/Dead cytotoxicity assay showing cell viability of type-I scaffolds at day 1 and 14 (D, x5). Green color indicates live cells and red color dead cells

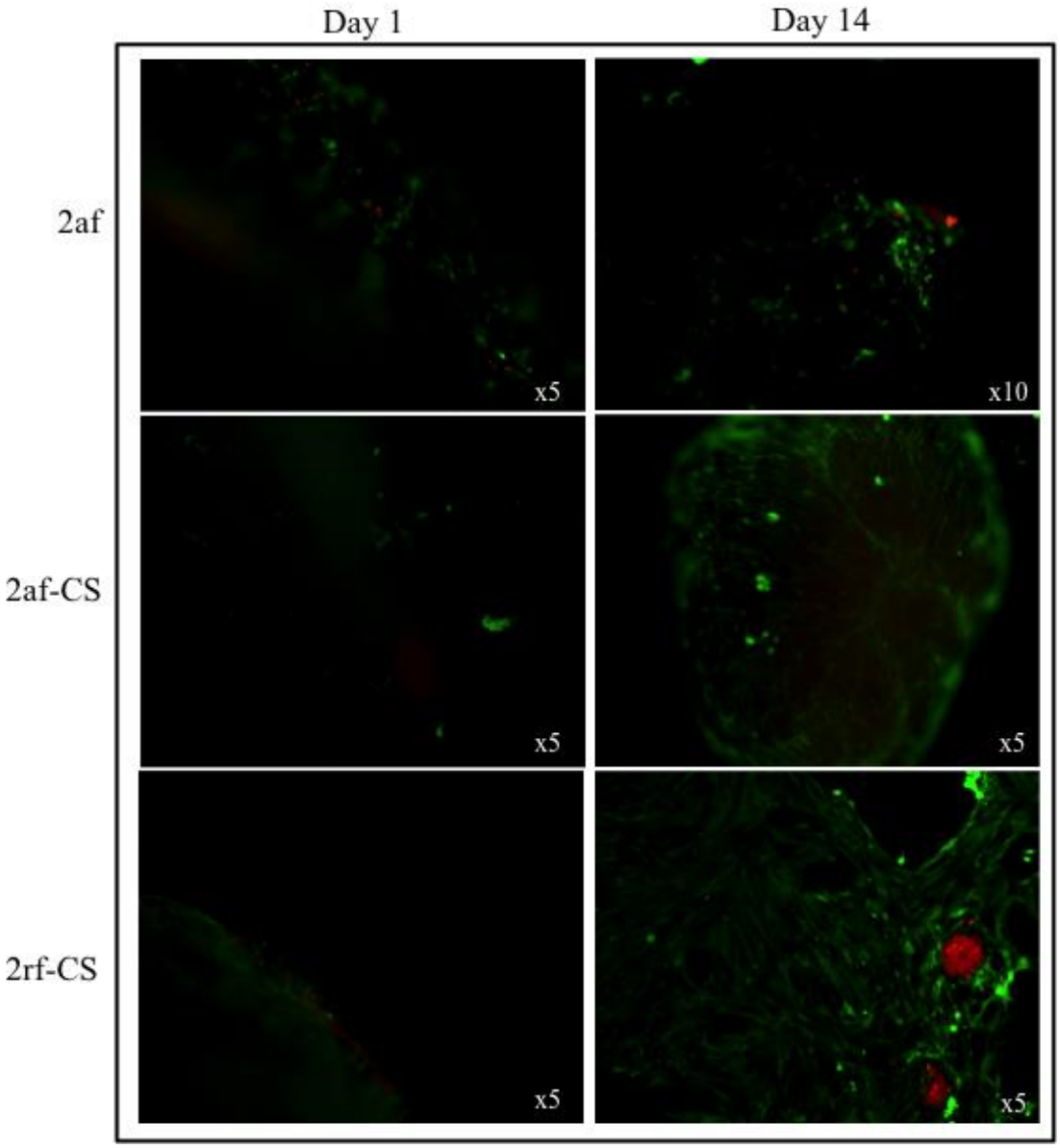


Figure 8.5 Live/Dead cytotoxicity assay showing cell viability of type-I scaffolds at day 1 and 14 (D, x5 and x10). Green color indicates live cells and red color dead cells

8.3.3 Cytoskeletal immunostaining (cell morphology)

In order to study cell spreading and actin development on different scaffolds, phalloidin actin staining and DAPI were used to stain the cytoskeletons and nuclei of cells, respectively. The actin staining shows the morphology of the cells and displays that they were distributed across the scaffold, forming a compact network with well-developed actin filaments. The actin structure of cells on all of the scaffolds was clear except for *2rf-CS* at day 1, where the actin organisation seemed to be more rounded rather than spread. At day 14 the structure seems to be highly developed on all of the scaffolds. Cells with relatively distinct nuclei and filaments were observed throughout the scaffold suggesting normal growth of cells (see Figure 8.6 and Figure 8.7). However due to the high density of cells it was not possible to distinguish a single cell cytoskeleton.

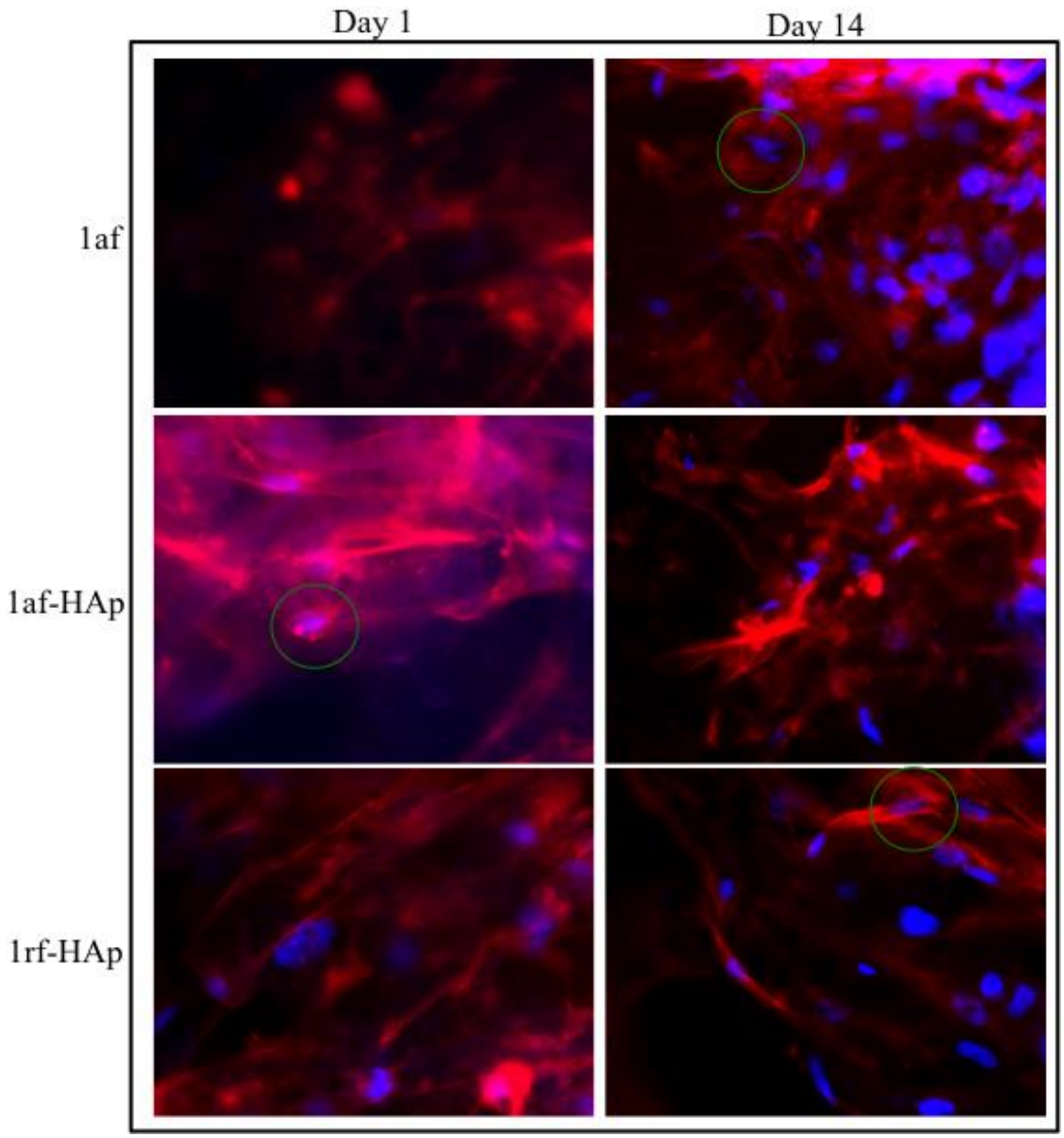


Figure 8.6 Cytoskeletal and DAPI images of type-I scaffolds; red indicates the cytoskeletal of cells; blue indicates the cell nuclei. Green circles indicate a cell and its cytoskeleton. Magnification 40x

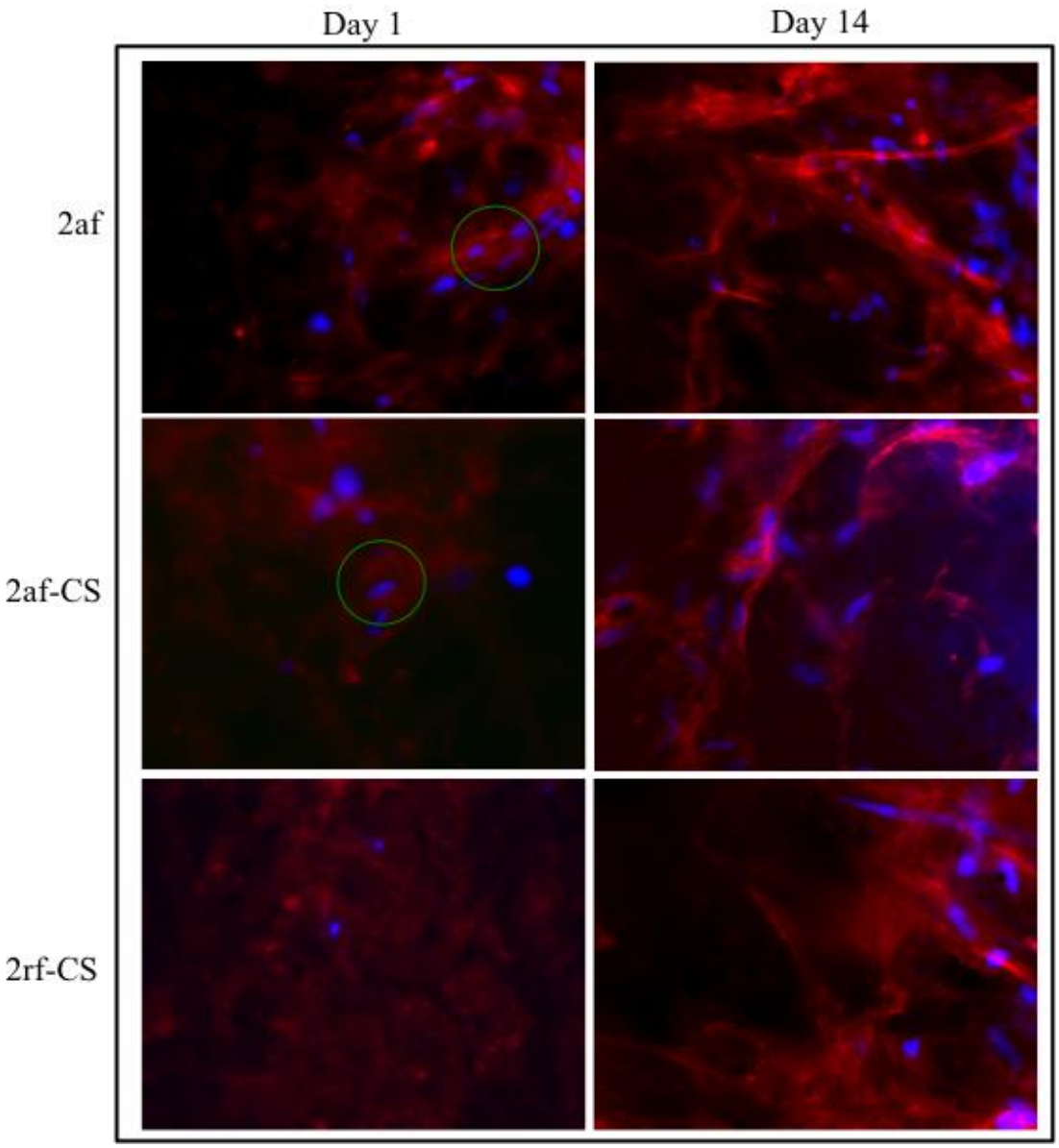


Figure 8.7 Cytoskeletal and DAPI images of type-II scaffolds; red indicates the cytoskeletal of cells; blue indicates the cell nuclei. Green circles indicate a cell and its cytoskeleton. Magnification 40x

8.3.4 Alamar Blue

hBMMSCs were cultured on scaffolds for 28 days and the metabolic activity and the numbers of cells were determined at day 1 and day 7 and 28 to establish any proliferation / apoptosis of cells. All samples showed a slight decrease in metabolic activity over time, except for *1af-HAp* where the drop in Alamar Blue activity was significant.

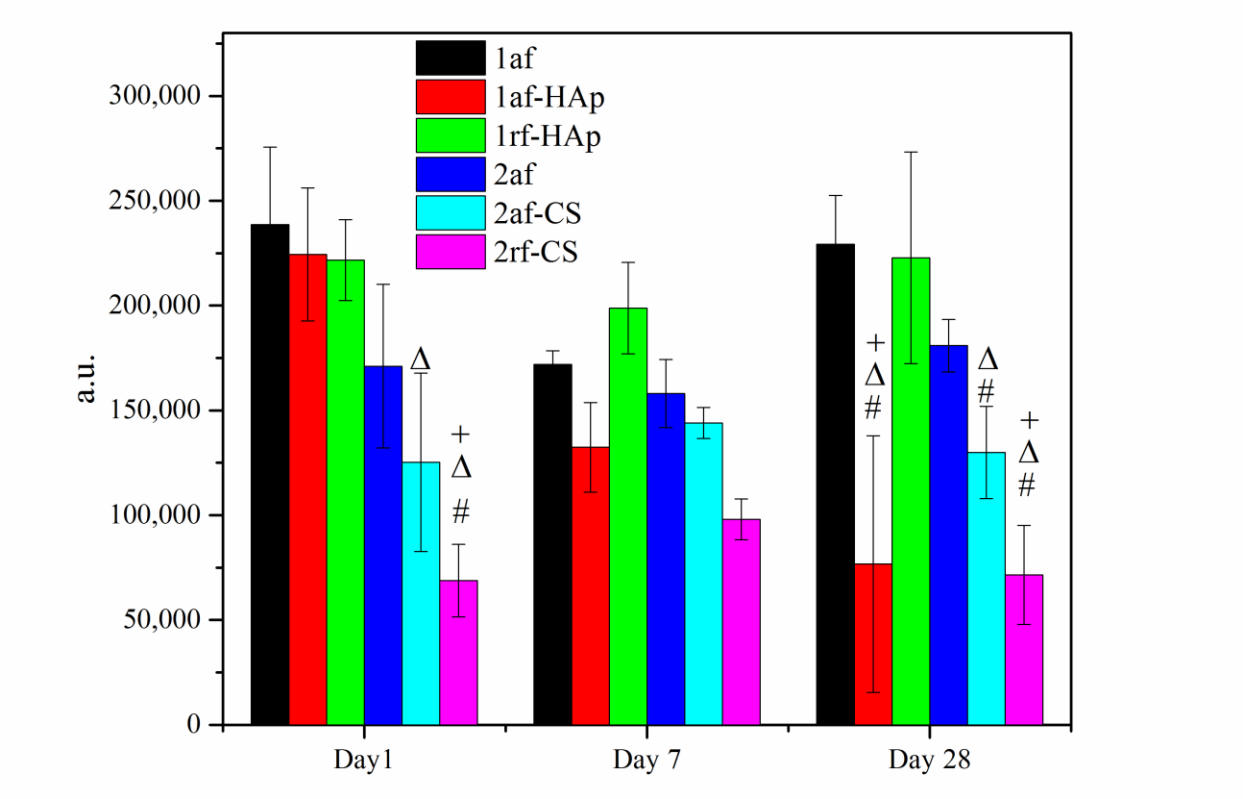


Figure 8.8 AlamarBlue activity of cells on different scaffolds on 1, 7 and 28 days. Symbols show the significant difference at level 0.05 in the same day: # significantly different from *1af*, Δ significantly different from *1rf-HAp* and + significant difference from *2af*. At day 7, *1af-HAp* and *2rf-CS* showed significantly lower activity compared to other scaffolds. Significant decrease in 1af-HAp at day 28 compared to day 7

The metabolic activity of cells on *2af-CS* and *2rf-CS* after 1 day were significantly lower than that on type-I scaffolds, with the cells on *2rf-CS* showing significantly lower activity than on *2af* (Figure 8.8). On day 7, the AlamarBlue (AB) activity of cells on *2rf-CS* was significantly lower than that on the rest of scaffolds. The cells were shown to be significantly (p<0.05) less

active on *1af-HAp* compared to other type-I scaffolds, while their activity on *1rf-HAp* was significantly higher than that of afibrillar type-II samples. On day 28, the metabolic activity of cells on *1af-HAp* and *2af-CS* were lower than the other type-I scaffolds. Cells on *2rf-CS* were less active than those on afibrillar type-I and pure afibrillar type-II (*2af*) scaffolds. After 28 days, the cells on *1af-HAp* showed a significant decrease in the AB activity compared to day 7, while the AB activity in the rest of the samples did not change significantly during the culture.

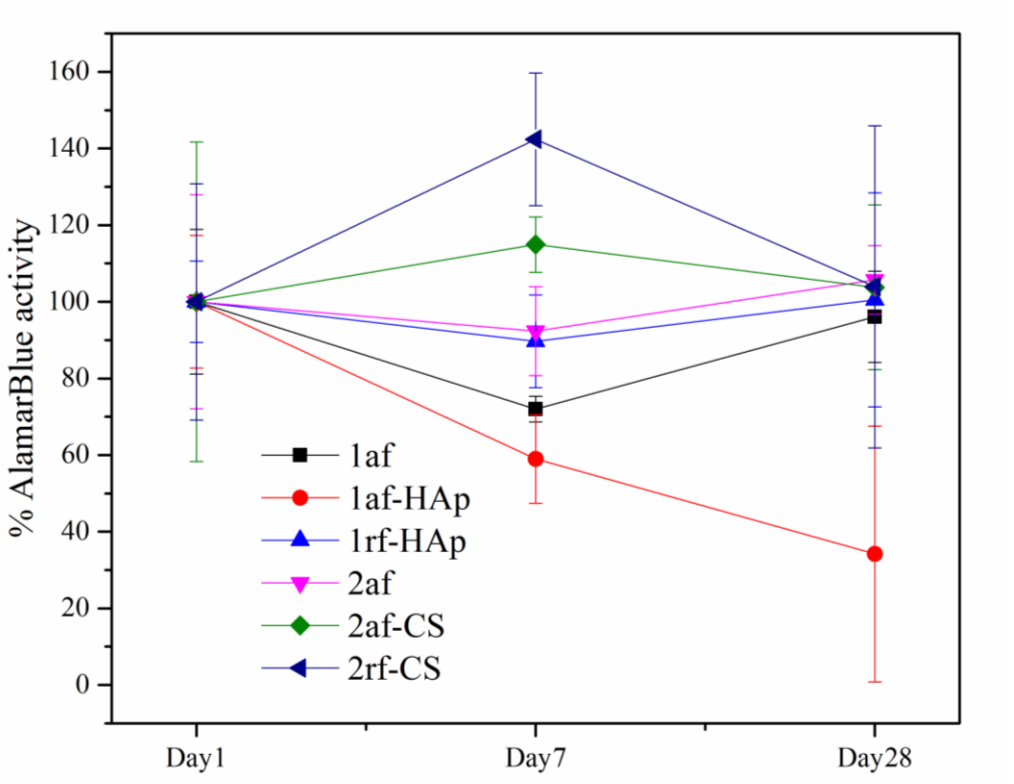


Figure 8.9 Alamar Blue activity change from day 1 in different groups

Presenting the results as the percentage of change in AB activity compared to day 1 in Figure 8.9, it can be seen that the metabolic activity of cells on *1af-HAp* decreased monotonically throughout the culture time on day 28 to ~30% of its initial value on day 1. Activity of cells increased 15% and 40% on CS-containing scaffolds *2af-CS* and *2rf-CS*,

respectively in the first week of culture before decreasing to slightly above its original value. On the other hand, AB activity showed a decrease on *2af* and type-I scaffolds in the first day of culture and increased to approximately their initial value (see Table 8.3).

Table 8.3 The % of change in Alamar Blue activity in different scaffolds after 7 and 28 days; SD denotes standard deviation (n=3).

	Day 1	SD	**Day 7**	SD	**Day 28**	SD
1af	100	±18.90	72.02	±3.35	96.05	±11.89
1af-HAp	100	±17.30	58.97	±11.61	34.18	±33.38
1rf-HAp	100	±10.65	89.68	±12.05	100.53	±27.90
2af	100	±27.93	92.33	±11.59	105.72	±8.97
2af-CS	100	±41.68	114.93	±7.20	103.78	±21.50
2rf-CS	100	±30.82	142.42	±17.31	103.90	±42.06

8.3.5 Histological examination

At the end of the cell culture experiment, the samples were fixed, embedded, sectioned and stained for different components. In this section, firstly the results of staining with H&E are presented, followed by trichrome and Alizarin Red stainings. The last part describes the outcome of immunohistochemistry for cell-produced type-I and II collagens.

8.3.5.1 H&E

Cell spatial distribution was shown by H&E staining of cell nuclei (dark purple/brown) and cytoplasm. From Figure 8.10, it can be seen that cells are present throughout the scaffold in *1af*, whereas in *1af-HAp* (Figure 8.11) they mainly exist as a cellular layer on the margin of

scaffold. From Figure 8.12 it can be seen that the pore structure of *1rf-HAp* scaffold has been relatively maintained with cells infiltrating into the scaffold. However, a dense layer of cells has been formed on the periphery of scaffold (~150um thick) which may indicated that many cells were not able to move into the scaffold.

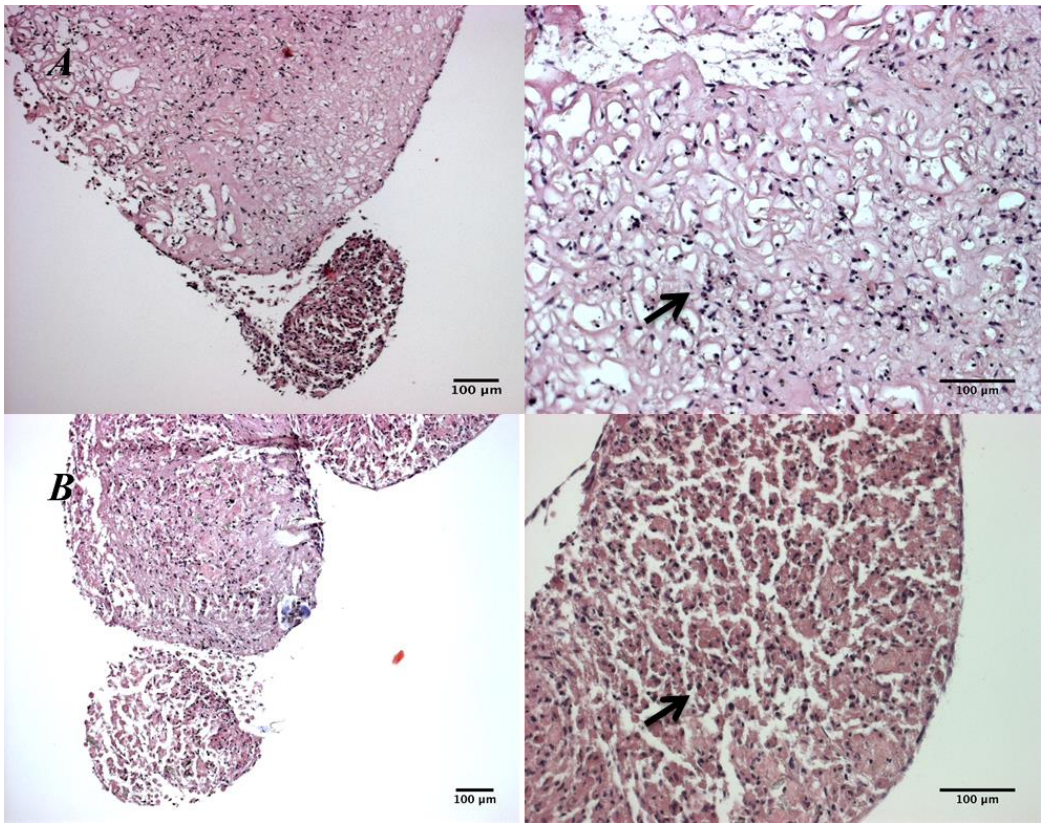


Figure 8.10 H&E staining of *1af* sections, at A) week 1 and B) week 4; black arrows show the cell nuclei

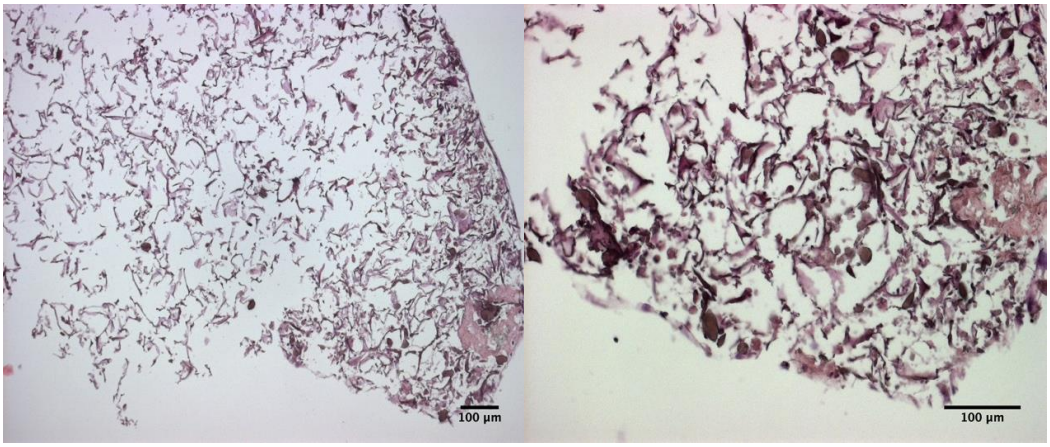


Figure 8.11 H&E staining of *1af-HAp* sections at week 4, cell nuclei stained dark brown

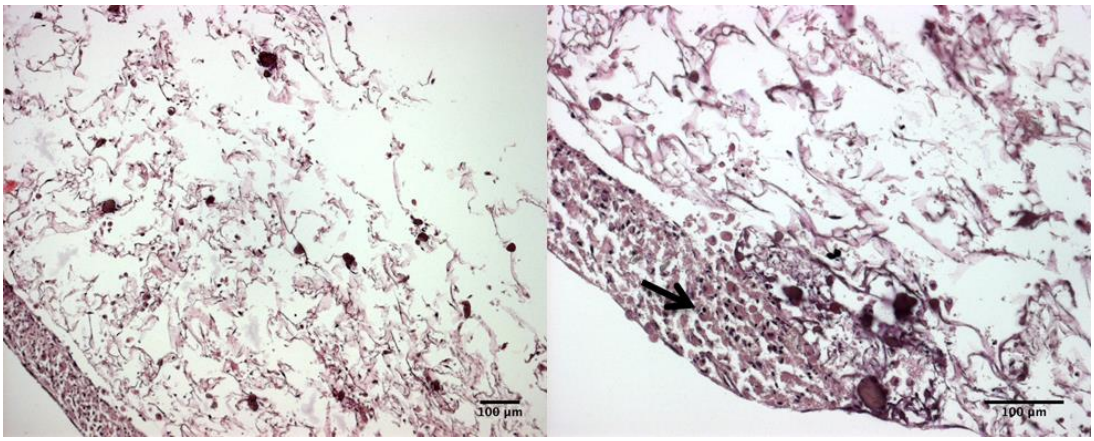


Figure 8.12 H&E staining of *1rf-HAp* sections at week 4; black arrow shows the cell nuclei

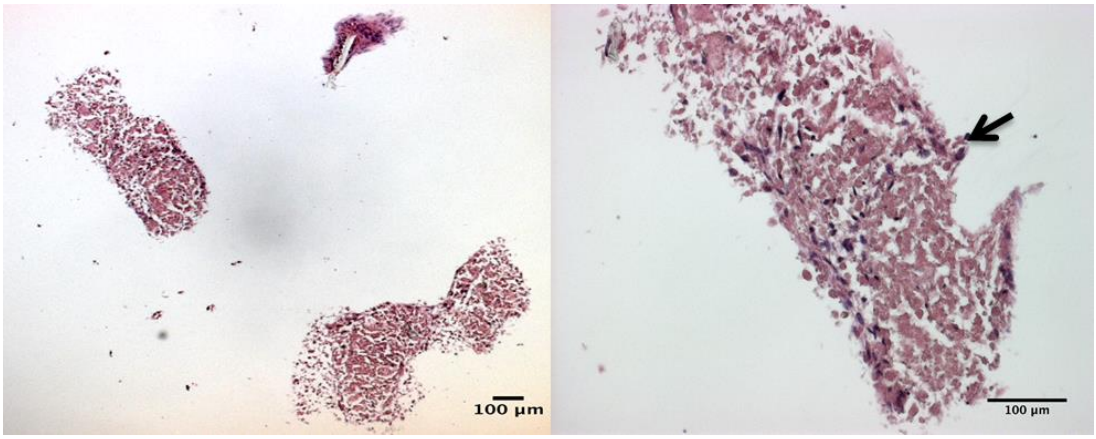


Figure 8.13 H&E staining of *2af* sections at week 4; black arrow shows the cell nuclei

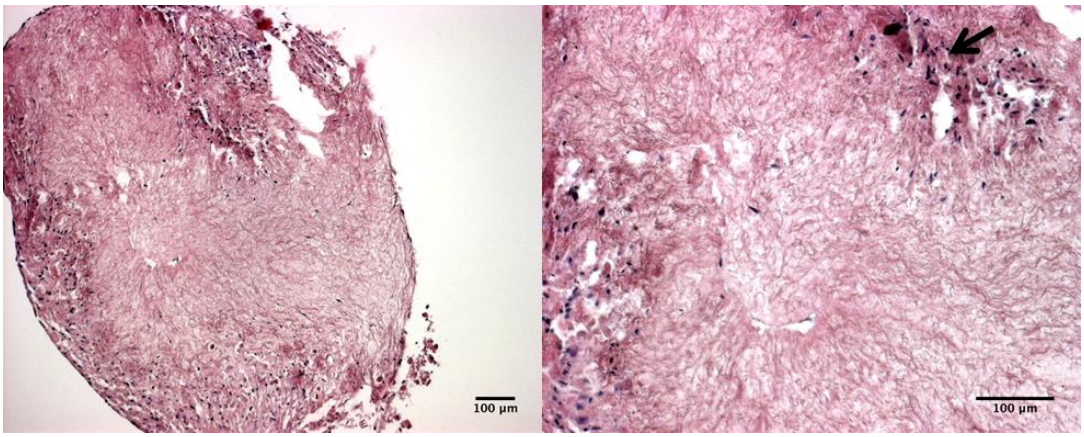


Figure 8.14 H&E staining of *2af-CS* sections at week 4; black arrow shows the cell nuclei

The cells have invaded the *2af* scaffold as can be seen in Figure 8.13. In contrast to *2af*, *2af-CS* scaffold has maintained its shape (Figure 8.14) but the pore structure seems to have collapsed. Ingrowth of cells into the centre of scaffold did not occur and they are mostly concentrated on the peripheries of the scaffold. This is in contrast to *2rf-CS* (see Figure 8.15), where pores/channels are still present in the scaffold, but the shape of scaffold has been altered, and a high number of cells are present throughout the scaffold.

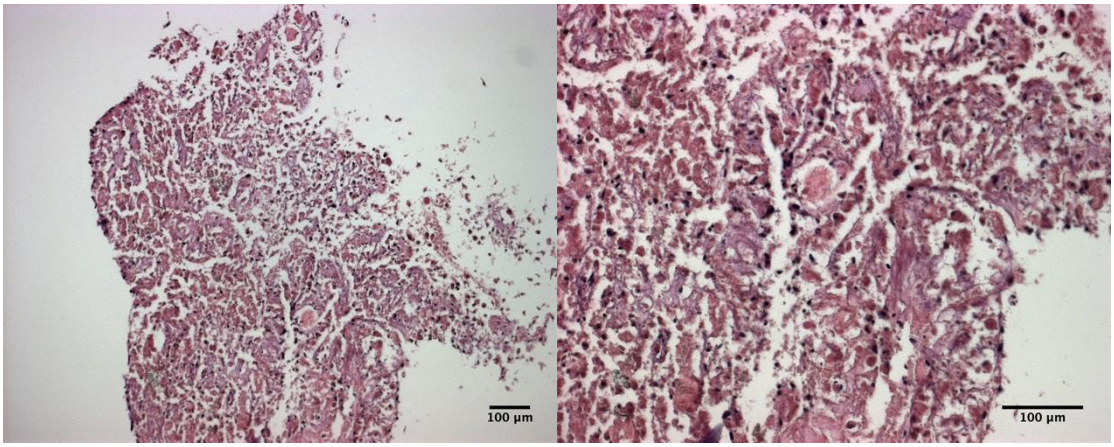


Figure 8.15 H&E staining of *2rf-CS* sections at week 4. Cell nuclei stained dark brown

8.3.5.2 Trichrome

The samples were stained for collagen (Picosirius-Red), GAG (Alcian Blue) and cells after 4 weeks of culture. Images were taken for *1af* and *1af-HAp* at week 1 as well.

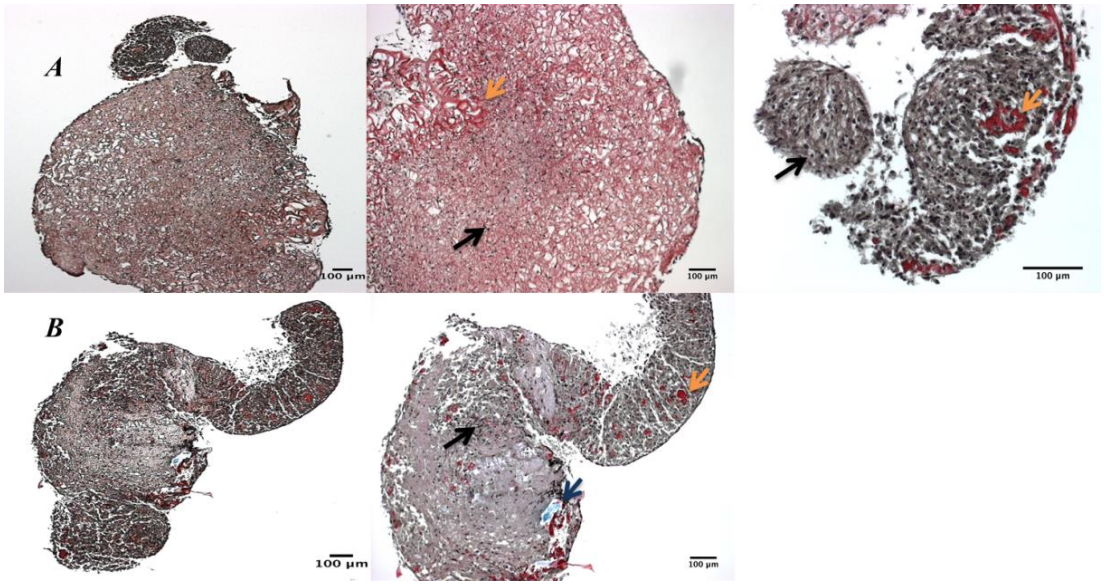


Figure 8.16 Trichrome staining of sample *1af* at A) week 1 and B) week 4 at different magnifications. Scale bar shown in image. Black arrows show the cell nuclei, orange arrows correspond to collagen and blue arrow shows GAGs

From Figure 8.16, it can be seen that at week 1 collagen is present evenly across the intact part of scaffold ("head"), with the disintegrating part showing compact zones of collagen between cells. At week 4, the amount of collagen has reduced considerably, with only patches of concentrated collagen throughout the sample. A small region of Alcian Blue stained GAG was also detected.

After 1 week, *1af-HAp* showed high amount of well distributed as well as compact collagen across the scaffold; cells were seen to be present throughout the sample, and a small

area stained for GAG was also observed (Figure 8.17). Interestingly, after 4 weeks, minimal amount of collagen was detected in the scaffold.

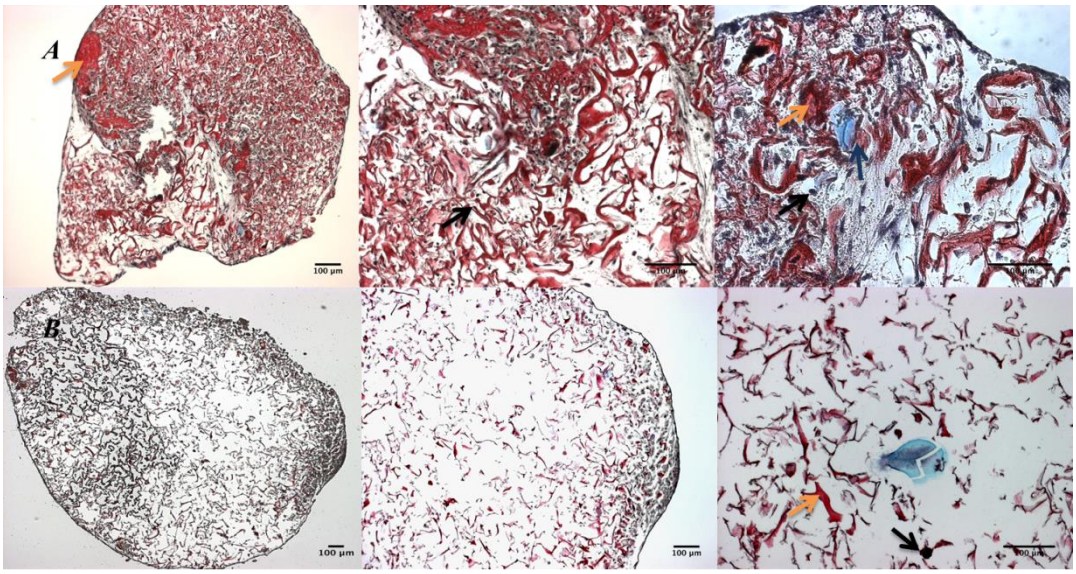


Figure 8.17 Trichrome staining of sample *1af-HAp* at A) week 1 and B) week 4 at different magnifications. Scale bar shown in image. Black arrows show the cell nuclei, orange arrows correspond to collagen and blue arrow shows GAGs

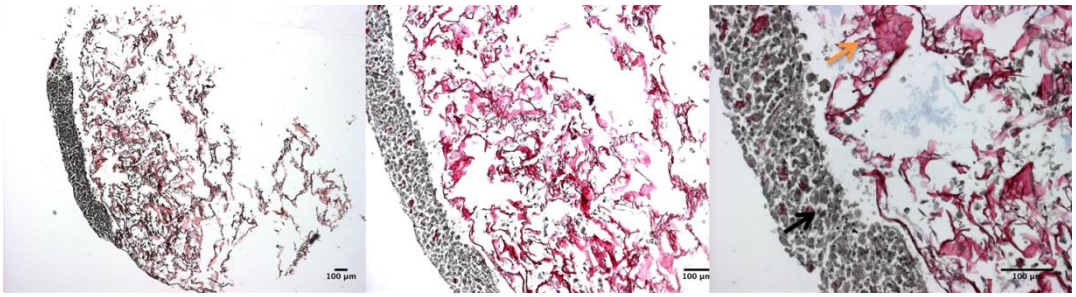


Figure 8.18 Trichrome staining of sample *1rf-HAp* at week 4 at different magnifications. Scale bar shown in image. Black arrows show the cell nuclei and orange arrows correspond to collagen

In *1rf-HAp* scaffolds (Figure 8.18), the cells were primarily observed on the edge of scaffold, however a large number also migrated into the centre. The edges seemed to be largely devoid of collagen (red staining). The collagen was concentrated mainly in other regions.

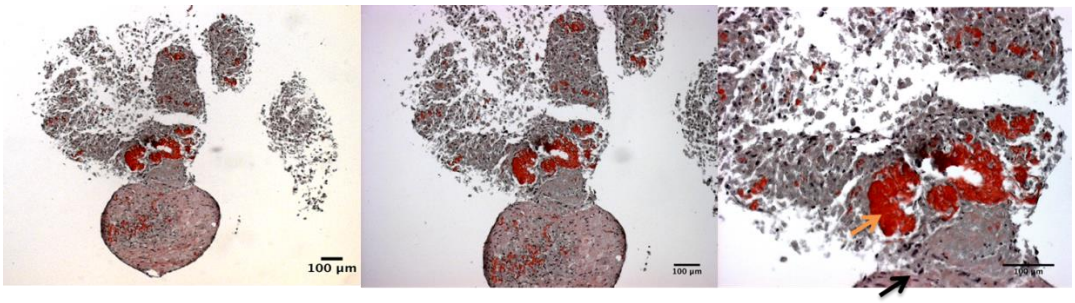


Figure 8.19 Trichrome staining of sample 2af at week 4 at different magnifications. Scale bar shown in image. Black arrows show the cell nuclei and orange arrows correspond to collagen

It can be seen that cells have infiltrated into *2af* scaffold and disintegrated it in some parts (Figure 8.19). The collagen has been stained red and can be seen in the intact region of scaffold (the "head" part), as well as in the neck, where scaffold has lost its original shape. The collagen in this part seems to be very concentrated. Its presence is also clear in some of areas of fragmented scaffold between the cells. No GAG production is shown by the lack of Alcian blue staining.

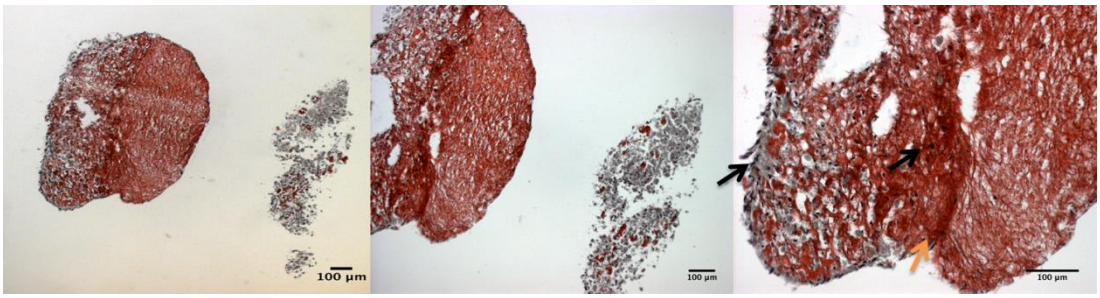


Figure 8.20 Trichrome staining of sample *2af-CS* at week 4 at different magnifications. Scale bar shown in image. Black arrows show the cell nuclei and orange arrows correspond to collagen

For the *2af-CS* scaffold the original shape and integrity have been maintained. The cells seem to have generated a separate colony with some collagen present. Interestingly, no GAG was observed, although CS was added to the scaffold during fabrication. It can be seen from Figure 8.20 that an extensive amount of collagen was present in the scaffold after 4 weeks.

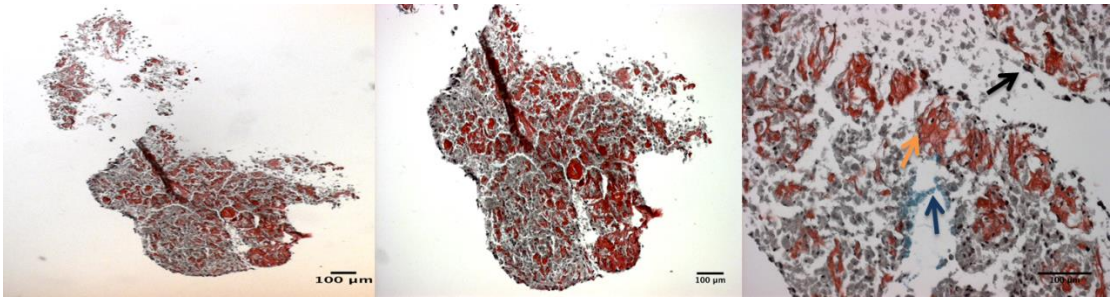


Figure 8.21 Trichrome staining of sample 2rf-CSat week 4 at different magnifications. Scale bar shown in image. Black arrows show the cell nuclei, orange arrows correspond to collagen and blue arrow shows GAGs

It can be seen that collagen is present in concentrated patches throughout *2rf-CS* (Figure 8.21) in contrast to *2af-CS* where it existed evenly across the scaffold (Figure 8.20). A small region of blue stain showed presence of GAGs.

8.3.5.3 Alizarin Red

Alizarin Red staining was used to mark the calcium-rich deposits in the scaffolds.

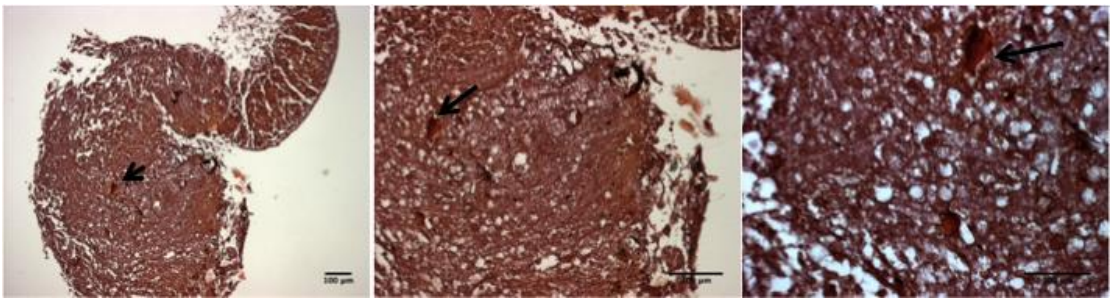


Figure 8.22 Alizarin Red staining of sample 1af at week 4; black arrow indicates an example of the regions stained positive for calcium.

It can be seen from Figure 8.22 that small regions of Alizarin Red staining occurred in *1af* scaffold, which originally did not contain any HAp. This shows that these calcium-rich residues were produced by cells.

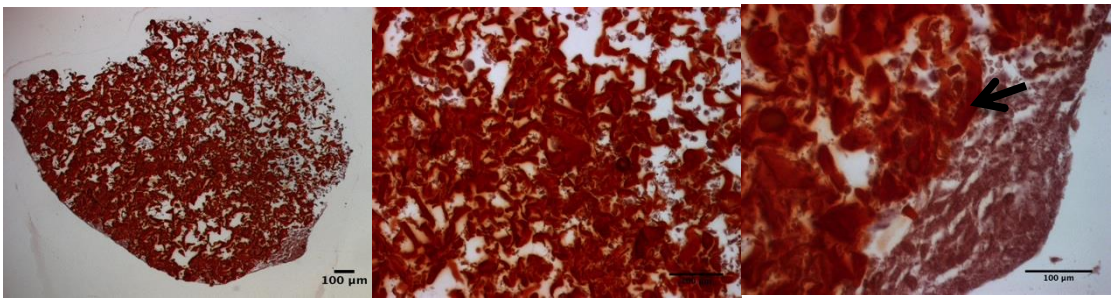


Figure 8.23 Alizarin Red staining of sample 1af-HAp at week 4; black arrow indicates an example of the regions stained positive for calcium

It can be seen (Figure 8.23) that most of *1af-HAp* surface is covered with calcium-rich deposits which are either the HAp added to scaffold during fabrication or they are produced by cells. Interestingly, this was not the case with the reconstituted fibrillar counterpart (Figure 8.24), where although regions of Ca-rich areas were present but they were spread out and the surface was not masked with them.

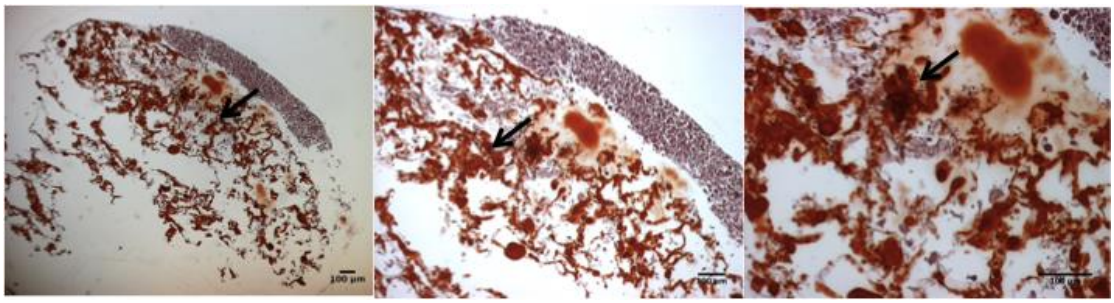


Figure 8.24 Alizarin Red staining of sample 1rf-HAp at week 4; black arrow indicates an example of the regions stained positive for calcium

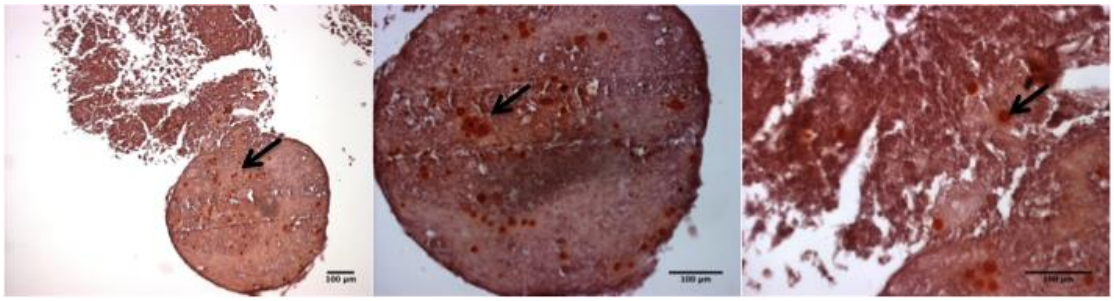


Figure 8.25 Alizarin Red staining of sample 2af at week 4; black arrow indicates an example of the regions stained positive for calcium

After 4 weeks of culture, Alizarin Red positive staining was evident in type-II afibrillar scaffold (Figure 8.25), showing the production of calcium-rich deposits by cells.

8.3.6 Immunohistochemistry

After 4 weeks, the samples were fixed, covered in wax, sectioned and processed for immunohistochemistry staining. The samples were stained with DAPI, and for collagen type-I and II produced by human cells.

It can be seen from Figure 8.26, Figure 8.27 and Figure 8.28 that minimal fluorescent staining for collagen-II was observed in type-I scaffolds (*1af, 1af-HAp* and *1rf-HAp).* The amount of produced type-I collagen by cells were higher especially in *1af* and *1rf-HAp,* where they were distributed relatively evenly (Figure 8.26 and Figure 8.28) compared to *1af-HAp* (Figure 8.27) where collagen-I seemed to be limited to the edged of scaffold.

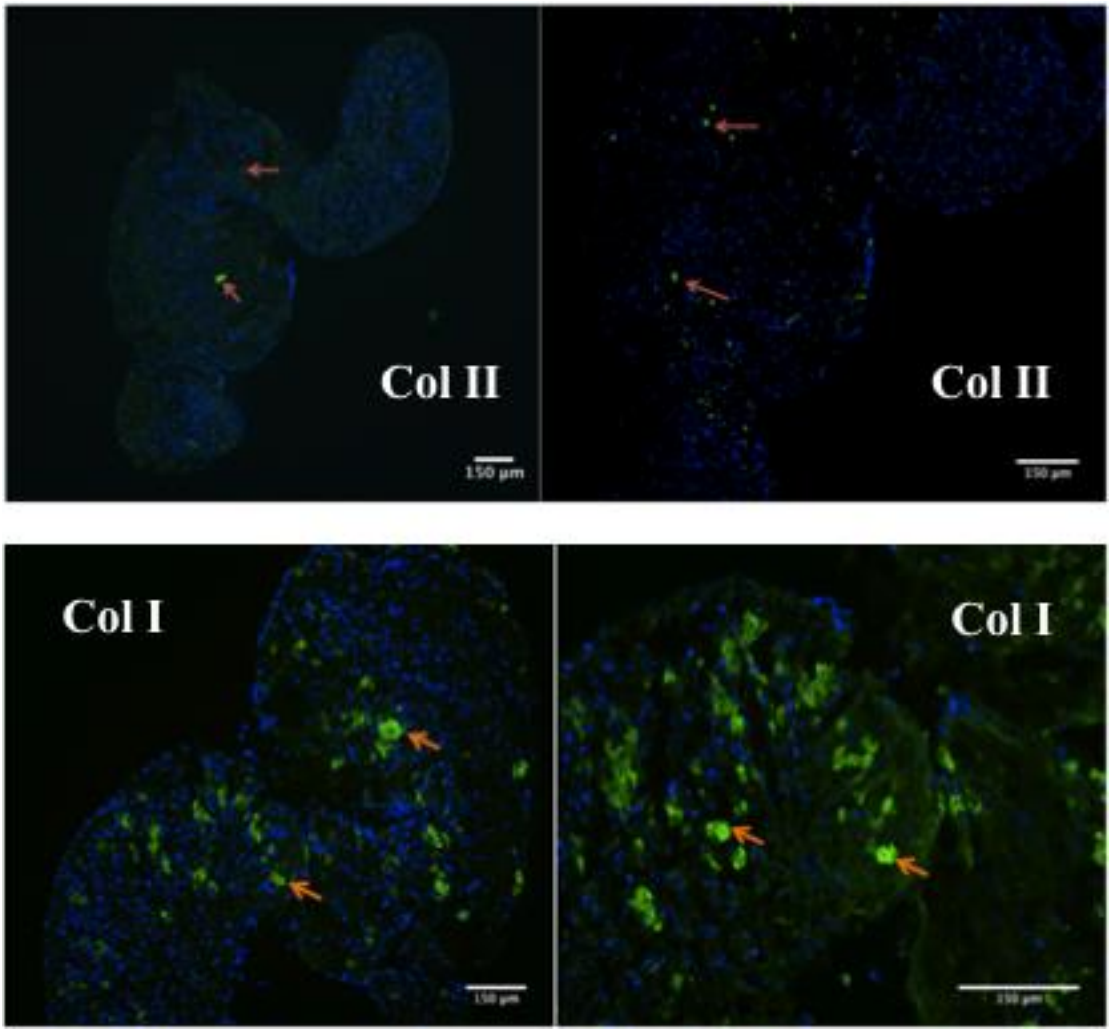


Figure 8.26 Col II and DAPI staining of 1af scaffolds at week 4 at different magnifications. Red arrows indicate examples of col II expressed by the BMMSCs

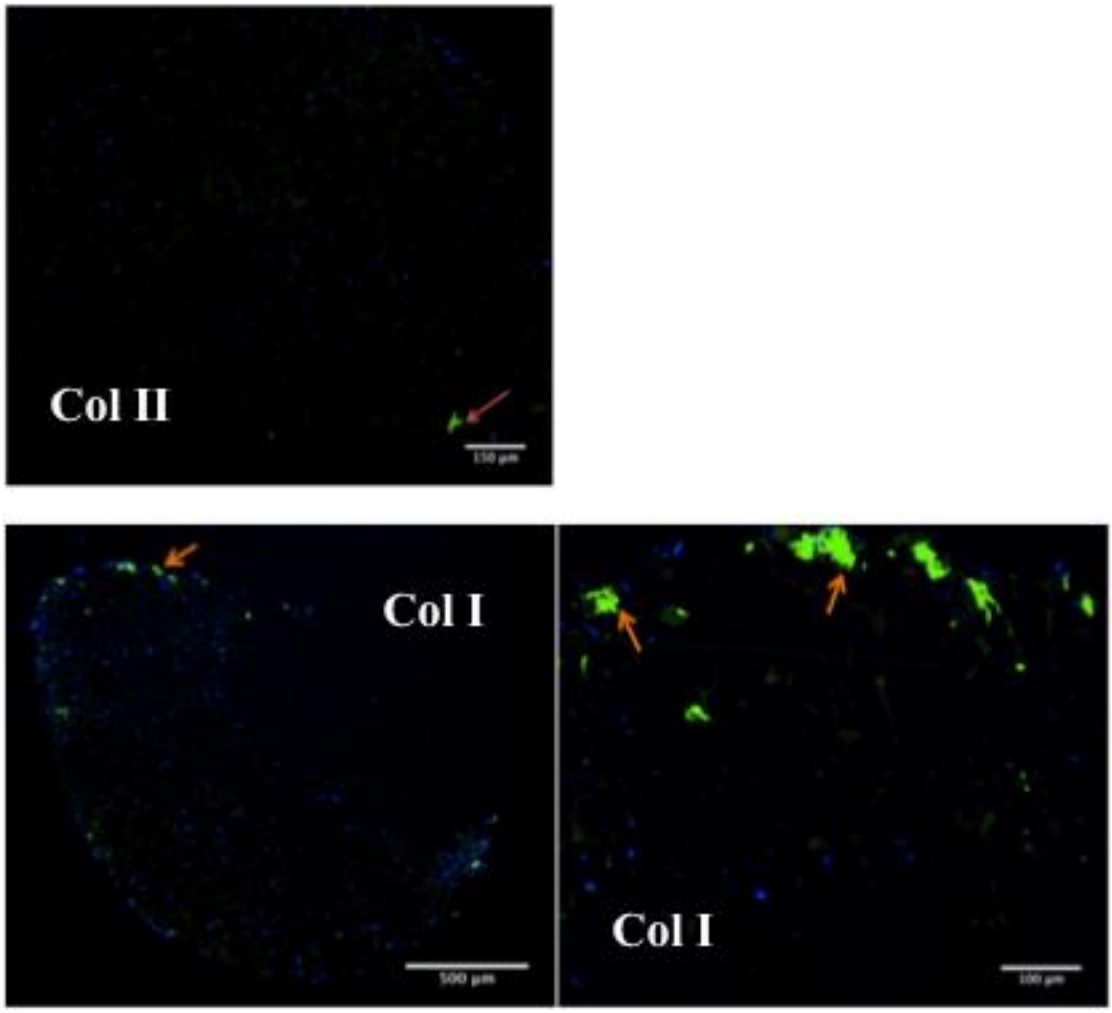


Figure 8.27 Col II and DAPI staining of 1af-HAp scaffolds at week 4. Red arrow indicates examples of col II expressed by the BMMSCs

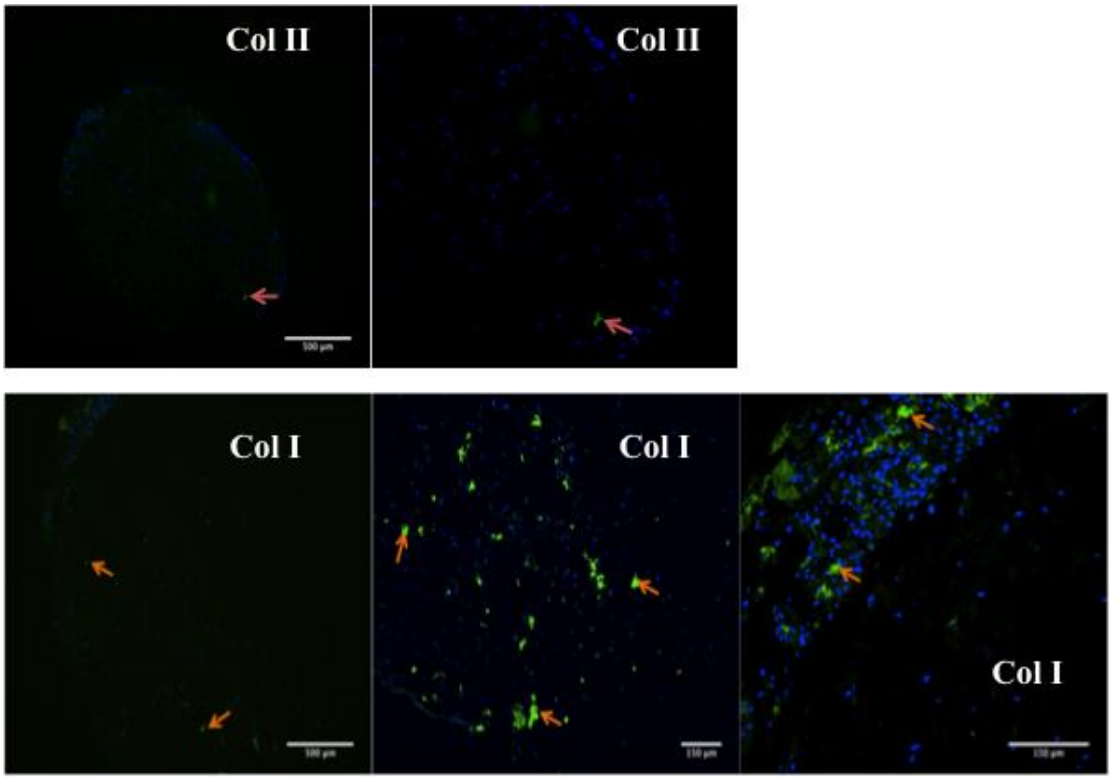


Figure 8.28 Col II and DAPI staining of 1rf-HAp scaffolds at week 4 at different magnifications. Red arrows indicate examples of col II expressed by the BMMSCs

In type-II afibrillar scaffold (Figure 8.29), especially on the "head" region (see Figure 8.19 for the light microscopy image) it can be seen that a relatively extensive fluorescent staining occurred for type-II collagen, concentrating on the peripheries but observed towards the centre as well. A small zone in the disintegrated part was also tagged for type-II. The rest of the disintegrated part showed positive staining for type-I collagen.

In afibrillar CS-containing scaffold (*2af-CS*), regions of fluorescent type-II collagen can only be seen on the edges of the intact part of scaffold (see Figure 8.20 for light microscopy image), where most cells (DAPI stained) are also present (see Figure 8.30). However, the disintegrated parts stained positive for type-I collagen.

Extensive type-II staining was observed in the intact part of *2rf-CS* scaffold, with a number of regions stained for type-I collagen produced by cells (Figure 8.31).

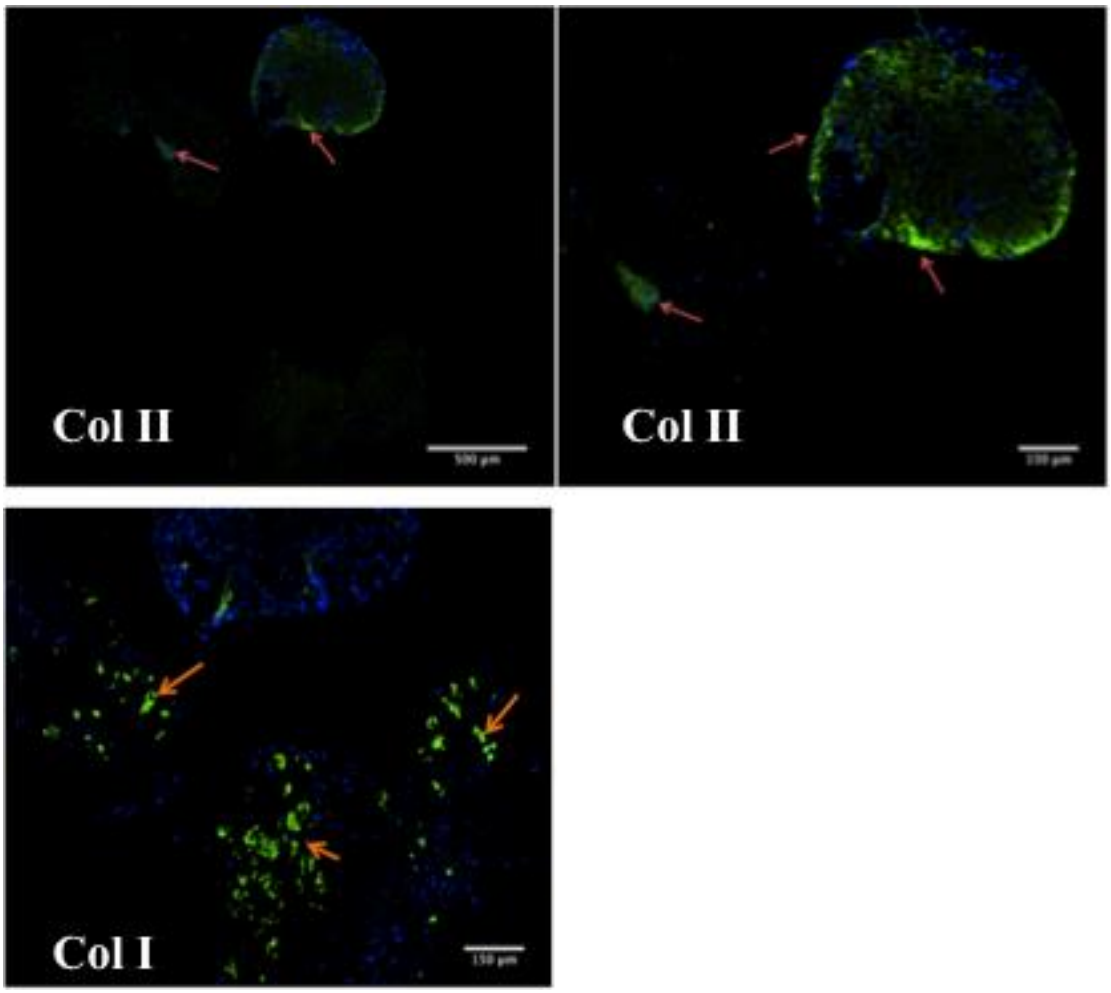


Figure 8.29 Col I and II and DAPI staining of 2af scaffolds at week 4 at different magnifications. Red arrows indicate examples of col I and II expressed by the BMMSCs

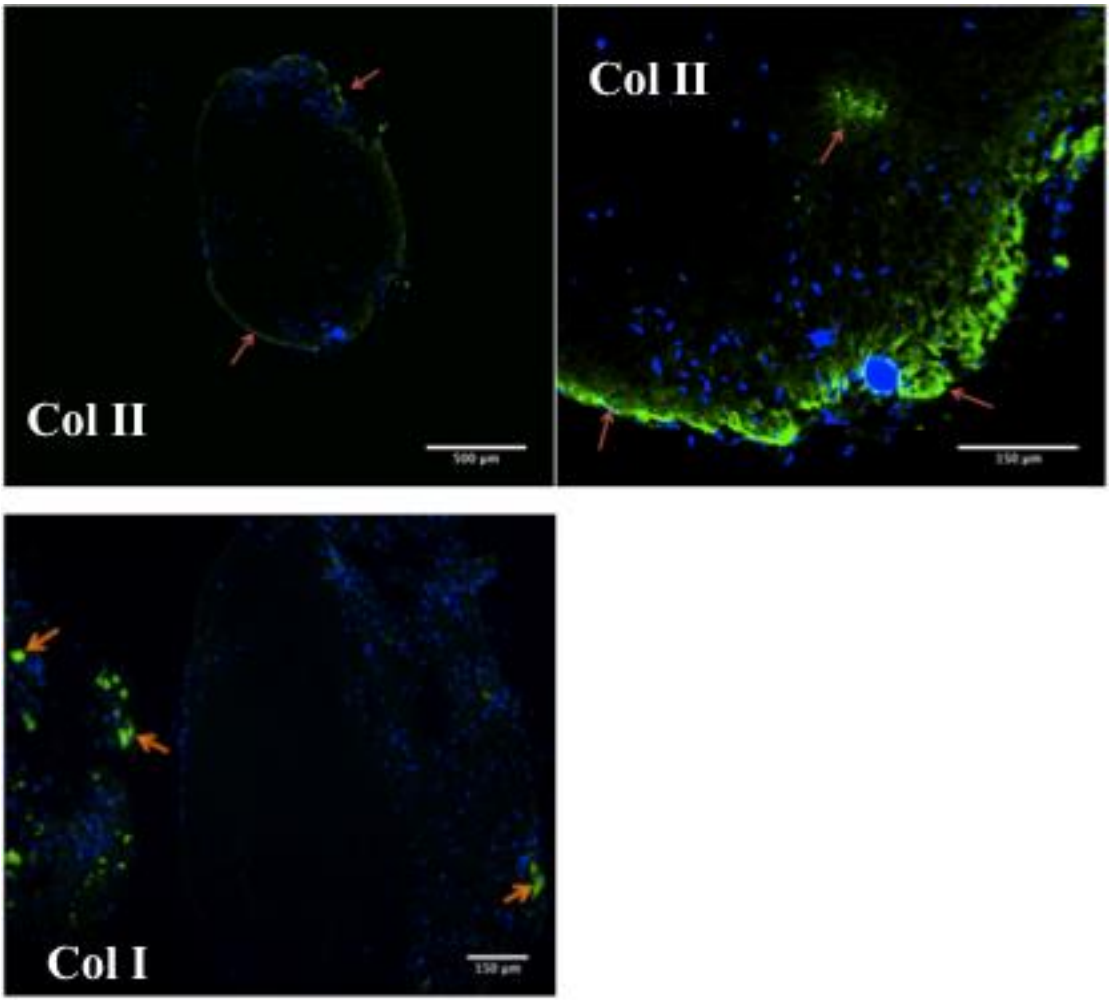


Figure 8.30 Col II and DAPI staining of 2af-CS scaffolds at week 4 at different magnifications. Red arrows indicate examples of col II expressed by the BMMSCs

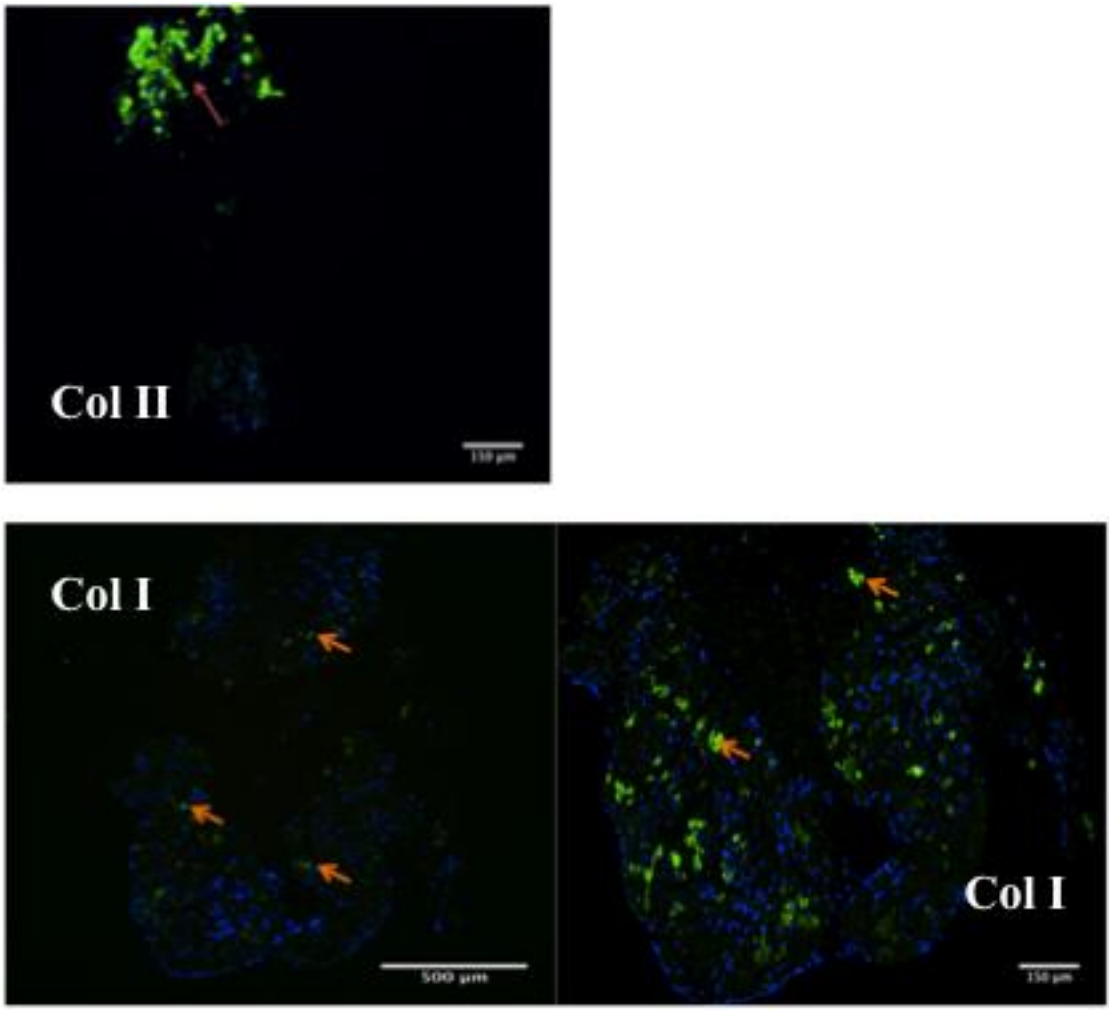


Figure 8.31 Col II and DAPI staining of 2rf-CS scaffolds at week 4 at different magnifications. Red arrows indicate examples of col II expressed by the BMMSCs

8.4 Discussion

This section discusses the results of cell culture on different types of collagen composite scaffolds. The contraction of scaffolds as a function of type and days in culture is examined. In addition, metabolic activity of cells on different types of scaffold is assessed. Histological and immunohistochemical observations are explained. Coupled with scaffold characterisation results, they assist to evaluate the performance of developed scaffolds for bone and cartilage tissue engineering.

8.4.1 Scaffold sterilization

The method of sterilisation for scaffolds was decided to be γ-irradiation; the reason to prefer this method to ethanol sterilisation was that it has been previously shown the less structurally stable type-II scaffolds did not survive the process of washing with ethanol (Walton, 2010). γ-irradiation is used widely clinically to sterilize metallic prosthetics, and therefore is a well-established method; however, in terms of biopolymers, there can be disadvantages to this technique. Firstly, there is a concern that the polymer chains are shortened by scission and/or crosslinking takes place. However, it has been shown that 50MRd did not alter collagen structure in dry state (Bowes and Moss, 1962) and at 1MRd little damage was caused to collagen peptide backbone (Cheung et al., 1990). Therefore, it is safe to assume that at the utilised energy level, the γ-irradiation did not destruct collagen structure.

8.4.2 Changes in scaffold sizes in culture

The changes in the sizes of scaffolds in culture media with and without the presence of cells were evaluated. Assuming the diameter of scaffold is a representation of its three

dimensional size, the cell-mediated changes (contraction and degradation) and solution-mediated changes could be distinguished (see Table 8.1).

8.4.2.1 Cell-mediated changes

The cell-mediated contractions of scaffolds have been observed previously (Mueller et al., 1999, Nehrer et al., 1997a, Veilleux and Spector, 2005, Dado and Levenberg, 2009), and have been attributed to the presence of myofibroblasts (Pieper et al., 2002, Nehrer et al., 1997a) and the expression of α-smooth muscle actin by cells (Veilleux and Spector, 2005, Shu et al., 2009). Collagen degradation in cell-seeded scaffolds occurs by production of collagenase (Rodrigues et al., 2013). Taking into account minimal cell-mediated degradation after 1 day, the cell-mediated changes (CMC) in Table 8.4 can refer to cell-mediated contraction, whereas after 28 days CMCs are a combination of cell-mediated degradation and contraction. Degradation and contraction could only be delineated in *2af-CS* with the high amount of residual collagen after 28 days (Figure 8.20 and Figure 8.30) and minimal cell-mediated changes (see Table 8.4). Here, the cells mostly lined the surface of scaffolds (Figure 8.20), preventing inner collagen degradation, but delivering slight circumferential contractile forces (Freyman et al., 2001b).

The initial (day 1) cell-mediated contractions seemed to be correlated to the bulk compressive modulus of scaffolds (see Table 8.4). The scaffolds with higher modulus (*1rf-HAp 1:1*, *2af-CS* and *2rf-CS*) did not experience a cell-mediated reduction in size. A study by Freyman (2001) attempted to measure the forces generated by fibroblasts on scaffolds found that each cell exerts 1nN force to the matrix (Freyman et al., 2001b), which can contract it depending on the stiffness of the matrix. It is worth mentioning that the bulk modulus maybe many times lower than the local modulus facing an individual cell (e.g. modulus of individual collagen-CS is

~103 times higher than the bulk modulus (Harley et al., 2007, Murphy et al., 2012)), and also the modulus in wet state is expected to be lower than in dry state. Thus it is suggested that initially it can be an indication of the contraction by cells collectively. However, over time the bulk dry compressive modulus becomes irrelevant, and mechanical properties of scaffolds would be far from the initial performance. This is most probably the reason that this trend was not kept during 28 days of culture.

Pore diameter did not seem to affect the cell-mediated changes in size (see Table 8.4), as was also observed by Lee et al. (2000) (Lee et al., 2000). Cell-mediated contraction, however, may have resulted in smaller pores in an attempt for cells to bridge the pores.

The cell-mediated increase in size in *2af* after 28 days indicates matrix synthesis by cells. This was further confirmed by histology and immunohistochemistry results (Figure 8.25 and Figure 8.29), where Alizarin Red showed positive staining for calcium and immunostaining was positive for cell-produced collagen.

8.4.2.2 Solution-mediated changes

The solution-mediated changes of unseeded scaffolds with time in culture media are due to a combination of factors; firstly, it is thought that the relief of residual strains in the matrices during the freeze-drying process due to additional removal of bound water may cause a reduction in scaffold size when placed in liquid, since water is a mild plasticizer for collagen (Lee et al., 2000). Secondly, it is possible that scaffold dissolution in cell culture media has caused a decrease in the size; this was evident in case of CS-containing scaffold, where no CS was observed by Alcian Blue staining in histology section (Figure 8.20 and Figure 8.21).

Among all scaffolds, after 28 days, solution-mediated changes were highest in CS-containing scaffolds while cell-mediate changes were minor; this is believed to be due to dissolution of unbound CS as well as electrostatically bound CS to collagen in media. The α-MEM media contains non-essential amino acids such as arginine, histidine and lysine, which - due to their high isoelectric point- are positively charged in pH 7.4 of media. The persistent exposure of the negatively charged CS to this condition may have attracted them away from collagen causing its dispersion in the media.

Table 8.4 Storage modulus, compressive modulus and pore sizes of scaffolds vs overal changes (OC) and cell-mediated changes (CMC) in size after 1 and 28 days.

Sample	Storage modulus (Pa)	Compressive modulus (Pa)	Pore size (μm)	% OC Day 1	% CMC Day 1	% OC Day 28	% CMC Day 28
1af	0.1	23 ±13	61	25.22	23.59	34.55	20.65
1af-HAp 1:1	0.4	40 ± 13	115	25.58	19.51	59.46	25.45
1rf-HAp 1:1	10	120± 19	78	8.1	-1.77	36.67	11.77
2af	0.002	17 ± 8	145	19.97	14.71	40.23	-6.97
2af-CS	3	287± 49	150	23.14	-3.03	62.75	0.87
2rf-CS	0.3	56 ± 8	140	38.02	-5.05	73.26	16.85

8.4.3 Cellular behaviours

The scaffold characteristics such as ECM specific surface area, composition (including collagen type, ultrastructure/*d*-banding) (Zhao et al., 2013, Murphy et al., 2013, Nehrer et al., 1997a, Fields, 1995, Palecek et al., 1997, Smith and Ma, 2004, Kleinman et al., 1976, Bacakova et al., 2011, Frey et al., 2006, Martino et al., 2012), microstructure and stiffness may affect cellular behaviour including attachment, proliferation and differentiation. These factors are considered in the following discussion of cells results.

8.4.3.1 Cell viability and scaffold biocompatibility

Most tissue-derived cells are anchorage dependent requiring attachment to a substrate for viability and growth (Woo et al., 2003, Bacakova et al., 2011). All of the scaffolds promoted cell attachment and viability throughout 4 weeks, showing biocompatibility of scaffolds, as observed by Live/Dead assay results (Figure 8.4, Figure 8.5). This is expected, since several sequences within the triple helical regions of collagen type I and II have been identified as cell adhesion sites (Fields, 1995). Collagen is believed to mediate the adhesion interaction between integrin and the substrate through specific Arg–Gly–Asp (RGD) sequences (Rodrigues et al., 2003, Boyan et al., 1996). It has been also found that in type I collagen, α1(I) chain of the triple helix is more active than the α2(I) chain, containing the most active peptide which corresponds to residue between 568 and 835; in case of type II collagen, a comparable region was found to be the only active site for cell binding (Kleinman et al., 1976).

HAp can have either a biocompatible or a cytotoxic effect on cells, depending on its concentration, size and shape and also the cell type (Filova et al., 2014). In form of nanoparticles, concentrations between 100-500 ug/mL have been shown to reduce viability and growth, where at 100 ug/mL HAp nanoparticles were found in lysosome and at concentrations greater than 250 ug/mL apoptotic changes in the cell nuclei were observed. This is thought to be due to relatively high release of Ca^{2+} ions (Filova et al., 2014). In this study the mineralised scaffolds containing HAp supported the cell viability, possibly by providing a source of calcium and phosphate ions that can be used by cells to create bone (Prosecka et al., 2014). However, their extensive deposition on 1af-HAp is thought to be detrimental to cell survival. It is also well-known that collagen-GAG scaffolds are natural polymer and therefore bioactive, allowing cells to maintain high metabolic rates over time (Tierney et al., 2009a).

It is known that the size and shape of cell spreading area is one of the decisive factors for migration, proliferation and differentiation of anchorage-dependent cells. Therefore, a small spreading area and rounded cells without spreading and focal adhesion will lead to apoptosis (Bacakova et al., 2004). Images of the actin cytoskeleton of cells (Figure 8.6 and Figure 8.7) showed well-developed actin filaments and spreading of cells on the scaffolds. Cells exhibited spread morphology, as was observed on randomly oriented fibres or zones of a scaffold by McCullen et al. (2013)(McCullen et al., 2012).

8.4.3.2 Cell attachment

Two sets of Alamar Blue experiments were conducted with different start dates and with cells from two different donors. In the first experiment however, the metabolic activity of cells decreased monotonically throughout 28 days, as opposed to the second experiment, where the metabolic activity either increased or decreased first and stabilised to nearly its initial value after 28 days. The reason for the unusual behaviour of cells in the first experiment is thought to be due to the quiescent nature of first donor cells; in the Alamar Blue experiment, it is assumed that all live cells are metabolically active, as opposed to quiescent. Therefore, in subsequent analysis only data from the second experiment are used.

The results of Alamar Blue at day 1 were considered to be an indication of initial cell attachment to the scaffolds (Moreau and Xu, 2009). One important point that needs to be considered while interpreting the Alamar Blue results is that cell metabolic activity, which is what to be deduced from this method, is not necessary an indication of number of cells; there might be a miscorrelation between metabolic activity and cell number, especially in BMMSCs as shown by (Quent et al., 2010), where the cell proliferation was over-estimated by Alamar Blue,

particularly pronounced over time and at high cell densities. This was the reason that the results were not presented in terms of cell number.

One of the factors affecting cellular adhesion is the scaffold specific surface area (surface to volume ratio)(Smith and Ma, 2004), which provides the cells integrins with sites for ligand binding (O'Brien et al., 2005, Palecek et al., 1997). Presenting sites for highly specific interactions between materials and surrounding cells has been achieved by introducing peptide ligands or ECM molecules in biomaterials surface to bind with cell surface receptors, and controlling the density of such ligands (Fields, 1995, Rowley and Mooney, 2002). Therefore, a high surface to volume ratio is believed to enhance cellular response (Smith and Ma, 2004).

It has been shown that an open-cell tetrakaidecahedron sufficiently describes the random microstructure of a cellular solid (O'Brien et al., 2005). In this case, the specific surface area (SA/V) can be described in terms of the pore diameter (d) and the relative density ($\frac{\rho^*}{\rho_s}$) by Equation 8.2:

$$SA/V = \frac{10.14}{d}\left(\frac{\rho^*}{\rho_s}\right)^{0.5} \qquad \text{Equation 8.2}$$

Therefore, the larger pore size (Murphy et al., 2010) and lower relative density provide smaller surface area for cell ligand binding; however after initial attachment bigger pore sizes are preferred to allow cell ingrowth and better proliferation (Mandal and Kundu, 2009, Murphy et al., 2010, McCullen et al., 2012). The results are presented in Table 8.5.

In type-I scaffolds, the initial AB activity was not statistically different among scaffolds (p<0.05) (see Table 8.5). This was not expected according to Equation 8.2, therefore, there must

be other factors influencing the cell metabolic activity. Firstly, the microstructure and composition (Wahl, 2007) of scaffolds differ due to presence of HAp (Zhao et al., 2013, Martino et al., 2012). Secondly, the surface roughness (Frey et al., 2006, Martino et al., 2012, Rodrigues et al., 2011, Rodrigues et al., 2013) is different in mineralised scaffolds. These factors, however, are not independent, because for instance HAp on the surface of collagen changes both the composition and the surface roughness of scaffolds. A rougher surface is expected to promote higher cell adhesion, as is also shown by Osathanon (2011) and Rodrigues (2013) (Rodrigues et al., 2013, Osathanon et al., 2011). This was not seen when comparing collagen and mineralised collagen scaffolds. The reason for this was not fully understood, but two possibilities are considered; firstly, the shape and size of HAp clusters may have not been optimum for cell attachment, or it is possible that the response to the surface roughness was affected by the cell type (Boyan et al., 1996).

Table 8.5 Scaffolds properties (surface area, compressive modulus and pore sizes) and Alamar Blue activity at day 1 (divided by 10000).

Sample	AlamarBlue Activity at day 1	Specific surface area (1/um)	Compressive modulus (Pa)	Pore size (μm)	% OC
1af	23.8	0.01458	23 ±13	61	34.55
1af-HAp 1:1	22.4	0.00785	40 ± 13	115	59.46
1rf-HAp 1:1	22.1	0.0131	120 ± 19	78	36.67
2af	17.1	0.00495	17 ± 8	145	40.23
2af-CS	12.5	0.00489	287 ± 49	150	62.75
2rf-CS	6.88	0.00502	56 ± 8	140	73.26

Veilleux et al. (2004) sought to study the difference in behaviour of chondrocytes seeded on type-I and II collagen scaffolds, and he found out that the cell adhesion was not different (Veilleux et al., 2004). This was not the case in this study. In type-II scaffolds, the release of CS into culture media may have functionalised the suspension well-plate, attracting the cells away from the scaffold, leading to the lower AB activity of CS-containing scaffolds compared to *2af* scaffold at all times. This might be why *2rf-CS*, while having the higher specific surface area among type-II scaffolds, showed a significantly lower AB activity at day 1. In general, highly deformable substrates do not tend to withstand traction forces exerted by cells during attachment, leading to less cell adhesion and consequently proliferation (Bacakova et al., 2011). Discharging CS from scaffold affects the compressive modulus of samples; therefore, it is not possible to comment on the effect of this parameter on the Alamar Blue activity of scaffolds.

8.4.3.3 Cellular metabolic activity

Over time the metabolic activity of cells decreased significantly in *1af-HAp 1:1*, while it was stabilised to nearly its original value in all other scaffolds after 28 days. Considering the results from the histology (Figure 8.23), this is believed to be due the blocking of pores because of the high amounts of residual/synthesized calcium-containing compounds (i.e. HAp). This may have prevented oxygen/nutrition and waste transportation to and from the cells leading to cell necrosis in central regions of scaffold after 28 days compared to day 14 (Figure 8.11), which justifies the significant reduction in AB activity in these scaffolds. Further, the overall contraction of scaffolds (Figure 8.2 and Figure 8.9) offered cells with smaller spaces for proliferation leading to cell overcrowding and their reduced metabolic activity. Similar behaviour was observed by meniscal cells in collagen matrices (Mueller et al., 1999).

It should be taken into consideration that there may be sub-populations of cells at different points in the lineage within these cultures that respond differently to the conditions they are subjected to. Therefore, some may continue to proliferate while others would start to differentiate and stop proliferating (Bernhardt et al., 2008).

8.4.4 Histological evaluations

In type-I scaffolds, cell in-growth occurred in all of the scaffolds, however, a layer of cells was also seen on the periphery, which had secreted extracellular matrix (, and). As a result it is possible that, diffusion of nutrients to the centre of the construct could become increasingly difficult resulting to acellular necrosis in the centre of scaffold (Gleeson et al., 2010). It is likely that the acellular necrosis, which was especially pronounced in *1af-HAp* after 4 weeks, was due to remaining/deposition of HAp, impeding fluid movement to cells in the centre.

It was seen that some of the cells grew on the surface and periphery of the constructs instead of infiltrating the pores of the scaffold; this could be particularly seen in *2af-CS*. It is believed that cell migration and ingrowth depends on scaffold pore size (Ohno et al., 2004, Ko et al., 2010) and stiffness. The pore size is not significantly different across type-II scaffolds; therefore, it cannot be the most influential factor. A stiff substrate is known to prompt a migratory response from cells (Dado and Levenberg, 2009), however, due to loss of CS in media (see Section 8.4.2) the compression modulus is likely to be reduced (see Table 8.5) and to be more comparable to *2af*. That the cells did not infiltrate into the scaffold and remained on periphery on *2af-CS* and not on other type-II scaffolds, is suggested to be due to discharge of a considerable amount of CS from scaffold into the culture (see Sections 8.4.2.2 and8.4.3.2) .

8.4.5 Matrix molecules production by cells

Qualitative analysis of immunohistology images showed that the cells produced more ECM collagen type-II on type-II scaffolds (Figure 8.29, Figure 8.30 and Figure 8.31) and negligible amount on type-I scaffolds. Type-I scaffolds (Figure 8.26, Figure 8.27 and Figure 8.28), especially mineralised scaffolds, showed increased excretion of ECM type-I collagen, which may be due to release of Ca^{2+} from HAp that is shown to increase osteogenic cell marker and gene expression (Filova et al., 2014). While synthesis and deposition of collagen type-I and calcium-containing compound may indicate cells in an osteoblastic path, production of collagen type-II and GAGs may imply that cells are going towards chondrogenic differentiation. The reason is that for example in osteogenesis, bone formation occurs by secretion of collagen (type I) from cells, followed by its calcification with the release of nHAp/Ca^{2+} ions (Kikuchi et al., 2001). Considering the results of Alizarin Red staining together with the immunohistochemistry, it can be concluded that afibrillar type-II scaffold incited a mixed response from cells by producing both markers for osteogenic and chondrogenic differentiation.

The stem cell fate is regulated by signals from its microenvironment. ECM to which the cell adheres is one of the components of this microenvironment, and its composition and physical properties (e.g. elasticity, topography, and microstructure) can direct the cell response (Trappmann et al., 2012).

Pore shape

Cells can be induced towards a specific lineage by artificially controlling their shape. It has been suggested that cell morphology could correlate with specific gene expression at

different levels (Rowley and Mooney, 2002). BMMSCs with a more rounded cell shape were associated with the higher expression of chondrogenic markers (McBride et al., 2008, Guilak et al., 2009). Therefore scaffolds with a more circular pore shape could be beneficial for chondrogenic differentiation. In type-II scaffolds for cartilage regeneration, composite scaffolds (*2af-CS* and *2rf-CS*) showed a more circular pore arrangements compared to *2af* (Figure 6.15). However, it can be qualitatively seen that the expressed collagen-II did not differ significantly across the scaffolds; therefore, this has not a strong effect on matrix molecule production in these scaffolds.

Scaffold stiffness

Scaffold stiffness is another factor affecting stem cell fate (Gleeson et al., 2010, Hadjipanayi et al., 2009, Engler et al., 2006, Discher et al., 2005, Even-Ram et al., 2006, Levental et al., 2007, Murphy et al., 2012, Vickers et al., 2010, Reinhart-King et al., 2008, Guilak et al., 2009, Trappmann et al., 2012). The cells response to mechanical properties of their matrix involve a feedback loop, where cells exert contractile forces on the matrix, producing strain in the substrate; this strain can be detected by other cells and they respond to this by adjusting their cytoskeleton and overall state (Discher et al., 2005, Murphy et al., 2013, Reinhart-King et al., 2008). Engler et al. (2006) showed (Figure 8.32) that human MSCs favoured differentiation into neuron-like cells on soft substrates, into myogenic lineage on substrates with moderate elasticity and into osteogenic lineage on rigid substrates (Engler et al., 2006).

Cells on stiffer type-I scaffolds (40-120 Pa) (Figure 7.2) in this study produced negligible type-II collagen but a considerable type-I collagen (Figure 8.26, Figure 8.27 and Figure 8.28),

one of the ECM markers of osteoblastic differentiation. The bulk stiffness of these scaffolds are far below the range specified by Engler (2006) or Discher et al. (2005), however as discussed earlier in Section 8.4.2, the high porosity of scaffolds means that the bulk modulus of elasticity would be lower from the local stiffness felt by cells by approximately 100 times (Harley et al., 2010b, Gleeson et al., 2010); due to the pore sizes of scaffolds (61-150um), it is expected that a high proportion of cells actually bridge the pores (Gleeson et al., 2010), so it is suggested that they feel a combination of local and the bulk stiffness of the scaffold, which may be in the stiffness range favoured by cells for osteogenesis.

In type-II scaffolds, as mentioned in Sections 8.4.2.2 and 8.4.3.2, CS is dissolved in cell culture media, thus it is expected that the stiffness of *2af-CS* was comparable to *2af*, with *2rf-CS* somehow higher due to fibrillogenesis, rendering all of them to be of much lower compression modulus compared to type-I scaffolds (Figure 7.2 and Figure 7.4). The increased type-II expression, which is a marker of chondrogenic differentiation, was seen on these scaffolds. Indeed, it was observed by Murphy et al. (2012) that lower stiffness (0.5 kPa) collagenous scaffolds induced up-regulation of SOX9, a phenotypic marker of chondrogenic differentiation and higher stiffness (1.5 kPa) scaffolds prompted up-regulation of RUNX2, a phenotypic marker of osteogenic differentiation (Murphy et al., 2012).

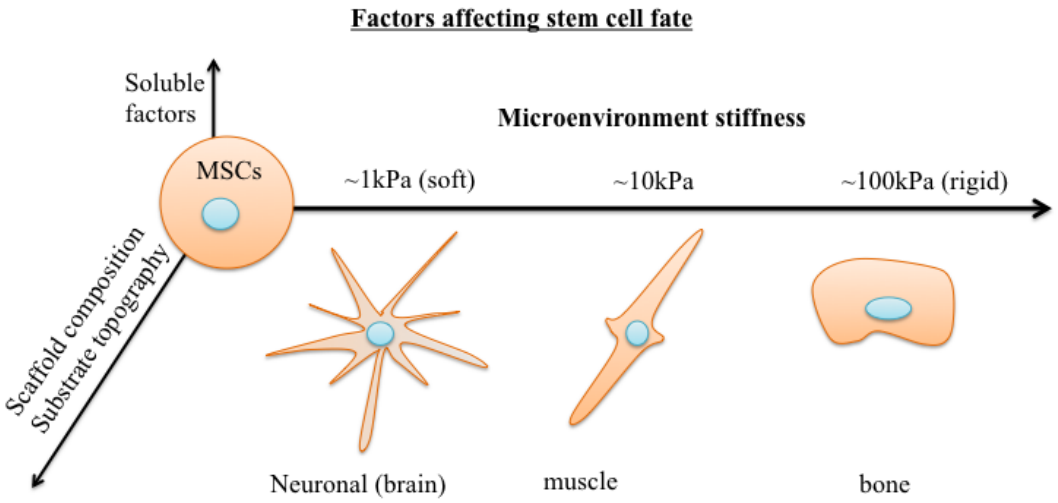


Figure 8.32 Effect of matrix elasticity on mesenchymal stem cell fate, adapted from (Engler et al., 2006); MSCs are initially small and round but develop increasingly branched, spindle, or polygonal shapes when grown on matrices respectively in the range typical of E brain (0.1–1 kPa), E muscle (~10 kPa), or E collagenous bone (~100kPa)

Size and pore size

It has been shown that the cartilage formation by mesenchymal stem cells(Shu et al., 2009) or chondroprogenitor cells (Vickers et al., 2010) requires an initial stage of "consdensation", where the intercellular space is reduced through cell aggregation and generation of cell-to-cell contacts which is then followed by condrogenic differentiation (Vickers et al., 2010, Sundelacruz and Kaplan, 2009, Veilleux and Spector, 2005). This was seen in *2af-CS* (Figure 8.30), where the cells resided densely on the edges of scaffold and deposited ECM marker collagen-II only in these parts.

Scaffold pore size may also play a role in directing the differentiation of stem cells. Nehrer showed that chondrocytes seeded on smaller pore size scaffolds are more closely packed and therefore the cell-cell interaction would affect the gene expression (Nehrer et al., 1997a). This may be extended to stem cells where condensation would be a pre-requisite of chondrogenesis. This means that higher type-II expression is expected in smaller pore size

scaffolds (*1af* and *1rf-HAp 1:1*- Table 8.5), which was not the case. This is probably due to the fact that pore size is only one of the many factors affecting cellular behavior as explained above, and the combination of these factors would determine cell fate, therefore, any attempt to identify effect of one without considering others would be unreasonable.

Scaffold composition

Scaffold composition is one of the most influential factors in cell differentiation (Nehrer et al., 1997a, Murphy et al., 2013). Collagen type (I and II in this study) as well as existence of HAp as explained in Section 8.4.5 are responsible for these specific matrix molecule production.

8.5 Summary

In summary, the microenvironment of cells, including the substrate properties on which they are seeded, has been shown to significantly influence cell behaviour in terms of attachment, metabolic activity and differentiation.

The cell attachment was affected by the combination of composition, microstructure and specific surface area in type-I scaffolds. In type-II scaffolds, the specific surface area did not differ among scaffolds but the lower attachment is suggested to be due to CS discharge. Over time, calcium containing compounds formed/remaining on *1af-HAp* may have led to acellular necrosis and reduced metabolic activity.

Cellular differentiation and production of ECM markers such as type-I and II collagen, was affected by scaffold elasticity, where stiffer type-I scaffolds promoted more type-I and less

type-II collagen secretion, and by scaffold composition, where collagen type and existence of HAp/CS affected the type of ECM marker production by cells.

8.6 Conclusion

The aims of this chapter were to examine the biocompatibility of scaffolds, and to determine whether the scaffolds alone would provide enough cues for MSCs differentiation. It was hypothesized that the chemical/molecular composition (Chapter 4 and 5), scaffold microstructures (Chapter 6) and mechanical properties (Chapter 7) would affect cellular response in terms of attachment, proliferation and differentiation. The results from this chapter were in accordance to the initial hypothesis: Cellular adhesion and metabolic activity were affected by a combination of microstructure (pore size) and composition (existence of HAp and CS), while cellular differentiation was affected by microstructure (pore shape, % of pores with appropriate size), mechanical properties and scaffold composition (collagen type, HAp and CS). It is concluded that cellular differentiation can be driven by a combination of collagen type, the presence of bioactive agents (CS and HAp), and physical features of the collagen scaffold itself. In short, the highly purified collagen may have provided a suitable foundation for the addition of specific factors to promote differentiation.

Chapter 9.Thesis Summary & Conclusions

Musculoskeletal and orthopaedic disorders have become a major issue in healthcare due to an aging population as well as tumour/trauma related injuries, and although the current treatments provide a fair improvement in conditions of patients (Section 2.6), they are still far from optimal. This thesis is concerned with manufacturing and characterisation of an osteochondral device mimicking the structure of natural tissue (Section 2.7). Following this approach the materials science of joints was studied (Section 2.2 and 2.3), and the importance of imitating the interface between the two tissue by providing a multi-layered scaffold with gradient change in properties was highlighted (Section 2.4), which led me to select monomeric type-I and type-II collagen with/without hydroxyapatite and chondroitin sulphate for this research as the materials of choice (Section 2.8.1).

The experimental work has been divided into six chapters. The aim of Chapter 3 was to fabricate pure and composite scaffolds. This was achieved by preparing Type I / Type II collagens into afibrillar/fibrillar atelocollagen with/without hydroxyapatite/chondroitin sulphate, liquids and freeze-dried scaffolds for physicochemical and biological characterisations.

In Chapter 4, the monolithic and composite scaffolds were characterized by Fourier Transform Infrared Spectroscopy. The aim was to develop an understanding of their properties and behaviours at the molecular level: it was shown that the triple helical structure of collagens in type-I was affected by addition of hydroxyapatite – possibly due to formation of new bonds between collagen amine groups/carboxylate groups and hydroxyapatite PO^{-3}_4/Ca^{2+}– and by fibrillogenesis – possibly due to a combination of collagen denaturation or packing of the triple helix by fibril formation. Triple helical structures of type-II scaffolds were not affected. In type-II scaffolds, it was suggested that the interaction between collagen and CS is electrostatic

involving the carbonyl group of hydroxyproline on collagen, as well as positively charged side chains and sulfate groups. This interaction was abolished by fibrillogenesis due to a combined effect of higher pH and ionic strength. These results were in accordance to the initial hypothesis of interactions between chondroitin sulfate/hydroxyapatite and different types of collagen (I and II) at molecular levels. It was further postulated that these chemical compositions and molecular interactions would have a multi-level effect on scaffolds characteristics: addition of CS/HAp and fibrillogenesis were shown to increase the viscosity of suspensions (Chapter 5), which was confirmed to affected the microstructure of especially Type-I scaffolds (Chapter 6), and compressive modulus of scaffolds (Chapter 7). The direct effect on cellular differentiation was observed by induction of chondrogenesis in Type-II scaffolds, especially those containing CS, and osteogenesis in Type-I scaffolds (Chapter 8). The conclusion that the interaction between type-II collagen and CS is purely of electrostatic nature, was confirmed by lack of any remaining CS in scaffolds once placed in cell culture media (Section 8.4.3.2). It was suggested that negatively charged CS were preferably attracted to positively charged amino acids in culture media rather than collagen. It was reasonable to relate the lower cell attachment and proliferation to this phenomenon.

The rheological properties of suspensions were studied in Chapter 5, and the aim was to understand the behaviour of suspensions at the molecular level before freeze-drying. This was achieved by looking at the changes in their molecular structure with fibrillogenesis and addition of chondroitin sulfate/hydroxyapatite. It was noted that collagen composite suspensions all showed shear thinning behaviour due to disturbance of equilibrium in forces between collagen/particles. It was determined that pure monomeric collagen solutions composing of semiflexible molecules were in semi-dilute state, mainly showing a viscous performance. Although some entanglements may be present between chains, they can move relatively freely upon applying strain. Upon adding CS, HAp or fibrillogenesis extensive rigidity of networks compared to monomeric solutions was detected. Overall, it was concluded that fibrillogenesis had a more pronounced effect on increasing the complex viscosity of suspensions than addition of HAp. These results verified the initial hypothesis that the molecular interactions between different constituents of scaffolds examined in Chapter 4, leads to differences in viscosity of suspensions and their rheological properties. Another hypothesis was that these rheological properties would affect the microstructure of resultant scaffolds (Chapter 6); this was corroborated by comparing the pore sizes of reconstituted fibrillar scaffolds with afibrillar scaffolds (Section 6.4.3).

The aim of Chapter 6 was to evaluate the microstructure of scaffolds in terms of pore structure (Section 6.4.2), size (Section 6.4.3) and shape (Section 6.4.4). It was shown that the microstructure of scaffolds will depend on the freezing of ice-crystals in suspensions. Whether the collagen/CS/hydroxyapatite are rejected from growing ice-crystal by diffusion or are pushed out by the ice-tip, as long as it is not entrapped in the ice-crystal a definable pore structure will form. It was shown that this was a result of forces on particles, where the main factors were

viscosity and thermal conductivity. It was concluded that especially in type-I preparations pore sizes are mainly growth rate dependent and they vary with the viscosity of the collagen suspensions. Furthermore, it was suggested that the resultant pores were best described as ellipses. Filtering the elliptical pore data for the desired pore sizes showed a moderate to high proportions of pores to be appropriate to support a specific cell type, or to promote a specific cell activity. However, biological assessments of scaffolds (Chapter 8) showed that having a high proportion of pores in a required size range does not necessarily lead to higher cell proliferation or specific differentiation; oxygen and nutrition transport to cells are suggested to be as influential. Proportion of pores with suitable sizes and their circularity, however, was shown to be one of the factors affecting chondrogenic differentiation in type-II/CS scaffolds.

The goal in Chapter 7 was to study the mechanical properties of scaffolds under compression. This was achieved by identifying the factors affecting the compressive modulus: it was concluded that the compression modulus was mainly affected by the modulus of the solid material rather than the relative density of scaffolds. This links the results from this chapter to Chapter 5, and further supports the hypothesis that molecular interactions affect subsequent viscosity, microstructure and mechanical properties. The clinical implication of the scaffolds behaviour under compression was that the scaffolds would be in their densification regime if implanted by press-fitting, where pore structure collapses and permanent change in size follows. Therefore, an alternative implantation technique needs to be employed, such as inserting the scaffold with tweezers instead of thumb. Fixation of scaffolds with fibrin glue could also be useful to avoid subsequent loosening.

The aim in Chapter 8 was to investigate the biological responses of scaffolds to human bone marrow mesenchymal stem cells. The interpretation and discussion of the results suggested that all of the scaffolds were biocompatible (Section 8.4.3.1). It was noted that the cell attachment and proliferation on the scaffolds was affected by composition, and bulk modulus (Section 8.4.3.2) of type-I scaffolds, while loss of CS during culture was possibly responsible for low cellular activities on CS-containing type-II scaffolds. It was concluded that stiffness, microstructure and material composition affects the extracellular matrix molecule deposition by cells. These results supported the overall hypothesis of this research: chemical/molecular interactions affect rheological properties of collagenous suspensions, which in turn influence the microstructure and mechanical properties. A combination of these factors then impacts cellular proliferation and differentiation.

The achievements of this research were three-fold:

Firstly, a comprehensive characterisation of rheological properties of suspensions with regards to their molecular state was performed. Although collagen suspensions have been previously studied in terms of their viscosity, an extensive examination of different collagen types (Type-I and II), ultrastructure (afibrillar/fibrillar) as well as their CS/HAp composites was lacking. It was established that rheological properties were linked with chemical/molecular interactions and that they affected microstructure and mechanical properties. Although the possible impact of viscosity on microstructure was previously explored, its effect on mechanical properties was relatively unknown.

Secondly, a thorough study of cell-scaffold interaction was implemented. Although biocompatibility of collagen-hydroxyapatite and collagen-chondroitin sulfate scaffolds has been

previously investigated, to author's knowledge, this is the first research to report the effect of collagen-type and composition on stem cell differentiation. To induce chondrogenesis/osteogenesis, researchers usually use chemical stimuli such as growth factors (e.g. TGF-b), however, in clinical situations sustainable delivery of growth factors to scaffolds is problematic (Tampieri et al., 2011), thus inducing differentiation without the need for growth factors is clinically very valuable. This research suggests that by selecting different types of collagen and additives (e.g. hydroxyapatite and CS) cellular differentiation can be controlled to a great extent, which may eliminate the need for differentiation supplements and/or some growth factors.

Thirdly, this research showed that to induce chondrogenesis, immobilisation of CS onto collagen scaffolds is not necessary; rather, mobilised CS in this research upregulated COL2 expression (data not shown) in BMMSCs. This allows for potentially quicker production by eliminating the need for crosslinking immobilisation of CS onto collagen scaffold.

The main limitations of these scaffolds were firstly their low compressive modulus and secondly their instability in cell culture media. The low compressive modulus would pose problems for future clinical use, as it needs to withstand forces during implantation. Collagen scaffold shrinkage is widely recognised and is quite problematic for tissue engineering. It can not only distort the shape and dimensions in the defect site, but also lead to constriction of pores affecting diffusive properties and cell migration (Itoh et al., 2001, Dawson et al., 2008). Improving the mechanical properties would resolve both issues.

Based on the results of this research the following scaffolds are suggested for further development in to clinical use:

For the cartilage section, the afibrillar *2af-CS* scaffold shows the highest potential; it has the highest compressive modulus, with a moderate percentage of pores (31%) suitable for chondrocytes. Furthermore, the combination of type-II collagen with CS has shown to induce chondrogenesis, in absence of any growth factors. For the bone section, on the other hand, the reconstituted fibrillar *1rf-HAp* (*1:1* and *1:3*) scaffolds are suggested. They had higher compressive modulus compared to their afibrillar counterparts, and although the percentage of pores suitable for osteoblasts were lower when compared to afibrillar scaffolds, cellular proliferation and COL1 upregulation was higher on *1rf-HAp 1:1*. Therefore, a composite scaffold of *2af-CS* and *1rf-HAp* (*1:1* and *1:3*) are proposed for further studies.

Chapter 10. Future Works

Parts of the thesis can be further developed. These include:

Fabrication and characterisation of scaffolds

- In a previous study by Walton (2010), the kinetics of fibrillogenesis of collagen from the same source was investigated. The same method was applied to generate fibrils in this thesis. However, further fibrillogenesis studies with mixtures of collagen, CS and HAp could be beneficial for a more accurate understanding about the effect of CS and HAp on degree and kinetics of fibrillogenesis, and the bonding between the constituents.

- It was concluded that the compressive moduli of monomeric/reconstituted fibrillar requires an alternative implantation technique in the defect sites. Thus further work in increasing the compressive moduli of these scaffolds would be beneficial. Developing appropriate methods of crosslinking could be a solution. Moreover, producing concentrated scaffolds, and therefore, increasing the elastic modulus of solid material, could be a starting point based on conclusions from this thesis.

- A systematic cell study is needed to determine the effect of fibrillogenesis, CS and HAp addition, and scaffold stiffness on cell behaviour, keeping other factors the same. Monitoring the rate of hydroxyapatite release and measuring the remaining HAp in scaffolds could give insights on the behaviour of the cells in terms of infiltration, proliferation and differentiation.

Development of the multi-layered composite scaffold for clinical use (see Figure 2.21)

- Suitable layers for cartilage and bone sections were identified in this research. The suggested scaffolds were *2af-CS* for cartilage and *1rf-HAp 1:1/1:3* for bone. Further work should be carried out to assemble these layers together and characterise their transition region in terms of microstructure and mechanical properties.
- An investigation on the cell attachment, proliferation and differentiation of layered scaffolds in the same culture environment should be carried out to explore the clinical applicability.
- Upon fabrication of a clinically suitable layered scaffold, *in vivo* animal studies should be done. In this case, large animals (e.g. sheep, horse, etc) would be more suitable, as they resemble the human conditions more closely, when compared to small animal models (rats, rabbits, etc). The newly formed tissue integration and its quality should be examined by histology, microCT, etc. Obtaining favourable results from *in vivo* studies, the next stage to develop a useable device would be clinical trials.

References

AIGNER, T. & STOVE, J. 2003. Collagens-major component of the physiological cartilage matrix, major target of cartilage degeneration, major tool in cartilage repair. *Collagen in drug delivery and tissue engineering,* 55**,** 1569-1593.

AKIZUKI, S., MOW, V. C., MULLER, F., PITA, J. C., HOWELL, D. S. & MANICOURT, D. H. 1986. Tensile Properties of Human Knee-Joint Cartilage .1. Influence of Ionic Conditions, Weight Bearing, and Fibrillation on the Tensile Modulus. *Journal of Orthopaedic Research,* 4**,** 379-392.

AL-MUNAJJED, A. A., PLUNKETT, N. A., GLEESON, J. P., WEBER, T., JUNGREUTHMAYER, C., LEVINGSTONE, T., HAMMER, J. & O'BRIEN, F. J. 2009. Development of a biomimetic collagen-hydroxyapatite scaffold for bone tissue engineering using a SBF immersion technique. *Journal of Biomedical Materials Research Part B: Applied Biomaterials,* 90B**,** 584-591.

AMIS, E. J., CARRIERE, C. J., FERRY, J. D. & VEIS, A. 1985. Effect of pH on collagen flexibility determined from dilute solution viscoelastic measurements. *International journal of biological macromolecules,* 7**,** 130-134.

AMJAD, Z., KOUTSOUKOS, P., TOMSON, M. B. & NANCOLLAS, G. H. 1978. Growth of Hydroxyapatite from Solution - New Constant Composition Method. *Journal of dental research,* 57**,** 909-909.

ANSELME, K. 2000. Osteoblast adhesion on biomaterials. *Biomaterials,* 21**,** 667-681.

ARIAS, C., YAGUE, A., RUEDA, C. & GARCIA BLANCO, F. 1998. Intrinsic viscosity calculated out of single point measurements for chondroitin-4-sulfate and chondroitin-6-sulfate solutions. *Biophysical chemistry,* 72**,** 307-312.

ARMSTRONG, C. G. & MOW, V. C. 1982. Variations in the Intrinsic Mechanical Proterties of Human Articular-Cartilage with Age, Degeneration, and Water-Content. *Journal of Bone and Joint Surgery-American Volume,* 64**,** 88-94.

ARRONDO, J. L. & GONI, F. M. 1999. Structure and dynamics of membrane proteins as studied by infrared spectroscopy. *Progress in biophysics and molecular biology,* 72**,** 367-405.

ASHBY, M. F. 2006. The properties of foams and lattices. *Philosophical Transactions of the Royal Society A: Mathematical, Physical and Engineering Sciences,* 364**,** 15-30.

ATESHIAN, G. A., LAI, W. M., ZHU, W. B. & MOW, V. C. 1994. An asymptotic solution for the contact of two biphasic cartilage layers. *Journal of Biomechanics,* 27**,** 1347-1360.

ATESHIAN, G. A. & WANG, H. 1995. A theoretical solution for the frictionless rolling contact of cylindrical biphasic articular cartilage layers. *Journal of Biomechanics,* 28**,** 1341-1355.

ATHANASIOU, K. A., ROSENWASSER, M. P., BUCKWALTER, J. A., MALININ, T. I. & MOW, V. C. 1991. Interspecies Comparisons of Insitu Intrinsic Mechanical-Properties of Distal Femoral Cartilage. *Journal of Orthopaedic Research,* 9**,** 330-340.

ATHANASIOU, K. A., ZHU, C. F., LANCTOT, B. S., AGRAWAL, C. M. & WANG, X. 2000. Fundamentals of biomechanics in tissue engineering of bone. *Tissue engineering,* 6**,** 361.

AZOUNI, M. A., KALITA, W. & YEMMOU, M. 1990. On the particle behaviour in front of advancing liquid-ice interface. *Journal of Crystal Growth,* 99**,** 201-205.

BACAKOVA, L., FILOVA, E., PARIZEK, M., RUML, T. & SVORCIK, V. 2011. Modulation of cell adhesion, proliferation and differentiation on materials designed for body implants. *Biotechnology Advances,* 29**,** 739-767.

BACAKOVA, L., FILOVA, E., RYPACEK, F., SVORCIK, V. & STARY, V. 2004. Cell adhesion on artificial materials for tissue engineering. *Physiol Res,* 53**,** S35-S45.

BAJAJ, P., SCHWELLER, R. M., KHADEMHOSSEINI, A., WEST, J. L. & BASHIR, R. 2014. 3D Biofabrication Strategies for Tissue Engineering and Regenerative Medicine. *Annual Review of Biomedical Engineering,* 16.

BANDEKAR, J. 1992. Amide modes and protein conformation. *Biochimica et Biophysica Acta (BBA) - Protein Structure and Molecular Enzymology,* 1120**,** 123-143.

BARAVIAN, C., BENBELKACEM, G. & CATON, F. 2006. Unsteady rheometry: can we characterize weak gels with a controlled stress rheometer? *Rheologica Acta,* 46**,** 577-581.

BARNES, H. A. 1997. Thixotropy- a review. *Journal of Non-Newtonian Fluid Mechanics,* 70**,** 1-33.

BARTH, A. 2007. Infrared spectroscopy of proteins. *Biochimica et Biophysica Acta (BBA) - Bioenergetics,* 1767**,** 1073-1101.

BEAR, R. S. 1952. The structure of collagen fibrils. *In:* ANSON, M. L., BAILEY, K. & EDSALL, J. T. (eds.) *Advances in protein chemistry, Volume 7.* New York: Academic Press.

BELLA, J., BRODSKY, B. & BERMAN, H. M. 1995. Hydration structure of a collagen peptide. *Structure,* 3**,** 893-906.

BERNHARDT, A., LODE, A., BOXBERGER, S., POMPE, W. & GELINSKY, M. 2008. Mineralised collagen-an artificial, extracellular bone matrix-improves osteogenic differentiation of bone marrow stromal cells. *Journal of materials science. Materials in medicine,* 19**,** 269.

BIRK, D. E. & SILVER, F. H. 1984. Collagen fibrillogenesis in vitro: Comparison of types I, II, and III. *Archives of Biochemistry and Biophysics,* 235**,** 178-185.

BLOND, G. 1988. Velocity of linear crystallization of ice in macromolecular systems. *Cryobiology,* 25**,** 61-66.

BOWES, J. H. & KENTEN, R. H. 1950. The swelling of collagen in alkaline solutions. 1. Swelling in solutions of sodium hydroxide. *Biochem.J.,* 46**,** 1-8.

BOWES, J. H. & MOSS, J. A. 1962. The Effect of Gamma Radiation on Collagen. *Radiation research,* 16**,** 211-223.

BOYAN, B. D., HUMMERT, T. W., DEAN, D. D. & SCHWARTZ, Z. 1996. Role of material surfaces in regulating bone and cartilage cell response. *Polymer Scaffolding and Hard Tissue Engineering,* 17**,** 137-146.

BRADT, J.-H., MERTIG, M., TERESIAK, A. & POMPE, W. 1999. Biomimetic mineralization of collagen by combined fibril assembly and calcium phosphate formation. *Chemistry of Materials,* 11**,** 2694-2701.

BRAND, D. D., KANG, A. H. & ROSLONIEC, E. F. Immunopathogenesis of collagen arthritis. Springer seminars in immunopathology, 2003. Springer, 3-18.

BRAND, D. D., LATHAM, K. A. & ROSLONIEC, E. F. 2007. Collagen-induced arthritis. *Nature protocols,* 2**,** 1269-1275.

BRAND, D. D., MYERS, L. K., WHITTINGTON, K. B., LATHAM, K. A., STUART, J. M., KANG, A. H. & ROSLONIEC, E. F. 2002. Detection of early changes in autoimmune T cell phenotype and function following intravenous administration of type II collagen in a TCR-transgenic model. *Journal of immunology (Baltimore, Md.: 1950),* 168**,** 490-498.

BRINCKMANN, J., NOTBOHM, H. & MULLER, P. K. 2005. *Primer in Structure, Processing and Assembly,* New York, Springer.

BUCKWALTER, J. A. & MANKIN, H. J. 1997a. Articular cartilage .1. Tissue design and chondrocyte-matrix interactions. *Journal of Bone and Joint Surgery-American Volume,* 79A**,** 600-611.

BUCKWALTER, J. A. & MANKIN, H. J. 1997b. Articular cartilage .Part II: Degeneration and Osteoarthrosis, repair, regeneration and transplantation. *Journal of Bone and Joint Surgery-American Volume,* 79A**,** 612-632.

BUCKWALTER, J. A. & MANKIN, H. J. 1998. Articular cartilage repair and transplantation. *Arthritis and Rheumatism,* 41**,** 1331-1342.

BUMA, P., PIEPER, J. S., VAN TIENEN, T., VAN SUSANTE, J. L. C., VAN DER KRAAN, P. M., VEERKAMP, J. H., VAN DEN BERG, W. B., VETH, R. P. H. & VAN KUPPEVELT, T. H. 2003. Cross-linked type I and type II collagenous matrices for the repair of full-thickness articular cartilage defects - A study in rabbits. *Biomaterials,* 24**,** 3255-3263.

CALIARI, S. R. & HARLEY, B. A. C. 2011. The effect of anisotropic collagen-GAG scaffolds and growth factor supplementation on tendon cell recruitment, alignment, and metabolic activity. *Biomaterials,* 32**,** 5330-5340.

CALIARI, S. R., RAMIREZ, M. A. & HARLEY, B. A. C. 2011. The development of collagen-GAG scaffold-membrane composites for tendon tissue engineering. *Biomaterials,* 32**,** 8990-8998.

CALIARI, S. R., WEISGERBER, D. W., RAMIREZ, M. A., KELKHOFF, D. O. & HARLEY, B. A. C. 2012. The influence of collagen-glycosaminoglycan scaffold relative density and microstructural anisotropy on tenocyte bioactivity and transcriptomic stability. *Special Issue on Tissue Engineering,* 11**,** 27-40.

CAO, H. & XU, S.-Y. 2008. EDC/NHS-crosslinked type II collagen-chondroitin sulfate scaffold: characterization and in vitro evaluation. *Journal of Materials Science-Materials in Medicine,* 19**,** 567-575.

CARTER, D. R., BEAUPRE, G. S., GIORI, N. J. & HELMS, J. A. 1998. Mechanobiology of skeletal regeneration. *Clinical orthopaedics and related research,* 355**,** S41-S55.

CEN, L., LIU, W., CUI, L., ZHANG, W. & CAO, Y. 2008. Collagen tissue engineering: development of novel biomaterials and applications. *Pediatric research,* 63**,** 492-496.

CHANG, M. C. & TANAKA, J. 2002. FT-IR study for hydroxyapatite/collagen nanocomposite cross-linked by glutaraldehyde. *Biomaterials,* 23**,** 4811-4818.

CHEN, Q., BRUYNEEL, A., CLARKE, K., CARR, C. & CZERNUSZKA, J. 2012. Collagen-Based Scaffolds for Potential Application of Heart Valve Tissue Engineering. *Journal of Tissue Science and Engineering,* S11.

CHEN, S., HIROTA, N., OKUDA, M., TAKEGUCHI, M., KOBAYASHI, H., HANAGATA, N. & IKOMA, T. 2011. Microstructures and rheological properties of tilapia fish-scale collagen hydrogels with aligned fibrils fabricated under magnetic fields. *Acta Biomaterialia,* 7**,** 644-652.

CHEUNG, D. T., PERELMAN, N., TONG, D. & NIMNI, M. E. 1990. The effect of gamma-irradiation on collagen molecules, isolated alpha-chains, and crosslinked native fibers. *Journal of Biomedical Materials Research,* 24**,** 581.

CHI, V. & CHANDY, K. G. 2007. Immunohistochemistry: Paraffin Sections Using the Vectastain ABC Kit from Vector Labsa. *J. Vis. Exp.,* 8**,** 308.

CHOW, A. W., FULLER, G. G., WALLACE, D. G. & MADRI, J. A. 1985. Rheooptical response of rodlike, shortened collagen protein to transient shear flow. *Macromolecules,* 18**,** 805-810.

COMPER, W. D. & VEIS, A. 1977. The mechanism of nucleation for in vitro collagen fibril formation. *Biopolymers,* 16**,** 2113-2131.

CREMER, M. A., ROSLONIEC, E. F. & KANG, A. H. 1998. The cartilage collagens: a review of their structure, organization, and role in the pathogenesis of experimental arthritis in animals and in human rheumatic disease. *Journal of Molecular Medicine-Jmm,* 76**,** 275-288.

CUI, W., WANG, Q., CHEN, G., ZHOU, S., CHANG, Q., ZUO, Q., REN, K. & FAN, W. 2011. Repair of articular cartilage defects with tissue-engineered osteochondral composites in pigs. *Journal of Bioscience and Bioengineering,* 111**,** 493-500.

CUNNIFFE, G. M., DICKSON, G. R., PARTAP, S., STANTON, K. T. & O'BRIEN, F. J. 2010. Development and characterisation of a collagen nano-hydroxyapatite composite scaffold

for bone tissue engineering. *Journal of Materials Science-Materials in Medicine,* 21**,** 2293-2298.

DA SILVA AQUINO, K. A. 2012. *Sterilization by Gamma Irradiation*.

DADO, D. & LEVENBERG, S. 2009. Cell-scaffold mechanical interplay within engineered tissue. *Regenerative Biology and Medicine: II and Patterning and Evolving the Vertebrate Forebrain,* 20**,** 656-664.

DAGALAKIS, N., FLINK, J., STASIKELIS, P., BURKE, J. F. & YANNAS, I. V. 1980. Design of an Artificial Skin .3. Control of Pore Structure. *Journal of Biomedical Materials Research,* 14**,** 511-528.

DAVIDENKO, N., GIBB, T., SCHUSTER, C., BEST, S. M., CAMPBELL, J. J., WATSON, C. J. & CAMERON, R. E. 2012. Biomimetic collagen scaffolds with anisotropic pore architecture. *Acta Biomaterialia,* 8**,** 667-676.

DAWSON, J. I., WAHL, D. A., CZERNUSZKA, J. T. & OREFFO, R. O. C. 2007a. Biomimetic collagen-hydroxyapatite composite scaffolds for osteo and chondrogenic conduction of STRO-1 immunoselected human bone marrow stromal cells. *Tissue engineering,* 13**,** 1644-1645.

DAWSON, J. I., WAHL, D. A., CZERNUSZKA, J. T. & OREFFO, R. O. C. 2007b. Bone marrow stromal cells and biomimetic collagen-hydroxyapatite scaffolds for skeletal tissue engineering. *Tissue engineering,* 13**,** 1377-1378.

DAWSON, J. I., WAHL, D. A., LANHAM, S. A., KANCZLER, J. M., CZERNUSZKA, J. T. & OREFFO, R. O. C. 2008. Development of specific collagen scaffolds to support the osteogenic and chondrogenic differentiation of human bone marrow stromal cells. *Biomaterials,* 29**,** 3105-3116.

DEVILLE, S. 2008. Freeze-Casting of Porous Ceramics: A Review of Current Achievements and Issues. *Advanced Engineering Materials,* 10**,** 155-169.

DEVILLE, S., MAIRE, E., LASALLE, A., BOGNER, A. S., GAUTHIER, C., LELOUP, J. R. M. & GUIZARD, C. 2009. In Situ X-Ray Radiography and Tomography Observations of the Solidification of Aqueous Alumina Particles Suspensions. Part II: Steady State. *Journal of the American Ceramic Society,* 92**,** 2497-2503.

DEVILLE, S., SAIZ, E. & TOMSIA, A. P. 2006. Freeze casting of hydroxyapatite scaffolds for bone tissue engineering. *Biomaterials,* 27**,** 5480-5489.

DEVILLE, S., SAIZ, E. & TOMSIA, A. P. 2007. Ice-templated porous alumina structures. *Acta Materialia,* 55**,** 1965-1974.

DISCHER, D. E., JANMEY, P. & WANG, Y. L. 2005. Tissue cells feel and respond to the stiffness of their substrate. *Science* 310**,** 1139-1143.

DOI, M. & EDWARDS, S. F. 1986. *The theory of polymer dynamics*, Clarendon Press.

DONNAN, F. G. 1924. The Theory of Membrane Equilibria. *Chemical reviews,* 1**,** 73-90.

DOUGLAS, T., HEINEMANN, S., BIERBAUM, S., SCHARNWEBER, D. & WORCH, H. 2006. Fibrillogenesis of Collagen Types I, II, and III with Small Leucine-Rich Proteoglycans Decorin and Biglycan. *Biomacromolecules,* 7**,** 2388-2393.

DOUGLAS, T., HEINEMANN, S., MIETRACH, C., HEMPEL, U., BIERBAUM, S., SCHARNWEBER, D. & WORCH, H. 2007. Interactions of Collagen Types I and II with Chondroitin Sulfates A-C and Their Effect on Osteoblast Adhesion. - *Biomacromolecules.* American Chemical Society.

DOYLE, B. B., BENDIT, E. G. & BLOUT, E. R. 1975. Infrared spectroscopy of collagen and collagen-like polypeptides. *Biopolymers,* 14**,** 937-957.

ENGLER, A. J., SEN, S., SWEENEY, H. L. & DISCHER, D. E. 2006. Matrix elasticity directs stem cell lineage specification. *Cell,* 126**,** 677-689.

ERISKEN, C., KALYON, D. M. & WANG, H. 2010. Viscoelastic and Biomechanical Properties of Osteochondral Tissue Constructs Generated From Graded Polycaprolactone and Beta-Tricalcium Phosphate Composites. *Journal of Biomechanical Engineering-Transactions of the Asme,* 132**,** 091013.

EVEN-RAM, S., ARTYM, V. & YAMADA, K. M. 2006. Matrix Control of Stem Cell Fate. *Cell,* 126**,** 645-647.

EYRE, D. 2002. Collagen of articular cartilage. *Arthritis Research,* 4**,** 30-35.

FARNDALE, R., SIXMA, J., BARNES, M. & DE GROOT, P. 2004. The role of collagen in thrombosis and hemostasis. *Journal of Thrombosis and Haemostasis,* 2**,** 561-573.

FARRELL, E., O'BRIEN, F. J., DOYLE, P., FISCHER, J., YANNAS, I., HARLEY, B. A., O'CONNELL, B., PRENDERGAST, P. J. & CAMPBELL, V. A. 2006. A collagen-glycosaminoglycan scaffold supports adult rat mesenchymal stem cell differentiation along osteogenic and chondrogenic routes. *Tissue engineering,* 12**,** 459-468.

FERRY, J. D. 1980. *Viscoelastic Properties of Polymers,* Wiley & Sons.

FICAI, A., ANDRONESCU, E., GHITULICA, C., VOICU, G., TRANDAFIR, V., MANZU, D., FICAI, M. & PALL, S. 2009. Collagen/hydroxyapatite interactions in composite biomaterials. *Mater Plast,* 46**,** 11-15.

FIELDS, G. B. 1995. The collagen triple-helix: correlation of conformation with biological activities. *Connective tissue research,* 31**,** 235-243.

FILOVA, E., SUCHY, T., SUCHARDA, Z., SUPOVA, M., ZALOUDKOVA¡, M., BALIK, K., LISA¡, V., SLOUF, M. & BACAKOVA¡, L. 2014. Support for the initial attachment, growth and differentiation of MG-63 cells: a comparison between nano-size hydroxyapatite and micro-size hydroxyapatite in composites. *Int J Nanomedicine,* 9**,** 3687.

FLORENCIO-SILVA, R., SASSO, G. R. D. S., SASSO-CERRI, E., SIMOES, M. J. & CERRI, P. S. 2015. Biology of Bone Tissue: Structure, Function, and Factors That Influence Bone Cells. *BioMed Research International,* 2015**,** 17.

FOOT, M. & MULHOLLAND, M. 2005. Classification of chondroitin sulfate A, chondroitin sulfate C, glucosamine hydrochloride and glucosamine 6 sulfate using chemometric techniques. *Journal of pharmaceutical and biomedical analysis,* 38**,** 397-407.

FOX, A. J. S., BEDI, A. & RODEO, S. A. 2009. The Basic Science of Articular Cartilage: Structure, Composition, and Function. *Sports Health,* 1**,** 461.

FREY, M. T., TSAI, I. Y., RUSSELL, T. P., HANKS, S. K. & WANG, Y.-L. 2006. Cellular Responses to Substrate Topography: Role of Myosin II and Focal Adhesion Kinase. *Biophysical journal,* 90**,** 3774-3782.

FREYMAN, T. M., YANNAS, I. V. & GIBSON, L. J. 2001a. Cellular materials as porous scaffolds for tissue engineering. *Progress in Materials Science,* 46**,** 273-282.

FREYMAN, T. M., YANNAS, I. V., YOKOO, R. & GIBSON, L. J. 2001b. Fibroblast contraction of a collagen-GAG matrix. *Biomaterials,* 22**,** 2883-2891.

FU, Q., RAHAMAN, M. N., DOGAN, F. & BAL, B. S. 2008. Freeze casting of porous hydroxyapatite scaffolds. I. Processing and general microstructure. *Journal of Biomedical Materials Research Part B: Applied Biomaterials,* 86B**,** 125-135.

GANDHI, N. S. & MANCERA, R. L. 2008. The Structure of Glycosaminoglycans and their Interactions with Proteins. *Chemical Biology & Drug Design,* 72**,** 455-482.

GELMAN, R. A. & BLACKWELL, J. 1973. Interaction Between Collagen and Chondroitin-6-Sulfate. *Connect Tissue Res,* 2**,** 31-35.

GELMAN, R. A., WILLIAMS, B. R. & PIEZ, K. A. 1979. Collagen fibril formation. Evidence for a multistep process. *Journal of Biological Chemistry,* 254**,** 180-186.

GEORGE, A. & VEIS, A. 1991. FTIRS in water demonstrates that collagen monomers undergo a conformational transition prior to thermal self-assembly in vitro. *Biochemistry,* 30**,** 2372-2377.

GIANNAKOPOULOS, A. E. 1998. Indentation of graded substrates. *Thin Solid Films,* 332.

GIBSON, L. J. & ASHBY, M. F. 1997. *Cellular Solids: Structure and Properties,* Cambridge, UK, Cambridge University Press.

GLEESON, J. P., PLUNKETT, N. A. & O'BRIEN, F. J. 2010. Addition of hydroxyapatite improves stiffness, interconnectivity and osteogenic potential of a highly porous collagen-based scaffold for bone tissue regeneration. *European Cells & Materials,* 20**,** 218-230.

GOTORA, D. & CZERNUSZKA, J. T. Mineralisation and cross-linking techniques to improve the mechanical properties of collagen-calcium phosphate (Coll-CaP) composites to be used as bone analogues. European Cells and Materials, 2004 2004. 55.

GREGORY, C. A., GRADY GUNN, W., PEISTER, A. & PROCKOP, D. J. 2004. An Alizarin red-based assay of mineralization by adherent cells in culture: comparison with cetylpyridinium chloride extraction. *Analytical Biochemistry,* 329**,** 77-84.

GRIFFON, D. J., SEDIGHI, M. R., SCHAEFFER, D. V., EURELL, J. A. & JOHNSON, A. L. 2006. Chitosan scaffolds: Interconnective pore size and cartilage engineering. *Acta Biomaterialia,* 2**,** 313-320.

GRYNPAS, M. D., EYRE, D. R. & KIRSCHNER, D. A. 1980. Collagen Type-II Differs from Type-I in Native Molecular Packing. *Biochimica et biophysica acta,* 626**,** 346-355.

GUILAK, F., COHEN, D. M., ESTES, B. T., GIMBLE, J. M., LIEDTKE, W. & CHEN, C. S. 2009. Control of stem cell fate by physical interactions with the extracellular matrix. *Cell stem cell,* 5**,** 17-26.

HADJIPANAYI, E., MUDERA, V. & BROWN, R. A. 2009. Close dependence of fibroblast proliferation on collagen scaffold matrix stiffness. *Journal of tissue engineering and regenerative medicine,* 3**,** 77-84.

HARLEY, B. A., LEUNG, J. H., SILVA, E. C. C. M. & GIBSON, L. J. 2007. Mechanical characterization of collagen-glycosaminoglycan scaffolds. *Acta Biomaterialia,* 3**,** 463-474.

HARLEY, B. A., LYNN, A. K., WISSNER-GROSS, Z., BONFIELD, W., YANNAS, I. V. & GIBSON, L. J. 2010a. Design of a multiphase osteochondral scaffold III: Fabrication of layered scaffolds with continuous interfaces. *Journal of Biomedical Materials Research Part a,* 92A**,** 1078-1093.

HARLEY, B. A., LYNN, A. K., WISSNER-GROSS, Z., BONFIELD, W., YANNAS, I. V. & GIBSON, L. J. 2010b. Design of a multiphase osteochondral scaffold. II. Fabrication of a mineralized collagen-glycosaminoglycan scaffold. *Journal of Biomedical Materials Research Part a,* 92A**,** 1066-1077.

HAYASHI, T. & NAGAI, Y. 1973. Effect of pH on the Stability of Collagen Molecule in Solution. *Journal of Biochemistry,* 73**,** 999-1006.

HAYES, W. C. & MOCKROS, L. F. 1971. Viscoelastic Properties of Human Articular Cartilage. *Journal of applied physiology,* 31**,** 562-&.

HORI, R. Y. & MOCKROS, L. F. 1976. Indentation tests of human articular cartilage. *Journal of Biomechanics,* 9**,** 259-268.

HSIEH, T.-T., TIU, C., SIMON, G. P. & YU WU, R. 1999. Rheology and miscibility of thermotropic liquid crystalline polymer blends. *Journal of Non-Newtonian Fluid Mechanics,* 86**,** 15-35.

HUNZIKER, E. B. 2002. Articular cartilage repair: basic science and clinical progress. A review of the current status and prospects. *Osteoarthritis and Cartilage,* 10**,** 432-463.

HUTMACHER, D. W. 2000. Scaffolds in tissue engineering bone and cartilage. *Biomaterials,* 21**,** 2529-2543.

HUTMACHER, D. W. 2001. Scaffold design and fabrication technologies for engineering tissues - state of the art and future perspectives. *Journal of Biomaterials Science-Polymer Edition,* 12**,** 107-124.

ITALA, A. I., YLANEN, H. O., EKHOLM, C., KARLSSON, K. H. & ARO, H. T. 2001. Pore diameter of more than 100 um is not requisite for bone ingrowth in rabbits. *Journal of Biomedical Materials Research,* 58**,** 679-683.

ITOH, H., ASO, Y., FURUSE, M., NOISHIKI, Y. & MIYATA, T. 2001. A honeycomb collagen carrier for cell culture as a tissue engineering scaffold. *Artif Organs,* 25**,** 213-7.

JACKSON, R. L., BUSCH, S. J. & CARDIN, A. D. 1991. Glycosaminoglycans - Molecular-Properties, Protein Interactions, and Role in Physiological Processes. *Physiological Reviews,* 71**,** 481-539.

JUNQUEIRA, L. C. U., BIGNOLAS, G. & BRENTANI, R. R. 1979. Picosirius staining plus polarization microscopy, a specific method for collagen detection in tissue sections. *Histochemicat Journal,* 11**,** 447-455.

KADLER, K. E., HOLMES, D. F., TROTTER, J. A. & CHAPMAN, J. A. 1996. Collagen fibril formation. *Biochemical Journal,* 316**,** 1-11.

KANUNGO, B. P. & GIBSON, L. J. 2009. Density-property relationships in mineralized collagen-glycosaminoglycan scaffolds. *Acta Biomaterialia,* 5**,** 1006-1018.

KANUNGO, B. P. & GIBSON, L. J. 2010. Density-property relationships in collagen-glycosaminoglycan scaffolds. *Acta Biomaterialia,* 6**,** 344-353.

KARAGEORGIOU, V. & KAPLAN, D. 2005. Porosity of 3D biomaterial scaffolds and osteogenesis. *Biomaterials,* 26**,** 5474-5491.

KASAPIS, S. & MITCHELL, J. R. 2001. Definition of the rheological glass transition temperature in association with the concept of iso-free-volume. *International journal of biological macromolecules,* 29**,** 315-321.

KEMPSON, G. E., FREEMAN, M. A. R. & SWANSON, S. A. V. 1971. Determination of a Creep Modulus for Articular Cartilage from Indentation Tests on Human Femoral Head. *Journal of Biomechanics,* 4**,** 239-250.

KEMPSON, G. E., MUIR, H., POLLARD, C. & TUKE, M. 1973. The tensile properties of the cartilage of human femoral condyles related to the content of collagen and glycosaminoglycans. *Biochimica et Biophysica Acta (BBA) - General Subjects,* 297**,** 456-472.

KEMPSON, G. E., MUIR, H., SWANSON, S. A. V. & FREEMAN, M. A. R. 1970. Correlations between stiffness and the chemical constituents of cartilage on the human femoral head. *Biochimica et Biophysica Acta (BBA) - General Subjects,* 215**,** 70-77.

KHOR, E. 1997. Methods for the treatment of collagenous tissues for bioprostheses. *Biomaterials,* 18**,** 95-105.

KIKUCHI, M., IKOMA, T., SYOJI, D., MATSUMOTO, H., KOYAMA, Y., ITOH, S., TAKAKUDA, K., SHINOMIYA, K. & TANAKA, J. 2004. Porous body preparation of hydroxyapatite/collagen nanocomposites for bone tissue regeneration. *Key Engineering Materials,* 254**,** 561-564.

KIKUCHI, M., ITOH, S., ICHINOSE, S., SHINOMIYA, K. & TANAKA, J. 2001. Self-organization mechanism in a bone-like hydroxyapatite/collagen nanocomposite synthesized in vitro and its biological reaction in vivo. *Biomaterials,* 22**,** 1705-1711.

KIM, T. G., SHIN, H. & LIM, D. W. 2012. Biomimetic Scaffolds for Tissue Engineering. *Advanced Functional Materials,* 22**,** 2446-2468.

KINNEBERG, K. R. C., NIRMALANANDHAN, V. S., JUNCOSA-MELVIN, N., POWELL, H. M., BOYCE, S. T., SHEARN, J. T. & BUTLER, D. L. 2010. Chondroitin-6-Sulfate Incorporation and Mechanical Stimulation Increase MSC-Collagen Sponge Construct Stiffness. *Journal of Orthopaedic Research,* 28**,** 1092-1099.

KLAWITTER, J. J. & HULBERT, S. F. 1971. Application of porous ceramics for the attachment of load bearing internal orthopedic applications. *Journal of Biomedical Materials Research,* 5**,** 161-229.

KLEINMAN, H. K., MCGOODWIN, E. B. & KLEBE, R. J. 1976. Localization of the cell attachment region in types I and II collagens. *Biochemical and biophysical research communications,* 72**,** 426-432.

KLEMUK, S. A. & TITZE, I. R. 2009. Determining motor inertia of a stress-controlled rheometer. *Journal of Rheology,* 53**,** 765-780.

KO, C.-S., HUANG, J.-P., HUANG, C.-W. & CHU, I. M. 2009. Type II collagen-chondroitin sulfate-hyaluronan scaffold cross-linked by genipin for cartilage tissue engineering. *Journal of Bioscience and Bioengineering,* 107**,** 177-182.

KO, Y.-G., GRICE, S., KAWAZOE, N., TATEISHI, T. & CHEN, G. 2010. Preparation of Collagen-Glycosaminoglycan Sponges with Open Surface Porous Structures Using Ice Particulate Template Method. *Macromolecular Bioscience,* 10**,** 860-871.

KONG, J. & YU, S. 2007. Fourier transform infrared spectroscopic analysis of protein secondary structures. *Acta Biochimica Et Biophysica Sinica,* 39**,** 549-559.

KURNIAWAN, N. A., WONG, L. H. & RAJAGOPALAN, R. 2012. Early Stiffening and Softening of Collagen: Interplay of Deformation Mechanisms in Biopolymer Networks. - *Biomacromolecules.* - American Chemical Society.

KUZNETSOVA, N. & LEIKIN, S. 1999. Does the triple helical domain of type I collagen encode molecular recognition and fiber assembly while telopeptides serve as catalytic domains? Effect of proteolytic cleavage on fibrillogenesis and on collagen-collagen interaction in fibers. *Journal of Biological Chemistry,* 274**,** 36083-36088.

LAI, G., LI, Y. & LI, G. 2008. Effect of concentration and temperature on the rheological behavior of collagen solution. *International journal of biological macromolecules,* 42**,** 285-291.

LANE, J. M. & WEISS, C. 1975. Review of Articular-Cartilage Collagen Research. *Arthritis and Rheumatism,* 18**,** 553-562.

LARSON, R. G. 1999. *The structure and rheology of complex fluids,* New York, Oxford University Press.

LAUDER, R. M. 2009. Chondroitin sulphate: A complex molecule with potential impacts on a wide range of biological systems. *Complementary therapies in medicine,* 17**,** 56-62.

LAWSON, A. C. & CZERNUSZKA, J. T. 1998. Collagen-Calcium Phosphate composites. *Proceedings of the Institution of Mechanical Engineers Part H-Journal of Engineering in Medicine,* 212**,** 413.

LAWSON, A. C. & CZERNUSZKA, J. T. 1999. Production and characterisation of collagen-calcium phosphate composite for use as a bone substitute. *Materials Researcch Society Symposium proceeding,* 550**,** 273.

LEE, C. R., BREINAN, H. A., NEHRER, S. & SPECTOR, M. 2000. Articular cartilage chondrocytes in type I and type II collagen-GAG matrices exhibit contractile behavior in vitro. *Tissue engineering,* 6**,** 555-565.

LEE, C. R., GRODZINSKY, A. J. & SPECTOR, M. 2001. The effects of cross-linking of collagen-glycosaminoglycan scaffolds on compressive stiffness, chondrocyte-mediated contraction, proliferation and biosynthesis. *Biomaterials,* 22**,** 3145-3154.

LENG, P., WANG, Y. & ZHANG, H. 2013. Repair of Large Osteochondral Defects With Mix-Mosaicplasty in a Goat Model. *Orthopedics,* 36**,** e331.

LEVENTAL, I., GEORGES, P. C. & JANMEY, P. A. 2007. Soft biological materials and their impact on cell function. *Soft Matter,* 3**,** 299-306.

LI, B.-Y. R., LI-JIAN; LI, YI-YI; GJUNTER, V.E. 2000. An Investigation of the Synthesis of Ti-50 At. Oct Ni Alloys through Combustionn Sythesis and Conventional Powder Sintering. *Metallurgical and Materials Transactions A,* 31A.

LI, W. L., LU, K. & WALZ, J. Y. 2012. Freeze casting of porous materials: review of critical factors in microstructure evolution. *International Materials Reviews,* 57**,** 37-60.

LIANG, W.-H., KIENITZ, B. L., PENICK, K. J., WELTER, J. F., ZAWODZINSKI, T. A. & BASKARAN, H. 2010. Concentrated collagen-chondroitin sulfate scaffolds for tissue engineering applications. *Journal of Biomedical Materials Research Part a,* 94A**,** 1050-1060.

LINDAHL, U. & HOOK, M. 1978. Glycosaminoglycans and Their Binding to Biological Macromolecules. *Annual Review of Biochemistry,* 47**,** 385-417.

LIU, C., HAN, Z. & CZERNUSZKA, J. T. 2009. Gradient collagen/nanohydroxyapatite composite scaffold: Development and characterization. *Acta Biomaterialia,* 5**,** 661-669.

LIVINGSTON, T. L., GORDON, S. & ARCHAMBAULT, M. 2003. Mesenchymal stem cells combined with biphasic calcium phosphate ceramics promote bone regeneration. UK: Chapman Hall.

LU, H. H., SUBRAMONY, S. D., BOUSHELL, M. K. & ZHANG, X. 2010. Tissue Engineering Strategies for the Regeneration of Orthopedic Interfaces. *Annals of Biomedical Engineering,* 38**,** 2142-2154.

LU, L., VALENZUELA, R. & YASZEMSKI, M. 2000. Articular cartilage tissue engineering. *e-biomed: The Journal of Regenerative Medicine,* 1**,** 99.

LYNN, A. K., BEST, S. M., CAMERON, R. E., HARLEY, B. A., YANNAS, I. V., GIBSON, L. J. & BONFIELD, W. 2010. Design of a multiphase osteochondral scaffold. I. Control of chemical composition. *Journal of Biomedical Materials Research Part a,* 92A**,** 1057-1065.

LYNN, A. K., BROOKS, R. A., BONFIELD, W. & RUSHTON, N. 2004a. Repair of defects in articular joints - Prospects for material-based solutions in tissue engineering. *Journal of Bone and Joint Surgery-British Volume,* 86B**,** 1093-1099.

LYNN, A. K., YANNAS, I. V. & BONFIELD, W. 2004b. Antigenicity and immunogenicity of collagen. *Journal of Biomedical Materials Research Part B: Applied Biomaterials,* 71B**,** 343-354.

MACKAY, A. M., BECK, S. C., MURPHY, J. M., BARRY, F. P., CHICHESTER, C. O. & PITTENGER, M. F. 1998. Chondrogenic differentiation of cultured human mesenchymal stem cells from marrow. *Tissue engineering,* 4**,** 415-428.

MACKINTOSH, F. C., KAS, J. & JANMEY, P. A. 1995. Elasticity of Semiflexible Biopolymer Networks. *Physical Review Letters,* 75**,** 4425-4428.

MADRY, H., VAN DIJK, C. N. & MUELLER-GERBL, M. 2010. The basic science of the subchondral bone. *Knee Surg Sports Traumatol Arthrosc,* 18**,** 419-33.

MANDAL, B. B. & KUNDU, S. C. 2009. Cell proliferation and migration in silk fibroin 3D scaffolds. *Biomaterials,* 30**,** 2956-2965.

MANSOUR, J. M. 2003. Biomechanics of Cartilage. *In:* OATIS, C. A. (ed.) *Kinesiology: Mechanics and Pathomechanics of Human Movement.* Philadelphia: Lippincott Williams and Wilkins.

MARTIN, I., MIOT, S., BARBERO, A., JAKOB, M. & WENDT, D. 2007. Osteochondral tissue engineering. *Journal of Biomechanics,* 40**,** 750-765.

MARTIN, J. A. & BUCKWALTER, J. A. 1996. Articular Cartilage Aging and Degeneration. *Sports Medicine and Anthroscopy Review,* 4**,** 263.

MARTINO, S., D'ANGELO, F., ARMENTANO, I., KENNY, J. M. & ORLACCHIO, A. 2012. Stem cell-biomaterial interactions for regenerative medicine. *Systems Biology for Biomedical Innovation,* 30**,** 338-351.

MCBRIDE, S. H., FALLS, T. & KNOTHE TATE, M. L. 2008. Modulation of stem cell shape and fate B: mechanical modulation of cell shape and gene expression. *Tissue Engineering Part A,* 14**,** 1573-1580.

MCCULLEN, S. D., AUTEFAGE, H., CALLANAN, A., GENTLEMAN, E. & STEVENS, M. M. 2012. Anisotropic fibrous scaffolds for articular cartilage regeneration. *Tissue Eng Part A,* 18**,** 2073.

MCCUTCHEN, C. W. 1962. The frictional properties of animal joints. *Wear,* 5**,** 1-17.

MEWIS, J. & WAGNER, N. J. 2009. Thixotropy. *Colloids, polymers and surfactants.Special Issue in honour of Brian Vincent,* 147-148**,** 214-227.

MONMATURAPOJ, N., SOODSAWANG, W. & THEPSUWAN, W. 2012. Porous hydroxyapatite scaffolds produced by the combination of the gel-casting and freeze drying techniques. *Journal of Porous Materials,* 19**,** 441-447.

MOREAU, J. L. & XU, H. H. K. 2009. Mesenchymal stem cell proliferation and differentiation on an injectable calcium phosphate -chitosan composite scaffold. *Biomaterials,* 30**,** 2675-2682.

MORITZ, T. & RICHTER, H.-J. R. 2007. Ice-mould freeze casting of porous ceramic components. *Journal of the European Ceramic Society,* 27**,** 4595-4601.

MORRISON, E. H., FERGUSON, M. W. J., BAYLISS, M. T. & ARCHER, C. W. 1996. The development of articular cartilage .1. The spatial and temporal patterns of collagen types. *Journal of anatomy,* 189**,** 9-22.

MOW, V. C., HOLMES, M. H. & LAI, W. M. 1984. Fluid Transport and Mechanical-Properties of Articular-Cartilage - a Review. *Journal of Biomechanics,* 17**,** 377-394.

MUELLER, S. M., SHORTKROFF, S., SCHNEIDER, T. O., BREINAN, H. A., YANNAS, I. V. & SPECTOR, M. 1999. Meniscus cells seeded in type I and type II collagen-GAG matrices in vitro. *Biomaterials,* 20**,** 701-709.

MULLEN, L. M., BEST, S. M., BROOKS, R. A., GHOSE, S., GWYNNE, J. H., WARDALE, J., RUSHTON, N. & CAMERON, R. E. 2010. Binding and Release Characteristics of Insulin-Like Growth Factor-1 from a Collagen-Glycosaminoglycan Scaffold. *Tissue Engineering Part C-Methods,* 16**,** 1439-1448.

MURPHY, C. M., HAUGH, M. G. & O'BRIEN, F. J. 2010. The effect of mean pore size on cell attachment, proliferation and migration in collagen-glycosaminoglycan scaffolds for bone tissue engineering. *Biomaterials,* 31**,** 461-466.

MURPHY, C. M., MATSIKO, A., HAUGH, M. G., GLEESON, J. P. & O'BRIEN, F. J. 2012. Mesenchymal stem cell fate is regulated by the composition and mechanical properties of collagen-glycosaminoglycan scaffolds. *Special Issue on Tissue Engineering,* 11**,** 53-62.

MURPHY, C. M., O'BRIEN, F. J., LITTLE, D. G. & SCHINDELER, A. 2013. Cell-scaffold interactions in the bone tissue engineering triad.

MYLLYHARJU, J. & KIVIRIKKO, K. I. 2001. Collagens and collagen-related diseases. *Annals of Medicine,* 33**,** 7-21.

NA, G. C. & PHILIPS, L. J. 1983. In vitro collagen fibril assembly: thermodynamic studies. - *Biochemistry.* - American Chemical Society.

NATIONAL CENTER FOR BIOTECHNOLOGY INFORMATION Chonsurid & Collagen-alpha chain. *PubChem Compound Database; CID=24766, and CID=6913668.*

NEHRER, S., BREINAN, H. A., RAMAPPA, A., SHORTKROFF, S., YOUNG, G., MINAS, T., SLEDGE, C. B., YANNAS, I. V. & SPECTOR, M. 1997a. Canine chondrocytes seeded in type I and type II collagen implants investigated In Vitro. *Journal of Biomedical Materials Research,* 38**,** 95-104.

NEHRER, S., BREINAN, H. A., RAMAPPA, A., YOUNG, G., SHORTKROFF, S., LOUIE, L. K., SLEDGE, C. B., YANNAS, I. V. & SPECTOR, M. 1997b. Matrix collagen type and pore size influence behaviour of seeded canine chondrocytes. *Biomaterials,* 18**,** 769-776.

NEWMAN, A. P. 1998. Articular cartilage repair. *American Journal of Sports Medicine,* 26**,** 309-324.

NICHOLSON, J. W. 1991. *The Chemistry of Polymers,* Cambridge, The Royal Society of Chemistry.

NISHIMURA, M., YAN, W., MUKUDAI, Y., NAKAMURA, S., NAKAMASU, K., KAWATA, M., KAWAMOTO, T., NOSHIRO, M., HAMADA, T. & KATO, Y. 1998. Role of chondroitin sulfate-hyaluronan interactions in the viscoelastic properties of extracellular matrices and fluids. *Biochimica et Biophysica Acta (BBA) - General Subjects,* 1380**,** 1-9.

O'BRIEN, F. J., HARLEY, B. A., YANNAS, I. V. & GIBSON, L. 2004. Influence of freezing rate on pore structure in freeze-dried collagen-GAG scaffolds. *Biomaterials,* 25**,** 1077-1086.

O'BRIEN, F. J., HARLEY, B. A., YANNAS, I. V. & GIBSON, L. J. 2005. The effect of pore size on cell adhesion in collagen-GAG scaffolds. *Biomaterials,* 26**,** 433-441.

O'SHEA, T. M. & MIAO, X. 2008. Bilayered Scaffolds for Osteochondral Tissue Engineering. *Tissue Engineering Part B-Reviews,* 14**,** 447-464.

OBRINK, B. 1973. A Study of the Interactions between Monomeric Tropocollagen and Glycosaminoglycans. *European Journal of Biochemistry,* 33**,** 387-400.

OBRINK, B., LAURENT, T. C. & CARLSSON, B. 1975. The binding of chondroitin sulphate to collagen. *FEBS letters,* 56**,** 166-169.

OCHSNER, A., MURCH, G. E. & DE LEMOS, M. J. S. 2008. *Cellular and porous materials: thermal properties simulation and prediction*, John Wiley & Sons.

OHNO, T., TANISAKA, K., HIRAOKA, Y., USHIDA, T., TAMAKI, T. & TATEISHI, T. 2004. Effect of type I and type II collagen sponges as 3D scaffolds for hyaline cartilage-like tissue regeneration on phenotypic control of seeded chondrocytes in vitro. *International Symposium on Cell Biomechanics and Tissue Engineering at the University of Tokyo,* 24**,** 407-411.

OSATHANON, T., BESPINYOWONG, K., ARKSORNNUKIT, M., TAKAHASHI, H. & PAVASANT, P. 2011. Human osteoblast-like cell spreading and proliferation on Ti-6Al-7Nb surfaces of varying roughness. *Journal of oral science,* 53**,** 23-30.

OTTANI, V., MARTINI, D., FRANCHI, M., RUGGERI, A. & RASPANTI, M. 2002. Hierarchical structures in fibrillar collagens. *Micron,* 33**,** 587-596.

PALECEK, S. P., LOFTUS, J. C., GINSBERG, M. H., LAUFFENBURGER, D. A. & HORWITZ, A. F. 1997. Integrin-ligand binding properties govern cell migration speed through cell-substratum adhesiveness. *Nature,* 385**,** 537-540.

PANDAY, S. & CORAPCIOGLU, M. Y. 1991. Solute rejection in freezing soils. *Water Resources Research,* 27**,** 99-108.

PEPPIN, S. S. L., WETTLAUFER, J. S. & WORSTER, M. G. 2008. Experimental verification of morphological instability in freezing aqueous colloidal suspensions. *Physical Review Letters,* 100**,** 238301.

PETITE, H., VANDAMME, K., MONFOULET, L. & LOGEART-AVRAMOGLOU, D. 2011. Strategies for improving the efficacy of bioengineered bone constructs: A perspective. London: Springer International.

PIECHOCKA, I. K., VAN OOSTEN, A. S. G., BREULS, R. G. M. & KOENDERINK, G. H. 2011. Rheology of Heterotypic Collagen Networks. *Biomacromolecules,* 12**,** 2797-2805.

PIEPER, J. S., HAFMANS, T., VEERKAMP, J. H. & VAN KUPPEVELT, T. H. 2000. Development of tailor-made collagen-glycosaminoglycan matrices: EDC/NHS crosslinking, and ultrastructural aspects. *Biomaterials,* 21**,** 581-593.

PIEPER, J. S., OOSTERHOF, A., DIJKSTRA, P. J., VEERKAMP, J. H. & VAN KUPPEVELT, T. H. 1999. Preparation and characterization of porous crosslinked collagenous matrices containing bioavailable chondroitin sulphate. *Biomaterials,* 20**,** 847-858.

PIEPER, J. S., VAN DER KRAAN, P. M., HAFMANS, T., KAMP, J., BUMA, P., VAN SUSANTE, J. L. C., VAN DEN BERG, W. B., VEERKAMP, J. H. & VAN KUPPEVELT, T. H. 2002. Crosslinked type II collagen matrices: preparation, characterization, and potential for cartilage engineering. *Biomaterials,* 23**,** 3183-3192.

PITTENGER, M. F., MACKAY, A. M., BECK, S. C., JAISWAL, R. K., DOUGLAS, R., MOSCA, J. D., MOORMAN, M. A., SIMONETTI, D. W., CRAIG, S. & MARSHAK, D. R. 1999. Multilineage Potential of Adult Human Mesenchymal Stem Cells. *Science,* 284**,** 143-147.

PLACE, E. S., EVANS, N. D. & STEVENS, M. M. 2009. Complexity in biomaterials for tissue engineering. *Nature Materials,* 8**,** 457-470.

PORTER, J. R., RUCKH, T. T. & POPAT, K. C. 2009. Bone Tissue Engineering: A Review in Bone Biomimetics and Drug Delivery Strategies. *Biotechnology progress,* 25**,** 1539-1560.

PROSECKA, E., RAMPICHOVA, M., LITVINEC, A., TONAR, Z., KRALIKOVA¡, M., VOJTOVA, L., KOCHOVA, P., PLENCNER, M., BUZGO, M., MIKOVA¡, A., JANA¡, J. & AMLER, E. 2014. Collagen/hydroxyapatite scaffold enriched with polycaprolactone nanofibers, thrombocyte-rich solution and mesenchymal stem cells promotes regeneration in large bone defect in vivo. *Journal of Biomedical Materials Research Part A***,** n/a-n/a.

PUPPI, D., CHIELLINI, F., PIRAS, A. M. & CHIELLINI, E. 2010. Polymeric materials for bone and cartilage repair. *Topical Issue on Biomaterials,* 35**,** 403-440.

QUENT, V. M. C., LOESSNER, D., FRIIS, T., REICHERT, J. C. & HUTMACHER, D. W. 2010. Discrepancies between metabolic activity and DNA content as tool to assess cell proliferation in cancer research. *Journal of Cellular and Molecular Medicine,* 14**,** 1003-1013.

REDAELLI, A., VESENTINI, S., SONCINI, M., VENA, P., MANTERO, S. & MONTEVECCHI, F. M. 2003. Possible role of decorin glycosaminoglycans in fibril to fibril force transfer in relative mature tendons-a computational study from molecular to microstructural level. *Bone Cell and Tissue Mechanics,* 36**,** 1555-1569.

REINHART-KING, C. A., DEMBO, M. & HAMMER, D. A. 2008. Cell-Cell Mechanical Communication through Compliant Substrates. *Biophysical journal,* 95**,** 6044-6051.

RIEPPO, L., SAARAKKALA, S., NÃ¤RHI, T., HELMINEN, H. J., JURVELIN, J. S. & RIEPPO, J. 2012. Application of second derivative spectroscopy for increasing molecular specificity of fourier transform infrared spectroscopic imaging of articular cartilage. *Osteoarthritis and Cartilage,* 20**,** 451-459.

RODRIGUES, C. V. M., SERRICELLA, P., LINHARES, A. B. R., GUERDES, R. M., BOROJEVIC, R., ROSSI, M. A., DUARTE, M. E. L. & FARINA, M. 2003. Characterization of a bovine collagen-hydroxyapatite composite scaffold for bone tissue engineering. *Biomaterials,* 24**,** 4987-4997.

RODRIGUES, M. R. T., GOMES, M. E. & REIS, R. L. 2011. Current strategies for osteochondral regeneration: from stem cells to pre-clinical approaches. *Tissue, cell and pathway engineering,* 22**,** 726-733.

RODRIGUES, S. C., SALGADO, C. L., SAHU, A., GARCIA, M. P., FERNANDES, M. H. & MONTEIRO, F. J. 2013. Preparation and characterization of collagenâ€• nanohydroxyapatite biocomposite scaffolds by cryogelation method for bone tissue engineering applications. *Journal of biomedical materials research Part A,* 101**,** 1080-1094.

ROEDER, R. K., CONVERSE, G. L., KANE, R. J. & YUE, W. 2008. Hydroxyapatite-reinforced polymer biocomposites for synthetic bone substitutes *JOM,* 60**,** 38-45.

ROSENBLATT, J., DEVEREUX, B. & WALLACE, D. G. 1993. Dynamic rheological studies of hydrophobic interactions in injectable collagen biomaterials. *Journal of Applied Polymer Science,* 50**,** 953-963.

ROTH, V. & MOW, V. C. 1980. The Intrinsic Tensile Behavior of the Matrix of Bovine Articular-Cartilage and its Variation with Age. *Journal of Bone and Joint Surgery-American Volume,* 62**,** 1102-1117.

ROWLEY, J. A. & MOONEY, D. J. 2002. Alginate type and RGD density control myoblast phenotype. *Journal of Biomedical Materials Research,* 60**,** 217-223.

ROY, T. D., SIMON, J. L., RICCI, J. L., REKOW, E. D., THOMPSON, V. P. & PARSONS, J. R. 2003. Performance of degradable composite bone repair products made via three-dimensional fabrication techniques. *Journal of Biomedical Materials Research Part A,* 66A**,** 283-291.

RYAN, B. F. & MACKLIN, W. C. 1968. The growth of ice in supercooled aqueous solutions. *Journal of Crystal Growth,* 2**,** 337-340.

SAARAKKALA, S., RIEPPO, L., RIEPPO, J. & JURVELIN, J. S. 2010. Fourier Transform Infrared (FTIR) Microspectroscopy of Immature, Mature and Degenerated Articular Cartilage. *In:* MENDEZ-VILAS, A. & DIAZ, J. (eds.) *Formatex Microscopy Series No 4, Vol. 1.* Spain.

SACHLOS, E. & CZERNUSZKA, J. T. 2003. Making tissue engineering scaffolds work: Review on the application of solid freeform fabrication technology to the production of tissue engineering scaffolds. *European Cells & Materials,* 5**,** 29-40.

SACHLOS, E., REIS, N., AINSLEY, C., DERBY, B. & CZERNUSZKA, J. T. 2003. Novel collagen scaffolds with predefined internal morphology made by solid freeform fabrication. *Biomaterials,* 24**,** 1487-1497.

SCHAEFER, D., MARTIN, I., SHASTRI, P., PADERA, R. F., LANGER, R., FREED, L. E. & VUNJAK-NOVAKOVIC, G. 2000. In vitro generation of osteochondral composites. *Biomaterials,* 21**,** 2599-2606.

SCHOOF, H., APEL, J., HESCHEL, I. & RAU, G. 2001. Control of pore structure and size in freeze-dried collagen sponges. *Journal of Biomedical Materials Research,* 58**,** 352-357.

SCHOOF, H., BRUNS, L., FISCHER, A., HESCHEL, I. & RAU, G. 2000. Dendritic ice morphology in unidirectionally solidified collagen suspensions. *Journal of Crystal Growth,* 209**,** 122-129.

SCOTT, J. E. 1988. Proteoglycan-fibrillar collagen interactions. *Biochem.J.,* 252**,** 313.

SHARMA, B. & ELISSEEFF, J. H. 2004. Engineering Structurally Organized Cartilage and Bone Tissues. *Annals of Biomedical Engineering,* 32**,** 148-159.

SHOULDERS, M. D. & RAINES, R. T. 2009. Collagen Structure and Stability. *Annu.Rev.Biomed,* 78**,** 929.

SHU, K., THATTE, H. & SPECTOR, M. Chondrogenic differentiation of adult mesenchymal stem cells and embryonic stem cells. Bioengineering Conference, 2009 IEEE 35th Annual Northeast, 2009 2009. 1-2.

SIKAVITSAS, V. I., TEMENOFF, J. S. & MIKOS, A. G. 2001. Biomaterials and bone mechanotransduction. *Biomaterials,* 22**,** 2581-2593.

SILVER, F. H., EBRAHIMI, A. & SNOWHILL, P. B. 2002. Viscoelastic Properties of Self-Assembled Type I Collagen Fibers: Molecular Basis of Elastic and Viscous Behaviors. *Connect Tissue Res,* 43**,** 569-580.

SILVER, F. H. & TRELSTAD, R. L. 1979. Linear aggregation and the turbidimetric lag phase: Type I collagen fibrillogenesis in vitro. *Journal of theoretical biology,* 81**,** 515-526.

SINGH, A. 2012. Hydroxyapatite, a biomaterial: Its chemical synthesis, characterization and study of biocompatibility prepared from shell of garden snail, Helix aspersa. *Bulletin of Materials Science,* 35**,** 1031-1038.

SINGH, M., BERKLAND, C. & DETAMORE, M. S. 2008. Strategies and Applications for Incorporating Physical and Chemical Signal Gradients in Tissue Engineering. *Tissue Engineering Part B-Reviews,* 14**,** 341-366.

SIONKOWSKA, A. & KOZÅ‚OWSKA, J. 2013. Properties and modification of porous 3-D collagen/hydroxyapatite composites. *International journal of biological macromolecules,* 52**,** 250-259.

SLOSARCZYK, A., PALUSZKIEWICZ, C., GAWLICKI, M. & PASZKIEWICZ, Z. 1997. The FTIR spectroscopy and QXRD studies of calcium phosphate based materials produced from the powder precursors with different CaP ratios. *Ceramics International,* 23**,** 297-304.

SLYNARSKI, K. & DESZCZYNSKI, J. Algorithms for articular cartilage repair. Transplantation proceedings, 2006 2006. Elsevier, 316-317.

SMITH, L. A. & MA, P. X. 2004. Nano-fibrous scaffolds for tissue engineering. *Biointerfaces and Nanotechnology,* 39**,** 125-131.

SNOWDEN, J. M. & SWANN, D. A. 1980. Effects of glycosaminoglycans and proteoglycan on the in vitro assembly and thermal stability of collagen fibrils. *Biopolymers,* 19**,** 767-780.

STOCKWELL, R. A. 1979. *Biology of Cartilage Cells,* London, Cambridge University Press.

STOLZ, M., RAITERI, R., DANIELS, A. U., VANLANDINGHAM, M. R. & BASCHONG, W. 2004. Dynamic Elastic Modulus of Porcine Articular Cartilage Deteremined at Two Different Levels of Tissue Organization by Indentation-Type Atomic Force Microscopy. *Biophysical journal,* 86**,** 3269.

STUART, K. & PANITCH, A. 2008. Influence of chondroitin sulfate on collagen gel structure and mechanical properties at physiologically relevant levels. *Biopolymers,* 89**,** 841-851.

SUCHANEK, W. & YOSHIMURA, M. 1998. Processing and properties of hydroxyapatite-based biomaterials for use as hard tissue replacement implants. *Journal of Materials Research,* 13**,** 94-117.

SUNDELACRUZ, S. & KAPLAN, D. L. 2009. Stem cell- and scaffold-based tissue engineering approaches to osteochondral regenerative medicine. *Regenerative Biology and Medicine: II and Patterning and Evolving the Vertebrate Forebrain,* 20**,** 646-655.

SURESH, S. 2001. Graded materials for resistance to contact deformation and damage. *Science* 292**,** 2447-2451.

SUSI, H. & BYLER, D. M. 1983. Protein-Structure by Fourier-Transform Infrared-Spectroscopy - 2nd Derivative Spectra. *Biochemical and biophysical research communications,* 115**,** 391-397.

TAMADDON, M. & CZERNUSZKA, J. T. 2013. The need for hierarchical scaffolds in bone tissue engineering. *Hard tissue,* 2**,** 4-37.

TAMADDON, M., WALTON, R. S., BRAND, D. D. & CZERNUSZKA, J. T. 2013. Characterisation of freeze-dried type II collagen and chondroitin sulfate scaffolds. *Journal of Materials Science-Materials in Medicine,* 24**,** 1153-1165.

TAMPIERI, A., LANDI, E., VALENTINI, F., SANDRI, M., D'ALESSANDRO, T., DEDIU, V. & MARCACCI, M. 2011. A conceptually new type of bio-hybrid scaffold for bone regeneration RID F-5365-2011. *Nanotechnology,* 22**,** 015104-015104.

TEMENOFF, J. S. & MIKOS, A. G. 2000a. Injectable biodegradable materials for orthopedic tissue engineering. *Biomaterials,* 21**,** 2405-2412.

TEMENOFF, J. S. & MIKOS, A. G. 2000b. Review: tissue engineering for regeneration of articular cartilage. *Biomaterials,* 21**,** 431-440.

TENHUISEN, K. S., MARTIN, R. I., KLIMKIEWICZ, M. & BROWN, P. W. 1995. Formation and Properties of a Synthetic Bone Composite - Hydroxyapatite-Collagen. *Journal of Biomedical Materials Research,* 29**,** 803-810.

TIAN, H., LI, C., LIU, W., LI, J. & LI, G. 2013. The influence of chondroitin 4-sulfate on the reconstitution of collagen fibrils in vitro. *Colloids and Surfaces B: Biointerfaces,* 105**,** 259-266.

TIERNEY, C. M., HAUGH, M. G., LIEDL, J., MULCAHY, F., HAYES, B. & O'BRIEN, F. J. 2009a. The effects of collagen concentration and crosslink density on the biological,

structural and mechanical properties of collagen-GAG scaffolds for bone tissue engineering. *Papers from the Second International Conference on the Mechanics of Biomaterials and Tissues,* 2**,** 202-209.

TIERNEY, C. M., JAASMA, M. J. & O'BRIEN, F. J. 2009b. Osteoblast activity on collagen-GAG scaffolds is affected by collagen and GAG concentrations. *Journal of Biomedical Materials Research Part A,* 91**,** 92-101.

TRAPPMANN, B., GAUTROT, J. E., CONNELLY, J. T., STRANGE, D. G. T., LI, Y., OYEN, M. L., STUART, M. A. C., BOEHM, H., LI, B. & VOGEL, V. 2012. Extracellular-matrix tethering regulates stem-cell fate. *Nature materials,* 11**,** 642-649.

TUCKWELL, D. S., AYAD, S., GRANT, M. E., TAKIGAWA, M. & HUMPHRIES, M. J. 1994. Conformation dependence of integrin-type II collagen binding. Inability of collagen peptides to support alpha 2 beta 1 binding, and mediation of adhesion to denatured collagen by a novel alpha 5 beta 1-fibronectin bridge. *Journal of cell science,* 107**,** 993-1005.

VAN SUSANTE, J. L. C., PIEPER, J., BUMA, P., VAN KUPPEVELT, T. H., VAN BEUNINGEN, H., VAN DER KRAAN, P. M., VEERKAMP, J. H., VAN DEN BERG, W. B. & VETH, R. P. H. 2001. Linkage of chondroitin-sulfate to type I collagen scaffolds stimulates the bioactivity of seeded chondrocytes in vitro. *Biomaterials,* 22**,** 2359-2369.

VASILEV, M. P., KOTETSKII, V. V., PUKHOVA, Z. I., VOLF, L. A. & ISTRANOV, L. P. 1973. Collagen precipitation from solutions. *Fibre Chemistry,* 4**,** 486-488.

VEILLEUX, N. & SPECTOR, M. 2005. Effects of FGF-2 and IGF-1 on adult canine articular chondrocytes in type II collagen-glycosaminoglycan scaffolds in vitro. *Osteoarthritis and Cartilage,* 13**,** 278-286.

VEILLEUX, N. H., YANNAS, I. V. & SPECTOR, M. 2004. Effect of passage number and collagen type on the proliferative, biosynthetic, and contractile activity of adult canine articular chondrocytes in type I and II collagen-glycosaminoglycan matrices in vitro. *Tissue engineering,* 10**,** 119-127.

VICKERS, S. M., GOTTERBARM, T. & SPECTOR, M. 2010. Cross-linking affects cellular condensation and chondrogenesis in type II collagen-GAG scaffolds seeded with bone

marrow-derived mesenchymal stem cells. *Journal of Orthopaedic Research,* 28**,** 1184-1192.

VILLA, M. M., WANG, L., HUANG, J., ROWE, D. W. & WEI, M. 2014. Bone tissue engineering with a collagen-hydroxyapatite scaffold and culture expanded bone marrow stromal cells. *Journal of Biomedical Materials Research Part B: Applied Biomaterials***,** 243-253.

WAHL, D. A. 2007. *Collagen-Hydroxyapatite Scaffolds for Bone Tissue Engineering.* D.Phil., Department of Materials, University of Oxford.

WAHL, D. A. & CZERNUSZKA, J. T. 2006. Collagen-Hydroxyapatite composites for hard tissue repair. *European Cells & Materials,* 11**,** 43.

WAHL, D. A., SACHLOS, E., LIU, C. & CZERNUSZKA, J. T. 2007. Controlling the processing of collagen-hydroxyapatite scaffolds for bone tissue engineering. *Journal of Materials Science-Materials in Medicine,* 18**,** 201-209.

WALLACE, D. 1985. The role of hydrophobic bonding in collagen fibril formation: A quantitative model. *Biopolymers,* 24**,** 1705-1720.

WALTON, R. S. 2010. *Preparation and analysis of type I/ type II collagens for tissue engineering scaffolds Â.* Dissertation/Thesis, University of Oxford.

WALTON, R. S., BRAND, D. D. & CZERNUSZKA, J. T. 2010. Influence of telopeptides, fibrils and crosslinking on physicochemical properties of type I collagen films. *J Mater Sci Mater Med,* 21**,** 451-461.

WANG, Y., YANG, C., CHEN, X. & ZHAO, N. 2006. Biomimetic Formation of Hydroxyapatite/collagen Matrix Composite. *Advanced Engineering Materials,* 8**,** 97-100.

WEGST, U. G. K., SCHECTER, M., DONIUS, A. E. & HUNGER, P. M. 2010. Biomaterials by freeze casting. *Philosophical Transactions of the Royal Society A-Mathematical Physical and Engineering Sciences,* 368**,** 2099-2121.

WILLIAMS, B. R., GELMAN, R. A., POPPKE, D. C. & PIEZ, K. A. 1978. Collagen fibril formation. *J.biol.Chem,* 253**,** 6578-6585.

WOO, K. M., CHEN, V. J. & MA, P. X. 2003. Nano-fibrous scaffolding architecture selectively enhances protein adsorption contributing to cell attachment. *Journal of Biomedical Materials Research Part A,* 67A**,** 531-537.

WU, S., LIU, X., YEUNG, K. W. K., LIU, C. & YANG, X. 2014. Biomimetic porous scaffolds for bone tissue engineering. *Materials Science and Engineering: R: Reports,* 80**,** 1-36.

XIE, X., ZHOU, Y., BI, H., YIN, K., WAN, S. & SUN, L. 2013. Large-range control of the microstructures and properties of three-dimensional porous graphene. *Scientific reports,* 3.

XU, D. & CRAIG, S. L. 2011. Strain Hardening and Strain Softening of Reversibly Cross-Linked Supramolecular Polymer Networks. *Macromolecules,* 44**,** 7478-7488.

YANG, P. J. & TEMENOFF, J. S. 2009. Engineering Orthopedic Tissue Interfaces. *Tissue Engineering Part B: Reviews,* 15**,** 127.

YANG, Y.-L. & KAUFMAN, L. J. 2009. Rheology and Confocal Reflectance Microscopy as Probes of Mechanical Properties and Structure during Collagen and Collagen/Hyaluronan Self-Assembly. *Biophysical journal,* 96**,** 1566-1585.

YANNAS, I. V. 1972. Collagen and Gelatin in Solid-State. *Journal of Macromolecular Science-Reviews in Macromolecular Chemistry and Physics,* C 7**,** 49-106.

YASZEMSKI, M. J., PAYNE, R. G., HAYES, W. C., LANGER, R. & MIKOS, A. G. 1996. Evolution of bone transplantation: molecular, cellular and tissue strategies to engineer human bone. *Polymer Scaffolding and Hard Tissue Engineering,* 17**,** 175-185.

YIN HSU, F., CHUEH, S.-C. & JIIN WANG, Y. 1999. Microspheres of hydroxyapatite/reconstituted collagen as supports for osteoblast cell growth. *Biomaterials,* 20**,** 1931-1936.

YOSHIMURA, K., CHONAN, Y. & SHIRAI, K. 1999. Preparation and Dynamic Viscoelastic Characterization of Pepsin-Solubilized Collagen from Shark Skin Compared with Pig Skin. *Nihon Chikusan Gakkaiho,* 70**,** 227-234.

YUNOKI, S., IKOMA, T., MONKAWA, A., OHTA, K., KIKUCHI, M., SOTOME, S., SHINOMIYA, K. & TANAKA, J. 2006. Control of pore structure and mechanical property in hydroxyapatite/collagen composite using unidirectional ice growth. *Materials Letters,* 60**,** 999-1002.

ZEHBE, R., GOEBBELS, J., IBOLD, Y., GROSS, U. & SCHUBERT, H. 2010. Three-dimensional visualization of in vitro cultivated chondrocytes inside porous gelatine scaffolds: A tomographic approach. *Acta Biomaterialia,* 6**,** 2097-2107.

ZHANG, M., CHEN, Y., LI, G. & DU, Z. 2010. Rheological properties of fish skin collagen solution : Effects of temperature and concentration. *Korea-Australia Rheology Journal,* 22**,** 119.

ZHANG, Q., LU, H., KAWAZOE, N. & CHEN, G. 2014. Pore size effect of collagen scaffolds on cartilage regeneration. *Acta Biomaterialia*, 10**,** 2005-2013.

ZHAO, C., TAN, A., PASTORIN, G. & HO, H. K. 2013. Nanomaterial scaffolds for stem cell proliferation and differentiation in tissue engineering. *Pearl (30th) Anniversary Edition: Nanotechnology & Regenerative Medicine,* 31**,** 654-668.